

Investigating Resistance of Glioblastoma Multiforme to Radiotherapy and Chemotherapy

Submission for the degree of Master of Science (by Research), MSc (Res), in Oncology

Aaron Simpson

Somerville College, Oxford

Supervisor: Dr Valentine Macaulay

Trinity 2016

Student Number: 739651

Table of Contents

List of Figures **6**

List of Tables **10**

List of Abbreviations **11**

Acknowledgments **13**

Abstract **14**

1 Chapter I: Introduction **16**

1.1 Glioblastoma multiforme **16**

1.1.1 Classifications of GBM 17

1.1.2 Paediatric GBM 20

1.1.3 Difficulties in treating GBM 22

1.2 Radiotherapy and radio-resistance of GBM **22**

1.3 Chemotherapy and chemo-resistance of GBM **26**

1.4 Insulin-like growth factor type 1 receptor **29**

1.4.1 IGF-1R axis 29

1.4.2 IGF-1R signalling 30

1.5 IGF-1R in tumour biology **34**

1.6 IGF-1R in GBM **35**

1.7 Aims of the Project **36**

2 Chapter II: Materials and Methods **37**

2.1 Data Extraction from The Cancer Genome Atlas **37**

2.2 Immunohistochemistry (IHC) for IGF-1R **37**

2.3 Cell Lines and Reagents **38**

2.4 Cell Culture **40**

2.5 Irradiation 40

2.6 Subline Generation 40

2.6.1 TMZ Resistant Cell Lines 40

2.6.2 Repeatedly Irradiated Cells 41

2.7 Protein Extraction 41

2.7.1 Protein Extraction from Monolayer Cultures 41

2.7.2 Protein Extraction from Cell Pellets 41

2.8 Sodium Dodecyl Sulphate Polyacrylamide Gel Electrophoresis (SDS-PAGE) and Electrotransfer 42

2.9 Western Blotting 43

2.10 Clonogenic Assays 43

2.11 3D Environment Matrigel Assays 44

2.12 Viability Assays 44

2.12.1 CellTiter-Blue® (Promega) 44

2.12.2 CellTiter-Glo® 3D (Promega) 45

2.13 siRNA Knockdown 45

2.13.1 siRNA Sequences 45

2.13.2 Transfection 46

2.14 Flow Cytometry 46

2.14.1 Cell Cycle Analysis 46

2.14.2 CD24 Analysis 47

2.15 Immunofluorescence 48

2.15.1 IGF-1R and Podoplanin 48

2.15.2 γH2A.X 48

2.16 RNA Extraction 49

2.17 Gene Expression Microarray 50

2.18 Reverse Transcription 51

2.19 Real Time quantitative Polymerase Chain Reaction (qRT-PCR) 51

2.19.1 Primer Sequences 51

2.19.2 qRT-PCR Cycles for Relative Gene Expression Comparison 53

2.20 Chemotaxis Transwell® Assay 54

2.21 Statistical Analyses 54

3 Chapter III: Investigation of the expression and role of IGF-1R in GBM 56

3.1 Introduction 56

3.2 Results 57

3.2.1 IGF-1R expression in GBM 57

3.2.2 IGF-1R activity in GBM cells and inhibition of IGF-1R signalling 72

3.2.3 Effect of IGF-1R inhibition on clonogenicity of GBM cells 81

3.2.4 Effect of IGF-1R inhibition on radio- and chemo-sensitivity of GBM cells 89

3.2.5 Effect of *IGF1R* knockdown in GBM cells 98

3.3 Discussion 105

4 Chapter IV: Investigation of resistance to temozolomide in GBM 113

4.1 Introduction 113

4.2 Results 114

4.2.1 Characterisation of temozolomide resistance and the role of MGMT in GBM cell lines 114

4.2.2 Generation and characterisation of cell lines with acquired temozolomide resistance 119

4.2.3 Effect of temozolomide on GaMG and GaMG sublines 127

4.2.4 Effect of O6BG on the sensitivity of GaMG sublines to temozolomide 135

4.3 Discussion 137

5 Chapter V: Investigation of the effects of fractionated ionising radiation on GBM cells 140

5.1 Introduction 140

5.2 Results 141

5.2.1 Response of GBM cells to repeated irradiation 141

5.2.2 Characterisation and comparison of IR60 sublines and parental cell lines 146

5.2.3 Validation of differentially expressed genes in response the clinical dose of ionising radiation 162

5.2.4 siRNA Knockdown of CD24 169

5.3 Discussion 174

6 Chapter VI: Future Work 182

7 Chapter VII: Appendices 186

7.1 List of Primary Antibodies 186

7.2 List of Secondary Antibodies 187

7.3 Recipes 188

7.3.1 Gels 188

7.3.2 Buffers 189

7.4 Additional Microarray Comparisons 192

8 Chapter VIII: References 197

Word Count: 28,410

List of Figures

Figure 1.1: Mechanisms of DNA repair in response to TMZ. 28

Figure 1.2: IGF-1R cellular signalling. 33

Figure 3.1: Relative expressions of IGF-1R in GBM samples where query genes are altered or unaltered. 59

Figure 3.2: Positive and negative controls for IGF-1Rβ IHC staining.. 62

Figure 3.3: Schematic of scale used to score intensity of IGF-1R IHC staining. 63

Figure 3.4: IGF-1R IHC staining of a normal brain sample. 63

Figure 3.5: IGF-1R IHC staining of adult brain tumour tissue microarrays. 65

Figure 3.6: IGF-1R IHC staining of paediatric brain tumour tissue microarrays. 67

Figure 3.7: Comparison of adult and paediatric IGF-1R IHC staining scores. 68

Figure 3.8: Kaplan-Meier Survival Curves for adult and paediatric brain tumour patients by absence or presence of IGF-1R. 69

Figure 3.9: Kaplan-Meier Survival Curves for adult and paediatric brain tumour patients by intensity of IGF-1R IHC staining. 70

Figure 3.10: Characterisation of the IGF-1R RTK signalling axis in GBM cell lines. 74

Figure 3.11: BMS-754807 target inhibition of IGF-1R in GBM cells.. 76

Figure 3.12: BI-836845 target inhibition of IGF-1R in GBM cells. 79

Figure 3.13: Inhibition of basal IGF-1R signalling in GBM cells. 80

Figure 3.14: Effect of BMS-754807 on clonogenicity of GBM cells.. 84

Figure 3.15: Effect of BI-836845 on clonogenicity of GBM cells. 85

Figure 3.16: Schematic of the 3D environment Matrigel format used to assay effects on 3D cellular growth. 86

Figure 3.17: Images of 3D cellular growth of adult GBM cell lines.. 86

Figure 3.18: Dose response of adult GBM cells to IGF-1R inhibition in 2D and 3D viability assays.. 87

Figure 3.19: IGF-1R immunofluorescence in GBM cells. 88

Figure 3.20: Dose response of GBM cells to IR. 91

Figure 3.21: Response of GBM cells to IR combined with IGF-1R inhibition. 93

Figure 3.22: Raw colony counts of IR + IGF-1R inhibition combination clonogenic assays. 94

Figure 3.23: Response of GBM cells to TMZ in combination with IGF-1R inhibition. 96

Figure 3.24: Raw colony counts of TMZ + IGF-1R inhibition combination clonogenic assays. 97

Figure 3.25: Knockdown of *IGF1R* in GBM cells. 99

Figure 3.26: Cell cycle distribution of GBM cells following *IGF1R* knockdown. 103

Figure 3.27: Knockdown of the IGF-1R protein for cell cycle distribution analysis. 104

Figure 4.1: Basal sensitivities of GBM cell lines to TMZ. 116

Figure 4.2: Combination of TMZ and O6BG in TMZ resistant cell lines. 118

Figure 4.3: Schematic of generation of TMZ resistant GaMG cells. 120

Figure 4.4: TMZ dose response of GaMG and TMZ-resistant GaMG sublines. 122

Figure 4.5: Growth properties of GaMG and GaMG sublines.. 124

Figure 4.6: Characterisation of MGMT protein expression and RTK signalling axes in GaMG and GaMG sublines. 126

Figure 4.7: Assessment of TMZ-induced apoptosis on GaMG and GaMG sublines. 128

Figure 4.8: γH2A.X induction and resolution in GaMG and GaMG sublines in response to TMZ. 134

Figure 4.9: Effect of O6BG on the TMZ sensitivity of GaMG sublines. 136

Figure 5.1: Dose schedule applied to GBM cells. 143

Figure 5.2: Radiation dose response of LN-18 and LNIR60 cells. 143

Figure 5.3: Images of LN-18 and LNIR60 colonies at different doses of radiation. . 144

Figure 5.4: Radiation dose response and colony morphologies of GaMG and GaMGIR60 cells. 145

Figure 5.5: Viability of parental GBM cells and IR60 sublines over time. 147

Figure 5.6: Comparison of growth in Matrigel of GaMG and GaMGIR60. 148

Figure 5.7: Chemotaxis of GaMG and GaMGIR60 cells. 151

Figure 5.8: Characterisation of levels and activation of signalling proteins in parental GBM cell lines and their IR60 sublines. 154

Figure 5.9: Design of Illumina microarray gene expression analysis experiment. ... 155

Figure 5.10: Differential gene expressions between parental GBM cell lines and their IR60 sublines. 158

Figure 5.11: Validation of differentially expressed genes at the RNA level. 164

Figure 5.12: Testing for expression of podoplanin in GBM cells at the protein level. 166

Figure 5.13: Validation of differential expression of CD24 in GaMG and GAMGIR60 cells at the protein level.. 168

Figure 5.14: Knockdown of *CD24* in GaMG and GaMGIR60. 171

Figure 5.15: Effect of *CD24* knockdown on viability of GaMG and GaMGIR60. ... 172

Figure 5.16: Morphologies of GaMG and GaMGIR60 following *CD24* knockdown..

..... 173

List of Tables

Table 3.1: Top 10 most significantly altered proteins when *PTEN* is altered. 58

Table 3.2: Top 10 most significantly altered proteins when *PTEN* is mutated. 58

Table 3.3: Results of tests assessing for statistically significant differences in survival distributions between two groups of patients separated by their expression of IGF-1R in brain tumour tissue. 71

Table 3.4: DER values for IR when combining with IGF-1R inhibition in KNS42. .. 95

Table 3.5: Statistical testing of the raw colony numbers in the IGF-1R inhibition plus IR combination clonogenic assay with KNS42.. 95

Table 4.1: Statistical testing of the TMZ dose response of GaMG, GaMG TMZ 100, and GaMG TMZ 300. 123

Table 5.1: List of upregulated genes in GaMGIR60 relative to GaMG. 159

Table 5.2: List of upregulated genes in GaMG relative to GaMGIR60. 159

Table 5.3: List of upregulated genes in LNIR60 relative to LN-18. 160

Table 5.4: List of upregulated genes in LN-18 relative to LNIR60. 161

List of Abbreviations

APE-1	AP endonuclease
ATM	ataxia telangiectasia mutated
ATR	ataxia telangiectasia and Rad3-related protein kinase
BER	base excision repair
BrdU	5-bromo-2'-deoxyuridine
CC3	cleaved caspase 3
CD24	cluster of differentiation 24
Chk1	checkpoint kinase 1
Chk2	checkpoint kinase 2
CSC	cancer stem cell
CTB	CellTiter-Blue®
DAPI	4',6-diamidino-2-phenylindole
DDR	DNA damage response
DER	dose enhancement ratio
DMSO	dimethyl sulfoxide
DNA-PK_{cs}	DNA-dependent protein kinase catalytic subunit
DSB	double strand break
EGFR	epidermal growth factor receptor
Erk	extracellular signal-regulated kinase
FBS	foetal bovine serum
GBM	glioblastoma multiforme
Grb2	growth factor receptor-bound protein 2
GSC	glioma stem cell
HR	homologous recombination
IGF-1	insulin-like growth factor 1
IGF-1R	insulin-like growth factor 1 receptor
IGF-2	insulin-like growth factor 2
IGFBP	insulin-like growth factor-binding protein
IHC	immunohistochemistry
INSR	insulin receptor
IR	ionising radiation

IRS	insulin receptor substrate
Mek	MAPK/ERK kinase
MGMT	*O6*-alkylguanine-DNA alkyltransferase
MMR	mismatch repair
mTORC	mammalian target of rapamycin complex
NHEJ	non-homologous end-joining
O6BG	O6-benzylguanine
PARP	poly (ADP-ribose) polymerase
PBS	phosphate-buffered saline
PDGFR	platelet-derived growth factor receptor
PDPN	podoplanin
PI3K	phosphatidylinositide-3-kinase
PIP2	phosphatidylinositol 4,5-bisphosphate
PIP3	phosphatidylinositol 3,4,5-trisphosphate
PTEN	protein phosphatase and tensin homologue
qRT-PCR	real time quantitative polymerase chain reaction
Rb	retinoblastoma protein
RPE	R-phycoerythrin
RPPA	reverse phase protein array
RTK	receptor tyrosine kinase
SGK1	serum and glucocorticoid-regulated kinase 1
SH2	Src homology 2
Sos	son of sevenless
SSB	single strand break
ssDNA	single-stranded DNA
TBST	Tris-buffered saline with 0.1% Tween-20
TCGA	The Cancer Genome Atlas
TKI	tyrosine kinase inhibitor
TMA	tissue microarray
TMZ	temozolomide
γH2A.X	phosphorylated histone H2A.X

Acknowledgments

I would like to thank my supervisor Dr Valentine Macaulay for the life-changing opportunity she gave to me by allowing me to complete this research degree as a member of her laboratory. She has been supportive, considerate, and interested in a warm and welcoming manner throughout the duration of my project, and having a supervisor who has been so willing to discuss ideas, results, and experiments has made this an invaluable learning and life experience. As well as allowing me to learn about the world of research, this degree has helped me to achieve my ambition of attending medical school, and Dr Macaulay has been incredibly supportive of this goal from day one. Dr Macaulay is a person who has helped me to pursue the most successful career that I can, for which I will have everlasting gratitude.

I would equally like to thank Dr Frances Willenbrock and Dr Tamara Aleksic for their continual support, guidance, and friendship from the moment I first stepped foot into the laboratory. They have kindly shared much of their wisdom with me and as a result I have been able to develop as a scientist throughout my course.

In addition, I give my thanks to the other members of our laboratory: Nicholas Coupe, Guillaume Rieunier, Wilfride Petnga Kamdoum, Christopher Towers, Lina Guo, Victoria Ma, and Avinash Gupta, who have been encouraging and helpful during my time in the laboratory.

Lastly, I of course thank my fiancée Andrea, for, quite simply, putting up with me through all journeys in the past, present and future!

Abstract

Glioblastoma multiforme (GBM) is the most common and aggressive type of brain tumour. Despite treatment with surgery, radiotherapy and temozolomide (TMZ) chemotherapy, patient survival remains poor, suggesting that GBM cells evade and resist these therapies. The insulin-like growth factor 1 receptor (IGF-1R) is a receptor tyrosine kinase that signals towards cellular survival, proliferation and motility. Previous work from our laboratory showed that IGF-1R inhibition sensitises other tumour types to ionising radiation (IR) and TMZ. The first aim of this project was to assess IGF-1R expression in brain tumour tissue microarrays by immunohistochemistry. IGF-1R was found to be upregulated in adult and paediatric tumours relative to normal brain. In paediatric brain tumour patients, higher IGF-1R expression was found to associate with reduced patient survival, but no association was observed for adult brain tumour patients. The second aim sought to assess the effect of IGF-1R inhibition on the sensitivities of GBM cell lines to IR and TMZ. Adult and paediatric GBM cells showed varied expression and activation of IGF-1R and downstream signalling components. Use of two IGF-1R axis inhibitors showed that paediatric, but not adult GBM cells were sensitive to IGF-1R inhibition. In addition, there was evidence that IGF-1R inhibition sensitised paediatric GBM cells to IR. These results suggest that the IGF-1R could be an important target in paediatric GBM. However, sensitisation to TMZ was not observed. The third aim of this project was to assess the effects of repeated TMZ or IR treatment on adult GBM cells in order to identify mediators of treatment resistance. Repeated treatment with TMZ allowed previously sensitive cells that lacked *O6*-alkylguanine-DNA alkyltransferase (MGMT) to acquire different degrees of resistance to TMZ. Characterisation of the induced resistance sublines showed detectable MGMT expression. However, unlike the TMZ resistance detected in two cell lines that expressed endogenous

MGMT, the induced TMZ resistance in the repeatedly treated cells did not depend on MGMT activity. These MGMT-independent resistant cells may be useful to investigate novel strategies to overcome TMZ resistance. Finally, two repeatedly irradiated GBM sublines were established and characterised. One subline developed relative resistance to IR, the other developed a more motile phenotype. Microarray analysis showed differential expression of 122 genes across both cell line pairs, including upregulation of the stem cell marker CD24 in the more motile repeatedly irradiated subline. CD24 upregulation was validated at the mRNA and protein levels. Further investigation of differentially expressed genes may provide insights into novel mechanisms by which GBM cells evade or resist radiotherapy, and may help to guide development of new targeted treatments for GBM patients.

1 Chapter I: Introduction

1.1 Glioblastoma multiforme

The brain is the centre of the nervous system and is composed of many different types of cells. Billions of cells called neurons are responsible for the cognitive functions of the brain, but once differentiated, these cells cease to proliferate and neural stem cells become the source of new neurons (Gage and Temple, 2013). Within the brain are also glial cells. Glial cells support the function and environment of neurons in the central nervous system and peripheral nervous system and include astrocytes, oligodendrocytes, ependymal cells, and microglia. Glioma is the name given to a tumour that arises from the supportive tissue of the brain. The establishment of malignant gliomas is the result of a multistep process that includes sequential and cumulative genetic alterations resulting from intrinsic and environmental factors, which, over time, culminates in glial cells acquiring the Hallmarks of cancer, including self-sufficiency in growth signals, evasion of apoptosis, and tissue invasion and metastasis (Hanahan and Weinberg, 2011). However, despite identification of potential risk factors and causative genetic and molecular alterations, in most cases, owing to the heterogeneity of the tumours, the exact aetiologies are unknown (Omuro and DeAngelis, 2013). Brain tumours were formerly classified by the World Health Organisation (WHO) into four histological grades (I-IV), with grade III and grade IV tumours representing malignant gliomas (Louis et al., 2007). Glioblastoma multiforme (GBM) (grade IV) is the most aggressive and common type of brain tumour, with 10,743 diagnoses in England between 2007 and 2011 (an incidence of 4.64/100,000/year), 6.1 months median survival overall, and 3.4% 5-year survival over this time period (Brodbelt et al., 2015).

1.1.1 Classifications of GBM

One way of classifying gliomas is by their cell of origin. Different glioma subtypes have been proposed to link to various potential cells of origin, including neural stem cells, astrocytes, and oligodendrocyte-, astrocyte-, and glial-restricted progenitor cells (Zong et al., 2012). Multipotent, self-renewing neural stem cells have been suggested as a potential source of glioma establishment, particularly from within the subventricular and subgranular zones in the CNS (Sanai et al., 2005). The properties of neural stem cells, such as robust proliferative potential, self-renewal, association with blood vessels, and high motility, enable behaviour that is characteristic of gliomas, and lend themselves to development of neoplastic growth, which can happen through a diverse array of molecular mechanisms that potentially result from an increased susceptibility to transformation (Sanai et al., 2005). However, evidence also exists for gliomas arising from more differentiated cell lineages. For example, in mouse models, lineage tracing showed that oligodendrocyte precursor cells were the only cells to exhibit aberrant growth characteristics prior to malignancy that was generated through induction of p53 and NF1 protein mutations in neural stem cells (Liu et al., 2011). One potential mechanistic explanation for transformation of oligodendrocyte precursor cells may be loss of asymmetrical segregation of the epidermal growth factor receptor (EGFR) by the proteoglycan NG2 during mitosis. Decreased asymmetrical division led cells that would normally differentiate (those with low NG2 and EGFR) to retaining EGFR, maintaining EGFR-mediated proliferative capacity, and developing tumour-initiating potential (Sugiarto et al., 2011). Furthermore, gliomas have been demonstrated to arise from differentiated astrocytes and neurons through a process of de-differentiation following introduction of distinct genetic alterations. These alterations generated neural stem cells or progenitors that were capable of initiating and sustaining tumour progression, and giving rise to heterogeneous cell populations (Friedmann-Morvinski et al., 2012).

Two major subclasses of GBM exist based upon the distinctive genetic alterations and clinical presentations of each: primary GBM (*de novo*, usually in patients of >45 years) and secondary GBM (progressive from lower grade diffuse glioma, usually in patients of <45 years) (Furnari et al., 2007). While difficult to distinguish histologically, primary GBMs have been shown to account for 95% GBMs and secondary GBMs 5% (Ohgaki et al., 2004). Both primary and secondary GBMs develop genetic dysfunctions that lead to common fundamental tumour characteristics, such as cell cycle dysregulation, enhanced mitogenic signalling, and altered p53 tumour suppressor protein function, but the main difference between the two subtypes is how and when these dysregulations occur (Furnari et al., 2007). For example, two of the most commonly affected genes that lead to development of GBM, *EGFR* (encoding the EGFR), and *TP53*, undergo distinct evolutions of alterations in primary and secondary GBM (Watanabe et al., 1996). *TP53* mutations (e.g. point mutations or loss of chromosome 17p), are rarer in primary GBM than in secondary GBM, but *EGFR* overexpression is more common in primary GBM (Louis, 1994; Watanabe et al., 1996). In contrast, p53 function in primary GBMs is more commonly affected by deletion of the tumour suppressor P14ARF or MDM2 overexpression rather than direct mutation in *TP53* (Fulci et al., 2000).

Genomic characterisation has allowed further division of GBM into the subtypes of Classical, Mesenchymal, Proneural, and Neural (Verhaak et al., 2010). These subtypes were based on the expression and aberration statuses of *EGFR, NF1*, and *PDGFRA* and *IDH1* for Classical, Mesenchymal, and Proneural subtypes respectively, highlighting the genetic heterogeneity of different tumours. In addition, it was found that each subtype responded differently to therapy: the greatest efficacy was evident in the Classical subtype, whereas the Proneural subtype did not benefit (Verhaak et al., 2010). Other genomic characterisations have led to identification of new mutations and genes that were not previously thought to be

altered in GBM, and have helped to characterise the vast landscape of genetic alterations that give rise to the molecular mechanisms involved in the generation of GBM (Cancer Genome Atlas Research, 2008; Parsons et al., 2008).

Following these genomic studies, in 2016, a new classification system, The 2016 World Health Organization Classification of Tumours of the Central Nervous System, was established to encompass the accumulating knowledge of the genetic diversity of CNS tumours, advancing on the previous WHO classification established in 2007 (Louis et al., 2016). Whereas the 2007 classification was based largely on histology, the 2016 classification factors in the molecular parameters that contribute towards the heterogeneity between different tumours, with the intent of pursuing more detailed, accurate, and personal diagnoses in CNS tumour patients. Various major changes were therefore made to the 2007 classifications, in particular, an algorithm was developed for stratifying diffuse gliomas (including GBM) based on histology and subsequent genetic analysis of *IDH1/2* status (wildtype or mutant) and 1p/19q co-deletion status, e.g.: glioblastoma, *IDH* wild-type; oligodendroglioma, *IDH* mutant and 1p/19q co-deleted. This allows separation of distinct genetic entities that would otherwise be classified together in groups such as 'oligoastrocytoma, not otherwise specified'. Within GBM, *IDH* wild-type tumours account for ~90% of cases and correspond most frequently with the clinically-defined primary GBM, whereas *IDH*-mutant GBMs (~10%) closely correspond to secondary GBM. The third type of GBM, wherein *IDH* status is not defined, is classified as not otherwise specified. *IDH* status is important in GBM because *IDH* mutation has been shown to mediate extensive remodelling of the methylation of the genome (the methylome), inducing a glioma CpG island methylator phenotype, known as G-CIMP, that is a powerful determinant of tumour pathogenicity (Turcan et al., 2012). Providing a dynamic classification based on both

phenotype and genotype is predicted to have important implications on how patients with different types of brain tumours should be managed.

1.1.2 Paediatric GBM

Further complexity arises when considering the differences between adult and paediatric GBM. Paediatric high-grade gliomas are recognised to harbour tumour-driving genetic and epigenetic changes that are distinct from those in adult GBMs, suggesting that they should be considered separately with regards to their biology and treatment (Jones et al., 2017). For example, in 2010, two separate studies showed differences in copy number aberrations between adult and paediatric tumours (Bax et al., 2010; Paugh et al., 2010). One showed that *PDGFRA* is a target of focal amplification in paediatric tumours, which consequently experience deregulated signalling from the platelet-derived growth factor receptor (PDGFR) alpha. In addition, paediatric tumours show greater gain of chromosome 1q, and less frequent chromosome 7 gain and 10q loss than adult GBMs (Paugh et al., 2010). Further analysis of the genomic profiles and correlation with clinical prognosis allowed sub classification of paediatric high-grade gliomas into four categories, those with: stable genomes, associated with better prognoses; highly re-arranged genomes; aneuploidy; and amplifier genotypes, which have significantly worse prognoses (Bax et al., 2010). This latter study also supported the findings of decreased chromosome 7 gain and 10q loss (a defining feature of adult GBM) and increased 1q gain in paediatric tumours, and showed that genetic aberrations that deregulate 'core signalling pathways' in adult GBM are underrepresented in paediatric gliomas, highlighting that significant and important differences exist between the biology of adult and paediatric gliomas.

Two landmark studies further demonstrated the unique biology of paediatric gliomas by identifying mutations in histones and chromatin remodelling genes (Schwartzentruber et al., 2012; Wu et al., 2012). A key finding was recurrent mutations in *H3F3A* and *HIST1H3B*,

which encode histone variants H3.3 and H3.1 respectively. The mutations result in amino acid residue substitutions at two key positions in the histone tail that are important in regulatory post-translational modifications: K27M and G34R/G34V. These mutations, along with mutations in ATRX (α-thalassaemia/mental retardation syndrome X-linked) and DAXX (death-domain associated protein), both of which form parts of a chromatin remodelling complex, were observed in 31% of all tumours analysed (Schwartzentruber et al., 2012). The importance of these mutations lies in that they are not found in adult glioblastomas, providing further evidence that unique molecular processes give rise to adult and paediatric gliomas; they demarcate subsets of paediatric gliomas; and they alter the epigenome (Jones and Baker, 2014).

The K27M mutant in histone H3.3 leads to reduced levels of methylation at this site (H3K27me3) by PRC2-mediated inhibition of the methyltransferase EZH2, resulting in hypomethylation of DNA and heightened gene expression (Bender et al., 2013). However, while reduced globally, an increase in H3K27me3 and EZH2 has also been observed at promoters of various genetic loci in H3.3K27M patient cells, which alters the expression of genes known to be associated with a variety of cancer pathways, suggesting that the K27M-induced changes in the epigenome may represent key drivers of tumorigenesis (Chan et al., 2013). The G34 mutation gives rise to a unique gene expression signature that includes features of neural stem cells, including those of self-renewal. Strikingly, *H3F3A* G34 mutations were found to induce upregulation of the potent oncogene MYCN, suggesting a potential causative role of G34 mutations in paediatric GBM (Bjerke et al., 2013).

Therefore, it is clear that adult and paediatric gliomas have very different mechanisms of tumorigenesis, and even within the groups of adult and paediatric tumours, multiple sub classifications exist to encompass the vast differences between genetic profiles. However, despite better understanding and stratification of the genetic elements giving rise

to GBM, the enormous complexity relating to the genomic aberrations make it a very difficult cancer to treat.

1.1.3 Difficulties in treating GBM

The standard-of-care treatment for GBM patients is surgical resection, followed by radiotherapy and concomitant and/or adjuvant temozolomide (TMZ) chemotherapy (Omuro and DeAngelis, 2013). The low rate of survival in GBM patients is thought to be due to the nature of the disease itself. The topographically diffuse and invasive histology of the disease make 100% surgical resection almost impossible, which is why, even after the best possible surgical outcomes, patients are treated with radiotherapy and chemotherapy (Holland, 2000). Even with this multimodality treatment though, the outlook for GBM patients remains poor and recurrence is almost inevitable, despite recent significant, yet modest, improvements of survival reported in elderly patients that were treated with TMZ in combination with short-term radiotherapy (Hou et al., 2006; Perry et al., 2016). This implies that as well as evasion of surgical resection, GBM cells are either able to evade or resist radiotherapy and chemotherapy.

1.2 Radiotherapy and radio-resistance of GBM

The current standard-of-care for radiotherapy in GBM is 60 Gy of ionising radiation (IR), administered in fractions of 2 Gy over a period of six weeks (Barani and Larson, 2015). Radiotherapy utilises IR in an attempt to prevent further proliferation of tumour cells. IR is so named because as it passes through cells, it deposits energy into molecules to eject electrons, forming ions. Ionised molecules are highly reactive and can lead to a chain reaction of the breaking of chemical bonds, disrupting macromolecules such as DNA (Jackson and Bartek, 2009). The most lethal of these disruptions are DNA double strand breaks (DSBs), which, if not efficiently repaired, can lead to cell death. Cell death following

IR can occur early through one of several mechanisms: apoptosis, mitotic cell death (mitotic catastrophe), necrosis, or autophagy, or cells can be forced into senescence (permanent loss of proliferative capacity) (Baskar et al., 2012). Thus the aims of radiotherapy are to prevent tumour expansion and reduce viable tumour cells. While the intent of radiotherapy is the induction of cell death resulting from DNA damage, particularly through the generation of DSBs, cells experience endogenous DNA damage during normal replication, and have consequently evolved mechanisms by which they repair DSBs and single strand breaks (SSBs) to ensure maintenance of viability (Willers et al., 2004).

Cells respond to DSBs through multiple signalling cascades involving protein kinases and adaptor proteins, which signal the recruitment of the necessary protein apparatus to mediate the repair of DSBs, collectively referred to as the DNA damage response (DDR) (Jackson and Bartek, 2009). Broadly, the DDR response comprises signalling proteins categorised into sensors, transducers, mediators, and effectors. These groups of molecules mediate the repair of damaged DNA, and the delay of cell cycle progression at G1/S, S, and G2/M cell cycle checkpoints to prevent replication of damaged DNA (Polo and Jackson, 2011). Important sensors of DSBs are the proteins MRE11, RAD50 and Nbs1, which form a complex called MRN (Rupnik et al., 2010). Once bound to the DSB, MRN recruits and activates a central transducer of the DDR, the ataxia telangiectasia mutated (ATM) protein kinase, a protein kinase that functionally interacts with hundreds of effector targets, including AKT, MDM2, and p53, the latter of which can be activated to induce transcription of pro-apoptotic genes leading to IR-induced apoptosis (Lee and Paull, 2005; Saito et al., 2002; Shiloh and Ziv, 2013). An important substrate of ATM is checkpoint kinase 2 (Chk2), an effector which is activated by phosphorylation (Matsuoka et al., 2000). Chk2 activates the S phase checkpoint and a major mechanism by which it does this is through phosphorylation of the phosphatase Cdc25, causing Cdc25 inactivation, degradation, and

consequent inhibition of dephosphorylation of cyclin-dependent kinase 2 (CDK2), halting cell cycle progression and DNA replication (Falck et al., 2001; Mailand et al., 2000). Checkpoint kinase 1 (Chk1) also phosphorylates and inactivates Cdc25 (Chen et al., 2003). The transducer responsible for activating Chk1 is ataxia telangiectasia and Rad3-related protein (ATR) kinase, which is activated after recruitment to replication protein A (RPA)-coated single-stranded DNA (ssDNA) overhangs upon DSB end resection (Zou and Elledge, 2003). By halting cell cycle progression, the ATM-Chk2-Cdc25-CDK2 and ATR-Chk1 axes allow time for DNA repair and restoration of genome integrity.

The two major pathways to repair DSBs are homologous recombination (HR) and non-homologous end-joining (NHEJ) (Pardo et al., 2009). As its name suggests, HR uses undamaged homologous DNA to repair DSBs, wherein the undamaged DNA strand with an identical sequence is used as a template to repair the damaged strand. By contrast, NHEJ repairs DSBs by joining two ends of a DSB without the need for a homologous strand of DNA. In this, Ku70 and Ku80 heterodimers bind to the ends of DSBs, and recruit DNA-dependent protein kinase catalytic subunit (DNA-PK_{cs}) to tether the DNA ends together for removal of damaged bases and repair in a process that is more error-prone than HR (Gottlieb and Jackson, 1993; Hartlerode and Scully, 2009). The DSB repair pathway of choice largely depends upon the phase of the cell cycle the cell is in at the time of DNA damage: HR is favoured during S phase and early G2, whereas NHEJ predominates from G2/M through G1, but is active throughout the cell cycle (Hinz et al., 2005; Rothkamm et al., 2003).

Despite the 60 Gy dose regimen of radiotherapy in GBM, patient survival remains poor, indicating that the tumour cells are able to evade or resist the treatment. The DDR has been the subject of much study in the context of radio-resistance. Indeed, in glioma stem cells (GSCs), radio-resistance was found to be mediated by increased activation of DDR proteins and an enhanced DNA repair capacity (Bao et al., 2006). More recent work in the

group of Anthony Chalmers further characterised the radio-resistance of GSCs compared with bulk tumour cells by showing increased expression of ATM, ATR, Chk1 and poly (ADP-ribose) polymerase (PARP), with preferential activation of Chk1 following IR (Ahmed et al., 2015). Inhibition of several components of the DDR was able to overcome radio-resistance and restore radio-sensitivity in GSCs (Ahmed et al., 2015; Carruthers et al., 2015).

Outside the DDR, other mechanisms have been shown to mediate radio-resistance in GBM, including increased signalling by receptor tyrosine kinases (RTKs). In response to IR, the EGFR has been shown to induce survival signalling through the downstream effector AKT, and direct inhibition of EGFR or downstream signalling components reverses the resistance (Li et al., 2009). In addition, *EGFR* is overexpressed in >40% GBMs and >25% of GBMs express a mutant form of EGFR: EGFRvIII (deletion of exons 2-7) (Liu et al., 2005; Sugawa et al., 1990), which can mediate radio-resistance by binding DNA-PKcs and enhancing DSB repair (Mukherjee et al., 2009). In other tumour models, an EGFR monoclonal antibody, Cetuximab, is able to prevent translocation of EGFR to the nucleus, preventing activation of DNA-PKcs and sensitising those cells to IR (Dittmann et al., 2005). Crosstalk between different RTK signalling pathways, connected via the EGFR, has also been shown to confer radio-resistance (Toulany et al., 2005). Despite their preclinical data, EGFR inhibitors have seen limited efficacy in clinical trials in GBM (Hegi et al., 2011; Raizer et al., 2010).

Another RTK, the insulin-like growth factor 1 receptor (IGF-1R) has been shown to be upregulated in response to repeated irradiation in murine GSCs, and secretion of insulin-like growth factor 1 (IGF-1) ligand was able to induce radio-resistance via autocrine activation of the IGF-1R (Osuka et al., 2013). In addition, like the EGFR, work from our group showed that IGF-1R inhibition can promote radio-sensitivity in other tumour models

by impairing HR and NHEJ (Chitnis et al., 2014; Turney et al., 2012). Therefore, by targeting various different cell signalling molecules, it may be possible to reverse radio-resistance in GBM.

1.3 Chemotherapy and chemo-resistance of GBM

TMZ is the most frequently used chemotherapy in GBM and when used in conjunction with radiotherapy, confers a survival benefit of an additional 2.5 months to GBM patients (Stupp et al., 2009; Stupp et al., 2005). Results of a very recent phase III trial did show significantly improved survival of elderly patients when TMZ was added to short-course radiotherapy concomitantly or as adjuvant therapy (Perry et al., 2016). Doses administered are 75 mg/m^2 daily during concomitant treatment with IR, and 150 mg/m^2 for five days on 28-day cycles during adjuvant therapy. TMZ is administered orally as a prodrug and is activated by the alkaline pH surrounding brain tumour tissue (Rottenberg et al., 1984). TMZ is a DNA alkylating agent and cytotoxicity is mediated through its formation of *O6*-MeG, *N7*-MeG, and *N3*-MeA adducts, of which, *O6*-MeG is the most toxic (Drablos et al., 2004). If left unrepaired, *O6*-MeG mispairs with thymine during DNA replication. The mismatch repair (MMR) machinery recognises the mispairing and excises the thymine, which is again mispaired with the *O6*-MeG in multiple futile cycles (Drablos et al., 2004; Margison, 2010). Repeated DNA SSBs eventually lead to replication fork collapse, DSBs, and ATR/Chk-1 mediated cell cycle arrest in cycling cells, leading to apoptosis (D'Atri et al., 1998; Margison, 2010; Stojic et al., 2004). Thus functional MMR is required to achieve TMZ cytotoxicity. Two other mechanisms of DNA repair are involved in the response to TMZ: base excision repair (BER) and direct repair. BER mediates removal of *N7*-MeG, and *N3*-MeA lesions through the activity of alkylpurine-DNA-*N*-glycosylase, the silencing of which enhances TMZ-induced apoptosis, and overexpression of which induces TMZ resistance (Agnihotri et al., 2012). Alkylpurine-DNA-*N*-glycosylase generates an abasic site

that is recognised by AP endonuclease (APE-1), which cleaves the phosphodiester backbone to leave a gap containing 3'-OH and 5'-deoxyribose phosphate, allowing DNA polymerases and ligases to fill and seal the gap, repairing the DNA (Robertson et al., 2009). In direct repair, the enzyme *O6*-alkylguanine-DNA alkyltransferase (MGMT) can stoichiometrically remove alkyl adducts on guanine residues before undergoing degradation via the proteasome, restoring guanine and eliminating the toxic effects of *O6*-MeG (Zhang et al., 2012). Therefore, as well as mediating the toxicity of TMZ, DNA repair mechanisms can also confer resistance to TMZ (Figure 1.1).

Direct repair by MGMT is thought to be the main mechanism of resistance to TMZ in GBM (Kitange et al., 2009). Hypermethylation of the *MGMT* promoter, which has been detected in 40%-68% of patient tumours, reduces MGMT activity in GBM by preventing its transcription, altering the response of patients to DNA alkylating drugs (Esteller et al., 2000). It is well established that *MGMT* methylation status can be used as a predictor of responsiveness to alkylating agents in GBM. Clinical studies have demonstrated, though not universally, a greater sensitivity to TMZ and other alkylating agents in patients whose tumours contained methylated *MGMT*, resulting in enhanced survival relative to patients whose tumours did not have methylated *MGMT* (Blanc et al., 2004; Hegi et al., 2004; Hegi et al., 2005). Expression of MGMT therefore represents a major marker of resistance to TMZ in GBM. However, expression of MGMT does not universally correlate with MGMT activity and TMZ resistance (Meyer et al., 2015; Zhukovskaya et al., 1992). Indeed, the direct inhibition of MGMT in phase II trials did not significantly enhance the effects of TMZ in adult or paediatric GBM patients (Quinn et al., 2009a; Warren et al., 2012). Additionally, various studies have demonstrated sensitisation to TMZ without directly targeting MGMT,

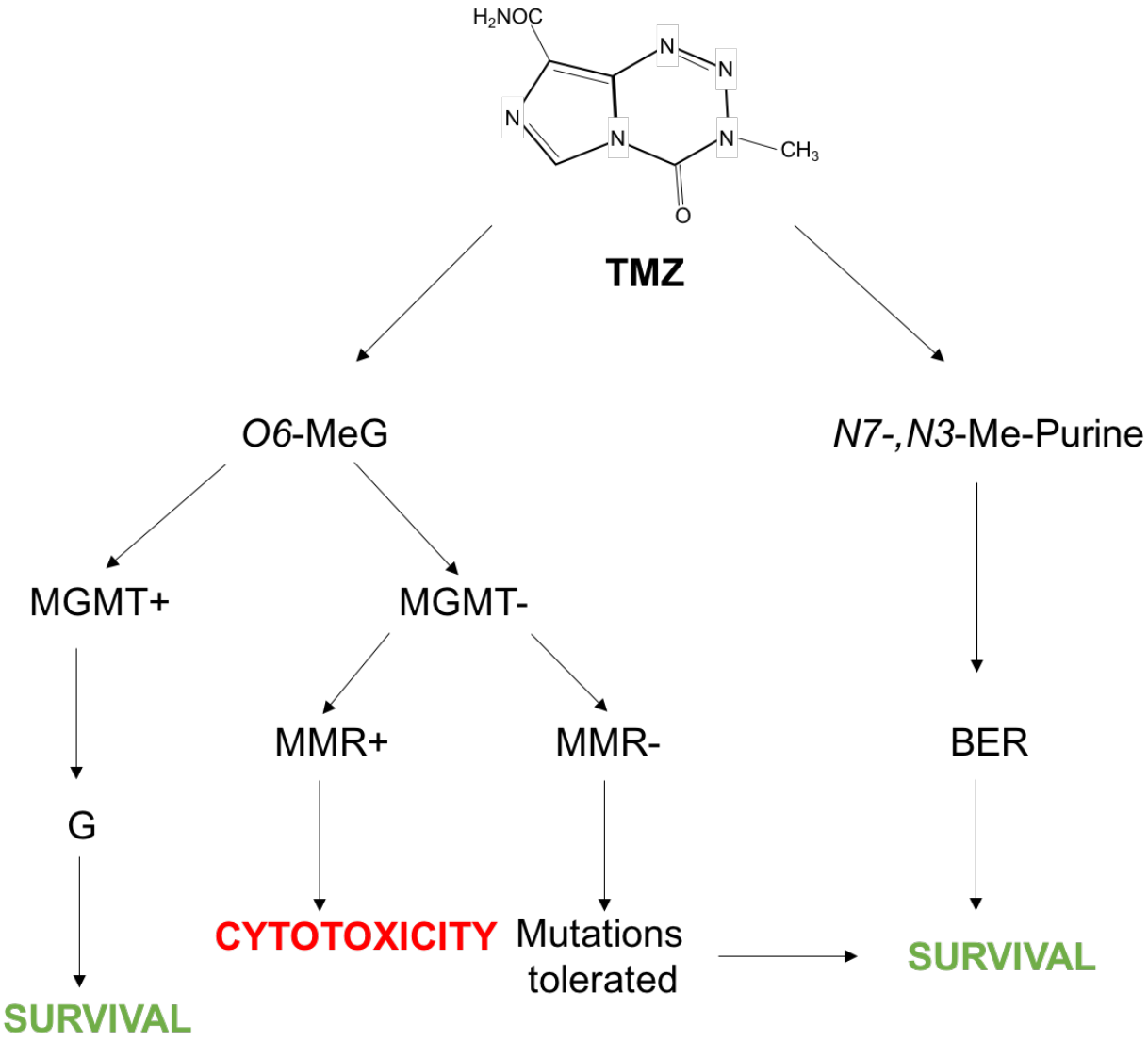


Figure 1.1 Mechanisms of DNA repair in response to TMZ. Adapted from Zhang *et al*. (2012).

including through inhibition of NF-κB, PARP, and RTK axes signalling components (Daniel et al., 2010; He et al., 2015; Wang et al., 2015). Therefore, it is clear that resistance to TMZ in GBM is more complex than simple expression of MGMT.

1.4 Insulin-like growth factor type 1 receptor

The IGF-1R is an RTK that transmits extracellular signals across the plasma membrane to the cell interior. IGF-1R is one of 518 protein kinases and 58 RTKs within the kinase complement of the human genome (Manning et al., 2002). IGF-1R, along with the insulin receptor (INSR), belongs to RTK class 2: the insulin receptor family. There are 20 RTK families, including the EGFR and the PDGFR families, and all are activated by extracellular ligands to become central nodes of cell signalling through recruitment of intracellular signalling molecules (Lemmon and Schlessinger, 2010).

1.4.1 IGF-1R axis

The IGF-1R axis consists of three ligands, two main receptors, seven ligand-binding proteins, and four insulin receptor substrates (IRSs) that bind directly to IGF-1R and INSR upon receptor activation. The ligands in the IGF-1R axis are insulin, IGF-1 and insulin-like growth factor 2 (IGF-2). The IGF-1R binds circulating IGF-1 with the highest affinity, followed by IGF-2, then insulin, the latter of which binds with >500-fold lower affinity (De Meyts et al., 1994). The insulin-like growth factor-binding proteins (IGFBPs) are circulating proteins that control the stability and the availability of IGF ligands to bind to their receptors by sequestration, thereby limiting IGF-induced signalling through IGF-1R and hybrid receptors (Firth and Baxter, 2002). IGFBPs 1-6 are the best characterised, but IGFBP7 has also been shown to block the activation of IGF-1R by IGF-1 (Evdokimova et al., 2012). Despite their inhibitory roles on IGF-1R signalling, IGFBPs have also been shown to

enhance the binding of IGF-1 to IGF-1R, indicating complex regulatory mechanisms (Jones et al., 1993).

The IGF-1R is a heterotetrameric RTK, consisting of two extracellular, ligand-binding alpha subunits linked via disulphide bonds to two transmembrane beta subunits, which contain the kinase domain and are responsible for signal transduction (Ullrich et al., 1986). Similarly, the INSR has a tetrameric structure, and can exist as two isoforms: INSRA, which functions like IGF-1R, and INSRB, which is the classic INSR that mediates glucose uptake (Belfiore and Malaguarnera, 2011). IGF-1R and INSR share a high degree of homology: 84% in the kinase domain and ~70% overall (Ullrich et al., 1986). Consequently, IGF-1R and INSR are able to form six different hybrid receptor species, each with varying binding abilities for IGF and insulin ligands (Pollak, 2012). The downstream signalling effects of hybrid receptors depends upon their specific composition; though IGF-1R:INSRA and IGF-1R:INSRB, like IGF-1R, are able to stimulate cell proliferation and migration (Pandini et al., 2002).

1.4.2 IGF-1R signalling

Signalling downstream of IGF-1R has been extensively studied (Chitnis et al., 2008; Girnita et al., 2014) and the classical signalling pathways are outlined in Figure 1.2. Upon binding of IGF-1/2 to the extracellular alpha subunits, a conformational change in the receptor takes place to liberate the intrinsic kinase activity of the beta subunit, which autophosphorylates tyrosines 1131, 1135, and 1136 to achieve full kinase activity (Favelyukis et al., 2001). Upon activation, the IGF-1R signals, broadly, towards cell survival, growth and proliferation through multi-kinase signal transduction and induction of gene expression (Figure 1.2). Autophosphorylation of juxtamembrane and carboxyl terminal tyrosine residues creates docking sites for the Src homology 2 (SH2) domains of the adaptor protein Shc, the phosphotyrosine binding domain of IRSs, and SH2 domains of class 1a

phosphatidylinositide-3-kinases (PI3Ks) (Girnita et al., 2014). Through subsequent phosphorylation of tyrosine residues in Shc and the C-terminal of IRSs, the IGF-1R recruits SH2 domain-containing proteins by binding the newly phosphorylated tyrosine residues in motif-specific manners (Rocchi et al., 1995). The recruited proteins are able to transmit the activation signal through multiple signalling cascades, two of which are well-characterised.

PI3K-AKT signalling is a major mediator of the effects of IGF-1R activation. Upon binding of the p85 subunit of class 1a PI3K to phosphotyrosine residues in IRS proteins and the IGF-1R itself, the catalytic p110 subunit becomes activated and phosphorylates phosphatidylinositol 4,5-bisphosphate (PIP2) to phosphatidylinositol 3,4,5-trisphosphate (PIP3), a process that can be reversed by the tumour suppressor protein phosphatase and tensin homologue (PTEN) (Backer et al., 1992; Cantley, 2002; Fukushima et al., 2012; Sun et al., 1999). PIP3 recruits AKT to the membrane by creating a docking site for AKT's pleckstrin homology domain (Frech et al., 1997). At the membrane, AKT is partly activated by direct phosphorylation of Thr 308 by phosphoinositide-dependent kinase 1, which is also recruited to the membrane by PIP3 (Alessi et al., 1997). Full activation of AKT is achieved by a second phosphorylation at Ser 473, which is thought to be mediated by activation, possibly via IGF-1R, of the mammalian target of rapamycin complex 2 (mTORC2) (Alessi et al., 1996; Sarbassov et al., 2005). Phosphorylated AKT then becomes an activated signalling hub that induces stimulatory and inhibitory phosphorylation of many substrates, leading ultimately to activation of mammalian target of rapamycin complex 1 (mTORC1), which promotes ribosomal assembly and translation, resulting in cell growth (Bhaskar and Hay, 2007). AKT inhibits pro-apoptotic proteins, including the pro-apoptotic BCL-2 family member BAD, leading to cell survival (Figure 1.2) (Datta et al., 1997; Manning and Cantley, 2007). AKT also acts on cell cycle regulatory proteins, inducing inhibitory phosphorylation of glycogen synthase kinase-3 beta, p21, p27, and FOXO transcription factors to promote

cell cycle progression (Brunet et al., 1999; Cross et al., 1995; Shin et al., 2002; Zhou et al., 2001).

The second major signalling pathway activated by IGF-1R also results in growth and proliferation. Once Shc has bound to phosphotyrosine residues on the IGF-1R, the SH2 domain of another adaptor protein, growth factor receptor-bound protein 2 (Grb2), binds to phosphotyrosines on Shc, and the Src homology 3 domain of Grb2 binds to proline-rich regions of a guanine nucleotide exchange factor, son of sevenless (Sos) (Girnita et al., 2014). Sos facilitates the exchange of GTP for GDP that is bound to membrane-bound Ras, which becomes activated and recruits Raf serine/threonine kinases to the membrane where they also become activated (Aronheim et al., 1994; Boriack-Sjodin et al., 1998; Leevers et al., 1994; Marais et al., 1995). A phosphorylation cascade through the mitogen-activated protein kinase kinases Mek 1 and 2, and extracellular signal-regulated kinase (Erk) 1 and 2, then culminates in the phosphorylation of numerous substrates, including ETS domain-containing protein Elk1, cAMP response element-binding protein, C-Fos and C-Jun (together, AP-1), and C-Myc (Dhillon et al., 2007; Kyriakis et al., 1992; McCubrey et al., 2007). By increasing transcription of cyclins, inhibitors of cell cycle inhibitors and the E2F transcription factor, C-Myc leads to downstream phosphorylation and inhibition of the retinoblastoma protein (Rb), allowing increased E2F activity, and transcription of genes that promote entry of the cell into S phase of the cell cycle, thus leading towards cell growth and proliferation (Figure 1.2) (Chellappan et al., 1991; Dynlacht et al., 1994; Hiebert et al., 1992; Kato et al., 1993; Mateyak et al., 1999; Ohtani et al., 1995). Therefore, through complex signalling mechanisms, the IGF-1R can convey to the cell instructions to survive, grow and divide. Since evasion of apoptosis, self-sufficiency in growth signals and tissue invasion and metastasis represent hallmarks of cancer (Hanahan and Weinberg, 2011), the oncogenic potential of IGF-1R has generated significant research interest in the context of cancer.

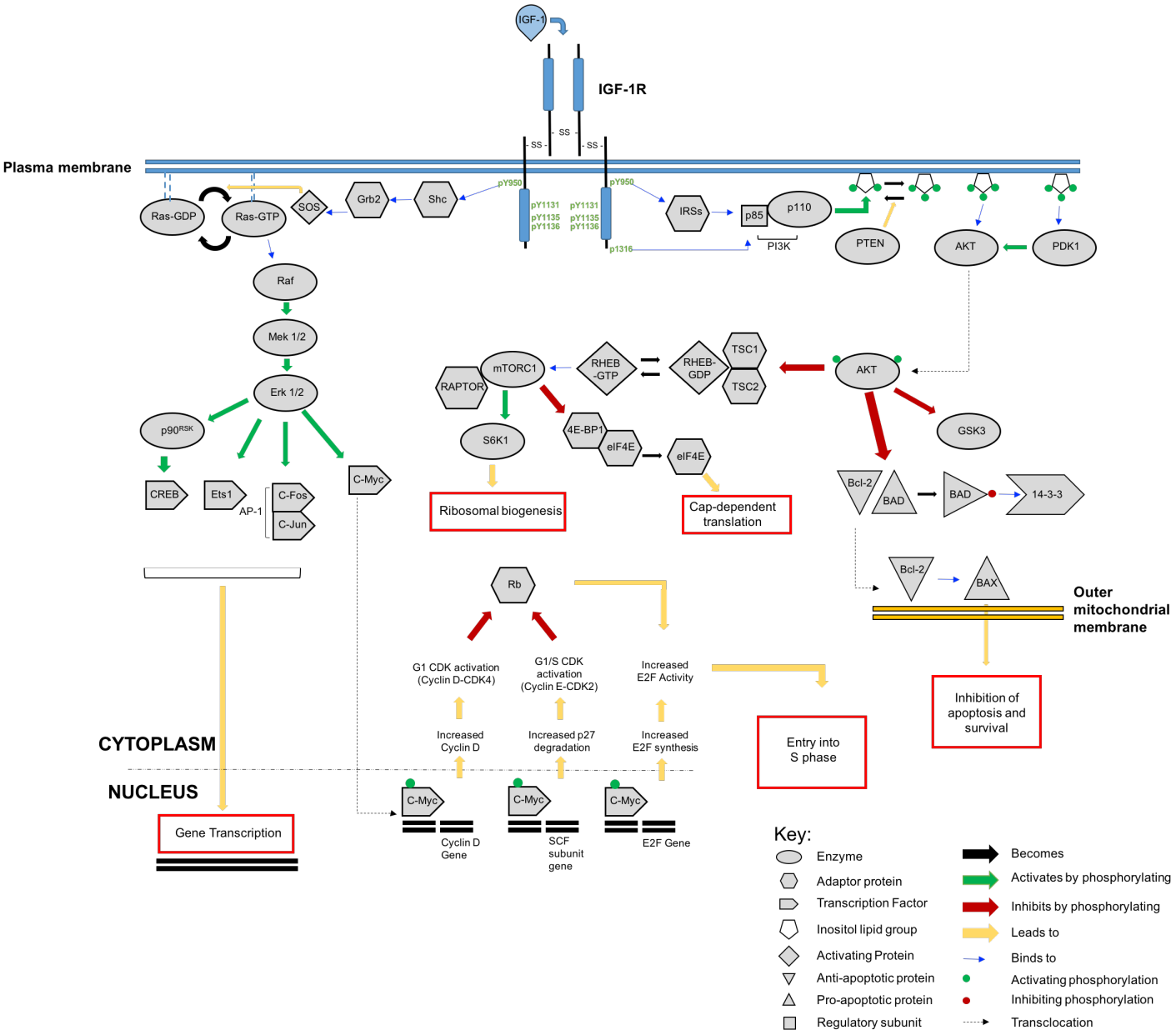


Figure 1.2: IGF-1R cellular signalling. Schematic diagram showing the effector components involved in signalling from the IGF-1R in response to ligand-induced activation. The diagram does not represent universal signalling responses in all cell types and it should be noted that cross-talk exists between many cell signalling pathways and signalling pathways are not linear. This figure was generated from information from references cited in the text.

1.5 IGF-1R in tumour biology

Countless studies have produced evidence that links IGF-1R expression and signalling with cancer. Particular founding studies came from early work in the group of Renato Baserga. Their work showed that without IGF-1R expression, mouse fibroblast cells are refractory to transformation by simian virus 40 large T antigen or oncogenic HRas, will not form anchorage-independent colonies in soft agar, and maintain density-dependent inhibition of growth, and re-expression of IGF-1R rescues transforming ability (Sell et al., 1994; Sell et al., 1993). The *IGF1R* gene is rarely mutated in human cancers;- only two cases of IGF-1R mutation in GBM were identified in the 2013 Glioblastoma study dataset available via TCGA (Brennan et al., 2013). However, many different tumour types can overexpress IGF-1R protein, which has been shown to result from loss of tumour suppressors such as TP53 and Wilm's tumour suppressor WT1 (Werner et al., 1996a; Werner et al., 1996b). Overexpression of IGF-1R has been observed to associate with a negative prognosis in various tumour types, including head and neck, bladder, ovarian, colorectal, and pancreatic cancers (Dale et al., 2015; Rochester et al., 2007; Spentzos et al., 2007; Takahari et al., 2009; Valsecchi et al., 2012). IGF-1R has also been shown to confer resistance to both traditional chemotherapies and targeted therapies in tumour cells (Schwartz et al., 2015; Vidal et al., 2015). Despite promising preclinical models and investigations, clinical trials of IGF-1R inhibition as a monotherapy have yielded disappointing results in all but a few cancer types, but rationally designed combination therapies and better patient selection have been suggested as potential avenues of increased efficacy for the future (King et al., 2014).

1.6 IGF-1R in GBM

IGF-1R and IGF-1 ligands are expressed in human brain tumour tissue (Sandberg-Nordqvist et al., 1993). Expression of IGF-1 in rat glioma cells was found to be crucial for tumorigenicity upon subcutaneous injection into rats, and IGF-1 antisense-transfected cells caused tumour regression of established GBMs distal to the injection site (Trojan et al., 1993). Early work with a human GBM cell line showed that IGF-1R expression affords autonomous and anchorage-independent growth, whereas IGF-1R silencing inhibits anchorage-independent growth, demonstrating the oncogenic potential of IGF-1R in GBM (Ambrose et al., 1994). Similarly, *IGF1R* siRNA inhibits both anchorage-independent and monolayer growth in rat GBM cells, and *IGF1R* siRNA-overexpressing rat cells are non-tumorigenic (Resnicoff et al., 1994). Subsequent studies showed that decreased expression and inhibition of IGF-1R attenuates GBM cell growth and causes apoptosis *in vitro* and in transplanted *in vivo* tumours (D'Ambrosio et al., 1996; Resnicoff et al., 1995a; Resnicoff et al., 1995b). Another study also showed that rat GBM cells transfected with antisense IGF-1R mRNA, but not sense IGF-1R mRNA, caused proliferation of CD8+ lymphocytes in response to wild-type rat GBM cells, showing that absence of IGF-1R signalling in GBM cells possibly stimulates an immune response (Resnicoff et al., 1996). The IGF-1R can also confer resistance to the traditional and experimental targeted therapies for GBM. Upregulation of IGF-1R allows GBM cells to resist inhibition of EGFR through induction of compensatory PI3K-AKT signalling, leading to enhanced cell survival (Chakravarti et al., 2002; Ma et al., 2016). In this context, dual targeting of EGFR and IGF-1R is reported to enhance the reduction of GBM cell growth relative to targeting either receptor alone. IGF-1R inhibition also enhances the effects of PDGFRα/β inhibition, where targeting both receptors effectively inhibits signalling through both the PI3K-AKT and Erk pathways (Bielen et al., 2011). In murine GSCs, as mentioned previously, activation of the IGF-1R

axis allows the development of an adaptive resistance to repeated irradiation, and subsequent blockade of IGF-1R activation reverses the resistant phenotype (Osuka et al., 2013). In addition, microRNAs have been shown to be tumour suppressors by acting to reduce IGF-1R expression (Zhang et al., 2014). A very recent report showed that tumour-associated macrophages are able to support GBM cells by provision of IGF-1 in the microenvironment, and that co-targeting of IGF-1R and colony-stimulating factor-1 receptor prolonged survival of transgenic PDGF-driven glioma mouse models (Quail et al., 2016).

1.7 Aims of the Project

Surgery, radiotherapy, and chemotherapy constitute the mainstay treatment for GBM. However, even this triple combination still affords very poor long-term survival for GBM patients. IGF-1R has been shown to contribute to GBM biology, and furthermore, previous work from our group showed that IGF-1R inhibition is capable of sensitising to IR and TMZ in other tumour models (Chitnis et al., 2014; Ramcharan et al., 2015; Turney et al., 2012). The above provides rationale for further investigation into whether IGF-1R expression and activation mediates resistance to radiotherapy and chemotherapy in human GBM. However, multiple mechanisms of radio- and chemo-resistance involving many different signalling pathways have been described in GBM. The aims of this project were thus three-fold:

1) To investigate IGF-1R expression in human gliomas and assess any associations with patient survival.
2) To investigate the effects of IGF-1R inhibition on the sensitivity of GBM cells to TMZ and IR.
3) To assess the effects of repeated TMZ and IR treatment on GBM cells, and characterise induced molecular changes associated with altered phenotypic response to TMZ and IR.

2 Chapter II: Materials and Methods

2.1 Data Extraction from The Cancer Genome Atlas

Publicly available cancer genomics data were from The Cancer Genome Atlas accessed through cBioPortal for Cancer Genomics (Cerami et al., 2012; Gao et al., 2013). Queries were run for specific genes within the Cell, 2013 Glioblastoma study dataset (Brennan et al., 2013). Protein expression data tables and scatter plots were generated for download through cBioPortal to reflect specific query conditions.

2.2 Immunohistochemistry (IHC) for IGF-1R

Formalin-fixed paraffin embedded sections of adult and paediatric brain tumour tissue microarrays (TMAs) and associated clinical data were kindly provided by Dr Chris Jones (Institute of Cancer Research, Surrey, UK). Permission to use human tissue under ethically approved study was approved by NRES Committee South Central – Oxford C. REC reference: 07/H0606/120; title: The role of insulin-like growth factor (IGF) signaling in tumour biology. Valid until November 2017.

Immunohistochemical staining for IGF-1Rβ was performed based on the method described by Aleksic *et al.* (Aleksic et al., 2016). Sections were dewaxed by two 8 min incubations in Citroclear (TCS Biosciences Ltd., UK) and rehydrated by incubation in graded ethanol solutions (100%, 95%, 80%, 70%, 50%) for 2 min intervals, followed by deionised water for 10 min. Antigen retrieval was performed in a decloaking chamber (Biocare Medical, model DC2002) with Tris/EDTA buffer (50 mM Tris + 2 mM EDTA, pH 9.0) at 125°C for 2 min, followed by 85°C for 10 min. Slides (in buffer) were cooled to room temperature on ice. Slides were washed 3 x 5 min in phosphate-buffered saline (PBS) before blocking endogenous peroxidase by incubation in 3% H_2O_2 (#H1009, Sigma) for 10 min at

room temperature. Slides were washed 3 x 5 min in PBS, then blocked in 5% bovine serum albumin (BSA)/5% goat serum (#G6767, Sigma) in PBS for 1 hr at room temperature. Slides were drained and placed into a humidified chamber with the tissue circled with PAP pen. IGF-1Rβ antibody (#9750, Cell Signaling Technology) was diluted 1:50 in blocking solution and added to completely cover the tissue for incubation overnight at 4°C. Slides were then washed 3 x 5 min in PBS. Detection of bound antibody was performed using a Rabbit HRP-Polymer detection kit (#MP-531-M3R100, Menarini Diagnostics); tissue was covered in rabbit probe (20 min, room temperature), followed by 3 x 5 min PBS washes, followed by incubation with rabbit HRP polymer (20 min, room temperature), followed by 3 x 5 min PBS washes. Slides were incubated with diaminobenzidine (#K3467, Dako) for 7 min to allow stain development, then were washed with water. Tissue was counterstained with haematoxylin for 30 secs then washed until water ran clear. Tissue was dehydrated by incubating slides in graded ethanol (50%, 70%, 80%, 95%, 100%) for 2 min intervals followed by a 5 min incubation in Citroclear. Slides were mounted using DePex reagent (VWR International).

Slides were scanned at x40 magnification on an Aperio ScanScope for analysis. Staining intensity was scored on a seven-point scale from negative to strong (see Figure 3.3), after training with consultant neuropathologist Professor Olaf Ansorge on examining brain tumour tissue. The scoring was verified with Prof Ansorge after completion.

2.3 Cell Lines and Reagents

Adult GBM cell lines GaMG and DK-MG were purchased directly from The Leibniz Institute DSMZ - German Collection of Microorganisms and Cell Cultures GmbH (DSMZ no. ACC 242 and ACC 277 respectively). The extensively characterised adult GBM cell line U87-MG (Clark et al., 2010) was obtained from Professor Adrian Harris (Department of

Oncology, University of Oxford, UK). The adult GBM cell line LN-18 (Diserens et al., 1981) was obtained via Dr Geoff Higgins from Professor Ian Tomlinson (Nuffield Department of Medicine, University of Oxford, UK). The paediatric GBM cell lines KNS42 (Takeshita et al., 1987) and SF-188 (Rutka et al., 1987) were obtained from Dr Chris Jones (Institute of Cancer Research, Surrey, UK). Cell lines were authenticated using the PCR-single-locus-technology services provided by Eurofins. All cells in culture were routinely tested for mycoplasma infection using the MycoAlert™ Mycoplamsa Detection Kit (#LT07-318, Lonza).

The IGF-1R/IR small molecule tyrosine kinase inhibitor (TKI) BMS-754807 was obtained commercially (#S1124, Selleck Chemicals) in powder form and reconstituted in dimethyl sulfoxide (DMSO) to a stock concentration of 10 mM. The fully human monoclonal antibody directed towards IGF-I and IGF-II, BI-836845, was obtained by Dr Valentine Macaulay from Boehringer Ingelheim for use through a Material Transfer Agreement and stored at 4°C. Temozolomide was a gift from Dr Geoff Margison (University of Manchester, UK) and was reconstituted from powder in DMSO to a 100 mM stock solution. Powdered IgG from human serum (#I4506, Sigma) was reconstituted in a saline solution (150 mM NaCl) to 11.7 mg/ml and stored at -20°C. O^6-Benzylguanine (#ab142739, Abcam), was obtained commercially in powdered form and reconstituted in DMSO to stock concentrations of 80 mM. Etoposide (#S1225, Selleck Chemicals) was purchased as a 10 mM stock in DMSO. Stock solutions in DMSO were stored in 5-200 µl aliquots at -20°C. Lyophilised recombinant human IGF-I (#I3769, Sigma) was reconstituted in 10 mM HCl to a 110 µM stock solution and stored at -80°C.

2.4 Cell Culture

U87-MG, GaMG, and LN-18 were maintained in high glucose Dulbecco's Modified Eagle Medium (DMEM) containing pyruvate (#41966-029, Gibco); KNS42 and SF-188 were maintained in DMEM-F12 (1:1) (#BE12-719F, Lonza); and DK-MG was maintained in RPMI-1640 (#21875-091, Gibco). All media were supplemented with 100 units/ml penicillin and 100 μg/ml streptomycin (#15140-122, Gibco), and 10% foetal bovine serum (FBS) (#10500-064, Gibco). GaMG medium was additionally supplemented with 4X MEM non-essential amino acids solution (#11140-035, Gibco). Cultures were grown at 37°C in 5% CO_2 (GaMG cultures were grown in 10% CO_2). During routine culture, cells were washed with sterile PBS, lifted in 5x Trypsin/EDTA solution (#LZBE02-007E, Lonza) and re-seeded into full medium. Cell lines were banked in a solution of 10% DMSO, 50% FBS, and 40% full medium and cooled at a rate of 1°C/min to -80°C. Vials were subsequently stored in liquid nitrogen.

2.5 Irradiation

Cells were irradiated in their culture vessels at doses between 2-10 Gy in a Gamma-Service Medical GmbH caesium-137 irradiator (GSR D1). Serial number: A0108, maximum activity: 197.1 TBq. Located in Old Road Campus Research Building, University of Oxford.

2.6 Subline Generation

2.6.1 TMZ Resistant Cell Lines

GaMG cells with acquired resistance to TMZ concentrations of 100 μM (GaMG TMZ 100) and 300 μM (GaMG TMZ 300) were generated by passaging cultures in medium containing TMZ. Cells were split into new flasks and the medium was replaced with medium

containing TMZ the following day and cells allowed to recover. Fresh medium containing TMZ was added if cells had not fully recovered to be passaged after 7 days. TMZ doses were increased by half log units (beginning with 10 μM) up to final concentrations of 100 μM or 300 μM.

2.6.2 Repeatedly Irradiated Cells

GaMG and LN-18 cultures in 75 cm flasks were subjected to the doses of IR received by GBM patients undergoing radiotherapy under the current standard-of-care treatment: 2 Gy fractions, five times per week for six weeks, totalling 60 Gy (Barani and Larson, 2015). After each five-day period, cells were subcultured and banked. Cells that completed the full IR dose course were designated GaMGIR60 and LNIR60. These were then banked and stored, and also maintained in culture for investigation of resistance mechanisms.

2.7 Protein Extraction

2.7.1 Protein Extraction from Monolayer Cultures

Six-well dishes were seeded with equal numbers of cells per well. After desired treatment, the medium was removed, and each well was washed twice on ice with ice-cold PBS. Cells were lysed and proteins denatured by adding 100 μl 3 x Laemmli Sample Buffer (containing 9% [w/v] sodium dodecyl sulphate [SDS], see Appendix 7.3) directly to each well. The contents of each well was scraped and collected, then denatured at 95°C for 10 min. Lysates were stored at -20°C until use.

2.7.2 Protein Extraction from Cell Pellets

After desired treatment(s), medium was removed from cells in 10-15 cm dishes and cells were washed on ice twice with ice-cold PBS. Cells were scraped and collected in ~1 ml ice-cold PBS, then centrifuged at 15,000 x *g* for 30 secs at 4°C. PBS was removed and

pellets were snap-frozen in dry ice and ethanol, and stored at -80°C until use. Cells from 75 cm culture flasks were lifted in trypsin/EDTA (see section 2.4), collected in full medium, and centrifuged at 220 x *g* for 5 min to pellet cells. The medium was removed, cells were re-suspended in ~1 ml sterile PBS, pelleted by centrifugation, and frozen as described above. Cell pellets were lysed on ice for 30 min in RIPA-100 lysis buffer (containing 0.1% [w/v] SDS, 0.5% [w/v] sodium deoxycholate, and 1% [v/v] triton X-100 see Appendix 7.3) supplemented with phosphatase inhibitor cocktails 2 and 3 (#P5726 and #P0044, Sigma), Pefabloc® SC (Roche), and cOmplete™ EDTA-free protease inhibitor cocktail (#11873580001, Roche). Lysates were centrifuged at 15,000 x *g* for 15 min at 4°C and supernatants collected. Lysates were subjected to a Pierce BCA Protein assay (#23225, ThermoFisher Scientific) to quantify soluble protein levels. Lysates were then diluted in RIPA-100 and 3 x Laemmli Sample Buffer to achieve equal amounts of protein, heated for 5 min at 95°C, and stored at -20°C until use.

2.8 Sodium Dodecyl Sulphate Polyacrylamide Gel Electrophoresis (SDS-PAGE) and Electrotransfer

Polyacrylamide resolving gels were cast at 8% or 15% according to the methods outlined in the appendices. Stacking gels were cast at 4%. NuPAGE™ Novex™ 4-12% Bis-Tris protein gradient gels were obtained commercially (#NP0335BOX, Invitrogen). Samples were denatured, centrifuged (15,000 x *g*, 2 min), and 30-50 µl loaded into lanes. Spectra™ multicolor broad range protein ladder (#26634, ThermoFisher Scientific) was used as a molecular weight marker. Electrophoresis proceeded at 125 V for ~70 min in running buffer (Appendix 7.3) to separate proteins. Electrotransfer onto nitrocellulose or polyvinylidene difluoride (PVDF) (pre-activated in methanol) membranes was performed at 35 mA/gel for 3 hr, or 150 mA/gel for 1 hr with semi-dry transfer buffer (Appendix 7.3),

or for 7 min at 1.3 A (25 V) using a Trans-Blot® Turbo™ Transfer System (Bio-Rad) with Trans-Blot® Turbo™ transfer buffer. Gradient gels were electrotransferred on the Turbo-Blot at 2.5 A (25 V) for 10 min.

2.9 Western Blotting

Following electrotransfer, membranes were blocked in 5% (w/v) non-fat dairy milk in Tris-buffered saline with 0.1% Tween-20 (TBST) for 1 hr at room temperature. Membranes were incubated with primary antibody for 1 hr at room temperature, or overnight at 4°C, washed 3 x 5 min in TBST, incubated for 1 hr at room temperature with horseradish peroxidase-conjugated secondary antibody, then washed a further 3 x 5 min in TBST. All incubations and washes were on a gyro-rocker. Bound antibodies were detected by electrochemiluminescence ECL Western Blotting Substrate (#W1015, Promega) and exposure to X-ray film. Film was developed using a Xograph Compact X4 Processor.

2.10 Clonogenic Assays

Single cells were seeded into 10 cm dishes at 3000 or 5000 cells/dish or at 1500 cells/well in six-well plates and incubated overnight at 37°C, 5% (GaMG: 10%) CO_2. The following day, triplicate dishes/wells were treated with their respective experimental conditions: IR, drug, or solvent control treatments (human IgG served as a control for BI-836845 as its solvent was not disclosed). Schedules of individual experiments where IR and drug treatments were used in combination are described in more detail in results chapters. Dishes/plates were incubated for 10-12 days (U87-MG, GaMG, LN-18), 8-10 days (SF-188), or 17-19 days (DK-MG, KNS42) until colonies of >50 cells had formed. Plates were washed with PBS and colonies fixed and stained with Coomassie stain (0.1% [w/v] brilliant

blue, 7% acetic acid, 50% methanol, dH_2O) for 25 min, then rinsed with water. Colonies were counted using a GelCount automated counter (Oxford Optronix).

2.11 3D Environment Matrigel Assays

This assay was adapted from the methods described by Lee *et al.* and Li and Lu (Lee et al., 2007; Li and Lu, 2011). The bottoms of wells of white-walled 96-well plates were coated in 40 µl of a 1:1 mixture of full medium and Matrigel (#354234, Corning) and incubated at 37°C for 30 min to solidify. Cells were lifted and seeded (500-2000 cells/well) into wells in medium containing 2% Matrigel for the '2% on-top assay', or medium containing 50% Matrigel for the 'embedded' assay (see Figure 3.16). Plates were incubated at 37°C with 5% or 10% (GaMG) CO_2 overnight, and experimental treatments were applied the following day. Drug treatments were added to wells in additional medium, typically at 5 x final concentration in one fifth of the final volume. Plates were incubated for 6-9 days to allow spheroidal colony growth. Plates were assayed with CellTiter-Glo® 3D Cell Viability Assay (#G9683, Promega).

2.12 Viability Assays

2.12.1 CellTiter-Blue® (Promega)

Cells were seeded into white-walled 96-well plates at 500-2000 cells/well and incubated at 37°C with 5% or 10% CO_2 overnight, and experimental treatments were applied the following day. Plates were incubated for 6-7 days, then assayed with the resazurin-based product CellTiter-Blue® (CTB) (#G8081, Promega) to ascertain viability levels. CTB was added to all experimental and blank (medium only) wells to 1/6 of the final volume. Plates were incubated at 37°C for 40 min and fluorescence was read on a POLARstar Omega plate reader spectrophotometer (BMG Labtech) at 10 min intervals up to 70 min ($560_{Ex}/590_{Em}$).

Values reported were based on blank-corrected raw values. All conditions were carried out in triplicates and where possible, quadruplicate.

2.12.2 CellTiter-Glo® 3D (Promega)

CellTiter-Glo® 3D Cell Viability Assay was used to assay cells that were grown in 3D environment Matrigel assays (section 2.11). After the desired incubation period, CellTiter-Glo® 3D was added to experimental and blank wells at an equal volume to the sample medium and the contents were mixed by shaking at 700 RPM in the POLARstar Omega plate reader spectrophotometer for 5 min. Plates were incubated in the dark at room temperature for 25 min before recording luminescence signal. Values reported were based on blank-corrected raw values.

2.13 siRNA Knockdown

2.13.1 siRNA Sequences

IGF1R (gene accession no. NM_000875) siRNAs were from Qiagen and Ambion and were reconstituted in RNase-free water to a stock of 20 μM and stored at -20°C as aliquots.

Qiagen siRNA sequences (5' → 3') were:

Sense: GGAGAAUAAUCCAGUCCUATT

Antisense: UAGGACUGGAUUAUUCUCCAT

Ambion siRNA sequences (5'→ 3') were:

Sense: GGAAUACAGGAAGUAUGGAtt

Antisense: UCCAUACUUCCUGUAUUCCtg

CD24 (gene accession no. NM_001291737.1) Stealth siRNA was from Invitrogen and was reconstituted in RNase-free water to a stock of 20 μM and stored at -20°C as aliquots. Sequences (5' → 3') were:

Sense: ACCCACGCAGAUUUAUUCCAGUGAA

Antisense: UUCACUGGAAUAAAUCUGCGUGGGU

For control transfections, Allstars Negative Control siRNA (#SI03650318, Qiagen) was used.

2.13.2 Transfection

For forward siRNA transfection, cells were seeded into 10 cm plates to achieve 30-40% confluence. The next day, cells were transfected with 50 nM of the relevant siRNA using Oligofectamine™ (OF) (#12252011, Invitrogen) in Opti-MEM® (OM) (#331985-047, Gibco). Per dish, 6.83 μl of thawed 20 μM siRNA stock was added to 1503 μl OM in one tube and incubated for 10 min. In a second tube, 12.3 μl OF was incubated with 410 μl OM for 10 min. The tubes were mixed and incubated for 25 min. Cells were washed twice with OM before 780 μl OM, followed by 1952 μl complexes were added to each dish. Dishes were then incubated for 4 hr at 37°C, 5% or 10% (GaMG) CO_2 before being topped up with 273 μl FBS and 11 ml full medium. Dishes were incubated for 24, 48, 72, or 96 hr before cells were harvested.

2.14 Flow Cytometry

2.14.1 Cell Cycle Analysis

At 48 hr and 96 hr post-transfection with *IGF1R*-targeted siRNA, cells were pulsed with 10 μM 5-bromo-2'-deoxyuridine (BrdU) (B5002, Sigma) for 30 min at 37°C. Cells were lifted with trypsin/EDTA, collected in the same medium (to harvest any dead cells),

and pelleted by centrifugation (220 x *g*, 5 min). Cells were resuspended in 100 µl PBS and fixed for >30 min in ice-cold excess 70% ethanol, added dropwise whilst vortexing. Fixed cells were stored at -20°C until use. Samples were centrifuged at 100 x *g* for 5 min, resuspended in 1 ml 2 M HCl containing 0.1 mg/ml pepsin (P6887, Sigma) and incubated at room temperature for 30 min. Cells were washed once with PBS, then once with 2% FBS/PBS. All washes involved centrifugation at 100 x *g* and removal of supernatant. Cells were resuspended in 100 µl 2% FBS/PBS containing 1 µl anti-BrdU monoclonal antibody (Appendix 7.1) (1:100 dilution) and incubated for 90 min at room temperature or overnight at 4°C. Cells were washed once with 1 ml 2% FBS/PBS, followed by resuspension in 100 µl 2% FBS/PBS containing 0.5 µl goat anti-mouse Alexa Fluor® 488 secondary antibody (1:200 dilution) and incubation for 1 hr at room temperature in darkness. Cells were washed with PBS, then resuspended in 400 µl PBS containing 5 µl 1 mg/ml propidium iodide stock (#P4864, Sigma). DNA content and BrdU uptake were analysed with a BD FACSCalibur. Results were analysed using the FlowJo Version 10 Data Analysis software.

2.14.2 CD24 Analysis

For analysis of expression of CD24 at the cell surface, cells were lifted in 3 mM EDTA in PBS to prevent any possible cleavage by trypsin. Cells were lifted, centrifuged at 220 x *g* for 5 min, and resuspended to give 10^6-10^7 cells in 95 µl PBS. Then 5 µl of R-phycoerythrin (RPE)-conjugated CD24 monoclonal antibody or IgG control were added to the tubes and incubated in darkness for 1 hr. Cells were washed once in PBS, centrifuged at 100 x *g* for 5 min, resuspended in 300 µl PBS, and RPE signal analysed with a BD FACSCalibur. Results were analysed with the FlowJo Version 10 Data Analysis software by Mick Woodcock.

2.15 Immunofluorescence

2.15.1 IGF-1R and Podoplanin

Sterile glass coverslips were placed into 6-well plates and 200,000 cells were seeded onto coverslips and incubated at 37°C overnight. Cells were fixed in 4% paraformaldehyde with 0.1% Triton-X100 in PBS for 20 min. Additional permeabilisation was performed with 0.5% Triton-X100 in PBS for 3 min. Solutions were aspirated and coverslips were washed in PBS. Blocking was performed with 5% BSA in PBS for 1 hr at room temperature. Coverslips were incubated with primary antibody in blocking solution (1:200 dilution) (IGF-1Rβ: #3027, Cell Signaling Technology; Podoplanin: #ab10288, Abcam) for 1 hr at room temperature or overnight at 4°C (in humidified 6-well plates). Coverslips were washed three times for 5 min in PBS and Alexa Fluor® 488 secondary antibody (donkey anti-rabbit [#A-21206, ThermoFisher Scientific] or goat anti-mouse [#A-11029, ThermoFisher Scientific]) in blocking solution (1:2000 dilution) was added to slides and incubated in darkness for 1 hr at room temperature. Antibody was removed and cells were washed three times for 5 min in PBS before mounting coverslips onto microscope slides with Mountant PermaFluor mounting medium (ThermoFisher Scientific) containing 2 μg/ml 4',6-diamidino-2-phenylindole (DAPI). Cells were visualised with a Nikon Eclipse 90i fluorescence microscope.

2.15.2 γH2A.X

For γH2A.X staining, cells were seeded onto coverslips at 50,000 cells/coverslip, and were fixed at specific time points post seeding and experimental treatment. Medium was removed from wells, and coverslips were washed for 1 min with PBS. Cells were fixed for 12 min with 4% paraformaldehyde in darkness, washed with PBS, then permeabilised for 5

min in permeabilisation solution (200 µl FBS, 25 µl Triton X-100 [20%], 4.8 ml PBS). Coverslips were washed in PBS then blocked with 10% BSA in PBS for 45 min. Coverslips were washed in PBS, then incubated with primary mouse monoclonal anti-γH2A.X antibody (#05-636, Millipore) (1:500 dilution) for 1 hr at room temperature in 1% BSA in PBS. Coverslips were washed in PBS, then incubated for 1 hr at room temperature with goat anti-mouse Alexa Fluor® 488 secondary antibody in 1% BSA in PBS in darkness. Coverslips were washed and mounted as above. Cells were visualised with a Zeiss LSM 710 Observer Z1 confocal microscope.

2.16 RNA Extraction

Cell pellets were made, snap frozen, and stored as described above (section 2.7.2). RNA was extracted from cells using the PureLink® RNA Mini Kit (#12183018A, Ambion). Briefly, pellets were resuspended in 600 µl lysis buffer containing 1% 2-mercaptoethanol and lysates homogenised through a syringe and 18 G needle. An equal volume of 70% ethanol was added to homogenates and the mixture was filtered through spin cartridges by spinning at 12,000 x *g* to bind RNA to the cartridge membranes. Wash buffers I and II were centrifuged through the cartridges, between which, 30 units of DNase in DNase I reaction buffer (PureLink® DNase set, #12185010, Invitrogen) were added to the membranes for a 15 min incubation at room temperature. After discarding excess flow-through wash buffer, 30 µl RNase-free water was added to spin cartridges and centrifuged at 12,000 x *g* for 2 min to elute the RNA. RNA quality (260/230 and 260/280 absorbance ratios) and concentration (ng/µl) was tested by a NanoDrop spectrophotometer. RNA samples were stored at -80°C.

2.17 Gene Expression Microarray

Cell pellets for gene expression analysis were prepared from 75 cm flasks (section 2.7.2) at various time-points post-treatment, and RNA was extracted as described above (section 2.16). For the design of the microarray experiment, see Figure 5.9. Microarray gene expression analysis was performed by the Oxford Genomics Centre High-Throughput Genomics Service (Wellcome Trust Centre for Human Genetics, University of Oxford, UK) using the Human HT12v4.0 Illumina array platform. For sample processing, >500 ng RNA/sample were required in 12 μl RNase-free water, plated in 96-well 0.2 μl skirted PCR plates sealed with adhesive seals. For quality control checks, 100-500 ng RNA/sample were submitted in 5 μl RNase-free water in separate plates. Expression data were transferred electronically and analysis was performed by Anastasia Samsonova (Bioinformatics Core Leader, Department of Oncology, University of Oxford, UK). Lists of differentially expressed genes in multiple sample comparisons were generated with the following outputs:

Genelist	One or more columns of probe annotation
logFC	log2-fold-change corresponding to the effect or contrast
AveExpr	Average log2-expression for the probe over all arrays and channels
t	Moderated t-statistic
P. Value	Raw p-value
Adj. P. Value	Adjusted p-value or q-value
B	Log odds that the gene is differentially expressed

Differentially expressed genes in individual comparisons were ranked by B values or adjusted P Values. Log2 transformed normalised expression values for each replicate were also generated. Volcano plots were generated for individual comparisons to display

differentially expressed genes with cut off values of ±1 for log2 fold change, and <0.01 for adjusted p-value.

2.18 Reverse Transcription

RNA conversion to complementary DNA (cDNA) was performed using the SuperScript® III First-Strand Synthesis SuperMix for qRT-PCR component kit (#11752050, Invitrogen). Per RNA sample, 1 μg RNA in RNase-free water was added to 10 μl 2X RT Reaction Mix and 2 μl RT Enzyme Mix, and made up to 20 μl with RNase free water in PCR tubes. Reaction mixtures were placed in a PCR thermal cycler and incubated at 25°C for 10 min, 50°C for 30 min, and reactions were terminated at 85°C for 5 min, before chilling on ice. Then 1 μl (2U) of *Escherichia coli* RNase H was added and incubated at 37°C for 20 min. cDNA concentrations were measured by NanoDrop. Storage was at -20°C.

2.19 Real Time quantitative Polymerase Chain Reaction (qRT-PCR)

2.19.1 Primer Sequences

Primers were designed using the web-based tool National Centre for Biotechnology Information (NCBI) Primer BLAST (Basic Local Alignment Search Tool). NCBI consensus coding sequences for each target were used for the design of primer pairs. Primers were reconstituted in RNase-free water to a concentration of 100 μM and pairs of primers were mixed 1:8 with water (50 μl of each primer in a pair, 300 μl water) to give 12.5 μM of each primer. Primer sequences were as follows:

CD24

Consensus CDS: CCDS75499.1

Pair 1

Forward: GCTCCTACCCACGCAGATTT

Reverse: GAGACCACGAAGAGACTGGC

Pair 5

Forward: GCTCCTACCCACGCAGATTTA

Reverse: GCCTTGGTGGTGGCATTAGT

SGK1

Consensus CDS: CCDS5170.1

Pair 2

Forward: GCCTGCCGCCTTTTTATAGC

Reverse: CCGCTTTGTCCTGTCCTTCT

Pair 3

Forward: TATGGCCTGCCGCCTTTTTA

Reverse: CAGGAGGTGTCTTGCGGAAT

IGFBP3

Consensus CDS: CCDS34632.1

Pair 2

Forward: CTGATCCCAAGTTCCACCCC

Reverse: CAACTTTGTAGCGCTGGCTG

Pair 3

Forward: AGAAAAAGCAGTGTCGCCCT

Reverse: TCCTTCCCCTTGGTGGTGTA

PDPN

Consensus CDS: CCDS30602.1

Pair 3

Forward: CCACGGAGAAAGTGGATGGA

Reverse: TAGGGCGAGTACCTTCCCG

Pair 7

Forward: GGGGTCTTACTAGCCATCGG

Reverse: TAGGGCGAGTACCTTCCCG

TUBA6 was used as the housekeeping reference gene to normalise differences in mRNA expression resulting from differences in loading.

Tubulin alpha 6 (TUBA6)

Forward: CCCCTTCAAGTTCTAGTCATGC

Reverse: ATTGCCAATCTGGACACCA

2.19.2 qRT-PCR Cycles for Relative Gene Expression Comparison

For each PCR reaction, cDNA (500-600 ng in 1 µl) was mixed with 8 µl RNase-free water, 10 µl SYBR Green PCR Master Mix (#4309155, ThermoFisher Scientific), and 1 µl reconstituted primer pairs (12.5 µM/primer), totalling 20 µl in skirted PCR plates. Plates were sealed with adhesive seals and centrifuged at 1700 x *g* for 1 min. PCR cycles were run on a 7500 Fast Real-Time PCR system (Applied Biosystems®) at Standard speed. Conditions were: 10 min hold at 95°C, then 40 cycles of 15 seconds at 95°C, 1 min at 60°C. Each reaction condition was performed in triplicate. A negative control containing RNase-free water without cDNA template was used for each primer pair. Quantification of

expression of target mRNAs relative to *TUBA6* was performed using the $2^{-\Delta CT}$ method (Livak and Schmittgen, 2001):

$\Delta C_T = C_T$ (target) – C_T (*TUBA6*)

where C_T = cycle threshold (no. of cycles required for fluorescent signal to cross threshold).

2.20 Chemotaxis Transwell® Assay

Prior to seeding, cells were starved in serum-free medium for 24 hr. Cells were lifted in 3 mM EDTA and seeded in serum-free medium at 5,000 or 10,000 cells/well of inserts in HTS Transwell®-96 Permeable Support plates with 8.0 μm pore polyester membranes (#3384, Corning). Serum-free medium or medium with 10% FBS was added to receiver wells. Plates were incubated at 37°C, 10% CO_2 for 24 hr. CTB (1/6 total volume) was combined with 10x Cell Dissociation Solution (CDS) (#3455-096-05, Trevigen) and dH_2O to give 1x CDS. Medium was removed from inserts and receiver wells and both were washed twice with PBS. Inserts were placed back into receiver wells containing 100 μl CTB/1x CDS and incubated for 30 min at 37°C, 10% CO_2. Inserts were removed and fluorescence was measured at 10 min intervals as in section 2.12.1.

2.21 Statistical Analyses

Kaplan-Meier survival curves were analysed with the Gehan-Breslow-Wilcoxon test and the Log-rank (Mantel-Cox) test for statistically significant differences between survival distributions. The Student's *t*-test was used to analyse differences between two groups, and a Holm-Šidák correction was used where multiple *t*-tests were applied. A one-way ANOVA was used to test for significance between more than two groups with one independent variable, and a two-way ANOVA was used for more than two groups with more than one

independent variable. Graphs were constructed and statistical analyses conducted using the GraphPad Prism 6.0 software.

3 Chapter III: Investigation of the expression and role of IGF-1R in GBM

3.1 Introduction

An IHC staining procedure for IGF-1R protein expression in clinical tissue samples has been optimised previously in our lab (Aleksic et al., 2010; Aleksic et al., 2016). The availability of adult and paediatric brain tumour tissue TMAs allowed for the opportunity to study IGF-1R expression in brain tumours using the aforementioned established protocol. Publicly accessible genomic data from GBM patients allowed for additional assessment of IGF-1R expression in GBM tissue and correlation of IGF-1R expression with common gene mutation statuses (Brennan et al., 2013; Cerami et al., 2012). The availability of two drugs that can inhibit IGF-1R phosphorylation, BMS-754807 and BI-836845, allowed for the study of the effects of IGF-1R inhibition on the growth characteristics of cultured GBM cells *in vitro*. Given previous evidence that IGF-1R may be an important target in GBM (Section 1.6), it was hypothesised that IGF-1R inhibition may sensitise GBM cells to TMZ and IR treatments used in GBM. Using a panel of adult and paediatric GBM cell lines, activation of components of the IGF axis was assessed and the effects of IGF-1R inhibition on GBM cells, alone and in combination with TMZ or IR, were investigated.

3.2 Results

3.2.1 IGF-1R expression in GBM

Previous bioinformatics analyses across 12 types of cancer for significantly mutated genes revealed *TP53*, *PTEN*, and *EGFR* as the top three most commonly mutated genes in GBM (Kandoth et al., 2013). TCGA-contained publicly available data from a GBM genomic study also reports these three genes as the most commonly mutated (Brennan et al., 2013). In light of this, these proteins were queried using cBioPortal to investigate any IGF-1R protein enrichments in the event of their mutation, deletion, up- or down-regulation. In patient samples for which reverse phase protein array (RPPA) data were available, 21% of samples had alterations (including homozygous deletion, mutation [missense, truncating, in-frame], RPPA upregulation, RPPA downregulation) in *PTEN*. Comparing altered *PTEN* against unaltered *PTEN* samples, protein enrichment analysis revealed IGF-1R to be the most statistically significantly altered protein, with samples where *PTEN* was unaltered containing higher levels of IGF-1R (Table 3.1; Figure 3.1A). Queries with *TP53* and *EGFR* revealed IGF-1R levels to be statistically significantly different when these genes were altered (*EGFR* altered > *EGFR* unaltered; *TP53* altered < *TP53* unaltered), but these were not as significant as the differences in total IGF-1R when *PTEN* was altered (Figure 3.1B, C). When mutations alone were queried, no statistically significant differences were seen in IGF-1R when comparing mutated *EGFR* and *TP53* samples with non-mutated samples, but IGF-1R was again the most statistically significantly altered protein when *PTEN* was mutated (*PTEN* mutated < *PTEN* non-mutated) (Table 3.2, Figure 3.1D). Importantly, a wide spread of IGF-1R expression was evident, demonstrating that IGF-1R is present in patients' GBM tissue at varying levels.

Table 3.1: Top 10 most significantly altered proteins when *PTEN* is altered. PTEN was altered in 21% of 580 samples with RPPA data. Alterations include homozygous deletion, mutation (missense, truncating, in-frame), RPPA upregulation, RPPA downregulation.

Target	Average abundance (z-scores)		P-Value	Up/down-regulation
Protein	**Unaltered**	**Altered**		
IGF1R	-0.65	-0.97	6.94e-7	↓
PIK3CA	-0.75	-0.90	4.21e-3	↓
PRKCA	0.41	0.07	4.74e-3	↓
MTOR	1.34	1.07	5.41e-3	↓
ERRFI1	-0.82	-0.70	6.19e-3	↑
AKT3	1.93	1.64	6.28e-3	↓
PEA15	0.98	0.69	7.45e-3	↓
PTEN	1.28	1.07	7.49e-3	↓
MAPK1	2.23	1.94	1.15e-2	↓
BIRC2	0.61	0.49	1.18e-2	↓

Table 3.2: Top 10 most significantly altered proteins when *PTEN* is mutated. 12% of 580 samples.

Target	Average abundance (z-scores)		P-Value	Up/down-regulation
Protein	**Unaltered**	**Altered**		
IGF1R	-0.70	-1.00	1.63e-4	↓
CDKN1B	-1.49	-1.75	3.21e-4	↓
FOXO3	-4.00	-4.15	6.24e-4	↓
RB1	-2.42	-2.53	3.63e-3	↓
BCL2L1	-1.91	-2.03	7.37e-3	↓
BID	-2.75	-2.83	8.15e-3	↓
MSH2	-3.17	-3.33	9.68e-3	↓
SMAD3	-1.15	-1.24	1.10e-2	↓
BAK1	-2.68	-2.77	1.10e-2	↓
CDH1	-1.72	-1.87	1.72e-2	↓

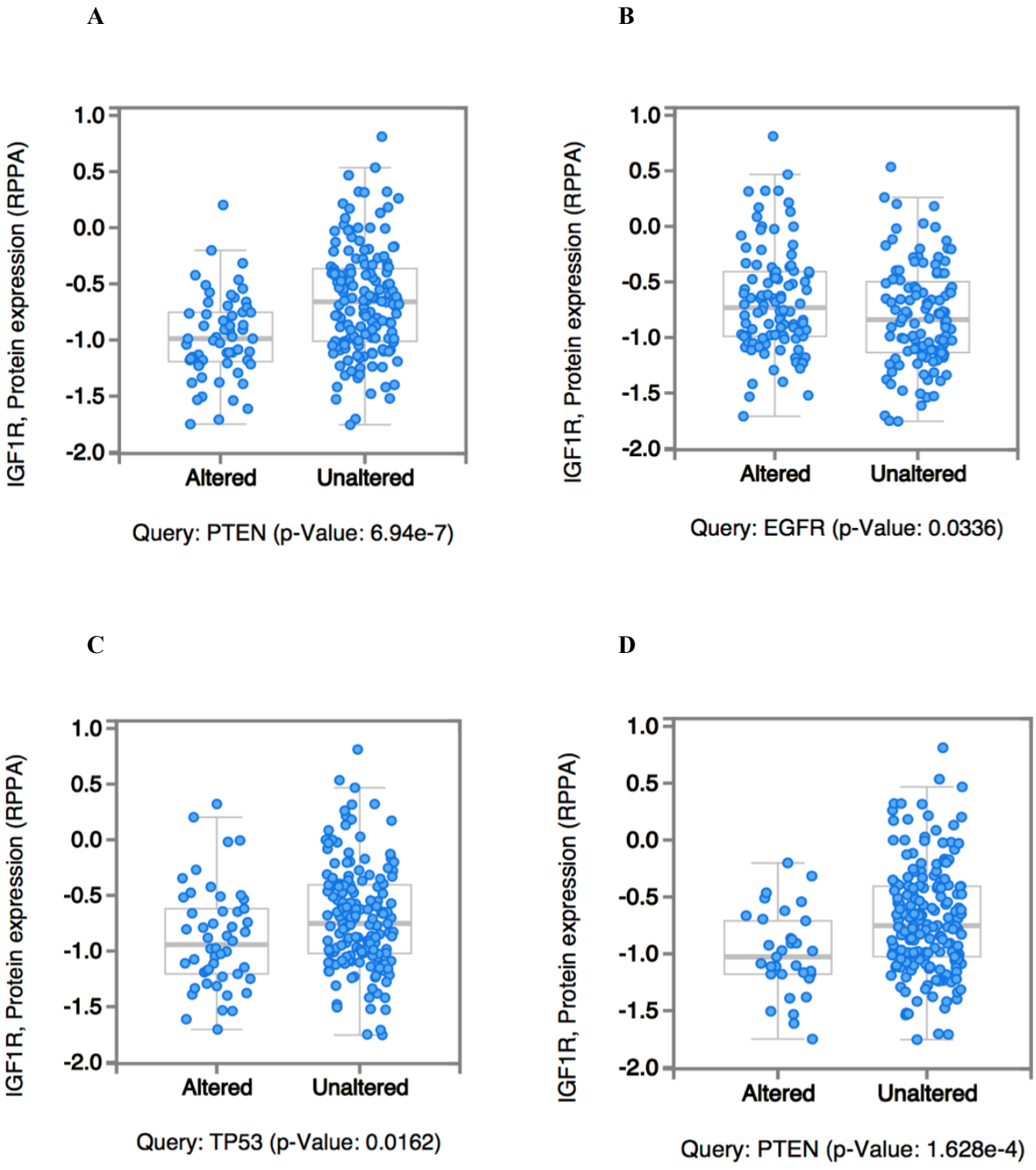


Figure 3.1: Relative expressions of IGF-1R in GBM samples where query genes are altered or unaltered. The top three most mutated genes in GBM were queried in cBioPortal to assess for statistically significant ($P < 0.05$) differences in IGF-1R protein levels when genes were altered vs unaltered. A) Comparison of IGF-1R levels when *PTEN* was altered vs unaltered. B) Comparison of IGF-1R levels when *EGFR* was altered vs unaltered. C) Comparison of IGF-1R levels when *TP53* was altered vs unaltered. D) Comparison of IGF-1R levels when *PTEN* was mutated vs not mutated. Graphs were generated through cBioPortal, which uses the Student's *t* test to derive p-values.

To assess directly the distribution of levels of expression of IGF-1R in human brain tumour tissue, and investigate associations with clinical parameters, adult and paediatric brain tumour samples (grade III and IV) were stained by IHC for IGF-1Rβ as in Aleksic *et al.* (2016). To do this, MCF-7 breast cancer cells, which highly express IGF-1R (Mukohara et al., 2009), with a high proportion localised at the membrane (Hartog et al., 2012), were used as a positive control for IGF-1Rβ staining. SKUT-1 human leiomyosarcoma cells, which have low expression of IGF-1R (Aleksic et al., 2016; Riedemann et al., 2007) were used as a second control, while staining of MCF-7 cells with no primary antibody was used for a secondary antibody control. MCF-7 cells displayed a high level of high intensity staining at the membrane, whereas SKUT-1 cells showed staining at a much lower intensity, and no staining was seen in the negative secondary antibody control (Figure 3.2).

A total of 305 adult and 103 paediatric brain tumour cores were stained for IGF-1Rβ, in addition to samples of normal brain. Samples were scored based on the intensity of staining for IGF-1Rβ using a seven-point scale (Figure 3.3). Total intensity alone was scored rather than scoring membrane, cytoplasmic and nuclear IGF-1R separately, as done previously in our group (Aleksic et al., 2010), due to the difficulty of distinguishing between membranes and cytoplasm in GBM histopathology (Dr. O. Ansorge, personal communication). There was a distinct difference in intensity of staining between normal brain tissue and tumour tissue (Figures 3.4 and 3.5), demonstrating clear upregulation of IGF-1R in tumour tissue relative to normal brain. Both adult and paediatric samples showed a wide range of staining intensity, covering all scores in the intensity scale (Figures 3.5 and 3.6 respectively), which was consistent with the wide range of IGF-1R expression values extracted from TCGA. However, normal brain samples were consistently negative. Of note, no nuclear IGF-1Rβ staining that has been observed in other tumour types (Aleksic et al., 2010) was observed here.

Comparing adult and paediatric samples, a higher proportion of paediatric samples than adult samples showed high scores for IGF-1Rβ IHC staining intensity, whereas the reverse was true for adult samples; a higher proportion of adult samples than paediatric samples had low scores for IGF-1Rβ IHC staining intensity (Figure 3.7A). Grouping raw scores into staining categories showed that adult samples had higher percentages of negative and weak staining, whereas paediatric samples had higher percentages of medium and strong staining (Figure 3.7B). This suggests that paediatric brain tumours are more likely to express IGF-1R and at a higher level than adult brain tumours.

IGF-1Rβ IHC intensity scores were next analysed with associated clinical data to assess for any associations between staining intensity and survival/prognosis. When patient samples were split into groups of IGF-1R positive tumours and IGF-1R negative tumours, no significant differences in survival distributions were seen for adult patients (Figure 3.8A). Median survivals were 253 days for IGF-1R negative patients, and 336 days for IGF-1R positive patients. Conversely, for paediatric patients, those with IGF-1R negative tumours showed a statistically significant improved survival relative to those with IGF-1R positive tumours (Figure 3.8B, Table 3.3), with median survivals at 30.7 months and 14.0 months respectively. In addition, further sorting of patients into negative/weak and medium-strong IGF-1Rβ IHC staining groups showed no difference in adult survival distributions (median survivals [days] were 312 [neg./weak], and 301 [medium-strong]) (Figure 3.9A), but again showed an improved survival for paediatric patients with lower intensity IGF-1Rβ IHC staining (Figure 3.9B) with greater statistical significance than the first grouping (Table 3.3). These analyses suggest that the expression of IGF-1R in paediatric patients, but not adult patients, may be associated with a worse survival, and that the level of IGF-1R expression may be an important factor for predicting patient outcome, with a higher expression possibly contributing to a poorer prognosis.

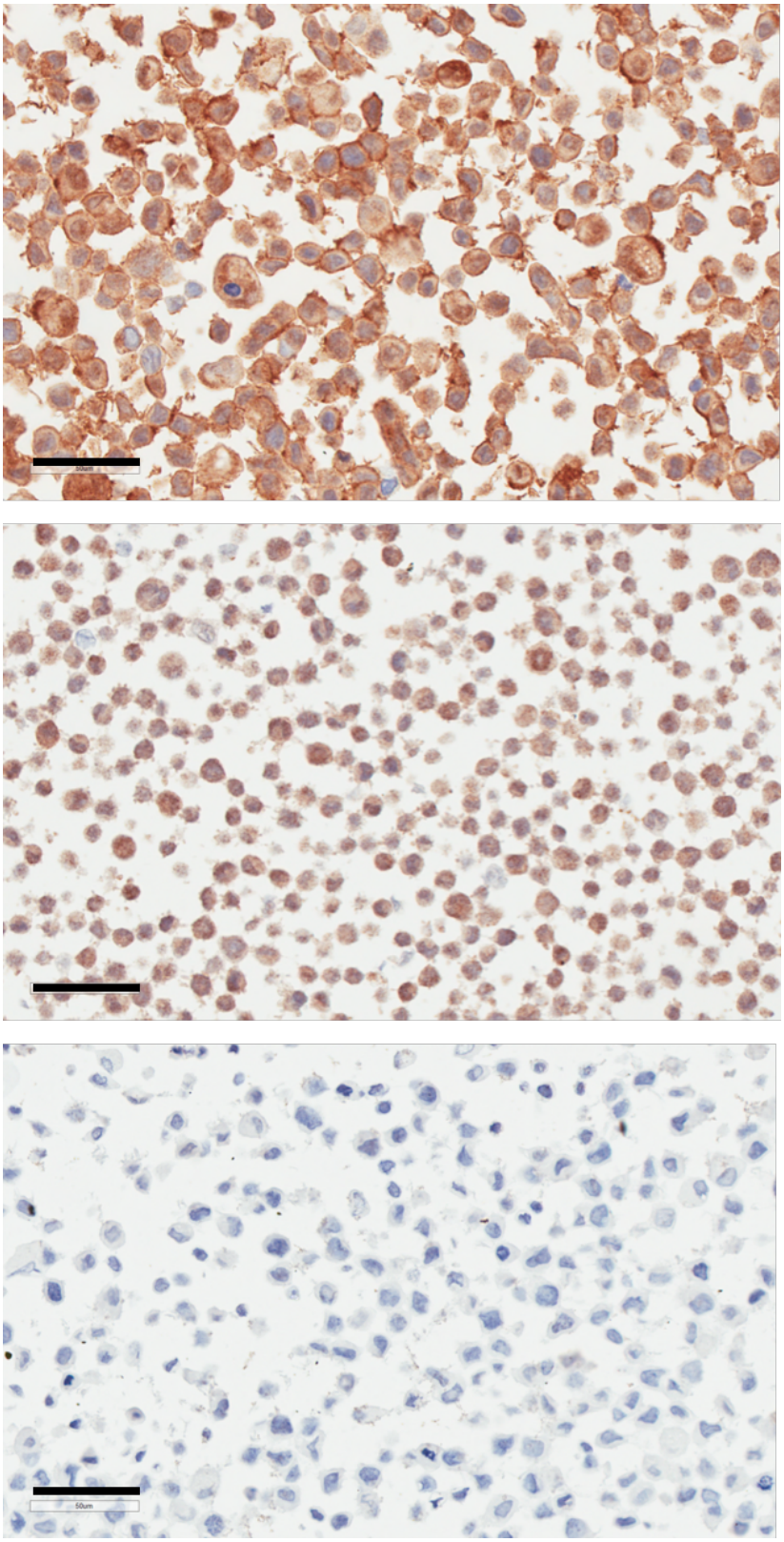


Figure 3.2: Positive and negative controls for IGF-1Rβ IHC staining. Staining of MCF-7 cells (top panel), SKUT-1 cells (middle panel), and MCF-7 cells incubated with no primary antibody (lower panel) was performed using an IGF-1Rβ monoclonal antibody (#9750, Cell Signaling Technology). Scale bars represent 50 μm. Original magnification x20.

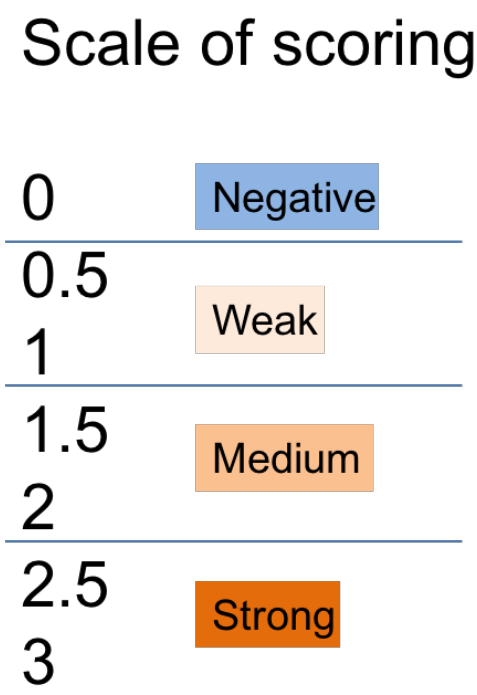


Figure 3.3: Schematic of scale used to score intensity of IGF-1R IHC staining.

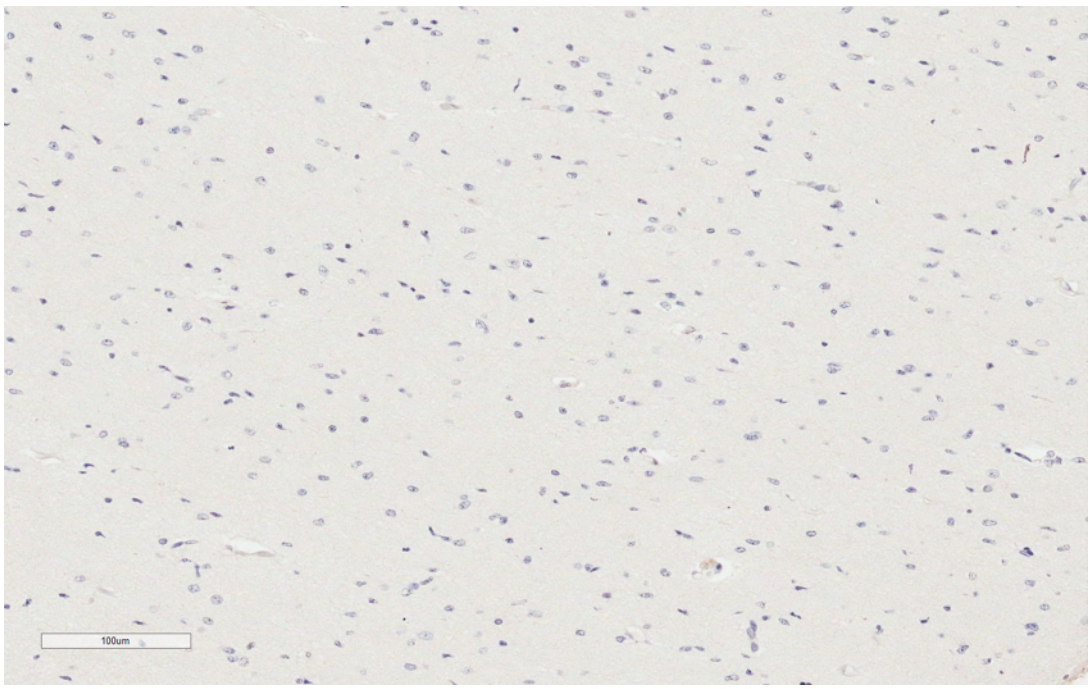
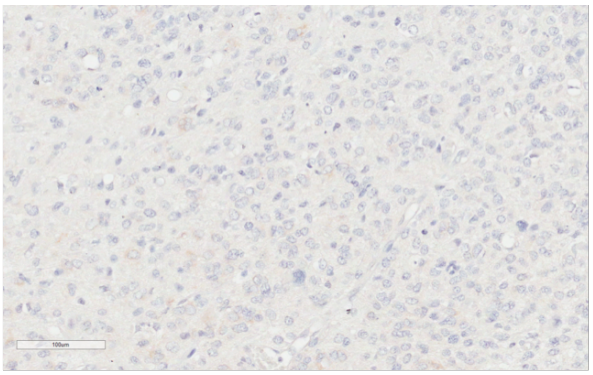
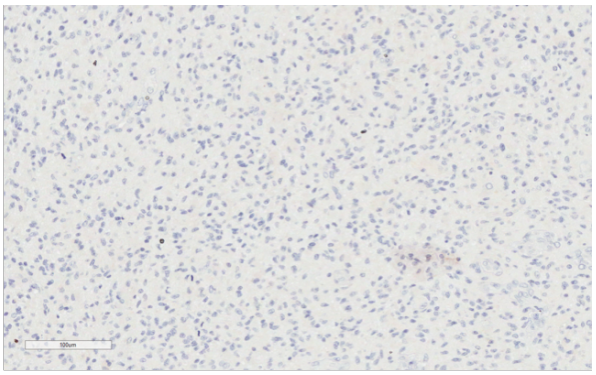


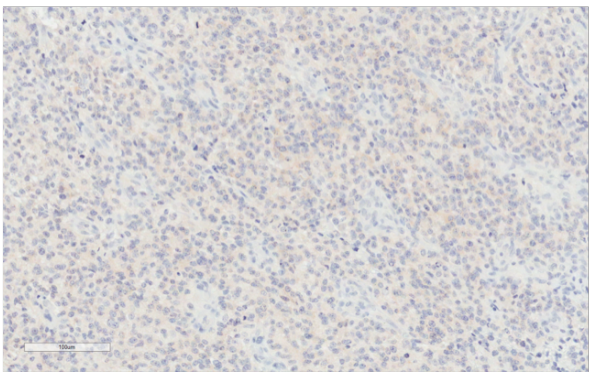
Figure 3.4: IGF-1R IHC staining of a normal brain sample. Normal brain samples were stained with IGF-1Rβ monoclonal antibody (#9750, Cell signaling Technology) as part of the brain tumour TMAs. Scale bar represents 100 μm. Original magnification x10.

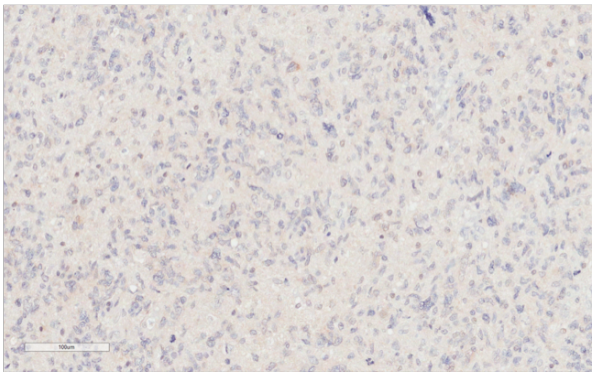
0



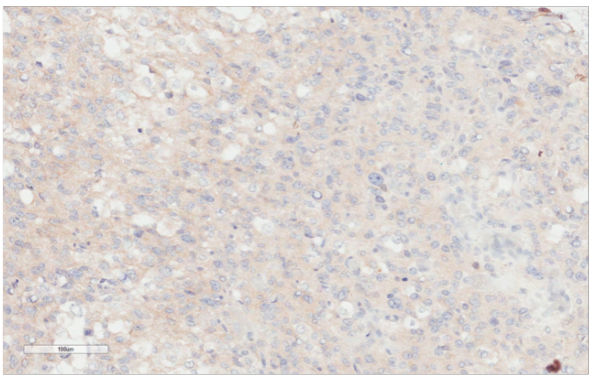


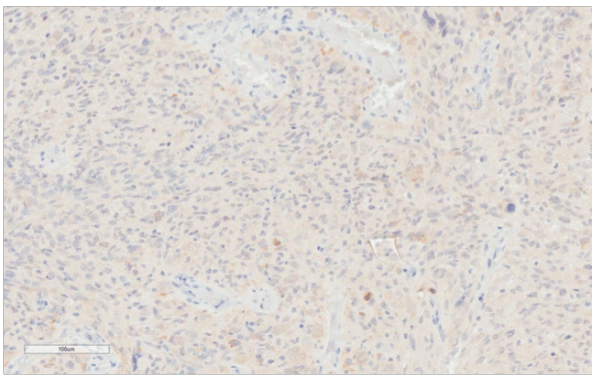
0.5



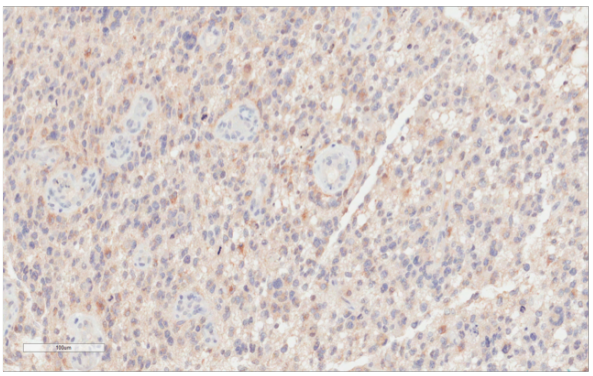


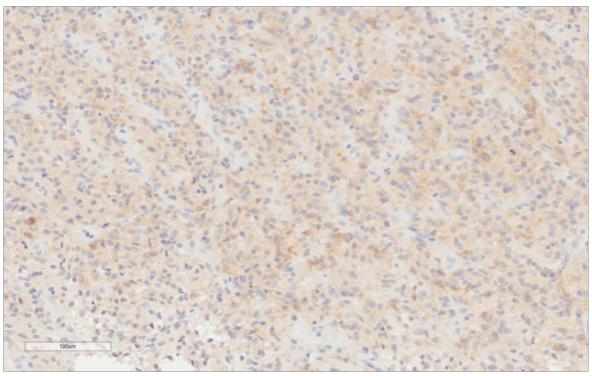
1



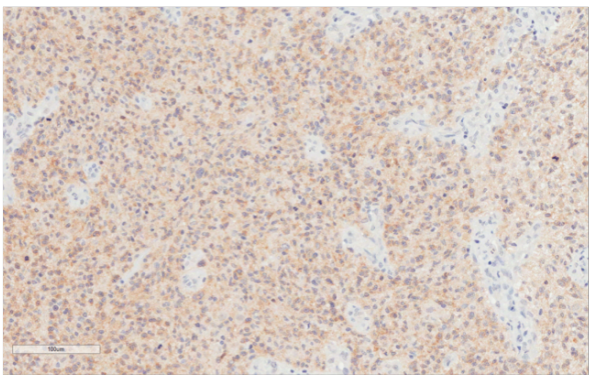


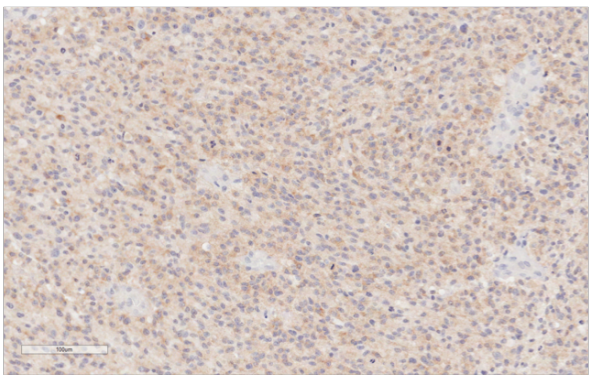
1.5





2





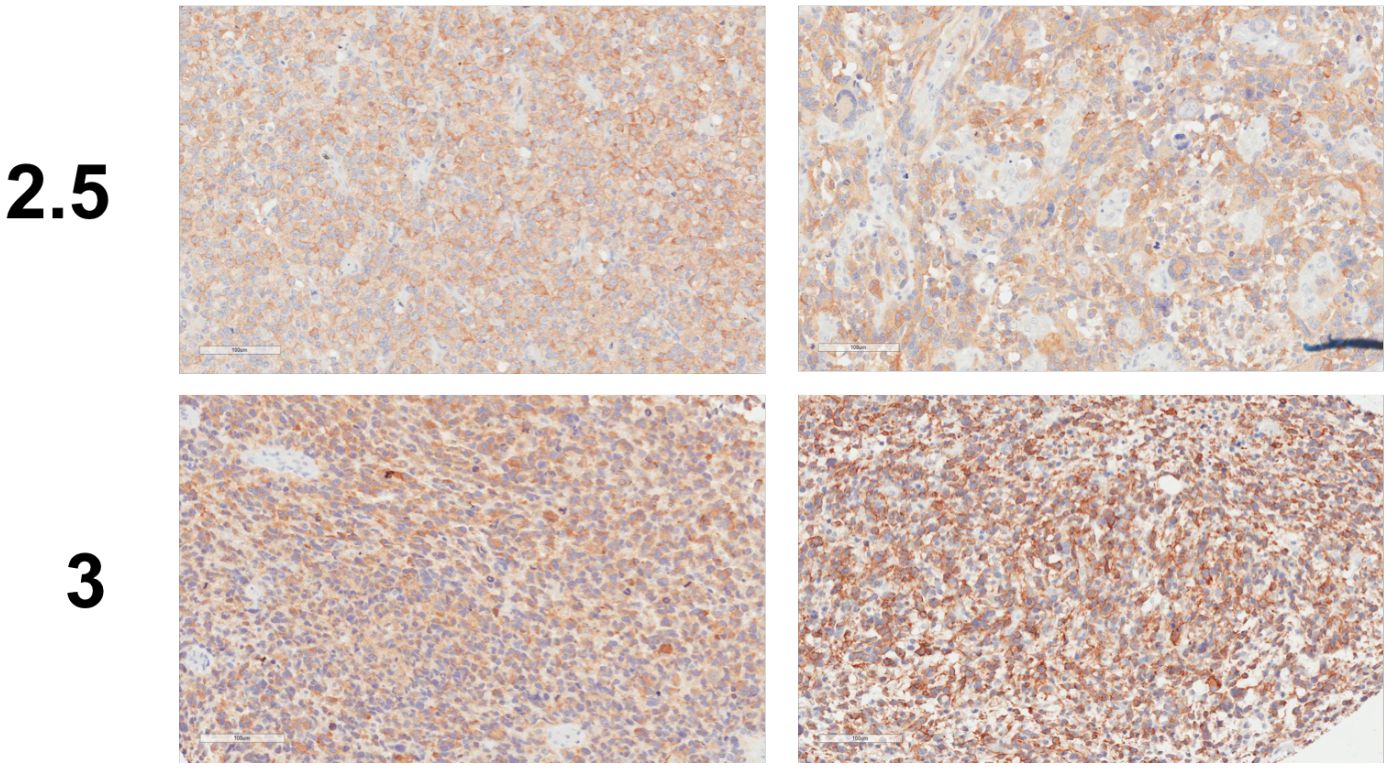
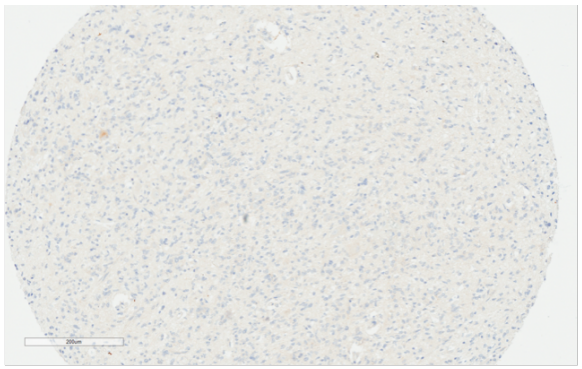
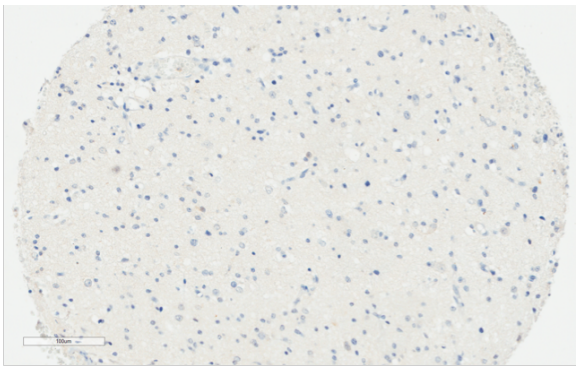


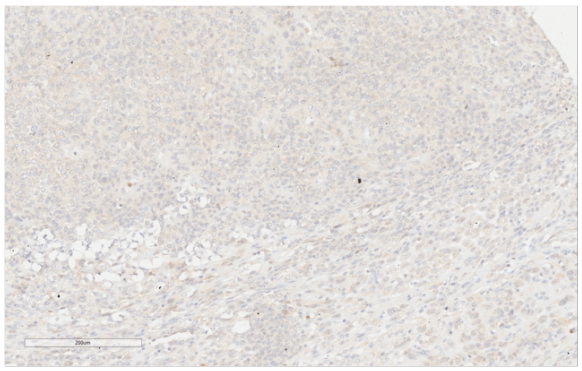
Figure 3.5: IGF-1R IHC staining of adult brain tumour tissue microarrays. TMAs were stained with IGF-1Rβ monoclonal antibody (#9750, Cell Signaling Technology) and scored for intensity of staining (left of images). Two samples of each intensity score are presented where a score of 0 represents negative staining. Scale bars represent 100 μm. Original magnification x10.

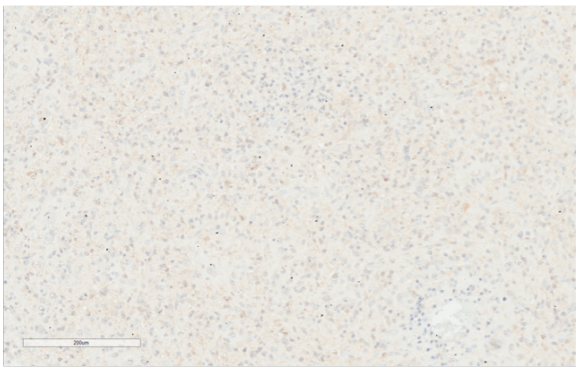
0



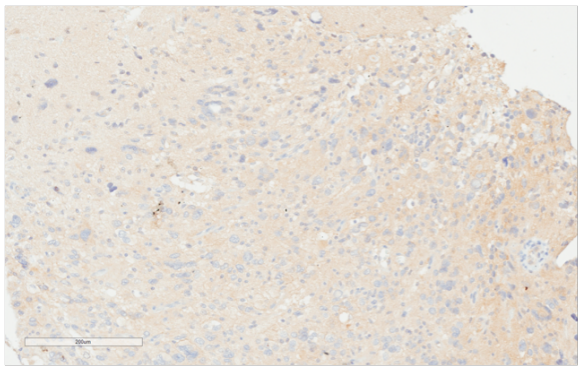


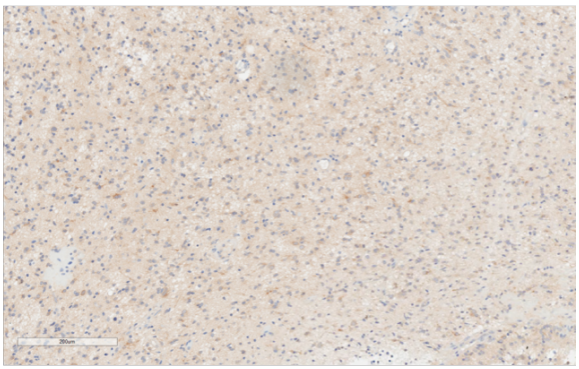
0.5



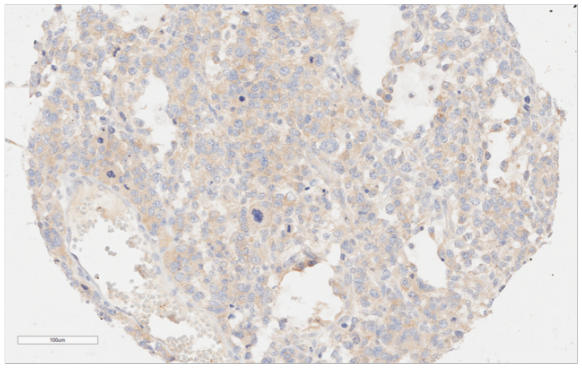


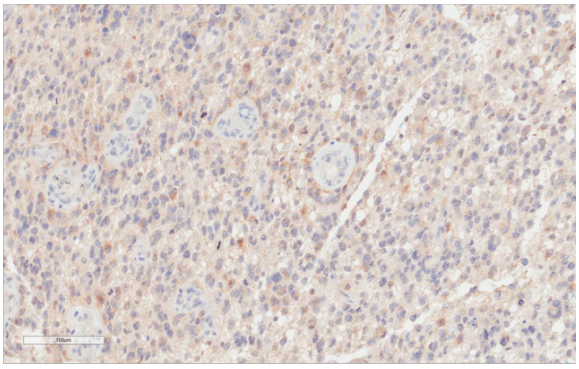
1



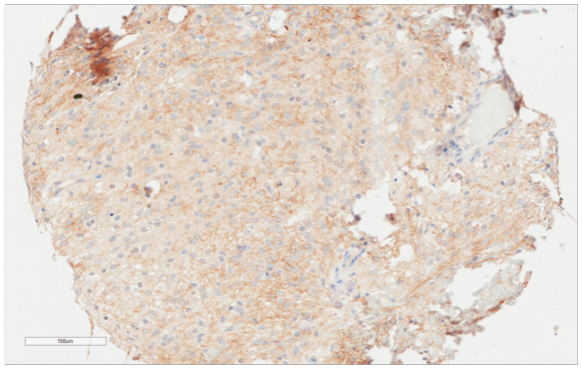


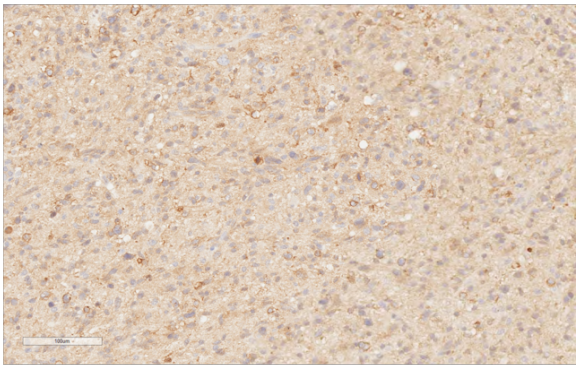
1.5



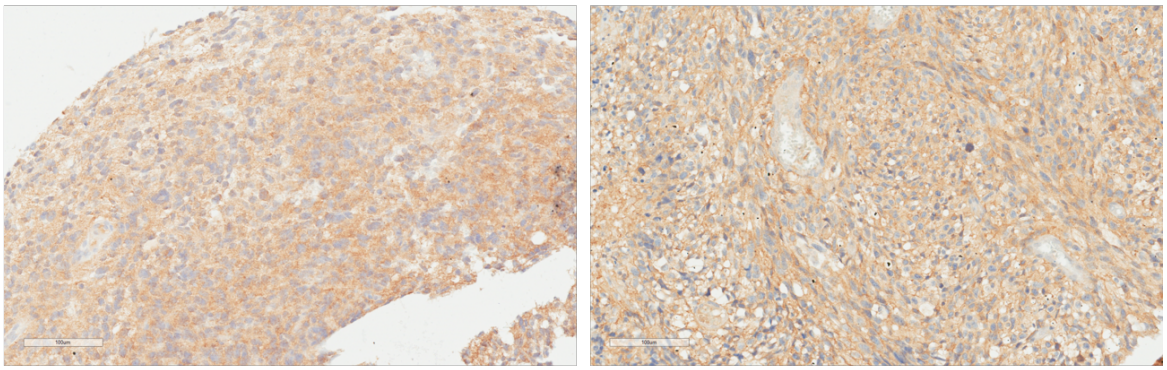


2





2.5



3

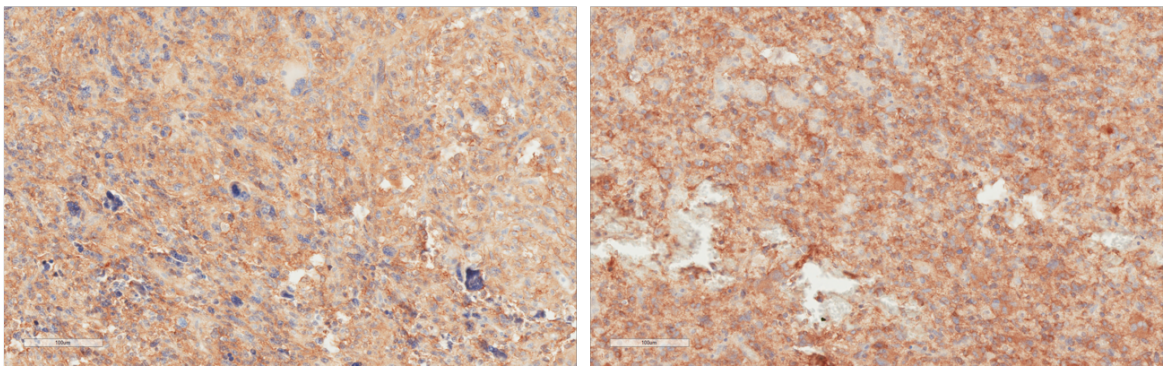
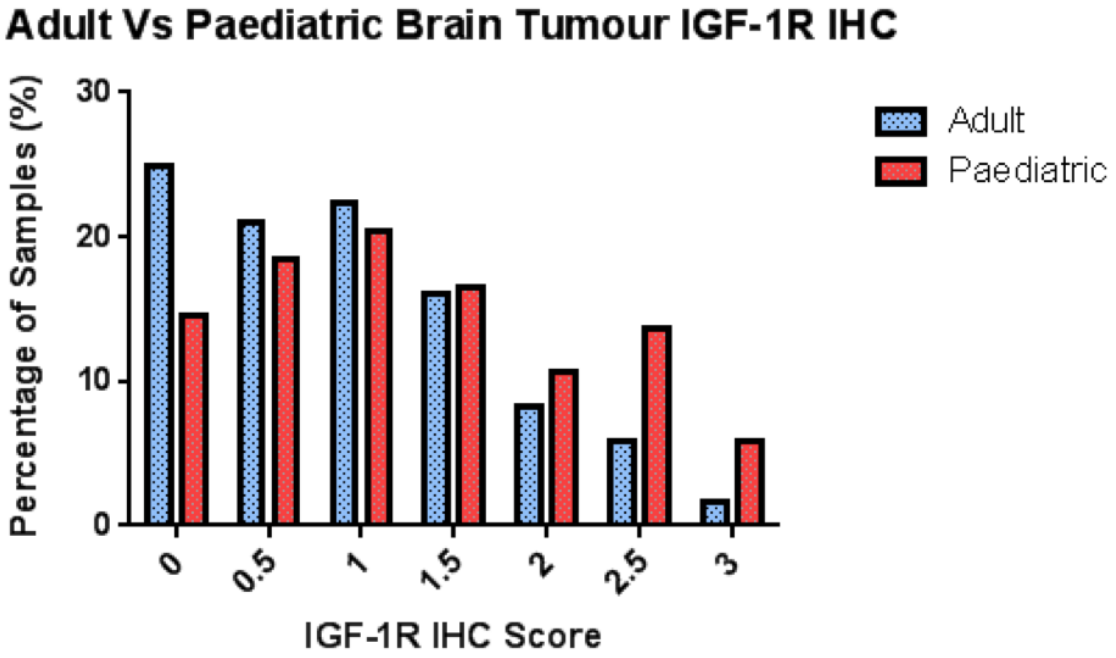


Figure 3.6: IGF-1R IHC staining of paediatric brain tumour tissue microarrays. TMAs were stained with IGF-1Rβ monoclonal antibody (#9750, Cell signaling Technology) and scored for intensity of staining. Staining was performed at a different time to the staining of the adult TMAs. Two samples of each intensity score are presented where a score of 0 represents negative staining. Scale bars represent 200 μm for scores 0.5-1 and left panel of score 0, and 100 μm for scores 1.5-3 and right panel of score 0. Original magnification x10.

A



B

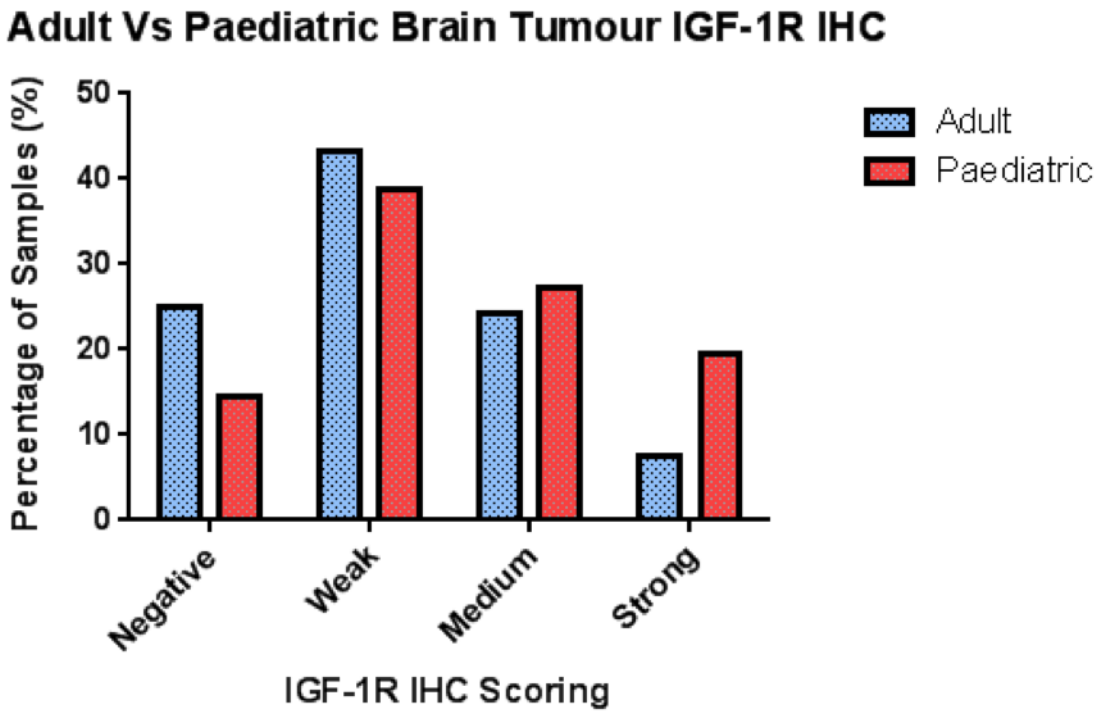
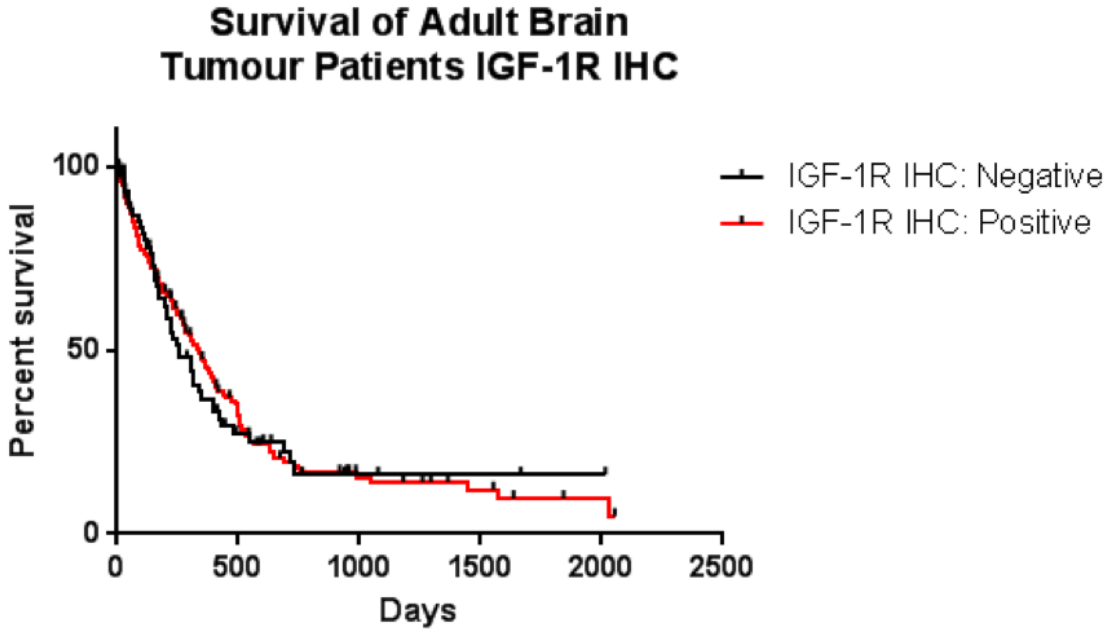


Figure 3.7: Comparison of adult and paediatric IGF-1R IHC staining scores. A) Percentages of adult and paediatric brain tumour samples scored at each level of the staining intensity scale. B) Comparison of adult and paediatric distribution of scores within the scoring categories assigned to raw score values. Negative: Score 0; Weak: Score 0.5-1; Medium: Score 1.5-2; Strong: Score 2.5-3. A total of 305 adult cases and 103 paediatric cases were present, stained, and scored.

A



B

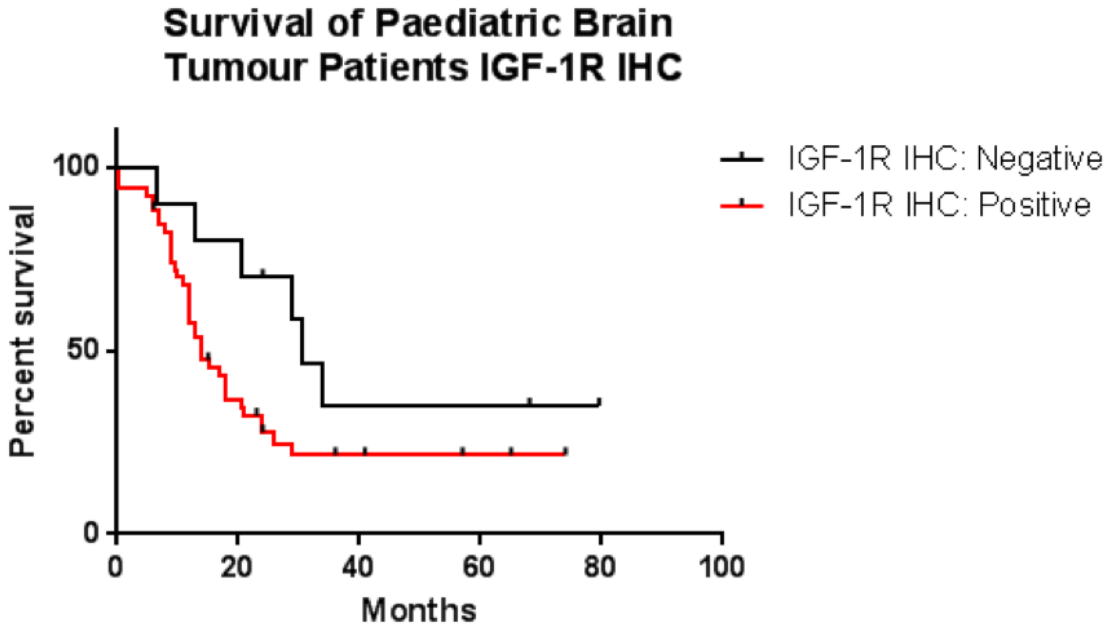
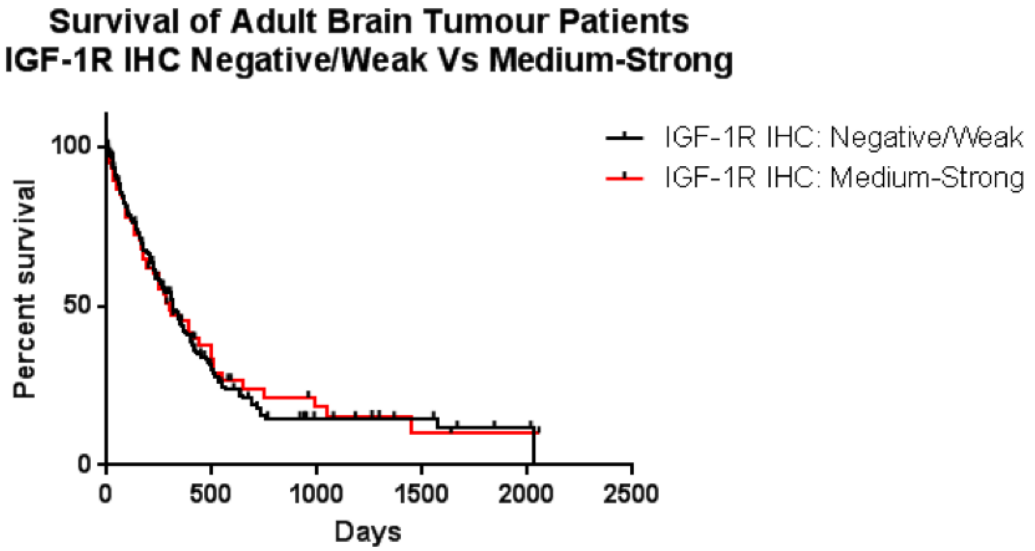


Figure 3.8: Kaplan-Meier Survival Curves for adult and paediatric brain tumour patients by absence or presence of IGF-1R. A) Survival of adult brain tumour patients (in days) grouped by IGF-1R negative tissue (score 0) and IGF-1R positive tissue (score 0.5-3). Of the 305 adult samples stained and scored, 260 samples had sufficient associated clinical data for incorporation into survival analysis. Median survival (days) was 253 : 336 (IGF-1R Negative : IGF-1R Positive). B) Survival of paediatric brain tumour patients (in months) grouped as in A. Of the 103 paediatric samples stained and scored, 62 samples had sufficient associated clinical data for incorporation into survival analysis. Median survival (months) was 30.7 : 14 (IGF-1R Negative : IGF-1R Positive). The remaining samples were either missing survival time, or survival information or both.

A



B

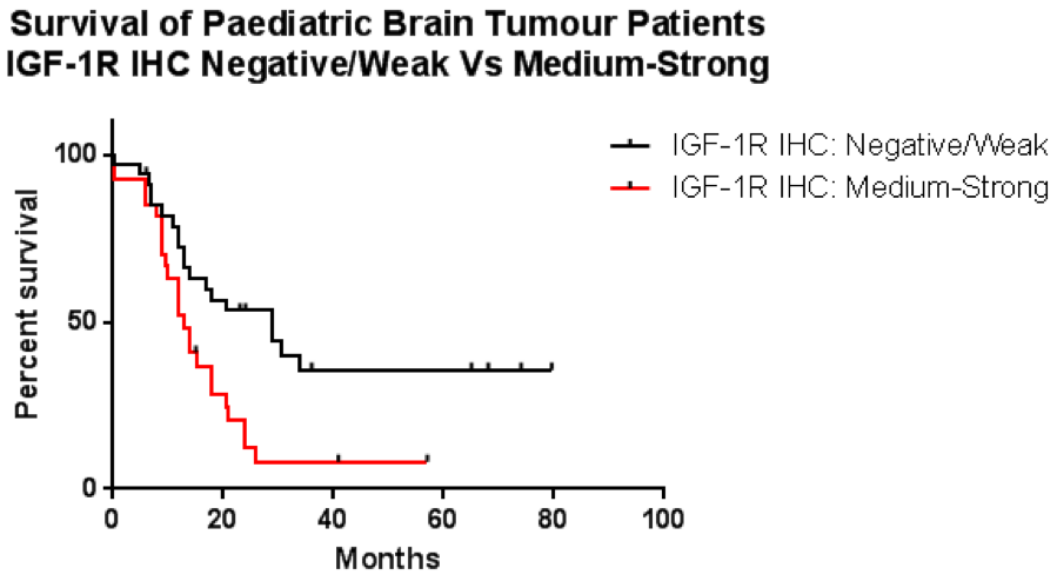


Figure 3.9: Kaplan-Meier Survival Curves for adult and paediatric brain tumour patients by intensity of IGF-1R IHC staining. A) Survival of adult brain tumour patients (in days) grouped by IGF-1R staining intensity. Negative/Weak staining represents cases scored at 0-1, Medium-Strong staining represents cases scored at 1.5-3. Samples analysed here are the same as those analysed in figure 3.8A (260 adult samples). Median survival (days) was 312 : 301 (IGF-1R Negative/Weak : IGF-1R Medium-Strong). B) Survival of paediatric brain tumour patients (in months) grouped as in A. Samples analysed here are the same as those analysed in figure 3.8B (62 paediatric samples). Median survival (months) was 29 : 13 (IGF-1R Negative/Weak : IGF-1R Medium-Strong).

Table 3.3: Results of tests assessing for statistically significant differences in survival distributions between two groups of patients separated by their expression of IGF-1R in brain tumour tissue. The four tests performed correspond to the Kaplan-Meier survival curves in Figures 3.8 and 3.9. (*p < 0.05; **p < 0.01).

Comparison	Log-rank (Mantel-Cox) Test P Value	Significance	Gehan-Breslow-Wilcoxon Test P Value	Significance
Adult: IGF-1R Positive Vs IGF-1R Negative	0.7702	NS	0.6886	NS
Paediatric: IGF-1R Positive Vs IGF-1R Negative	0.0913	NS	0.0482	*
Adult: IGF-1R Negative/Weak Vs Medium-Strong	0.8251	NS	0.9064	NS
Paediatric: IGF-1R Negative/Weak Vs Medium-Strong	0.0048	**	0.0185	*

3.2.2 IGF-1R activity in GBM cells and inhibition of IGF-1R signalling

The observations of a wide range of IGF-1R expression levels in patient tumours, statistically significant changes in IGF-1R levels following common gene alterations, and a possible association of high IGF-1R expression with worse survival in paediatric patients, prompted investigation into the activity of IGF-1R in brain tumours. If active, inhibition of the IGF-1R may bestow a survival benefit to patients. A panel of six GBM cell lines was assessed for baseline expression and phosphorylation levels of signalling components within the IGF-1R and other RTK signalling axes (Figure 3.10). This included four adult GBM cell lines: DK-MG, U87-MG (PTEN mutant), GaMG, and LN-18; and two paediatric GBM cell lines: SF-188 and G34V mutant KNS42 to represent the distinct genotypic, phenotypic, and molecular differences from adult GBM cell lines (Bax et al., 2009).

The six cell lines showed a varied expression of IGF-1R, with the two paediatric cell lines showing the highest basal expression of total protein, and KNS42 and GaMG showing the highest levels of phospho-IGF-1R in basal conditions (growing in full medium) (Figure 3.10). KNS42 also had the highest levels of IRS-1. DK-MG and the PTEN-mutant U87-MG cells showed the lowest levels of total IGF-1R, and LN-18 had the least phospho-IGF-1R. In addition, two cell lines, DK-MG and GaMG, showed high EGFR expression and activation. A band of lower molecular weight was also detected in these cells, which could represent the mutant form of EGFR commonly found in GBM: EGFRvIII (deletion of exons 2-7) (Sugawa et al., 1990). The paediatric cell lines showed low expression of EGFR, with the lowest total EGFR detected in KNS42. PDGFRβ expression also varied across the panel. GaMG showed lower levels relative to the other adult cell lines and SF-188, and PDGFRβ was not detected in KNS42 cells. Basal phospho-AKT was highest in U87-MG, GaMG, and LN-18, whereas basal phospho-Erk was quite uniform across all cell lines, with KNS42 showing slightly higher levels.

The relative lack of basal EGFR and PDGFRβ expression, yet abundance and activation of IGF-1R in KNS42 may indicate a possible signalling dependency on IGF-1R for these cells. Additionally, the high level of basal phospho-IGF-1R in GaMG may partly account for the relatively high basal level of phospho-, and thus active, AKT, enhancing their growth and survival. The next experiments tested the ability of two drugs to inhibit signalling through IGF-1R in GBM cells. BMS-754807 is a reversible small molecule inhibitor for the IGF-1R/IR family kinases, with a Ki of <2 nM and IC50 values of 5-365 nM in cell lines of different tumour types (Carboni et al., 2009; Wittman et al., 2009). BMS-754807 was effectively able to inhibit IGF-1-induced phosphorylation of IGF-1R in KNS42 cells at low concentrations (1 nM) (Figure 3.11A). AKT phosphorylation was reduced to serum-starved levels by 300 nM, and Erk phosphorylation was reduced to below serum-starved levels by 300 nM (Figure 3.11A). Similarly, low concentrations were able to completely inhibit IGF-1-induced phosphorylation of IGF-1R in GaMG cells, and were able to suppress IGF-1-induced phosphorylation of AKT to below serum-starved levels, but not in a linear fashion by concentration (Figure 3.11B). Phospho-Erk was reduced to serum-starved levels by 30 nM, and subsequently to below serum-starved levels as concentration increased. BMS-754807 had similar effects in other GBM cell lines (Figure 3.11C). These results show that BMS-754807 can inhibit IGF-1R phosphorylation and consequently reduce ligand-induced activation of downstream effector signalling components.

In addition to BMS-754807, the ability of BI-836845 to inhibit IGF-1R signalling was tested. BI-836845 is a fully human monoclonal antibody that binds to IGF-1 and IGF-2 with high affinity (Friedbichler et al., 2014). The advantage of this is that it can selectively

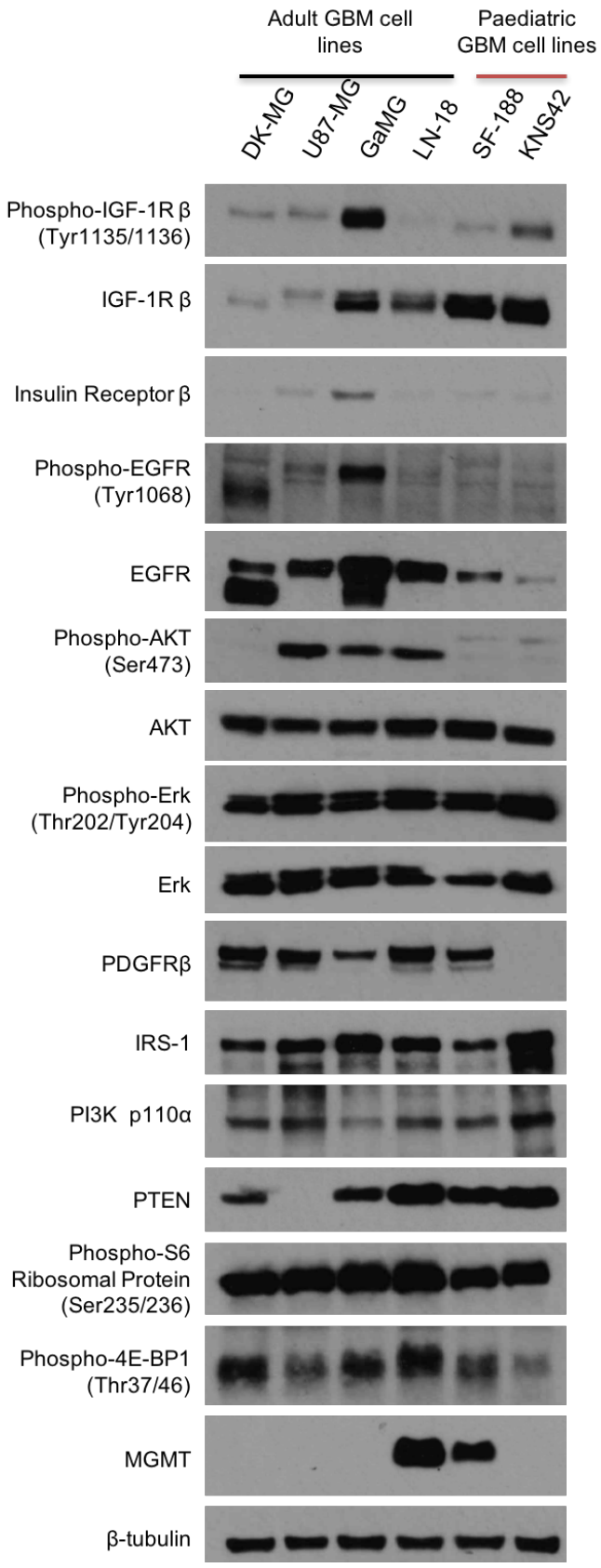
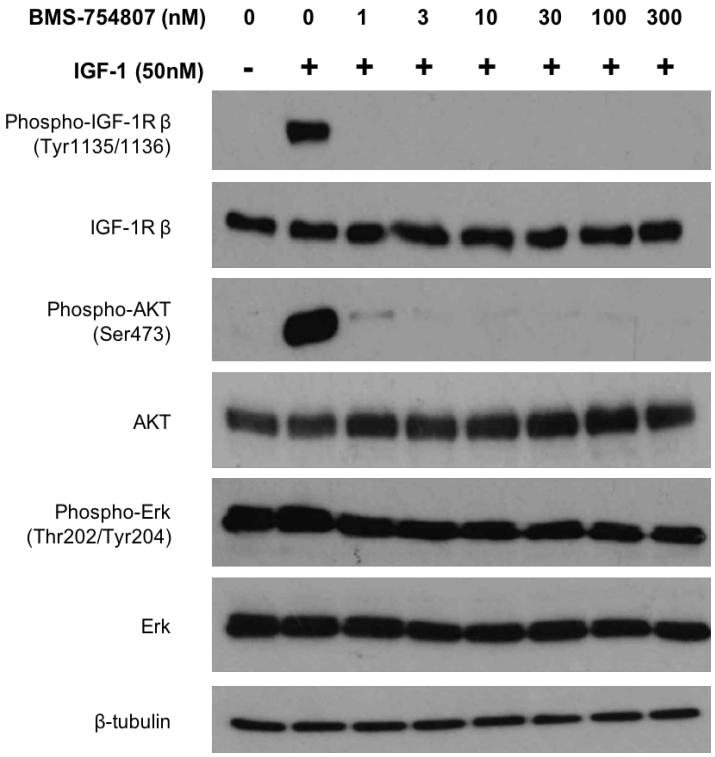
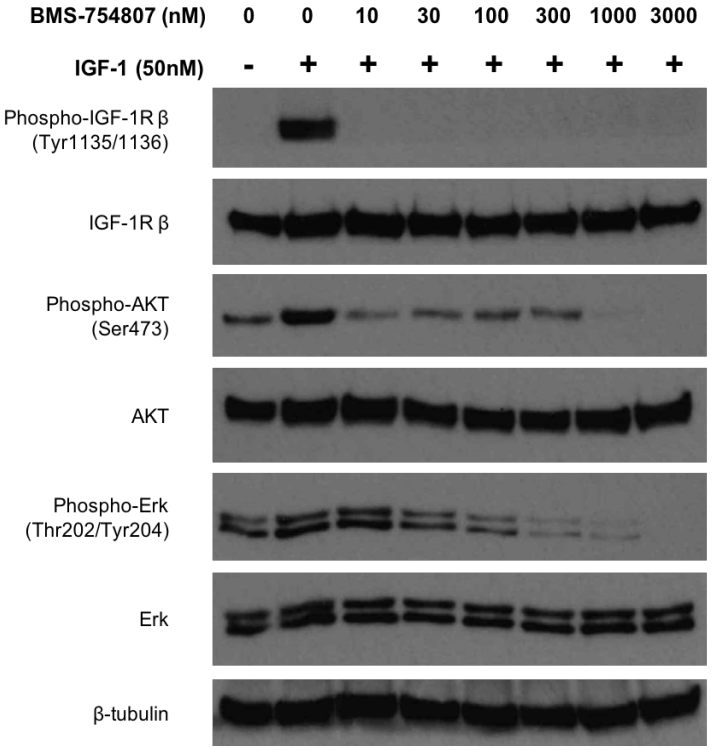


Figure 3.10: Characterisation of the IGF-1R RTK signalling axis in GBM cell lines. Western blot of whole cell lysates showing the basal levels of expression and phosphorylation of signalling proteins within the IGF-1R signalling axis. Protein was extracted from frozen cell pellets. MGMT expression status was also characterised. Similar results were seen on separate sets of blots.

A KNS42



B GaMG



C

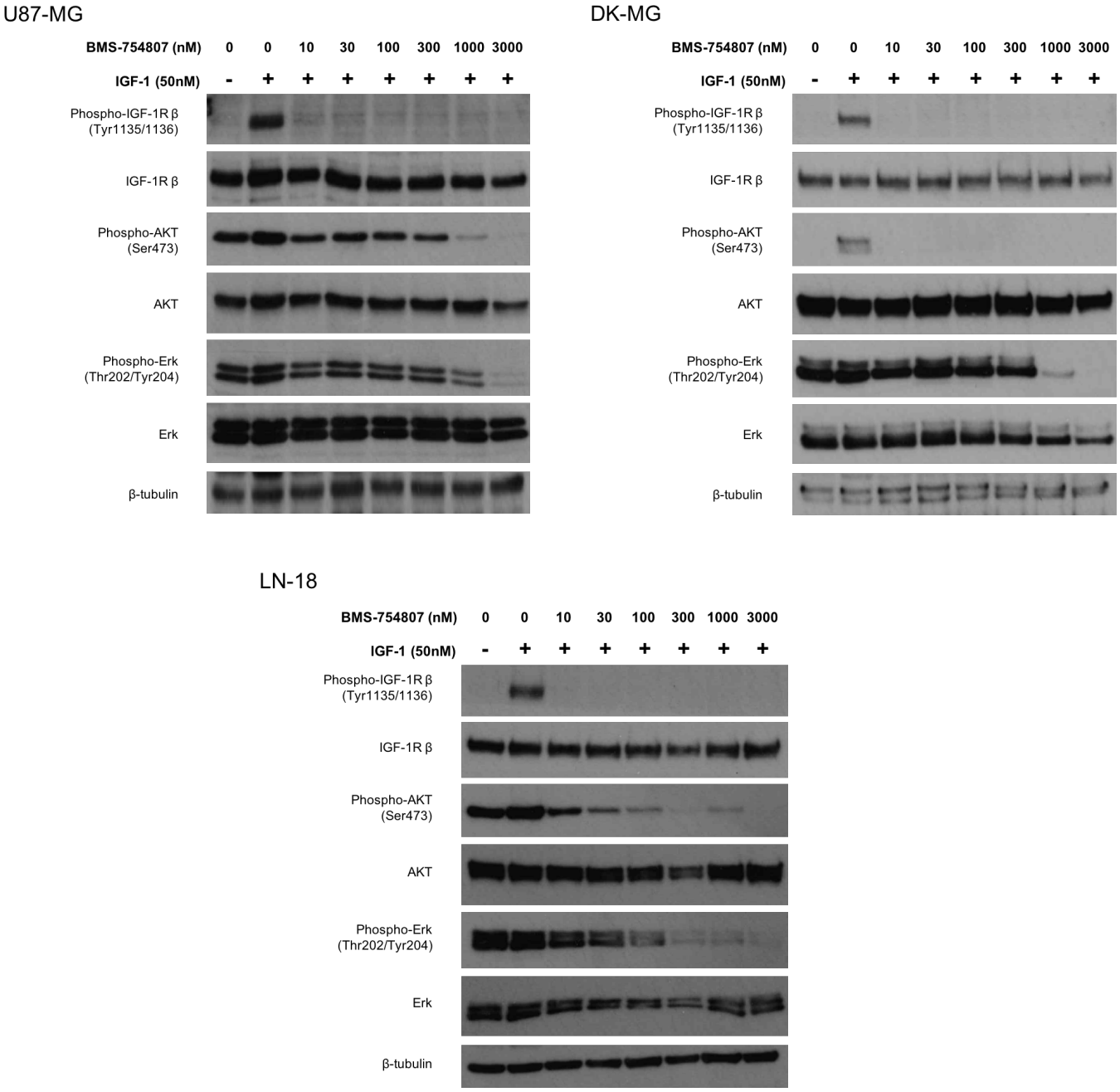


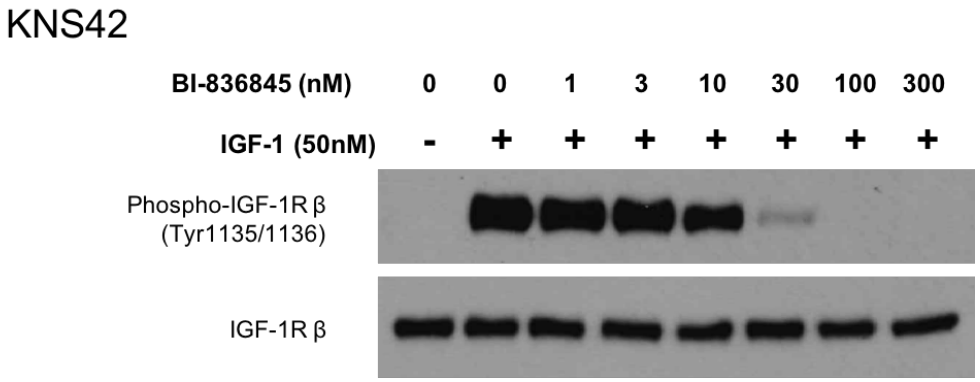
Figure 3.11: BMS-754807 target inhibition of IGF-1R in GBM cells. A) KNS42 cells were serum-starved for 24 hr then treated with BMS-754807 or DMSO solvent control for 1 hr. For an additional 15 min, cells were treated with 50 nM IGF-1 or HCl solvent. Whole cell lysates were prepared in dishes on ice and lysates were Western blotted to assess levels of IGF-1R phosphorylation. Phosphorylation of downstream signalling components AKT and Erk were also measured. B) GaMG cells were treated as in A, and phosphorylation of signalling components was assessed. C) Effects of BMS-754807 on U87-MG, DK-MG, and LN-18 cells. Similar results were obtained on separate blots.

inhibit the IGF-1R and INSR-A by binding IGF ligands and preventing them from activating their target receptors without inhibiting the INSR-B through its binding of insulin, which is the case with most TKIs directed towards IGF-1R due to the high degree of sequence homology between the two receptors. BI-836845 was able to fully inhibit IGF-1-induced IGF-1R phosphorylation in both KNS42 and GaMG cells at 100 nM (Figure 3.12A, B). These results show that BI-836845, although not as potent (likely due to the stoichiometric manner in which BI-836845 inhibits ligand binding), is equally as effective as BMS-754807 at preventing ligand-induced phosphorylation of IGF-1R in GBM cells.

To investigate whether BMS-754807 and BI-836845 had an effect on downstream signalling in basal growth conditions (full medium with 10% FBS), KNS42 and GaMG cells were treated with the drugs for two different time periods in full medium. In this experiment, phospho-IGF-1R was not detected in basal conditions, but was detected with an IGF-1-stimulated positive control in both cell lines (Figure 3.13). Consequently, phospho-IGF-1R was not detected after drug treatments but curiously, an unidentified band of ~115 kDa was identified by the phospho-IGF-1R/IR antibody in IGF-1R-inhibited GaMG cells. However, after a 3 hr incubation with BI-836845, phosphorylation and thus activation of both AKT and Erk in KNS42 cells had been reduced to below basal levels from normal culture conditions (Figure 3.13A). Interestingly, after a 1 hr incubation with BI-836845, phospho-Erk and phospho-AKT levels had increased in KNS42. BMS-754807 also increased phospho-AKT levels relative to basal conditions at both incubation times, and increased phospho-Erk after 1 hr, but reduced phospho-Erk after 3 hr, suggesting time-dependent inhibition of downstream signalling (Figure 3.13A). In GaMG cells, phospho-AKT was largely unaffected by incubation of cells with the two drugs (Figure 3.13B). However, after a 3 hr incubation with both drugs, phospho-Erk was reduced to below basal levels, though a 1 hr incubation had little effect (Figure 3.13B).

These data suggest that the IGF-1R does contribute to basal activation of the AKT and Erk signalling pathways in normal growth conditions in KNS42 cells, and that inhibition of the IGF-1R can suppress signalling of both of these pathways. IGF-1R also possibly contributes towards basal Erk activation, but not AKT activation, in GaMG cells, which too can be suppressed by inhibition of IGF-1R activation.

A



B

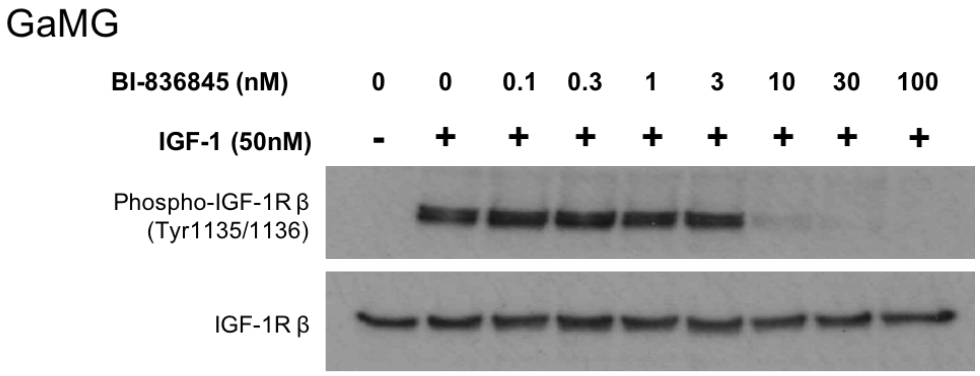


Figure 3.12: BI-836845 target inhibition of IGF-1R in GBM cells. A) KNS42 cells were serum-starved for 24 hr then treated with BI-836845 or human IgG control for 1 hr. For an additional 15 min, cells were also treated with 50 nM IGF-1 or solvent. Whole cell lysates were prepared in dishes on ice and lysates were Western blotted to assess levels of IGF-1R phosphorylation. B) GaMG cells were treated as in A, but with a slightly different dose range of BI-836845. IGF-1R phosphorylation was assessed in response to ligand and drug.

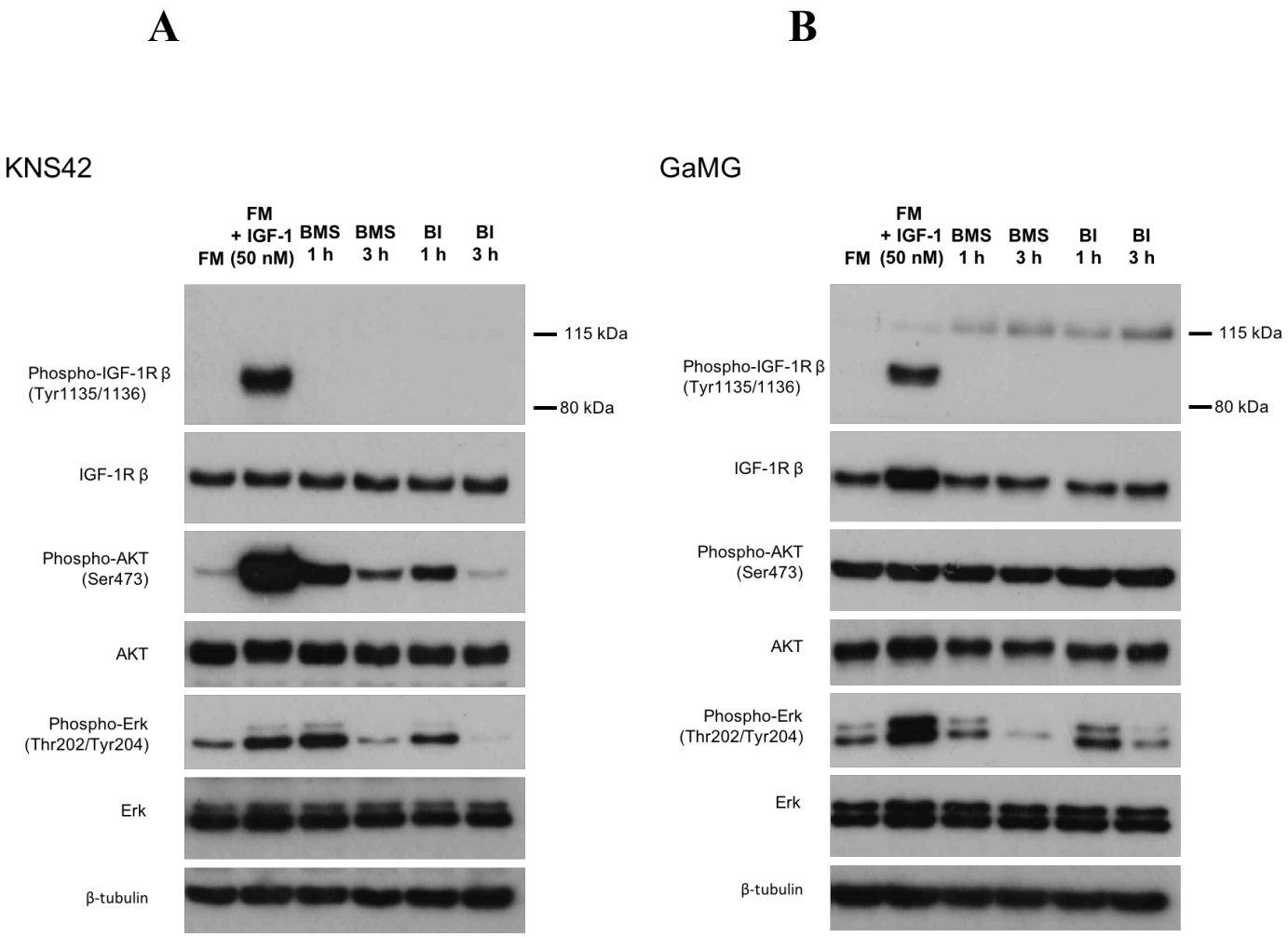


Figure 3.13: Inhibition of basal IGF-1R signalling in GBM cells. A) KNS42 cells were plated into 15 cm plates and cultured to 80% confluence in full medium. Dishes were treated with 100 nM BMS-754807 or BI-836845 for 1 hr or 3 hr, or with 50 nM IGF-1 in fresh full medium for 15 min as a positive control, or received no treatment. Cells were harvested on ice and protein extracted from thawed cell pellets. Lysates were western blotted to measure phosphorylation and expression of IGF-1R, AKT, and Erk basally and after treatment in full medium with drug or IGF-1. B) GaMG cells were treated as in A, and the effects of the drugs were assessed. Similar results were obtained from a second independent set of lysates. FM: full medium.

3.2.3 Effect of IGF-1R inhibition on clonogenicity of GBM cells

Following observations of inhibition of IGF-1R activation and downstream signalling by BMS-754807 and BI-836845, survival and proliferation of GBM cells were assessed in the presence of these two drugs. Clonogenic assays assess the ability of single cells to form colonies of 50 cells or more, so can be used to inherently measure both the survival and proliferation of cells in response to experimental treatments. GBM cells were therefore subjected to clonogenic assays in the presence of different concentrations of both drugs. BMS-754807, up to 300 nM, had little to no effect on the clonogenicity of adult GBM cells U87-MG, LN-18 and GaMG, but had some effect on DK-MG (Figure 3.14). Concentrations of 500-1000 nM saw a sharp decrease in clonogenicity for all these cell lines. The clonogenicity of KNS42 was inhibited in a dose-dependent manner from 1-1000 nM, and in SF-188 cells from 10-1000 nM (Figure 3.14).

It is known that TKIs can exert off-target effects due to the high degree of conservation of the kinase domain in protein kinases (Hanks and Hunter, 1995). In particular, known off-targets of BMS-754807 include c-MET, aurora kinases, and tropomyosin receptor kinases (Carboni et al., 2009). To test whether the reduced clonogenicity at >300 nM BMS-754807 was a specific effect of inhibition of the IGF-1R and its downstream signalling, dose response clonogenic assays were also performed with BI-836845. This allows a more specific inhibition of IGF-1R via steric hindrance of ligand binding, rather than by binding within the kinase domain. All adult GBM cell lines showed little to no inhibition of clonogenicity by BI-836845 up to 1000 nM (Figure 3.15), suggesting the reduced clonogenicity seen with >500 nM BMS-754807 was due to off-target effects of the drug. BI-836845 also had very little effect on the clonogenicity of SF-188 cells. However, KNS42 again showed a dose-dependent inhibition of clonogenicity with BI-836845 up to 1000 nM (Figure 3.15), with a greater reduction at 1 nM than with BMS-

754807, though a 50% reduction of clonogenicity (SF_{50}) was not observed. The sharp decrease in clonogenicity seen from 300-1000 nM BMS-754807 was not replicated with BI-836845, suggesting that reduced clonogenicity up to 300 nM BMS-754807 was likely due, at least in part, to specific effects of inhibition of the IGF-1R signalling axis, and suggesting that inhibition above 300 nM was unrelated to IGF-1R blockade.

The IGF-1R has been reported to be an important factor in mediating anchorage-independent growth in 3D environments, and IGF-1R inhibitors have been shown to inhibit growth in these culture formats (Ambrose et al., 1994; Garcia-Echeverria et al., 2004; Sell et al., 1993). Matrigel was used to design a 3D environment culture assay (Figure 3.16). Matrigel was preferred to soft agar due to the presence of extracellular matrix proteins, which enable Matrigel to better reflect an *in vivo* environment than soft agar. Initial assays tested spheroid growth when embedded in 50% Matrigel (Figure 3.16, upper). Adult GBM cell lines were successfully cultured in 3D, forming spheroid-like colonies in different planes in 96-well plates (Figure 3.17) as opposed to monolayers in standard 2D culture. The adult GBM cells GaMG and LN-18, which did not show reduced clonogenicity in 2D monolayers in response to IGF-1R inhibition, were tested in the 3D format to investigate whether IGF-1R inhibition becomes growth inhibitory in these different conditions. The '2% on-top' assay (Figure 3.16, lower) was used for these experiments to reduce Matrigel viscosity and ensure efficient delivery of drugs to cells. Cellular morphology remained the same as in the embedded assay (Figure 3.17), allowing confidence that there was similar 3D growth. Counterpart 2D 96-well viability assays were also performed in parallel. The effects of IGF-1R inhibition in 3D were very similar to the effects observed in 2D: BMS-754807 and BI-836845 did not show a reduction in viability in either cell line (Figure 3.18), aside from the presumed off-target effects of BMS-754807 above 300 nM.

It was surprising that IGF-1R inhibition had little to no effect on the clonogenicity or 3D growth of the GaMG cell line but did affect the clonogenicity of KNS42 in 2D, especially since both showed high levels and basal phosphorylation of IGF-1R (Figure 3.10). To investigate the possible reasons for this difference, the localisation of IGF-1R in KNS42 and GaMG cells was analysed by immunofluorescence staining of IGF-1Rβ (Figure 3.19). KNS42 cells showed a more diffuse cellular localisation for IGF-1R than did GaMG, wherein IGF-1R mainly localised to a perinuclear region; possibly the Golgi apparatus. The concentration of IGF-1R at this perinuclear region may explain why GaMG did not respond to blockade of extracellular ligand binding by BI-836845 treatment despite high basal phospho-IGF-1R signalling, but does not necessarily explain the lack of response to BMS-754807, which acts intracellularly.

These experiments show that one of the six GBM cell lines, the paediatric cell line KNS42, is affected by drugs that inhibit activation of IGF-1R, and is likely the only cell line which has some dependency on signalling mediated by the IGF-1R.

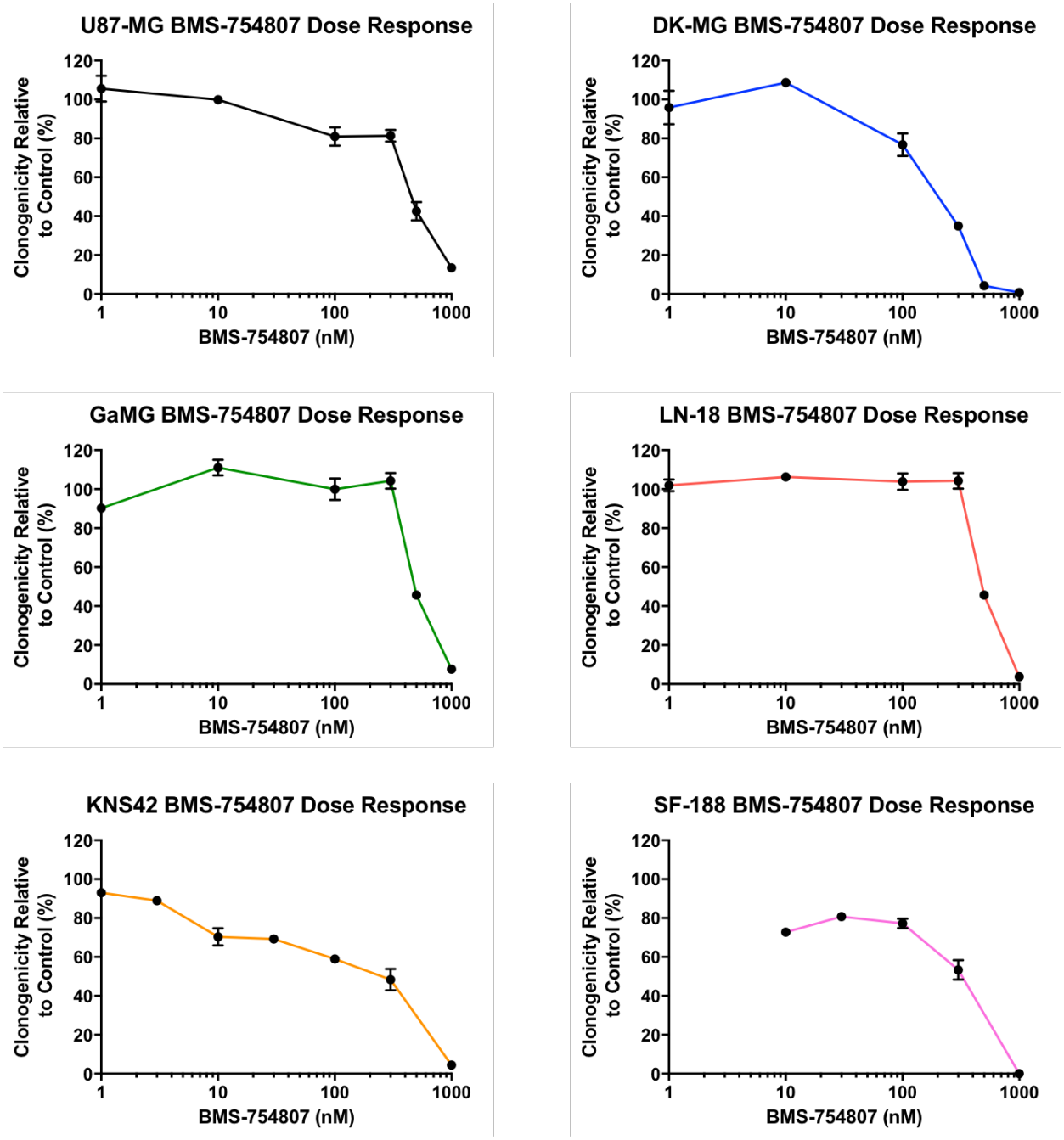


Figure 3.14: Effect of BMS-754807 on clonogenicity of GBM cells. GBM cells were subjected to a BMS-754807 dose response in clonogenic assays. Single cells were treated with various doses of BMS-754807 (1-1000 nM) or DMSO solvent control 24 hr after seeding and incubated to allow formation of colonies of >50 cells. The graphs show colonies as a percentage of solvent-treated controls. Points are the mean ± SEM of pooled data for triplicate values in each of two experiments (six data points).

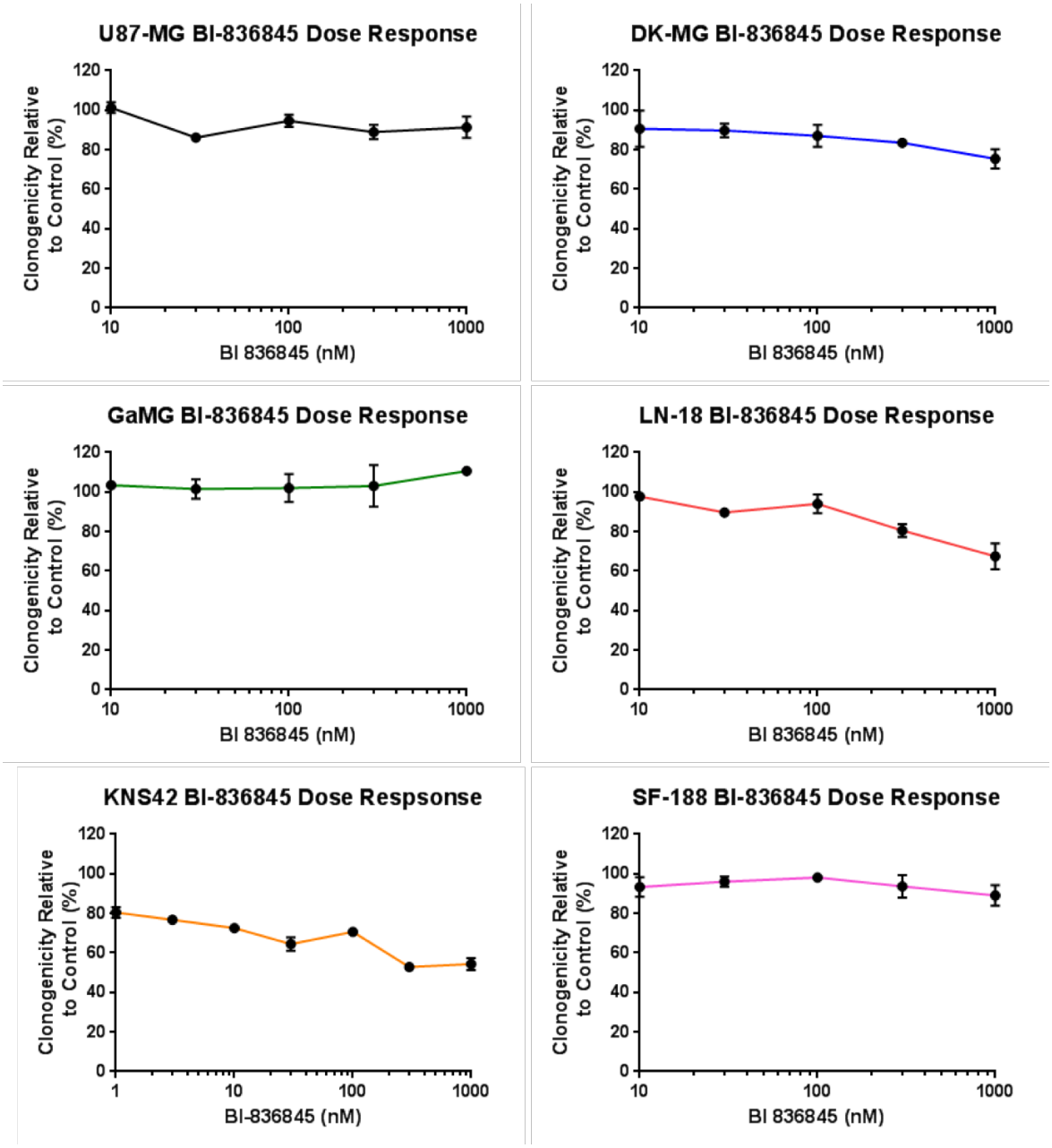


Figure 3.15: Effect of BI-836845 on clonogenicity of GBM cells. GBM cells were subjected to a BI-836845 dose response in clonogenic assays. Single cells were treated with of BI-836845 or human IgG control 24 hr after seeding and incubated to allow formation of colonies of >50 cells. The graphs show colonies as a percentage of IgG-treated controls. Points are the mean ± SEM of pooled data for triplicate values in each of two experiments (six data points).

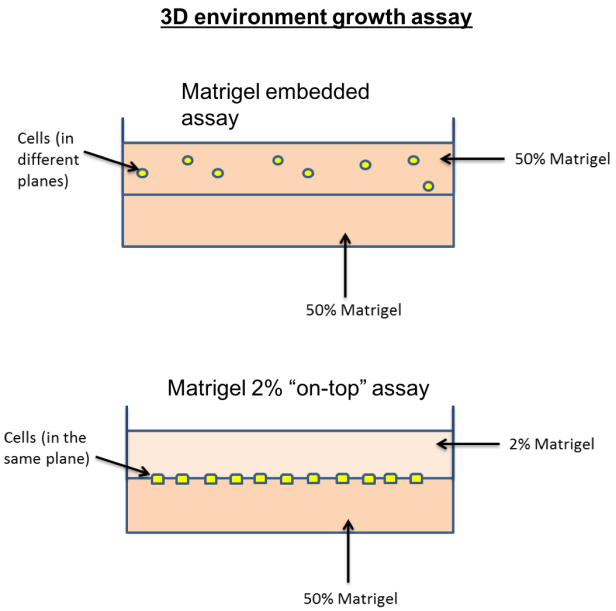


Figure 3.16: Schematic of the 3D environment Matrigel format used to assay effects on 3D cellular growth.

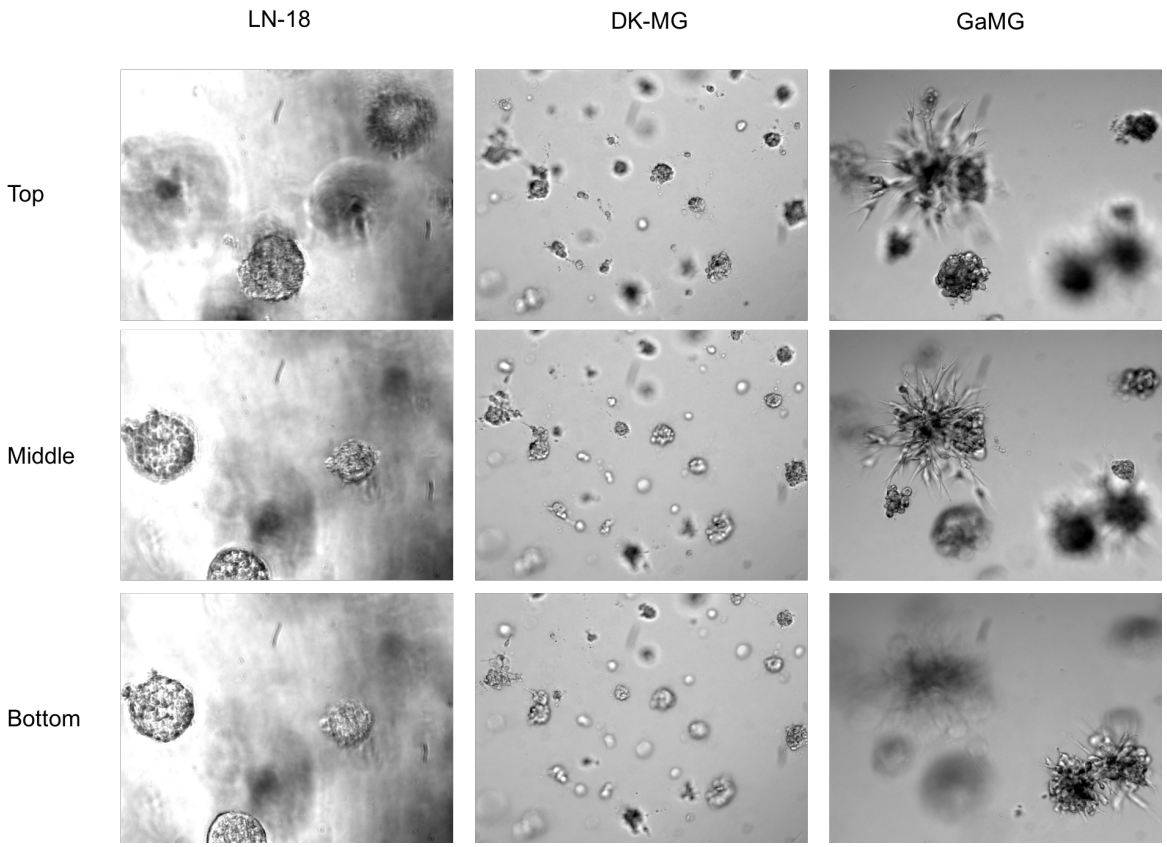


Figure 3.17: Images of 3D cellular growth of adult GBM cell lines. The 'embedded' assay was used here (Figure 3.16). Individual cells were seeded and grew to form discrete three dimensional colonies with strikingly different morphologies from each other and their counterpart 2D growth. Photographs were taken in three vertical planes with a Nikon Ti-E microscope. Original magnification x10.

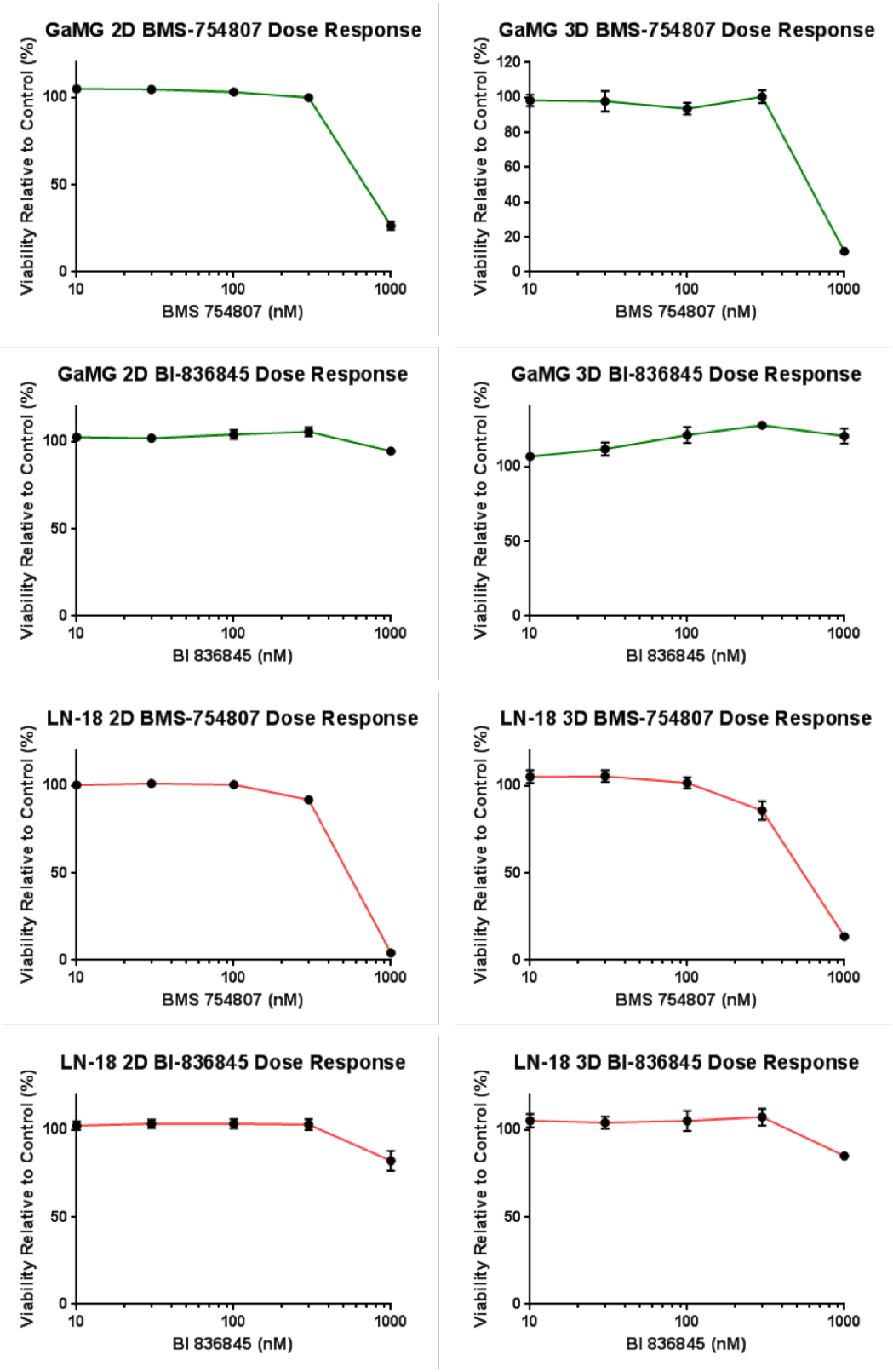


Figure 3.18: Dose response of adult GBM cells to IGF-1R inhibition in 2D and 3D viability assays. Adult GBM cells were seeded into 96-well plates either in their normal culture medium, or in a 3D environment Matrigel '2% on-top' assay as depicted in Figure 3.16. BMS-754807 or BI-836845 were added 24 hr after seeding and plates were incubated for 7 days before lysing and assaying for ATP to assess viability. Values are expressed as a percentage of solvent or IgG controls. Points are means ± SEM of triplicate readings. Graphs are representative of two individual experiments.

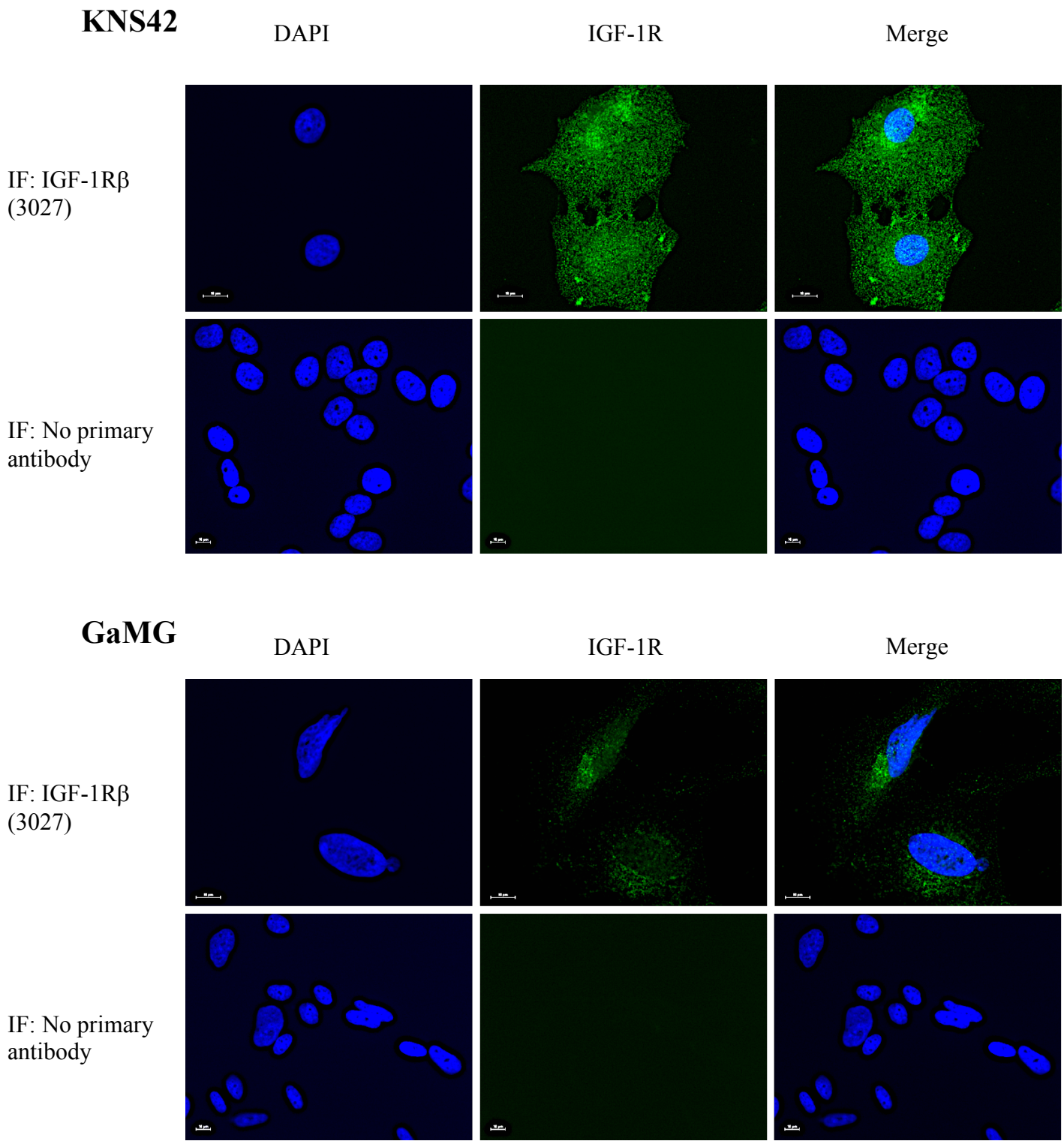


Figure 3.19: IGF-1R immunofluorescence in GBM cells. KNS42 (upper) and GaMG (lower) were grown on coverslips at 200,000 cells overnight and fixed the following day for immunofluorescence staining described in section 2.15.1. Cells were incubated with IGF-1Rβ primary antibody (#3027, Cell Signaling Technology) or no primary antibody and bound antibody was detected with secondary antibody conjugated to Alexa Fluor® 488. Nuclei were counterstained with DAPI. Cells were imaged with a Nikon Eclipse 90i fluorescence microscope. Scale bars represent 10 μm.

3.2.4 Effect of IGF-1R inhibition on radio- and chemo-sensitivity of GBM cells

Previous studies, including work from our group, have shown that expression of IGF-1R can confer radio-resistance in multiple tumour types, and that inhibition of IGF-1R can sensitise cancer cells to IR (Iwasa et al., 2009; Rochester et al., 2005; Turner et al., 1997; Turney et al., 2012). IGF-1R inhibition has been implied in radio-sensitivity in GBM (Carapancea et al., 2007; Osuka et al., 2013). Radiotherapy forms part of the current standard of care for GBM, but even after radiotherapy or chemo-/radiotherapy, patient survival remains poor (Stupp et al., 2009). The ability of IGF-1R inhibition to sensitise GBM cells to IR was tested in clonogenic assays, which are the standard method to assess radio-sensitivity (Tiwana et al., 2015). The basal sensitivities of GBM cells to IR were tested through dose response experiments of single IR doses ranging 2-10 Gy (Figure 3.20). DK-MG cells were relatively sensitive, but the other adult and paediatric (KNS42) (Figure 3.20A, B) GBM cells were quite radio-resistant, with 60-80% clonogenicity maintained post 2 Gy IR, and >10% clonogenicity after a single dose of 6 Gy. SF-188 cells were not tested, but have been shown to be radio-sensitive compared to other GBM cells, undergoing extensive apoptosis in a p53-independent manner involving tumour necrosis factor receptor type 1-associated death domain protein (Haas-Kogan et al., 1996; Yount et al., 2001).

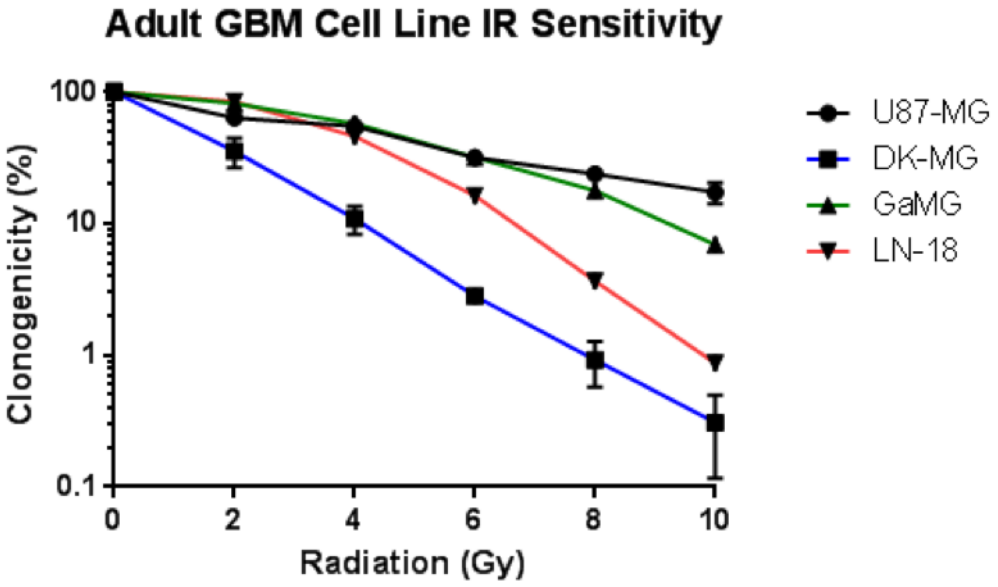
GaMG and KNS42 cells were selected for treatment with BMS-754807 or BI-836845 in combination with a range of IR doses to test for radio-sensitisation. In KNS42, 300 nM BMS-754807 was applied 24 or 4 hr before or 24 hr after irradiation. KNS42 cells showed evidence of sensitisation to IR upon addition of BMS-754807 either 4 hr before or 24 hr post IR (Figure 3.21A), and in these two schedules, all dose enhancement ratios (DERs) for doses of 4 Gy and above exceeded the potentially meaningful result of 1.2 (Table 3.4) (Harrington et al., 2011). However, none of the adult GBM cell lines were sensitised to

IR by BMS-754807 or BI-836845 (Figure 3.21B, C). Despite not showing any sensitivity to IGF-1R inhibition alone, the adult cell lines were tested because A) GaMG had high phospho-IGF-1R basally, and B) IR has been reported to directly activate the IGF-1R, which may give cells a survival advantage post IR (Cosaceanu et al., 2007). To clarify the effect on absolute versus relative cell survival, raw colony numbers were also assessed. Analysis of the raw colony numbers from each condition showed that despite the lack of sensitisation at lower IR doses, KNS42 formed significantly fewer colonies when IGF-1R inhibition was combined with IR than with IR alone (Figure 3.22A and Table 3.5). However, this was not true for GaMG (Figure 3.22B).

TMZ chemotherapy in combination with radiotherapy allows an additional survival benefit to GBM patients compared with radiotherapy alone, but the median survival is increased by only 2.5 months when TMZ is used as a single agent with radiotherapy (Stupp et al., 2005). Previous work from our group showed that IGF-1R inhibition was able to sensitise melanoma cells to TMZ (Ramcharan et al., 2015). However, treatment with BMS-754807 or BI-836845 did not sensitise KNS42, GaMG, or SF-188 cells to TMZ (Figure 3.23). Of note was that KNS42 (Figure 3.23A) and GaMG (Figure 3.23B) were more sensitive to TMZ basally than were SF-188 cells (Figure 3.23C), with SF-188 surviving 10-fold higher concentrations. Similar to experiments combining IGF-1R inhibition with IR, there were statistically significant reductions in raw colony numbers when adding IGF-1R inhibition to TMZ in KNS42 cells (Figure 3.24A), but not in GaMG (Figure 3.24B).

These results suggest that IGF-1R inhibition does not sensitise adult GBM cells to IR or TMZ. In paediatric GBM, IGF-1R inhibition could have a sensitisation effect to IR and an additional, independent effect that is able to further reduce the growth of GBM cells when added to TMZ chemotherapy.

A



B

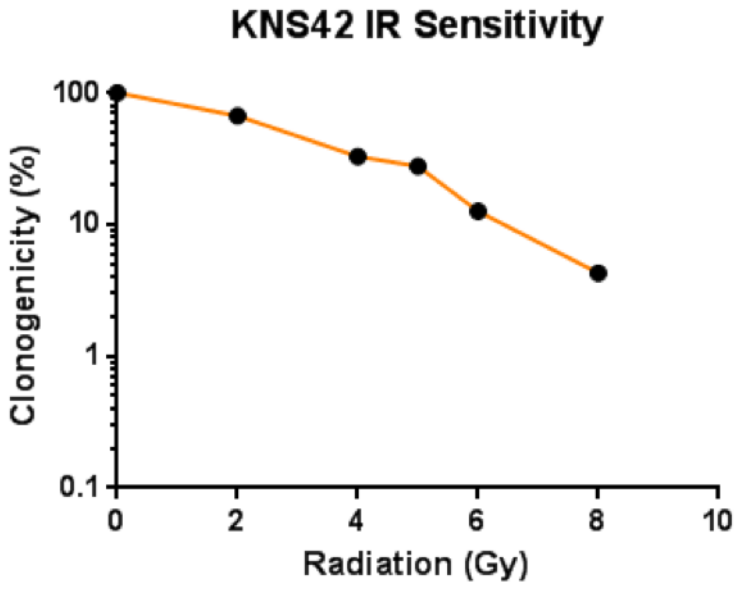
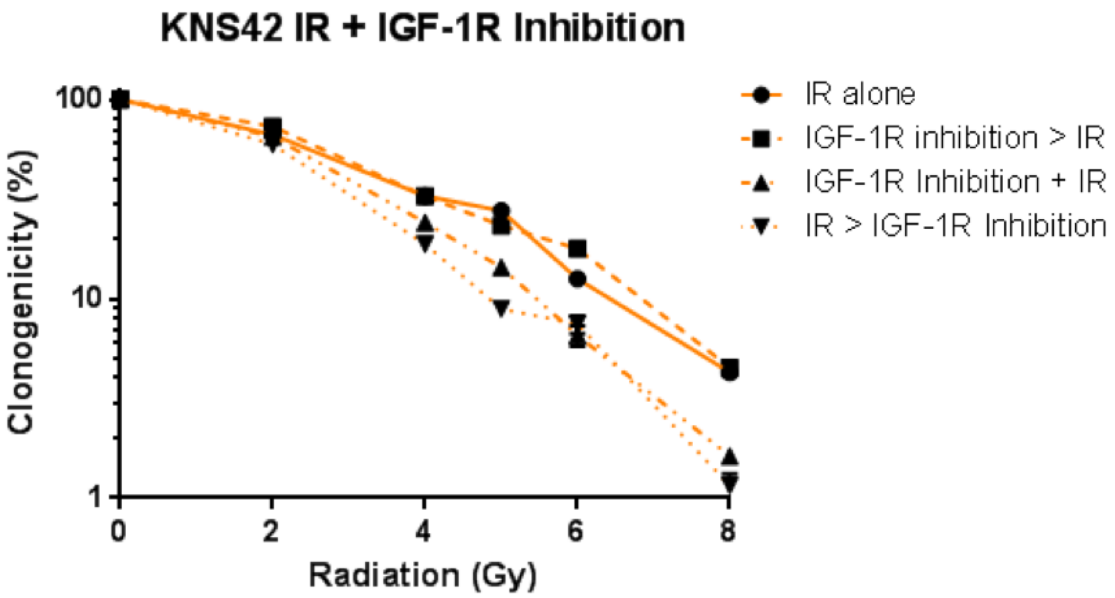
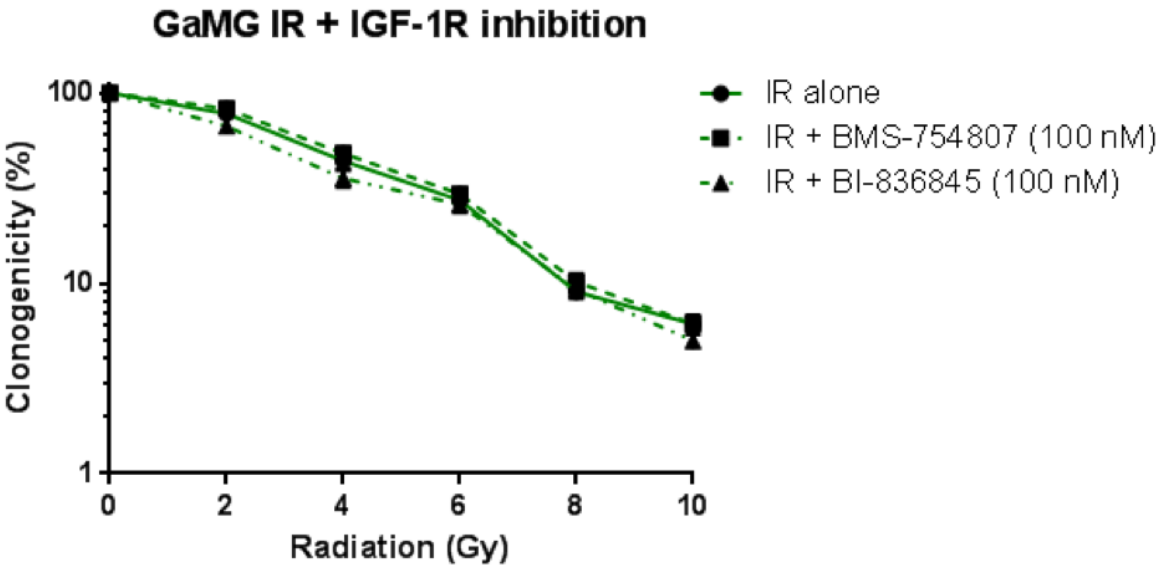


Figure 3.20: Dose response of GBM cells to IR. A) Adult GBM cell lines were seeded into clonogenic assays and irradiated the following day with single doses of IR up to 10 Gy**.** B) The paediatric cell line KNS42 was seeded into clonogenic assays and treated as in A, with doses up to 8 Gy. Plates were incubated to allow formation of colonies of >50 cells. Points represent the means ± SEM of pooled data for triplicate measurements across two independent experiments.

A


KNS42 IR + IGF-1R Inhibition
Clonogenicity (%)
100
10
1
0
2
4
6
8
Radiation (Gy)
IR alone
IGF-1R inhibition > IR
IGF-1R Inhibition + IR
IR > IGF-1R Inhibition

B


GaMG IR + IGF-1R inhibition
Clonogenicity (%)
100
10
1
0
2
4
6
8
10
Radiation (Gy)
IR alone
IR + BMS-754807 (100 nM)
IR + BI-836845 (100 nM)

C

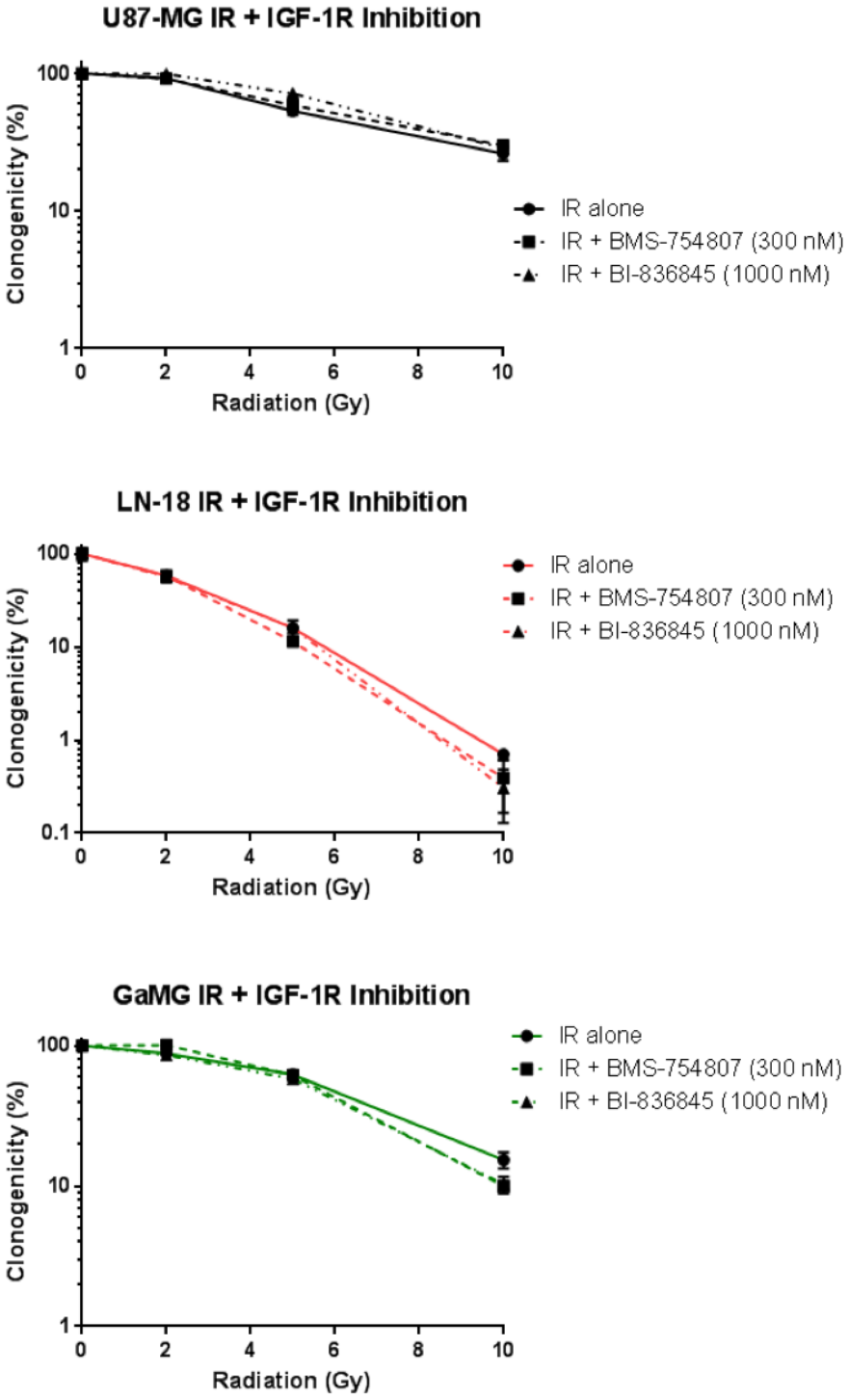
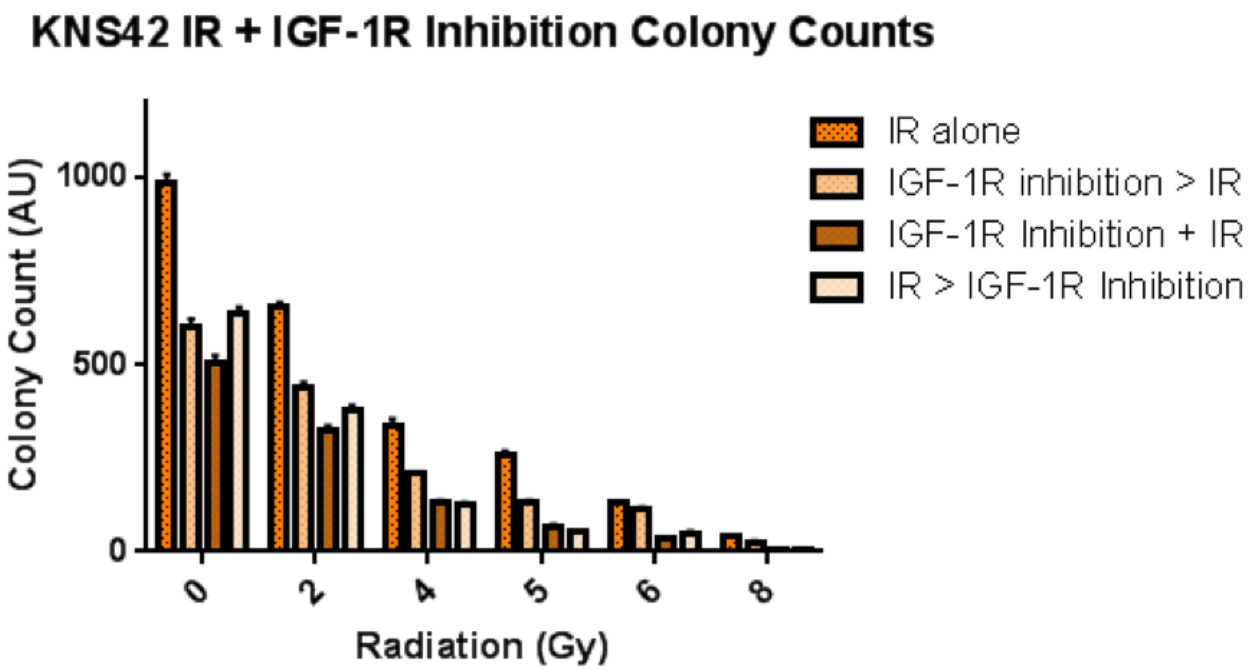


Figure 3.21: Response of GBM cells to IR combined with IGF-1R inhibition. A) KNS42 cells were seeded into clonogenic assays and were treated in triplicate with one of the following schedules: 300 nM BMS-754807 24 hr before irradiation (IGF-1R inhibition > IR), BMS-754807 4 hr before irradiation (IGF-1R inhibition + IR), or BMS-754807 24 hr after irradiation (IR > IGF-1R inhibition). B) GaMG cells were treated with BMS-754807, BI-836845, or DMSO solvent control 4 hr before irradiation. All IR doses were single doses. Dishes were incubated to allow formation of colonies of >50 cells. C) Clonogenic assays of adult GBM cells treated with IR and IGF-1R inhibition in the 6-well plate format. Points represent the means ± SEM from pooled data across two independent experiments for KNS42. For GaMG, this experiment was repeated in a 6-well clonogenic assay format (C), and for U87-MG and LN-18, the assay was performed once.

A



B

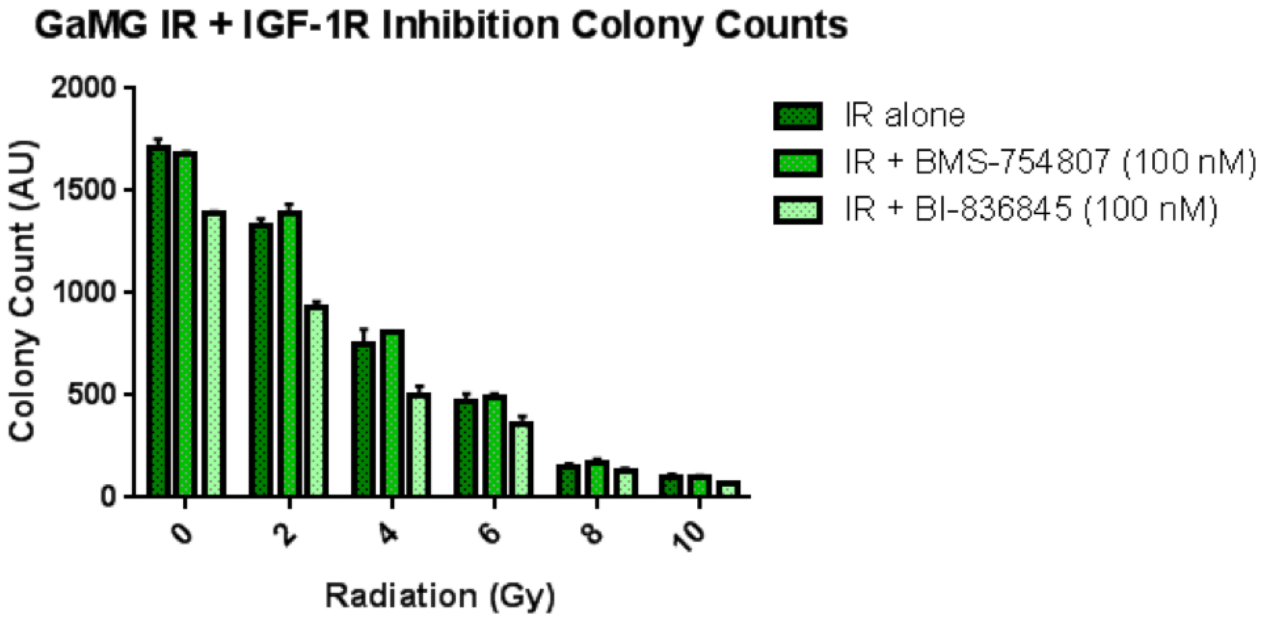


Figure 3.22: Raw colony counts of IR + IGF-1R inhibition combination clonogenic assays. Colony counts from experiments performed in Figure 3.21 are displayed as raw values. Counts were obtained on a GelCount. Bars are means ± SEM. Statistical analysis of these data is shown in Table 3.5.

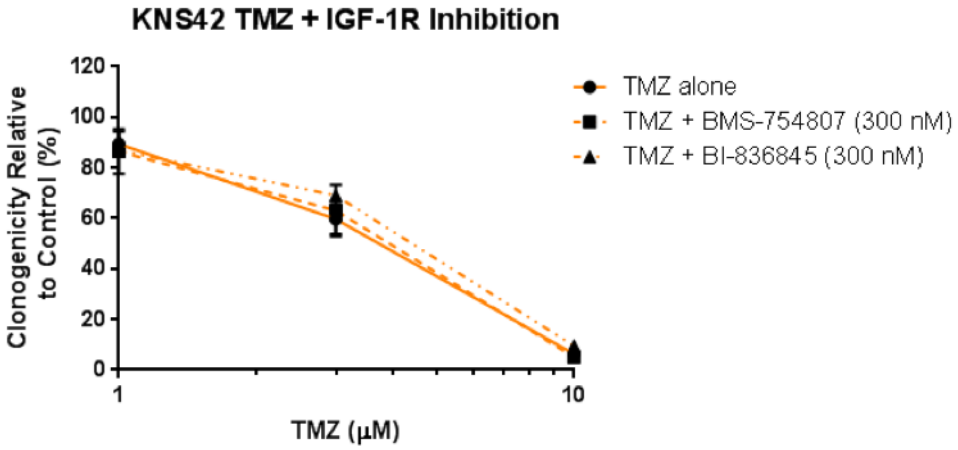
Table 3.4: DER values for IR when combining with IGF-1R inhibition in KNS42. DER = $\frac{\%\ Clonogenicity\ with\ IR\ dose\ alone}{\%\ Clonogenicity\ with\ IR\ dose\ and\ IGF{-}1R\ inhibition}$

IR (Gy)	IR Dose Enhancement Ratio for KNS42		
	IGF-1R Inhibition → IR	IGF-1R Inhibition + IR	IR → IGF-1R Inhibition
2	0.91	1.01	1.12
4	1.00	1.36	1.75
5	1.19	1.93	3.12
6	0.71	1.93	1.69
8	0.95	2.64	3.71

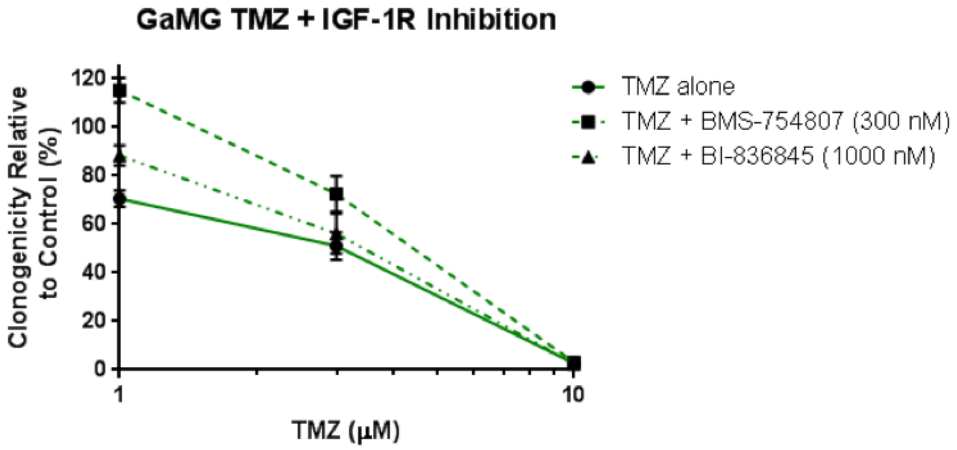
Table 3.5: Statistical testing of the raw colony numbers in the IGF-1R inhibition plus IR combination clonogenic assay with KNS42. Results from Figure 3.22A were analysed by two-way ANOVA (*p < 0.05; **p < 0.01; ****p < 0.0001).

IR Dose (Gy)	Comparison		
	IR alone Vs IGF-1R inhibition > IR	IR alone Vs IGF-1R inhibition + IR	IR alone Vs IR > IGF-1R inhibition
0	p < 0.0001 (****)	p < 0.0001 (****)	p < 0.0001 (****)
2	p < 0.0001 (****)	p < 0.0001 (****)	p < 0.0001 (****)
4	p < 0.0001 (****)	p < 0.0001 (****)	p < 0.0001 (****)
5	p < 0.0001 (****)	p < 0.0001 (****)	p < 0.0001 (****)
6	p = 0.9167 (NS)	p = 0.0021 (**)	p = 0.0140 (*)
8	p = 0.9416(NS)	p = 0.5796 (NS)	p= 0.5630 (NS)

A



B



C

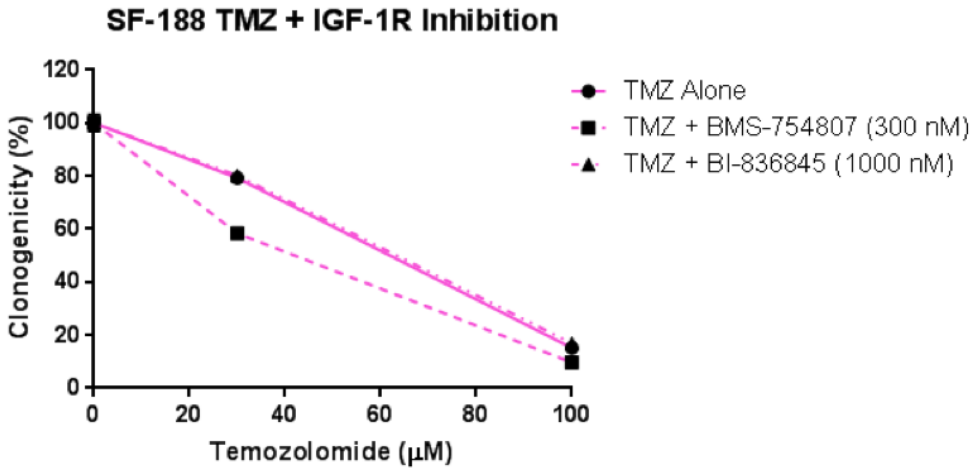
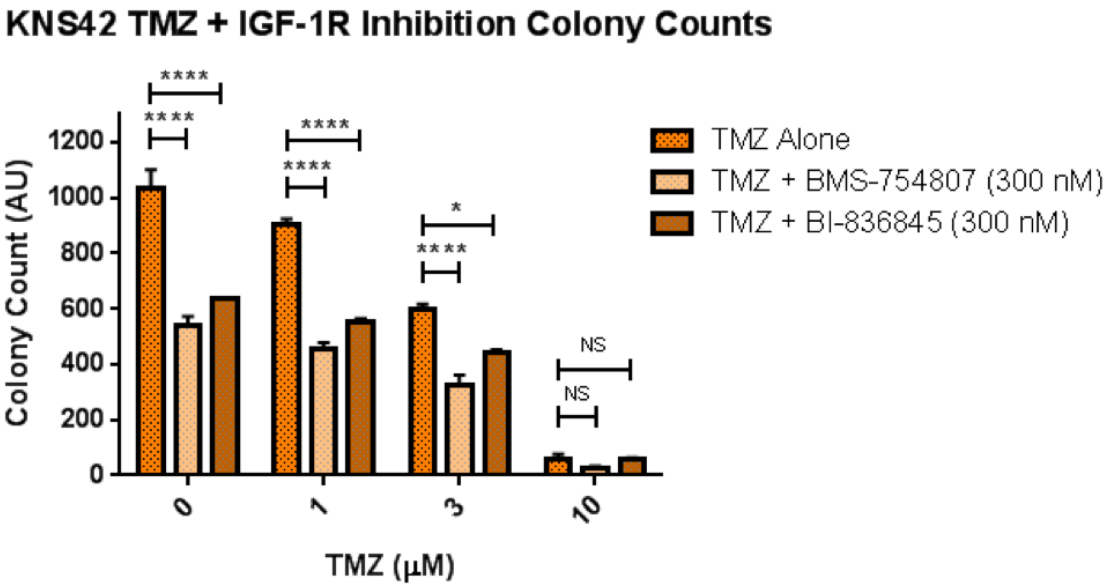


Figure 3.23: Response of GBM cells to TMZ in combination with IGF-1R inhibition. A) KNS42 cells were seeded into 10 cm plates for clonogenic assays and treated in triplicate with either TMZ alone, TMZ + BMS-754807, or TMZ + BI-836845. B) GaMG cells were seeded into 6-well plates for clonogenic assays and treated as in A. C) SF-188 cells were seeded into 6-well plates for clonogenic assays and treated as in A. Dishes were incubated to allow formation of colonies of >50 cells. Points represent the means ± SEM. KNS42 values are pooled data from triplicates across two independent experiments. GaMG and SF-188 data are triplicates from a single experiment.

A



B

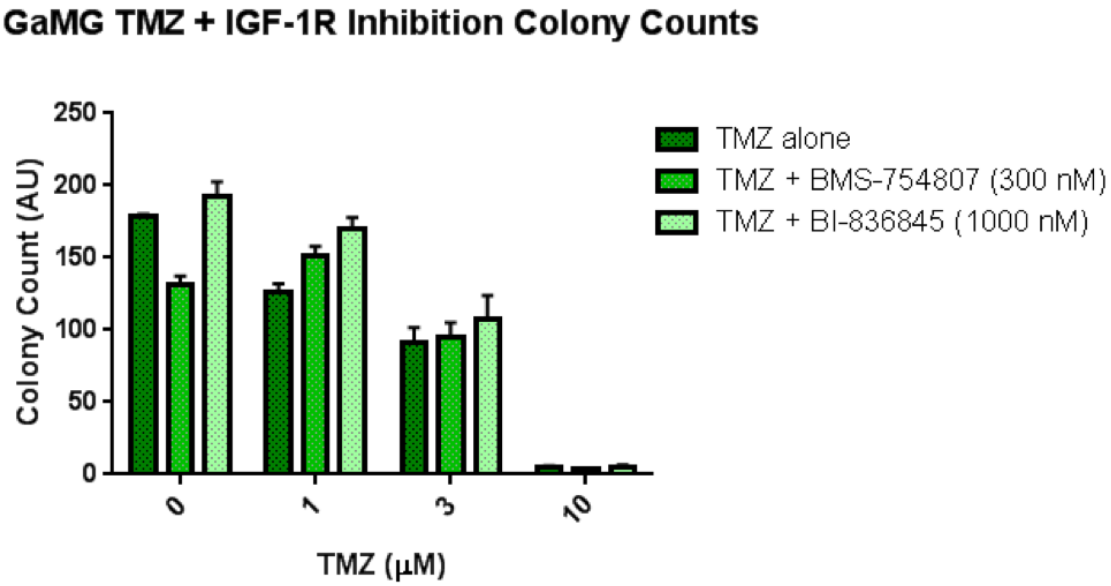


Figure 3.24: Raw colony counts of TMZ + IGF-1R inhibition combination clonogenic assays. Colony counts from experiments performed in Figure 3.23 are displayed as raw values. Counts were obtained on a GelCount. Bars are means ± SEM. Results in A were analysed by two-way ANOVA (*$p < 0.05$; ****$p < 0.0001$).

3.2.5 Effect of *IGF1R* knockdown in GBM cells

To investigate the possible reasons for the additional growth inhibitory effect IGF-1R inhibition had on KNS42 paediatric GBM cells when added to IR or TMZ, siRNA was used to knock down the IGF-1R in these cells and an adult GBM cell line, GaMG. It is well known that IGF-1R, through downstream AKT and Erk signalling pathways, can increase the transcription of pro-mitogenic genes such as cyclins to mediate progression through the cell cycle. Therefore, it was speculated that the reduced colony number of IGF-1R-inhibited KNS42 cells that received IR or TMZ, relative to that of cells that received IR or TMZ alone, may have been due to delayed cell cycle progression.

Two siRNAs were used to deplete IGF-1R. IGF-1R protein was efficiently knocked down by both siRNAs in KNS42 cells and was almost completely undetected by 72 hr in Western blots. This was accompanied by decreased phosphorylation of IGF-1R and AKT relative to control-transfected cells, but phospho-Erk levels remained rather constant (Figure 3.25A). Similarly, IGF-1R protein levels were decreased almost entirely in GaMG cells by 72 hr, but without a concomitant decrease in phospho-AKT or phospho-Erk levels (Figure 3.25B). Notably, when IGF-1R protein was knocked down in GaMG, the phospho-IGF-1R antibody detected a signal at a marginally lower molecular weight than the phospho-IGF-1R signals detected in control-transfected cells (Figure 3.25B, left), which could have been phosphorylation of the insulin receptor given the dual specificity of the antibody, suggesting the presence of a signalling mechanism that compensates for IGF-1R loss in these cells. Indeed, knockdown with the second (Ambion) *IGF1R* siRNA caused a slight increase in phospho-AKT levels relative to control-transfected samples, though no phospho-IGF-1R signals were detected on these blots. Again, an unidentified band was detected on the GaMG blots with the phospho-IGF-1R/IR antibody (Figure 3.25B), but this time at ~140 kDa, as opposed to the ~115 kDa seen in previous blots (Figure 3.13). The 140 kDa band was not

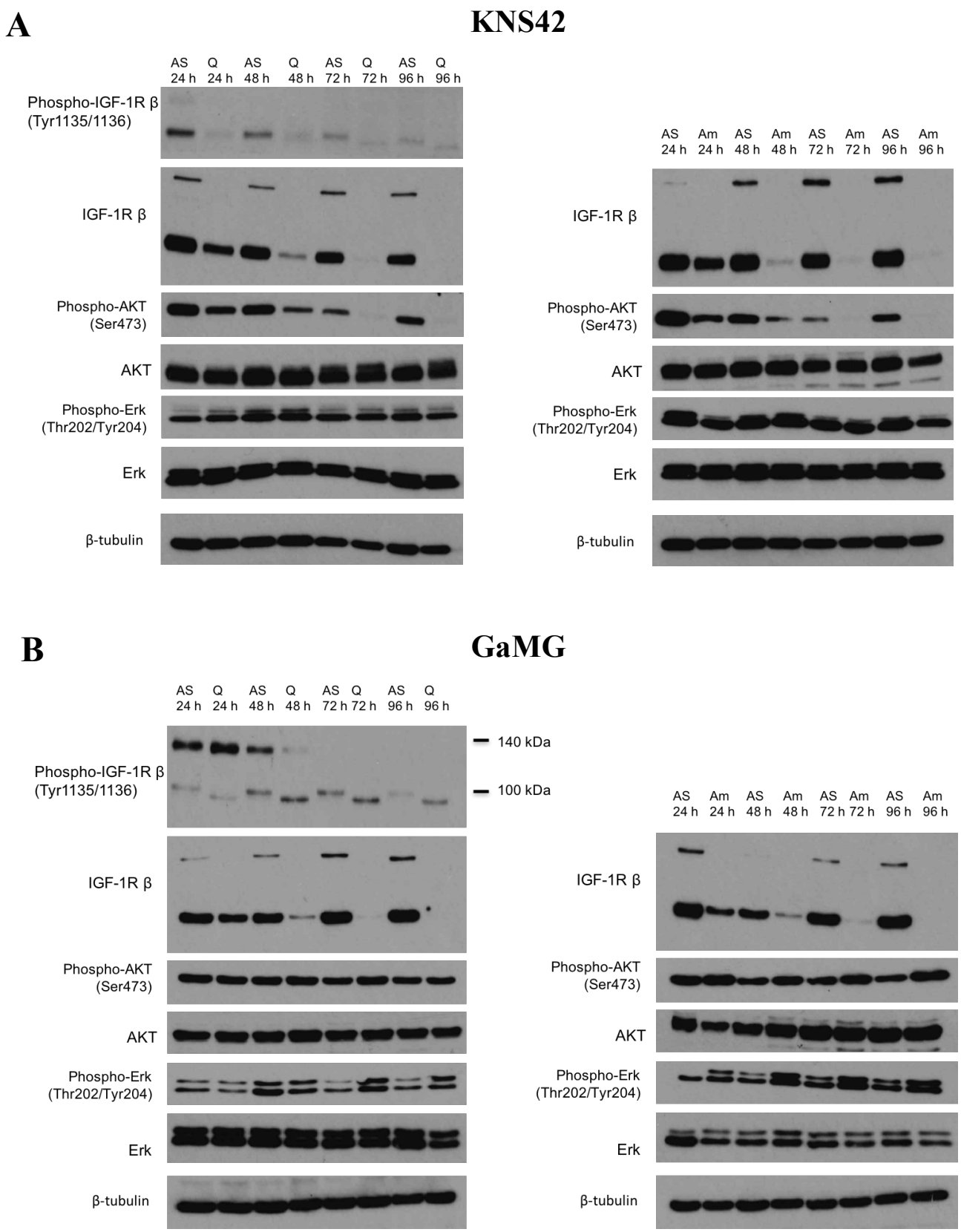


Figure 3.25: Knockdown of *IGF1R* in GBM cells. Cells were transfected with one of two (Qiagen – Q; Ambion – Am) *IGF1R* siRNAs or control, non-silencing siRNA (Allstars – AS), and harvested as cell pellets on ice at indicated time-points post-transfection. A) Western blot showing effects of *IGF-1R* knockdown on IGF-1R protein levels and downstream signalling in KNS42 cells with Qiagen siRNA (left) and Ambion siRNA (right). B) Similar analysis as in A with GaMG cells.

depleted 24 hr after the *IGF1R* siRNA transfection, but was reduced at 48 hr. Therefore, it is unclear whether this is a product of the *IGF1R* gene.

Following the testing of knockdown efficiency, the 48 hr and 96 hr time-points were chosen to assess the effects of *IGF-1R* knockdown on cell cycle distribution. KNS42 and GaMG cells were harvested post-siRNA transfection at these time-points and flow cytometry was used to assess the cell cycle distribution of untransfected, control-transfected, and *IGF1R* siRNA-transfected cells (Figure 3.26). *IGF1R* knockdown was tested and confirmed in parallel by Western blotting for IGF-1R protein levels (Figure 3.27). Comparing *IGF1R* siRNA-transfected with control-transfected KNS42 cells, at both 48 hr and 96 hr post-transfection, there was a reduction of the proportion of cells in S phase and an increased G1 population in cells with IGF-1R knockdown (Figure 3.26A). This might be partly explained by the observed decreased phospho-AKT levels when IGF-1R was knocked down relative to control-transfected cells (Figure 3.27). In addition, the proportion of cells in S phase was further reduced in IGF-1R-depleted cells at 96 hr, consistent with relative phospho-AKT signals at 48 hr and 96 hr. However, incorporated into these knockdown experiments were untransfected KNS42 controls. These samples had lower proportions of cells in S phase at both time-points and in parallel, had lower levels of phospho-AKT than transfected cells (Figure 3.27), suggesting that the siRNA transfection process caused signalling that stimulated entry into the cell cycle, possibly by means of a stress response. Consistent with previous results, phospho-Erk levels remained relatively unchanged by siRNA transfection.

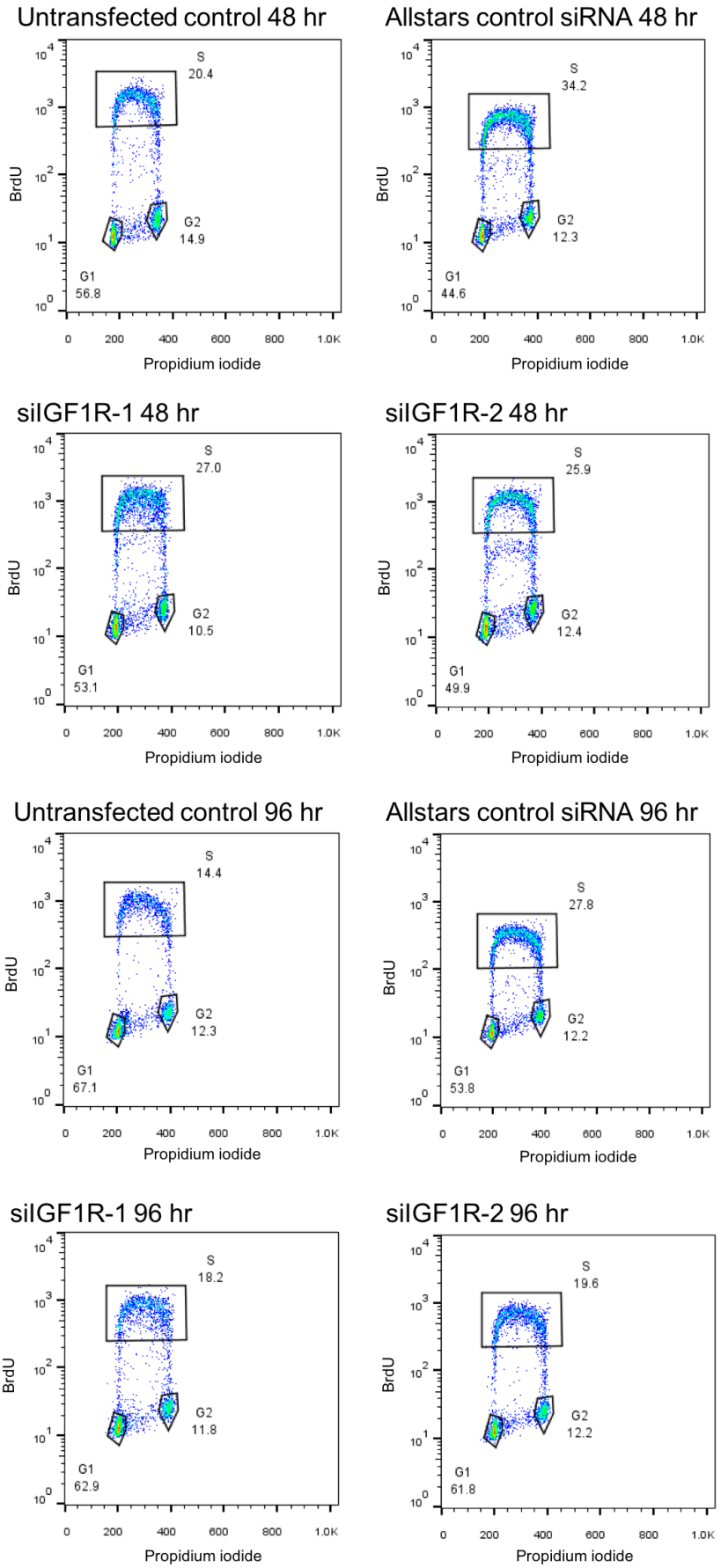
GaMG cells showed a pattern similar to KNS42 in their cell cycle distribution at 48 hr, with reduction in S phase in IGF-1R-depleted cells compared with Allstars transfections. However, at 96 hr, the distribution was not the same for the two siRNAs: Qiagen siRNA gave decreased G1 but increased S and G2 proportions relative to Allstars control, but the

Ambion knockdown showed a similar distribution to the Allstars control (Figure 3.26B). However, prominent in these cells after *IGF1R* siRNA transfection was detection of increased phospho-Erk (Figure 3.27). There was also detection of the faster mobility band using the phospho-IGF-1R/INSR antibody, possibly INSR phosphorylation, and detectable phospho-IGF-1R/INSR signal at ~115 kDa (Figure 3.27A), as seen previously (Figure 3.13). This finding could suggest possible reactive or compensatory signalling in the face of IGF-1R knockdown.

These results suggest that the IGF-1R can contribute towards entry into the cell cycle in KNS42 cells, paralleling changes in phospho-AKT. This effect could contribute to the reduced colony numbers seen in KNS42 cells when combining IGF-1R inhibition with IR or TMZ. There was only transient cell cycle delay in GaMG cells, which had not shown growth or survival inhibition on treatment with IGF-1R inhibitory drugs. However, the results of *IGF1R* knockdown do point towards possible compensatory signalling and redundancy for the IGF-1R in adult GBM cells.

A

KNS42


Untransfected control 48 hr
S 20.4
G2 14.9
G1 56.8
Allstars control siRNA 48 hr
S 34.2
G2 12.3
G1 44.6
siIGF1R-1 48 hr
S 27.0
G2 10.5
G1 53.1
siIGF1R-2 48 hr
S 25.9
G2 12.4
G1 49.9
Untransfected control 96 hr
S 14.4
G2 12.3
G1 67.1
Allstars control siRNA 96 hr
S 27.8
G2 12.2
G1 53.8
siIGF1R-1 96 hr
S 18.2
G2 11.8
G1 62.9
siIGF1R-2 96 hr
S 19.6
G2 12.2
G1 61.8
BrdU
Propidium iodide

GaMG

B

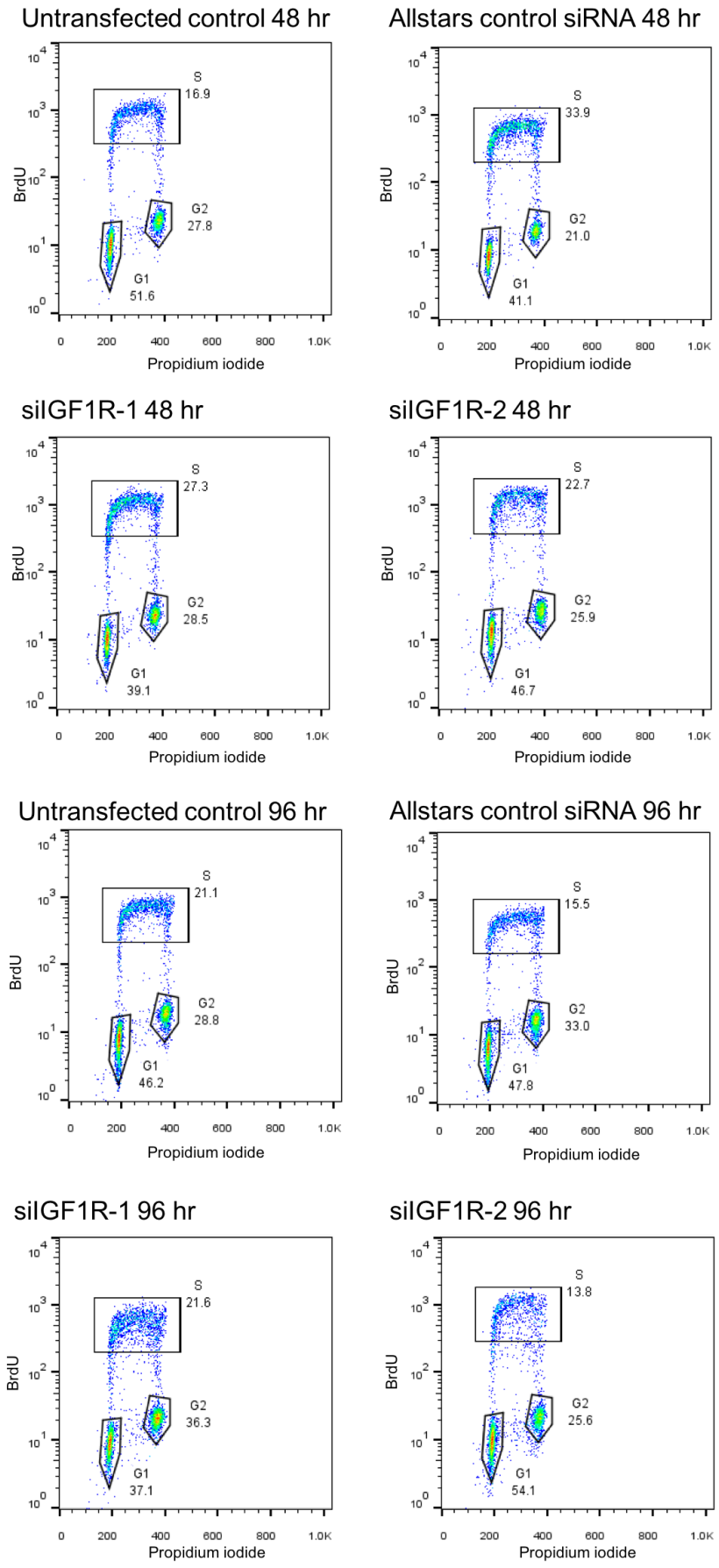


Figure 3.26: Cell cycle distribution of GBM cells following *IGF1R* knockdown. GBM cells were grown to 30-40% confluence and transfected with control (Allstars) siRNA, one of two *IGF1R* siRNAs, or were untransfected. Cells were pulsed for 30 min with BrdU and collected at 48 hr or 96 hr post-transfection and fixed for analysis by flow cytometry as described in section 2.14.1. A) KNS42 cells were analysed for cell cycle distribution by DNA quantification and BrdU incorporation into DNA after different treatment conditions. B) GaMG cells were analysed for cell cycle distribution as in A resulting from different treatment conditions. FlowJo software was used to gate live single cells and assign G1, S, and G2 phases of the cell cycle. Graphs show results from one of two independent experiments. siIGF1R-1: Qiagen siRNA; siIGF1R-2: Ambion siRNA.

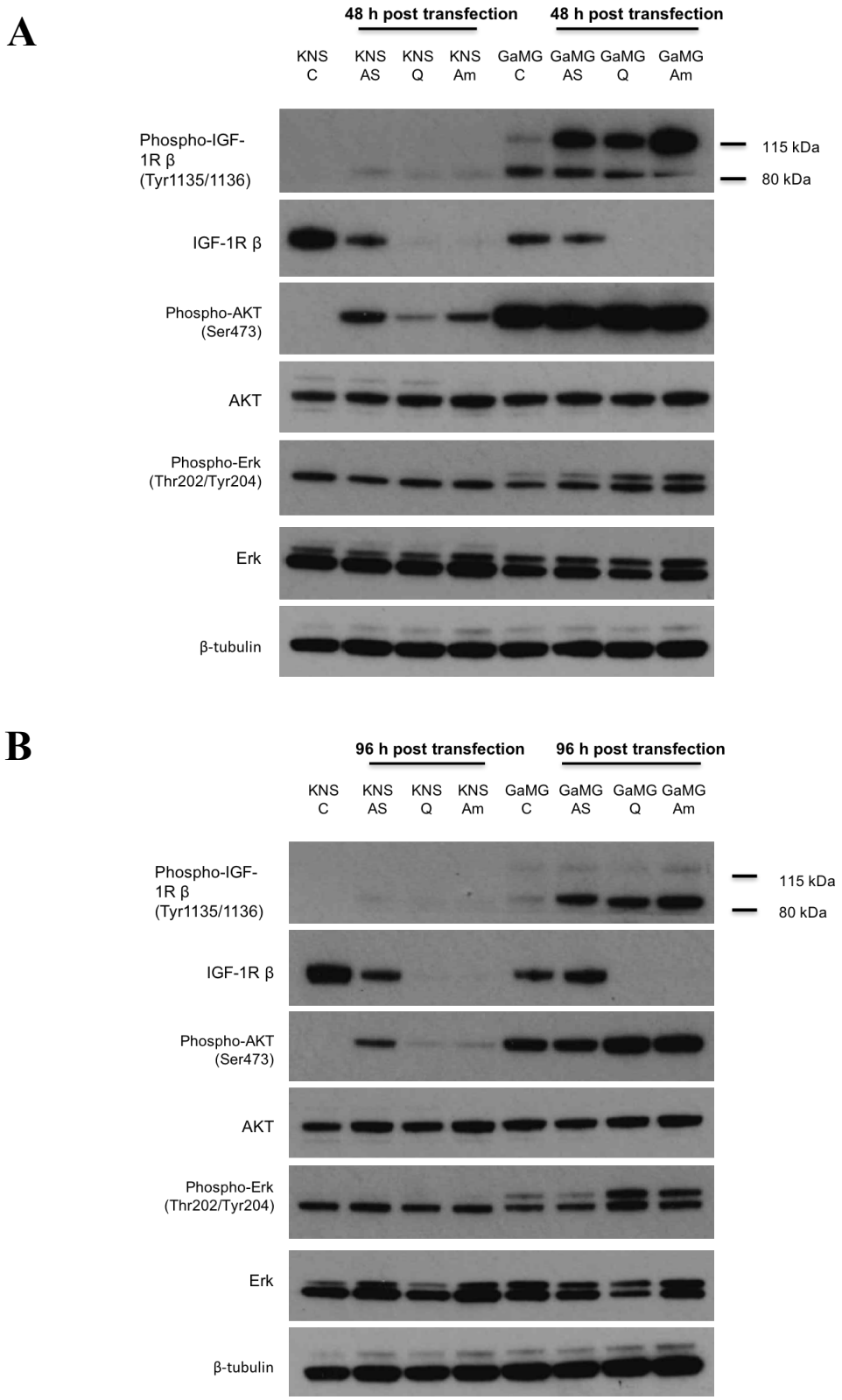


Figure 3.27: Knockdown of the IGF-1R protein for cell cycle distribution analysis. Parallel samples to those analysed by flow cytometry were transfected and harvested and frozen as cell pellets at 48 hr and 96 hr post-transfection. A) KNS42 cell pellets were lysed and Western blotted to check for knockdown of IGF-1R ahead of cell cycle analysis. IGF-1R expression and downstream signalling were assessed. B) GaMG cell pellets were lysed and analysed by Western blotting as in A. Separate parallel checks for knockdown of IGF-1R at the protein level were performed for the two individual cell cycle analysis experiments, and the blots presented here correspond to those samples that are presented in graphs in Figure 3.26.

3.3 Discussion

The results of this chapter demonstrated that IGF-1R expression in GBM was related to expression of wildtype PTEN in GBM patients, and that IGF-1R can be overexpressed in GBM relative to normal brain tissue. IGF-1R overexpression correlated with worse prognosis in paediatric, but not adult brain tumours, and inhibition of IGF-1R in a paediatric GBM cell line resulted in inhibition of growth and possible radio-sensitisation.

The tumour suppressor gene *PTEN* is one of the most commonly altered genes in GBM through point mutations or deletions, with frequent loss of heterozygosity (Wang et al., 1997). Analyses performed here using publicly available data also showed *PTEN* to be in the top three most commonly mutated genes in GBM, and that IGF-1R was the most statistically significantly altered protein when *PTEN* was altered. Conflicting reports exist on the relationship between PTEN and IGF-1R expression. Studies in pancreatic and prostate cancer cell lines demonstrated that active PTEN or PTEN overexpression reduced expression of IGF-1R in an AKT-dependent manner in pancreatic cancer, and in an AKT-independent manner in prostate cancer (Tanno et al., 2001; Zhao et al., 2004). In these reports, decreased IGF-1R expression was associated with decreased invasiveness and proliferation. Conversely, in the PTEN-negative GBM model U87-MG, PTEN expression or PI3K inhibition increased the expression of IGF-1R and INSR (Lackey et al., 2007). This agrees with the data extracted from TCGA here and is supported by other data that showed induction of IGF-1R expression and phosphorylation after AKT inhibition (Chandarlapaty et al., 2011). Lackey *et al.* (2007) also showed that Erk activation was not achieved in response to IGF-1 in U87-MG cells, but was achieved in response to EGF or PDGF, and that re-expression of PTEN led to sensitisation of IGF/insulin-stimulated Erk activation. The data presented here did confirm reduced expression of IGF-1R in U87-MG relative to other GBM cell lines, but phosphorylation of Erk was seen in U87-MG in response to IGF-1,

although this could reflect the differences in concentration of IGF-1 used: 13 nM in the Lackey *et al*. (2007) study versus 50 nM used here.

Given the large variation of PTEN status in GBM patients, a wide range of expression of IGF-1R was expected in patients' tumour tissue. Indeed, IGF-1R IHC staining intensity showed scores at every level of a seven-point intensity scale in the adult and paediatric brain tumour samples stained in this study. Most tumour samples showed more intense IGF-1R staining than normal brain, and paediatric tumours appeared to contain more IGF-1R than adult tumours. Analyses of IGF-1R expression and clinical data revealed a negative association between presence (and intensity) of IGF-1R staining and survival in paediatric patients with brain tumours, but not in adult patients. Lack of association of IGF-1R expression with decreased survival of adult patients contrasts with a recent study that found that IGF-1R was associated with poorer survival in adult GBM as assessed by IGF-1R IHC and associated clinical data (Maris et al., 2015). The authors also found that the benefit of patients from TMZ chemotherapy was greater in the IGF-1R-negative group. The samples analysed by Maris *et al.*, (2015) did not include any paediatric tumours for comparison. The contrasting results in adult brain tumours are likely consequences of differences in the IHC staining and scoring procedures, including the primary antibody and secondary detection methods. It should be noted that there were fewer paediatric samples (n = 62) than adult samples (n = 260) in the analyses performed here. To increase confidence in the results in the paediatric cohort, it would be interesting to examine a large number of paediatric samples. Univariate analysis could also be performed to assess other prognostic factors, including age and grade, then, multivariate analyses could test whether IGF-1R expression is of independent prognostic significance.

When interpreting IGF-1R IHC data and possible associations, it is important to remember that IHC reveals presence or absence of IGF-1R, and not whether it is active.

Lack of activation may contribute to the absence of association between increased IGF-1R and reduced survival in adult brain tumours. It is possible that, as well as having a higher proportion of high IGF-1R-expressing samples than adult brain tumours, paediatric tumours might have a greater proportion of active, functional IGF-1R.

The functional role of IGF-1R was next assessed in a panel of GBM cell lines, testing effects of IGF-1R inhibition on cell survival and response to TMZ and IR. A shortcoming of the results presented in this Chapter is that some experiments were performed only once. In order to make conclusions with greater certainty, additional repeats would be needed to confirm initial findings regarding effects of inhibiting IGF-1R, with and without IR or TMZ treatment.

Supporting the hypothesis that IGF-1R may be more functional in paediatric brain tumours are results generated in this study when the effect of IGF-1R inhibition was assessed in adult and paediatric GBM cell lines. There were differences in the baseline expression and phosphorylation of IGF-1R across the cell line panel. The paediatric cell lines, consistent with the IHC data, appeared to have the highest expression of IGF-1R, but the adult cell line GaMG, followed by the paediatric cell line KNS42, appeared to have the highest levels of phosphorylated IGF-1R. In testing whether the phosphorylated IGF-1R was functional, the effect of IGF-1R inhibition was assessed in all cell lines, first with the small molecule inhibitor BMS-754807.

BMS-754807 at concentrations of ≤ 300 nM had only very minor effects on the clonogenicity of all adult GBM cell lines except DK-MG. In contrast, clonogenicity of paediatric GBM cells was inhibited, which is consistent with the effects reported in paediatric GBM cell lines using the IGF-1R inhibitor NVP-AEW541 (Bielen et al., 2011). At 1000 nM of BMS-754807, there was a sharp decrease in clonogenicity in all cell lines. It is known that small molecule drugs exhibit off-target effects, and BMS-754807 is known to

inhibit TrkA, TrkB, and aurora kinases (Carboni et al., 2009). With off-target effects in mind, a second, more specific drug was used to block activation of IGF-1R: BI-836845, a fully humanised monoclonal antibody directed towards IGF-1 and IGF-2. Only KNS42 cells showed inhibition of clonogenicity by treatment with BI-836845 in a concentration-dependent manner. BI-836845, even up to 1000 nM, had very little effect on the other cell lines. These data suggest that the effects seen with BMS-754807 up to 300 nM in KNS42 may have been specific effects of IGF-1R inhibition, and that the decreases in clonogenicity at 1000 nM BMS-754807 resulted from off-target effects.

Thus, data presented here showed that in patient brain tumour samples and *in vitro* models, paediatric GBM cells have higher expression of IGF-1R than adult GBM cells. In addition, it is likely that IGF-1R has a more functional role in promoting the growth and proliferation of paediatric cells than adult cells, consistent with the finding that IGF-1R expression is associated with a worse prognosis in paediatric brain tumours, but not in adult brain tumours.

It was interesting that IGF-1R inhibition reduced the clonogenicity of KNS42 cells but did not affect GaMG clonogenicity, despite the high baseline signal for phospho-IGF-1R in GaMG cells. A possible reason for this may lie in the observed effects of IGF-1R inhibition on the downstream mediators of IGF-1R signalling. Despite being able to inhibit IGF-1-induced phosphorylation of AKT and Erk in all cell lines, BMS-754807 and BI-836845 inhibited phospho-AKT and phospho-Erk to a greater extent in KNS42 than in GaMG when the cells were treated with the IGF-inhibitory drugs in basal growth conditions. Indeed, in GaMG cells, phospho-AKT was not inhibited at all by either drug. This could be related to expression and function of other RTKs. The expression and baseline phosphorylation of EGFR in GaMG was found to be the highest of all the GBM cell lines examined here. GaMG cells also expressed PDGFRβ. Conversely, KNS42 expressed

relatively low amounts of EGFR, and no detectable baseline phospho-EGFR or expression of PDGFRβ, the latter contradicting findings of Bielen *et al.* (2011). It is possible that, even in the absence of phospho-IGF-1R, activation of AKT and Erk was still achieved in GaMG by compensatory signalling through other RTKs, possibly rendering IGF-1R signalling redundant. IGF-1R signalling may be less likely to be redundant in KNS42 cells, due to the relative lack of expression and activation of other RTKs. It would be interesting to compare the adult and paediatric patient samples stained in this study after staining for EGFR. The localisation of IGF-1R in GaMG cells may also help explain the lack of response to IGF-1R inhibition. A large proportion of IGF-1R in GaMG was in a perinuclear region and may not have been active, whereas KNS42 showed a more homogenous localisation, likely a combination of membrane and cytoplasmic/internalised IGF-1R in response to ligand. Co-staining with markers of specific sub-cellular locations would be required to confirm these differences.

The influence of IGF-1R inhibition on radio- and chemo-sensitivity in GBM cells was assessed. Previous work from our group and others showed that IGF-1R inhibition with small molecule inhibitors and antibodies directed towards IGF-1R can sensitise cancer cells to IR (Chitnis et al., 2014; Iwasa et al., 2009; Li et al., 2013; Turney et al., 2012). Our lab also demonstrated that IGF-1R inhibition sensitises melanoma cells to TMZ in a schedule-dependent manner, with the greatest sensitisation observed when IGF-1R is inhibited after treatment with TMZ (Ramcharan et al., 2015). In addition, in murine glioma stem cells, IGF-1R was found to confer radio-resistance in response to repeated irradiation (Osuka et al., 2013). Adult GBM cells were relatively radio-resistant, but co-treatment with IGF-1R inhibition and IR did not sensitise the cells to IR. The paediatric cell line KNS42 showed a similar response to adult cell lines when treated with IR alone, but there appeared to be a degree of radio-sensitisation when IGF-1R was inhibited 4 hr before IR or 24 hr after IR,

but not 24 hr before IR. The two highest DERs were seen in the 'IGF-1R inhibition 24 hr after IR' group: 3.11 and 3.71 at 5 Gy and 8 Gy respectively. At 4 Gy and above, the DERs were all greater than 1.3 for the '4 hr before' and '24 hr after' groups, indicating potentially meaningful radio-sensitisation, where DERs of >1.2 are proposed to represent a useful effect (Harrington et al., 2011). At 2 Gy, the greatest DER was 1.12, also observed in the '24 hr after' group. In addition, the absolute numbers of colonies were consistently and significantly lower when KNS42 cells were treated with both IR and BMS-754807 as opposed to IR alone. However, the biggest sensitisation effects were seen at doses above 2 Gy, the per fraction dose administered clinically, which questions the clinical relevance of the radio-sensitisation seen with these results. An interesting future experiment could involve treating KNS42 cells with repeat 2 Gy fractions with or without IGF-1R inhibition to test for sensitisation to fractionated IR.

The panel of GBM cell lines was also tested for response to chemotherapy. Paediatric SF-188 cells were relatively resistant to TMZ, whereas GaMG and KNS42 were relatively sensitive. KNS42 have previously been shown to harbour resistance to TMZ, which was reported to be due to a specific HOX gene expression signature (Gaspar et al., 2010), though this resistance was not observed here. In contrast to the radio-sensitisation seen in KNS42, no sensitisation was seen when combining IGF-1R inhibition with TMZ in any paediatric or adult GBM cell line, which also contrasted with the observed synergy between TMZ and IGF-1R inhibition in KNS42 cells reported by Bielen *et al.* (2011). However, in KNS42 but not GaMG cells, absolute colony numbers were again reduced when IGF-1R inhibition was combined with TMZ relative to when either treatment was used alone.

It was speculated that the apparent enhanced anti-proliferative effect (reduced colony counts above lower diameter threshold) of TMZ on KNS42 when combined with IGF-1R

inhibition may have been due to effects of IGF-1R on the cell cycle, independent of TMZ. In order to test how IGF-1R influences the cell cycle, *IGF1R* was silenced by siRNA to deplete IGF-1R protein and the cell cycles of KNS42 and GaMG were assessed. Compared with control-transfected cells, IGF-1R-depleted KNS42 cells had lower proportions of cells in S-phase and an accumulation of cells in G1 at both 48 hr and 96 hr post-transfection. IGF-1R-depleted GaMG cells had reduced proportions of S-phase cells at 48 hr, but the effects did not persist until 96 hr post-transfection, and there was no pattern of G1 accumulation. In considering differences between the two cell lines, it was noted that Western blotting of IGF-1R-depleted cells showed an increase in signal of a faster mobility (~90 kDa) band relative to ~95 kDa phospho-IGF-1R. This faster mobility band was more apparent in the GaMG cell line than KNS42, and was thought to represent phosphorylation of the INSR, which is also recognised by the phospho-IGF-1R antibody. The greater signal in GaMG than KNS42 suggests the presence of compensatory signalling in GaMG, but not in KNS42. This difference may possibly explain the greater effect seen in KNS42, compared with GaMG, on G1 accumulation and reduced clonogenicity caused by IGF-1R depletion and inhibition respectively. Reduced proliferation due to delayed cell cycle progression in KNS42 may also have occurred in the irradiation/IGF-1R inhibition combination experiments, but since sensitisation effects were observed in addition to reduced colony counts, it is possible that other mechanisms were at play beyond any effect of IGF-1R inhibition on cell cycle progression.

To assess the relative contributions of cell death and reduced proliferation to the radio-sensitisation seen when combining IGF-1R inhibition with IR in KNS42, it would have been beneficial to examine proliferation and apoptosis in response to single and combination treatments. Cleaved caspase 3 levels and pre-G1 DNA on flow cytometry could have been used to assess whether there was a greater increase in apoptosis in response to

combined IGF-1R inhibition and IR compared with either treatment alone, and cell cycle distributions from the same conditions could have been analysed in parallel. In addition, it would have been informative to assess how cell cycle distributions changed in response to BMS-754807 and BI-836845 compared with *IGF1R* siRNA. As seen when comparing the control-transfected with untransfected cells, the siRNA transfection procedure appeared to accelerate entry into the cell cycle.

Collectively, the results of this Chapter suggest that the IGF-1R may be a more important target in paediatric brain tumours than in adult brain tumours, and may contribute to the radio-resistance of paediatric GBM cells. However, IGF-1R inhibition did not appear to sensitise GBM cells to TMZ. The next steps were to investigate other possible mechanisms of chemo- and radio-resistance in GBM.

4 Chapter IV: Investigation of resistance to temozolomide in GBM

4.1 Introduction

Inhibition of IGF-1R showed some evidence of radio-sensitisation in a paediatric GBM cell line, but not in any adult GBM cell lines. In addition, IGF-1R inhibition did not sensitise any GBM cell lines to TMZ, suggesting that sensitisation to TMZ seen in melanoma cells when IGF-1R is inhibited (Ramcharan et al., 2015) did not extend to GBM cells. Since *MGMT* promoter methylation has been heavily linked to a better response of GBM patients to TMZ (Hegi et al., 2004; Hegi et al., 2005), the contribution of MGMT protein to TMZ resistance in GBM cells was assessed. However, *MGMT* methylation status does not always serve as a meaningful predictive marker of response to TMZ (Blanc et al., 2004). Therefore, it is possible that targets additional to MGMT may confer TMZ resistance in GBM cells, possibly as a result of the repeated exposure to TMZ through the course of chemotherapy. It was hypothesised that repeated exposure of GBM cells to TMZ could induce TMZ resistance in previously sensitive cells. Considering this idea, GBM cells were cultured in increasing concentrations of TMZ and their phenotype and molecular characteristics were assessed.

4.2 Results

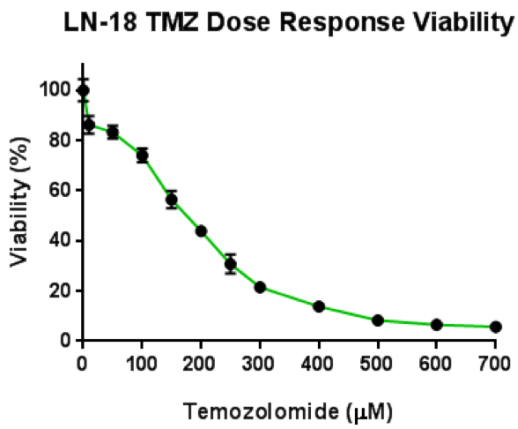
4.2.1 Characterisation of temozolomide resistance and the role of MGMT in GBM cell lines

The responses of adult and paediatric cell lines to TMZ were tested by viability or clonogenic assays. LN-18 was the most resistant cell line, and the paediatric cell line SF-188 was the next most resistant (Figure 4.1A, B). Comparing against other adult and paediatric GBM cell lines, these cells showed marked resistance to TMZ, with the concentration required to reduce survival by 50% (SF_{50}) being almost 10-fold higher in SF-188 than in the next most resistant cell line, GaMG, and the SF_{50} of LN-18 was double that of SF-188 (Figure 4.1C). The resistance to TMZ was found to directly correlate with MGMT protein levels (Figure 4.1D). LN-18 expressed the most MGMT protein, followed by SF-188. MGMT protein was not detected in U87-MG, DK-MG, GaMG, or KNS42.

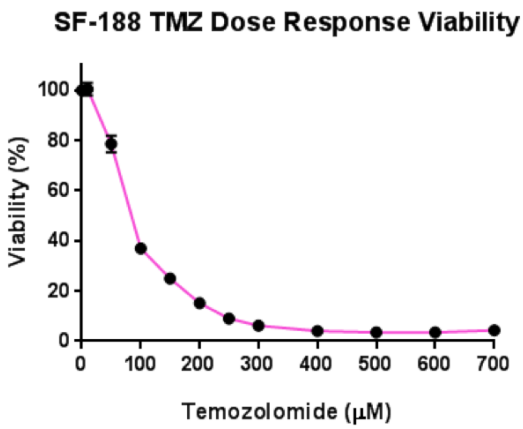
MGMT is a suicide enzyme that acts to stoichiometrically remove methyl adducts from guanine residues. Consequently, inhibition of MGMT can be achieved by a pseudosubstrate. O6-benzylguanine (O6BG) is a potent pseudosubstrate inhibitor of MGMT that can effectively decrease alkyltransferase activity of MGMT in human tumour cells to increase their sensitivity to DNA alkylating agents (Dolan et al., 1990). To test whether the expression of MGMT was responsible for TMZ resistance in LN-18 and SF-188, the cells were pre-incubated with O6BG in clonogenic and viability assay formats, and their responses to TMZ was assessed. Following pre-incubation with 20 μM O6BG, LN-18 cells showed a marked increase in sensitivity to TMZ, especially at higher concentrations (Figure 4.2A). This sensitisation was also seen in viability assay format, where the change in sensitisation was related to the O6BG concentration used (Figure 4.2B). SF-188 showed a similar pattern of sensitisation to LN-18 in both clonogenic (Figure 4.2C) and viability

assays (Figure 4.2D). For both cell lines, the SF_{50} value decreased to below 10 μM TMZ in the presence of 20 μM O6BG in viability assays. These results suggest that the basal resistance to TMZ in LN-18 and SF-188 was mainly attributable to MGMT expression, and that direct inhibition of MGMT reverses the resistant phenotype almost entirely. This highlights the rationale for targeting MGMT in GBM therapy to sensitise patient tumours to TMZ.

A



B



C

Cell Line	TMZ SF_{50} (μM) + 95% CI
LN-18	163.7 (151.4-177.0)
SF-188	81.4 (74.7-88.8)
GaMG	8.8 (7.8-10.0)
KNS42	3.8 (3.0-5.0)

D

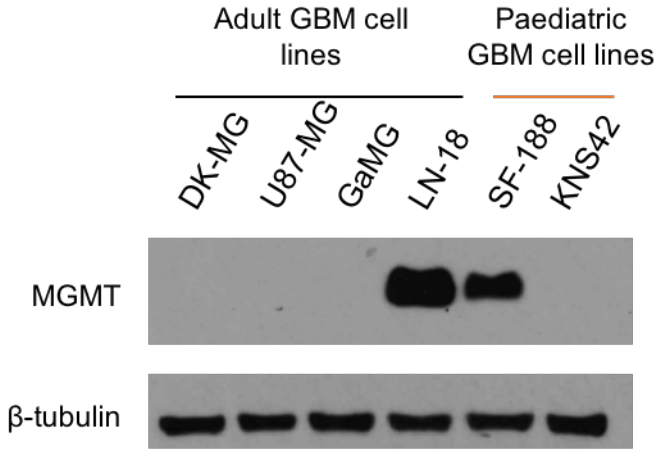
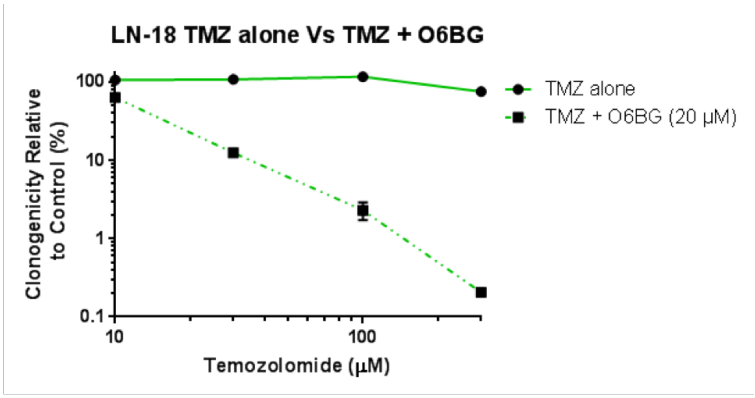


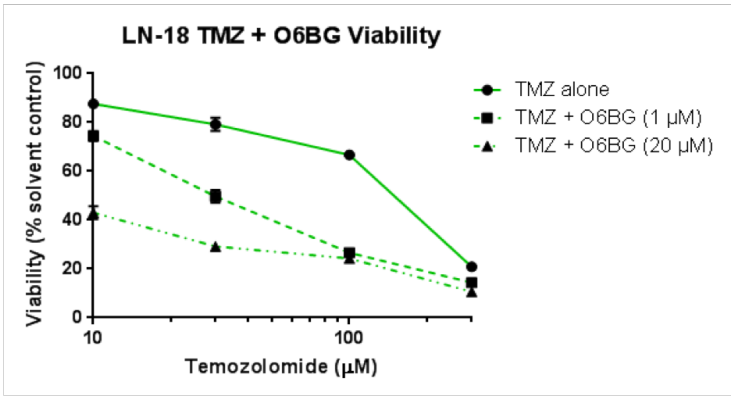
Figure 4.1: Basal sensitivities of GBM cell lines to TMZ. A) LN-18 cells were seeded into 96-well plates and treated in triplicate with a range of doses of TMZ the following day. Viability of cells was tested six days after seeding. B) SF-188 cells were seeded and treated as in A. Points are means ± SEM of triplicates representative of two independent experiments. C) TMZ SF_{50} values for four GBM cell lines. Values were interpolated from dose responses in GraphPad Prism 6.0 using the one phase decay model to fit the raw data. The SF_{50} for GaMG was calculated from results presented in a later graph (Figure 4.4). The SF_{50} value for KNS42 was calculated from clonogenic experiments reported in Chapter 3 (Figure 3.23). D) Part of Western blot displayed in Figure 3.10, showing the MGMT protein expression status of GBM cell lines.

A



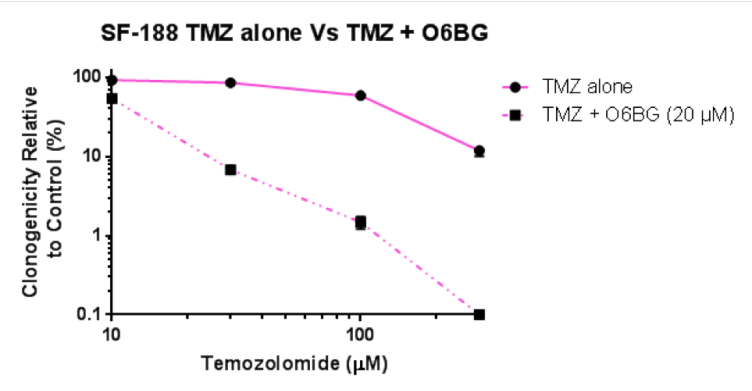
LN-18 Condition	TMZ SF_{50} (µM)
TMZ Alone	>300
TMZ + O6BG (20 µM)	12.8

B



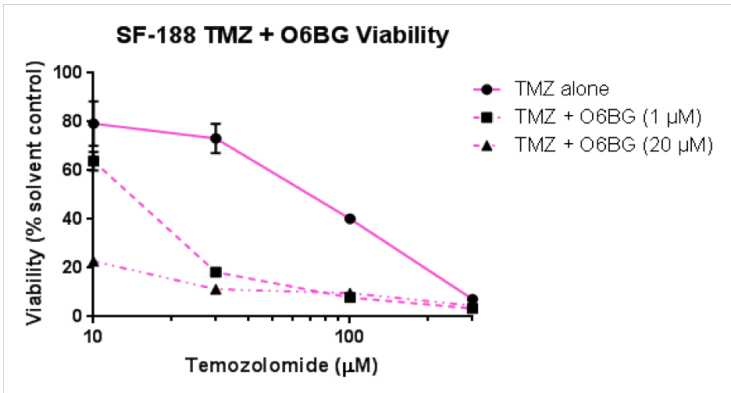
LN-18 Condition	TMZ SF_{50} (µM)
TMZ Alone	170.6
TMZ + O6BG (1 µM)	33.2
TMZ + O6BG (20 µM)	<10

C



SF-188 Condition	TMZ SF_{50} (µM)
TMZ Alone	128.3
TMZ + O6BG (20 µM)	10.6

D



SF-188 Condition	TMZ SF_{50} (µM)
TMZ Alone	75.6
TMZ + O6BG (1 µM)	13.6
TMZ + O6BG (20 µM)	<10

Figure 4.2: Combination of TMZ and O6BG in TMZ resistant cell lines. Cells were seeded into viability or clonogenic assays and incubated overnight. O6BG was added to the culture medium and cells were incubated for a further 2 hr. TMZ was then added to the culture medium and plates were incubated for 6 days for viability assays, and clonogenics for 11 days for LN-18, and 8 days for SF-188. A) Dose response of LN-18 to TMZ ± O6BG in clonogenic format. B) Dose response of LN-18 to TMZ ± O6BG in viability format. C) Dose response of SF-188 to TMZ ± O6BG in clonogenic format. D) Dose response of SF-188 to TMZ ± O6BG in viability format. Upper panels show the dose responses to TMZ for each condition, lower panels show the SF_{50} values calculated for each condition.

4.2.2 Generation and characterisation of cell lines with acquired temozolomide resistance

Several clinical trials have examined the effects of direct inhibition of MGMT in combination with TMZ therapy on patient survival. Despite promising preclinical results and phase I trials (Quinn et al., 2009b; Warren et al., 2005), the use of O6BG analogues in combination with TMZ in phase II trials did not significantly improve patient survival in adult or paediatric GBM patients (Quinn et al., 2009a; Warren et al., 2012). This suggests an important need for other agents that are able to sensitise GBM cells to TMZ. However, in order to best test the potential of other chemical inhibitors to sensitise GBM cells to TMZ, along with MGMT proficient cells, a model is required in which resistance to TMZ is not dependent upon the expression of MGMT.

It has been shown that introducing TMZ into cell culture medium can induce acquired resistance to TMZ in GBM cells, albeit through upregulation of MGMT expression (Kohsaka et al., 2012). In addition, patients undergo repeated dosing with TMZ during chemotherapy. To investigate whether MGMT upregulation occurs universally, and observe the effects of repeated TMZ exposure on GBM cells, the relatively TMZ-sensitive cell line GaMG was passaged with repeated doses of TMZ, increasing in concentration (Figure 4.3). Doses were increased by half log values to beyond the ~20 μM calculated to be clinically achievable in cerebrospinal fluid: clinical circulation Cmax of 60 μM, and cerebrospinal fluid has ~33% of the circulation levels (Agarwala and Kirkwood, 2000; Middleton et al., 2000). At 100 μM and 300 μM, TMZ concentrations were increased no further and cells were continually passaged with a single dose of these concentrations added at each new passage (every 6-7 days), generating the GaMG TMZ 100 and GaMG TMZ 300 sublines (Figure 4.3). It was unlikely that there was accumulation of TMZ above the intended concentrations because the half-life of TMZ is very short in aqueous solution (1.8 hr).

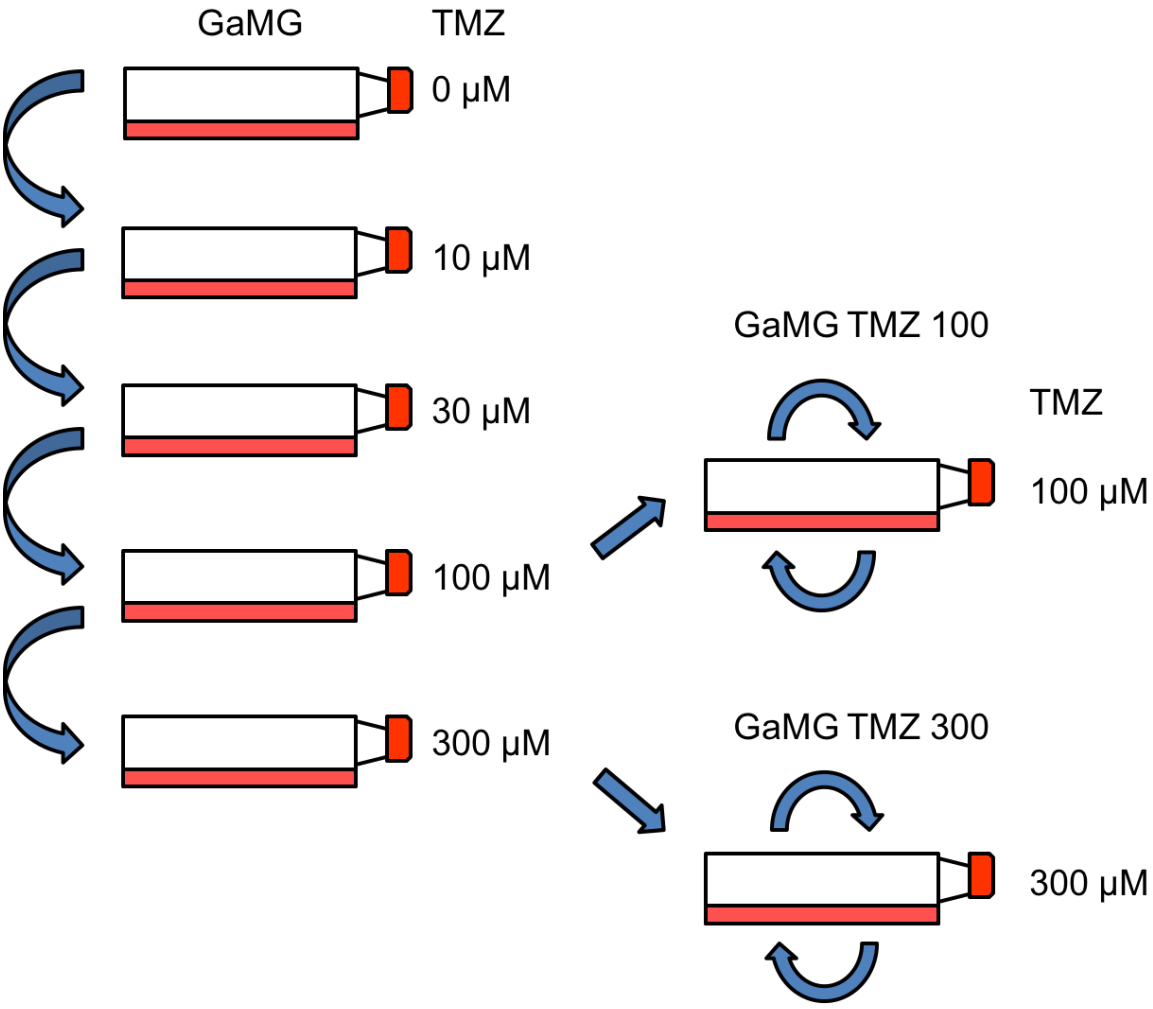
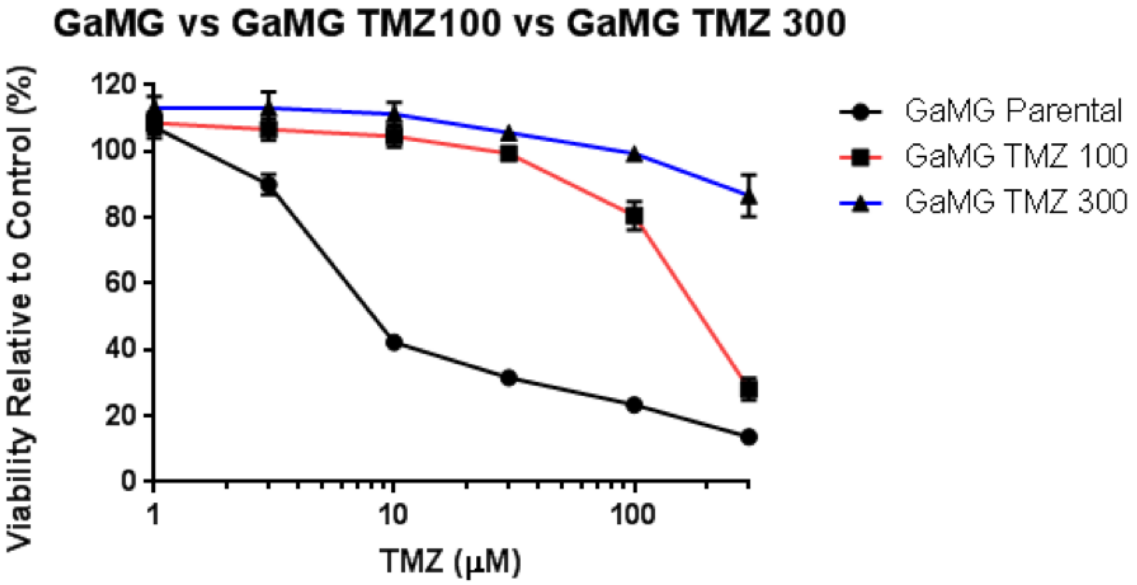


Figure 4.3: Schematic of generation of TMZ resistant GaMG cells. Cells were passaged with increasing doses of TMZ added to the culture medium. For details, see section 2.6.1.

To test whether TMZ resistance had been acquired by these GaMG cells, the viability of GaMG TMZ 100, GaMG TMZ 300, and GaMG parental cells was tested following incubation with TMZ. GaMG parental cells showed a sensitive phenotype, with a large reduction in viability at 10 μM TMZ and an SF_{50} value of 8.8 μM, whereas both GaMG TMZ 100 and GaMG TMZ 300 showed clear resistance to TMZ at these concentrations (Figure 4.4). The SF_{50} values for GaMG TMZ 100 and GaMG TMZ 300 were 215 μM and >300 μM respectively. Both GaMG TMZ sublines showed statistically significant increased viability relative to the GaMG parental cell line from 3-300 μM TMZ (Table 4.1). Interestingly, at the 100 μM and 300 μM TMZ concentrations, there were statistically significant differences between the viabilities of GaMG TMZ 100 and GaMG TMZ 300, with GaMG TMZ 300 maintaining relatively higher viability at these concentrations (Table 4.1, Figure 4.4). These results show that the GaMG TMZ 100 and GaMG TMZ 300 sublines acquired resistance to TMZ, and that the extent of resistance depended upon the concentration of TMZ that the cells were repeatedly exposed to.

In addition to the TMZ resistant phenotype, the GaMG TMZ 300 subline exhibited noticeably different growth characteristics during routine culture. When assayed for viability in the absence of TMZ, it was observed that these cells had a statistically significant lower basal viability relative to GaMG and GaMG TMZ 100 (Figure 4.5A). This could suggest that they proliferated more slowly, or had reduced metabolic activity or both. Observation under the microscope showed a less regular morphology of the GaMG TMZ 300 cells compared with GaMG and GaMG TMZ 100, which were indistinguishable in culture (Figure 4.5B). This may either indicate a different mechanism of resistance in GaMG TMZ 300 to GaMG TMZ 100, or that the damage from the higher concentration of TMZ took longer to repair, which may have influenced the cells' metabolism and/or proliferation.



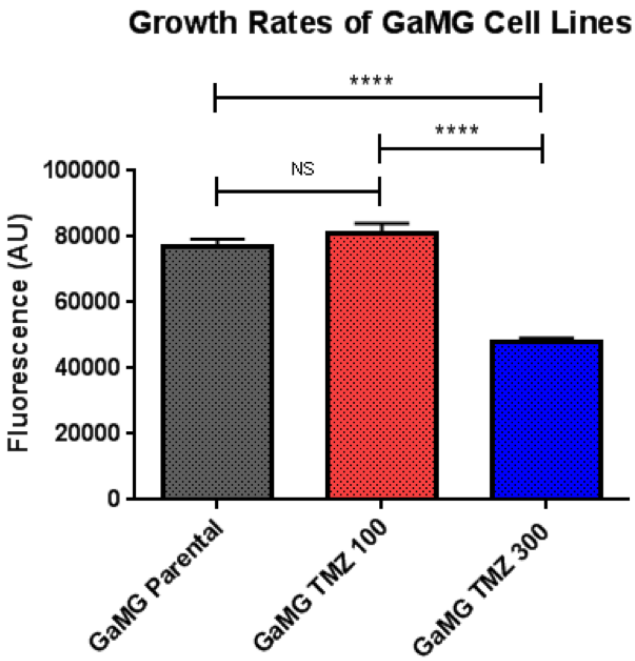
Cell Line	TMZ SF_{50} (µM)
GaMG	8.8
GaMG TMZ 100	214.9
GaMG TMZ 300	>300

Figure 4.4: TMZ dose response of GaMG and TMZ-resistant GaMG sublines. GaMG, GaMG TMZ 100, and GaMG TMZ 300 cells were seeded into 96-well plates and incubated overnight. Triplicate wells were treated the following day with a range of TMZ concentrations. Viability of cells was tested after 7 days. The upper panel shows the dose response of each cell line to the same concentration range of TMZ. The lower panel shows TMZ SF_{50} values for the parental GaMG and TMZ-resistant GaMG sublines. Points are means ± SEM of pooled triplicate values from three independent experiments (six independent experiments for GaMG parental).

Table 4.1: Statistical testing of the TMZ dose response of GaMG, GaMG TMZ 100, and GaMG TMZ 300. Results from Figure 4.4 were analysed by two-way ANOVA (**p < 0.01; ***p < 0.001; ****p < 0.0001).

Tukey's multiple comparisons test	Significant?	Summary
0 µM		
GaMG Parental vs. GaMG TMZ 100	No	ns
GaMG Parental vs. GaMG TMZ 300	No	ns
GaMG TMZ 100 vs. GaMG TMZ 300	No	ns
1 µM		
GaMG Parental vs. GaMG TMZ 100	No	ns
GaMG Parental vs. GaMG TMZ 300	No	ns
GaMG TMZ 100 vs. GaMG TMZ 300	No	ns
3 µM		
GaMG Parental vs. GaMG TMZ 100	Yes	***
GaMG Parental vs. GaMG TMZ 300	Yes	****
GaMG TMZ 100 vs. GaMG TMZ 300	No	ns
10 µM		
GaMG Parental vs. GaMG TMZ 100	Yes	****
GaMG Parental vs. GaMG TMZ 300	Yes	****
GaMG TMZ 100 vs. GaMG TMZ 300	No	ns
30 µM		
GaMG Parental vs. GaMG TMZ 100	Yes	****
GaMG Parental vs. GaMG TMZ 300	Yes	****
GaMG TMZ 100 vs. GaMG TMZ 300	No	ns
100 µM		
GaMG Parental vs. GaMG TMZ 100	Yes	****
GaMG Parental vs. GaMG TMZ 300	Yes	****
GaMG TMZ 100 vs. GaMG TMZ 300	Yes	***
300 µM		
GaMG Parental vs. GaMG TMZ 100	Yes	**
GaMG Parental vs. GaMG TMZ 300	Yes	****
GaMG TMZ 100 vs. GaMG TMZ 300	Yes	****

A



B

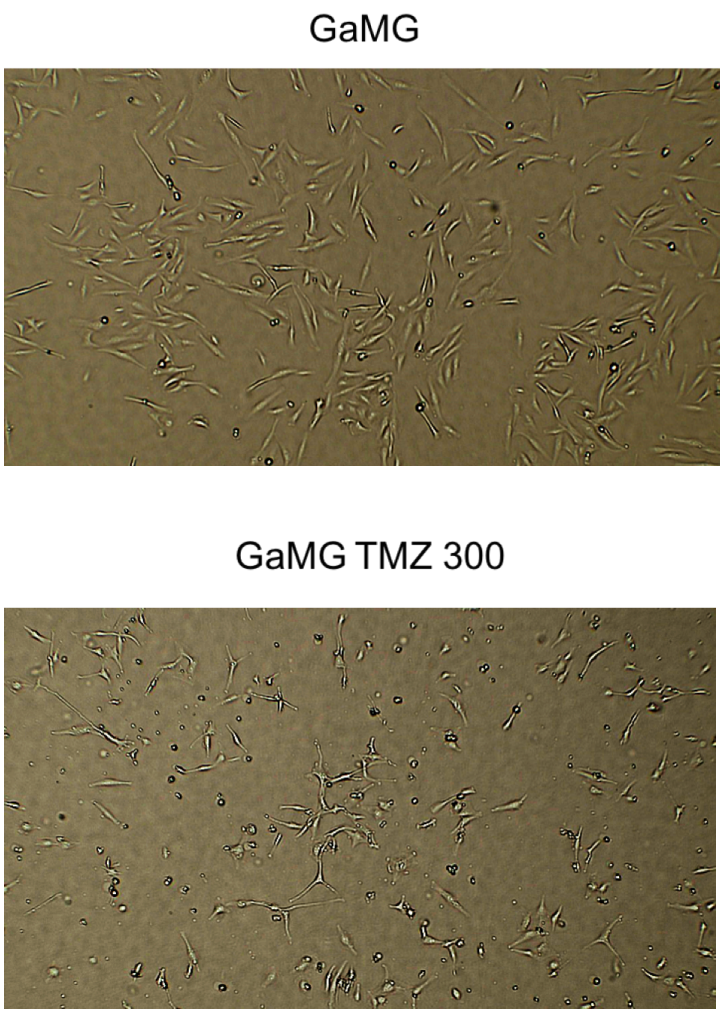


Figure 4.5: Growth properties of GaMG and GaMG sublines. A) Viability values after incubation for 7 days in the absence of TMZ. The same number of cells was seeded into each well. Values are derived from experiments presented in Figure 4.4 and represent mean ± SEM of pooled triplicate data from three independent experiments. Means were tested for statistically significant differences by one-way ANOVA (****$p < 0.0001$). B) Images of GaMG parental cell line (upper) and GaMG TMZ 300 subline (lower) during routine culture. Cells were visualised with a Motic AE2000 inverted microscope and photographs were taken with a Deltapix microscope camera.

To begin investigating the extent to which MGMT was responsible for these cells' resistance to TMZ, the next experiment assessed whether the GaMG TMZ sublines had upregulated expression of MGMT relative to parental GaMG. In concurrence with previous experiments, MGMT protein was not detected in GaMG parental cells, however, GaMG TMZ 100 had clear upregulation of MGMT, although the signal was not as strong as in LN-18 cells, which have high basal MGMT expression (Figure 4.6A). Conversely, MGMT was not detected in GaMG TMZ 300 cells, suggesting non-MGMT-mediated acquired resistance to TMZ.

It has been reported previously that signalling through the PI3K-AKT and Mek-Erk pathways can lead to upregulation of MGMT expression (He et al., 2015; Zhang et al., 2015). In light of this, and in keeping with earlier experiments, the IGF-1R and EGFR RTK axes were examined and compared in GaMG and its TMZ-resistant sublines to search for any indication of relatively increased or decreased signalling. Other than a possible increase in phospho-EGFR in GaMG TMZ 100, no major differences in signalling were found when examining representatives of both the PI3K-AKT and Mek-Erk pathways in all three sublines (Figure 4.6B).

Collectively, these results demonstrate that repeated exposure to TMZ, as is intended to be the case in the clinical setting, was capable of inducing acquired resistance and/or select for resistant subpopulations of GBM cells, even at doses higher than those achieved clinically. In addition, different degrees of TMZ resistance were achieved, which appeared to be concentration-dependent. Furthermore, chronic treatment with TMZ induced changes in growth characteristics in GBM cells and upregulated the direct repair protein MGMT. However, GaMG TMZ 300 cells did not show detectable MGMT, suggesting potential different mechanisms of resistance even in cells of the same origin.

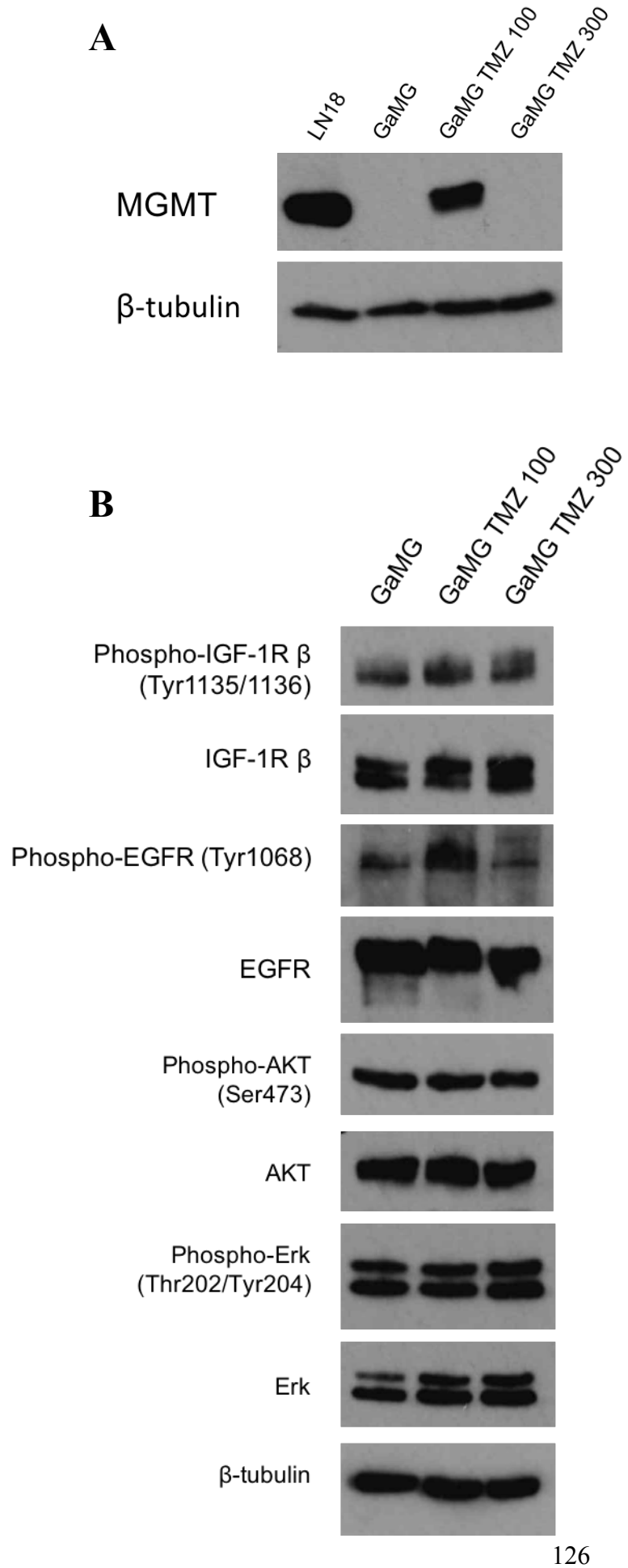


Figure 4.6: Characterisation of MGMT protein expression and RTK signalling axes in GaMG and GaMG sublines. Protein was extracted from thawed cell pellets and whole cell lysates were analysed by Western blotting. A) MGMT protein expression status of GaMG, GaMG TMZ 100, and GaMG TMZ 300. LN-18 was loaded as a positive control for MGMT protein detection. B) Expression and basal phosphorylation of key signalling components in the IGF-1R and EGFR signalling axes.

4.2.3 Effect of temozolomide on GaMG and GaMG sublines

GaMG TMZ 100 and GaMG TMZ 300 sustained high levels of viability relative to their parental cell line when treated with TMZ. To distinguish whether this difference was due to death of GaMG cells, arrested cell cycles and/or metabolic changes, GaMG and its TMZ-resistant sublines were treated with TMZ at 100 μM or 300 μM and examined at three time points for the extent of cell death. Analysing two separate markers of apoptosis, cleaved caspase 3 (CC3) and cleaved PARP, confirmed that GaMG cells underwent apoptosis more readily in response to TMZ than did GaMG TMZ 100 or GaMG TMZ 300 (Figure 4.7). Signals for CC3 and cleaved PARP in GaMG were evident three days after treatment with 100 μM TMZ, increased after four days, and were stronger and appeared sooner in cells that were treated with 300 μM, demonstrating that the extent of apoptosis was a property of the TMZ concentration with which the cells were treated (Figure 4.7A). Interestingly, for GaMG TMZ 100 cells, only 300 μM TMZ induced clear CC3 and cleaved PARP signal, showing that 100 μM was not enough to cause apoptosis in these cells (Figure 4.7B). This result confirmed their resistance to 100 μM but not 300 μM TMZ, mirroring the result of the viability assays (Figure 4.4). No induction of CC3 or cleaved PARP signal was detected in GaMG TMZ 300 cells at any time point or TMZ concentration (Figure 4.7C), consistent with their resistance to TMZ up to 300 μM.

MGMT was again not detected in GaMG or GaMG TMZ 300 in these experiments, but was detected in GaMG TMZ 100 and LN-18 controls. At day 2 in GaMG TMZ 100 cells treated with 100 μM TMZ, MGMT signal had decreased relative to untreated cells, but was restored by day 4 (Figure 4.7B). MGMT was also reduced to a greater extent by treatment with 300 μM TMZ than with 100 μM TMZ at each time point. The recovery of MGMT signal in the '100 μM, day 4' condition, and lower signal in 300 μM-treated cells suggests

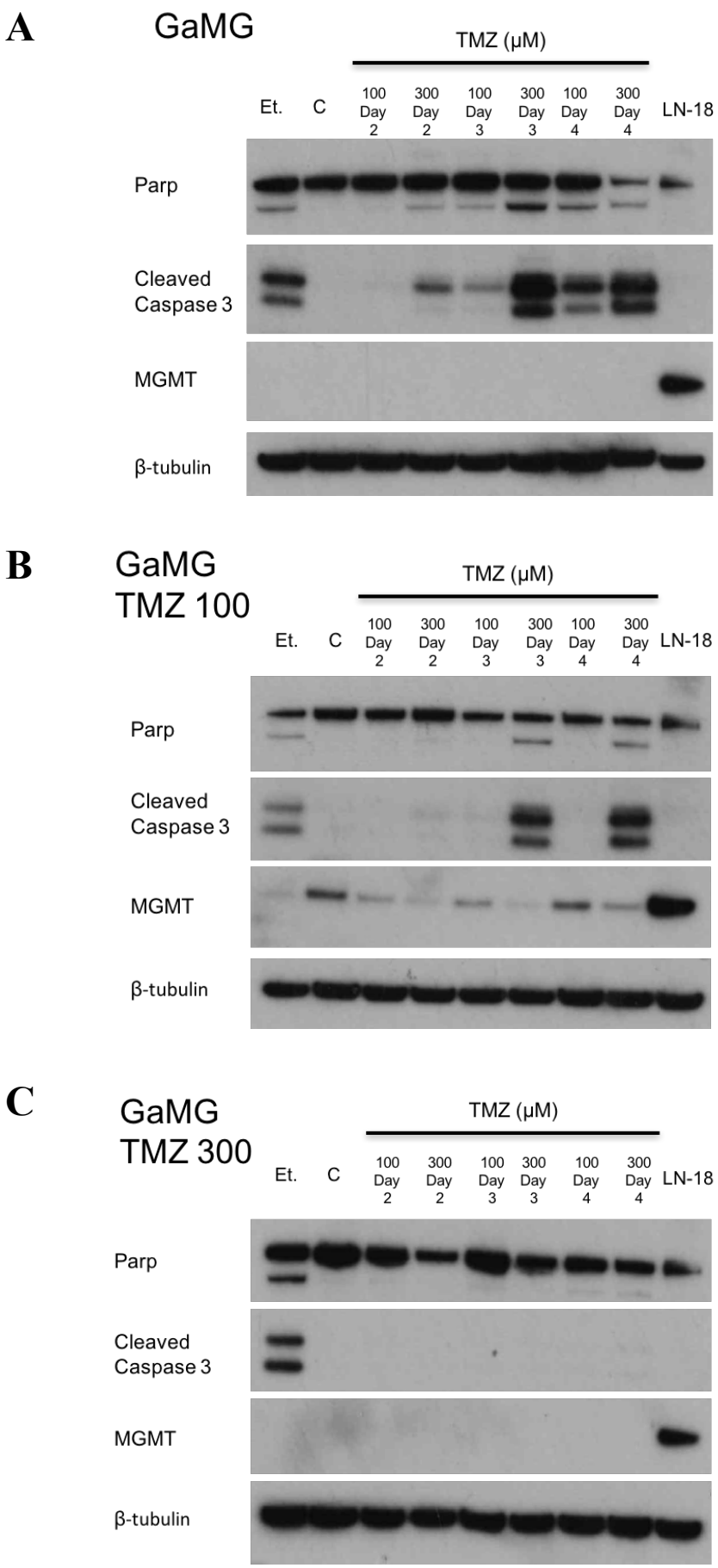


Figure 4.7: Assessment of TMZ-induced apoptosis on GaMG and GaMG sublines. Cells were seeded into 10 cm plates (500,000 cells/plate for GaMG, 300,000 cells/plate for sublines) and incubated overnight. TMZ (100 μM or 300 μM), DMSO control, or etoposide positive control for cell death (10 μM) treatments were added to the culture medium the following day and cells were incubated for various time points before harvesting and freezing cell pellets. Etoposide and DMSO controls were incubated for 48 hr before collection. Protein was extracted from thawed cell pellets and whole cell lysates were Western blotted for markers of cell death and MGMT, for which LN-18 lysates were loaded as a positive control. Assessment of cell death of A) parental GaMG cells, B) GaMG TMZ 100 cells, C) GaMG TMZ 300 cells. Blots represent one of two independent experiments.

that MGMT was stoichiometrically depleted as it removed the methyl adducts on guanine residues and was consequently degraded. The recovery at day 4 may have been the result of transcription and translation of new MGMT protein. However, the lack of recovery in 300 μM-treated cells suggests the possibility that the MGMT pool in GaMG TMZ 100 was enough to repair potential DNA damage induced by 100 μM TMZ, but not adequate to repair the damage caused by 300 μM.

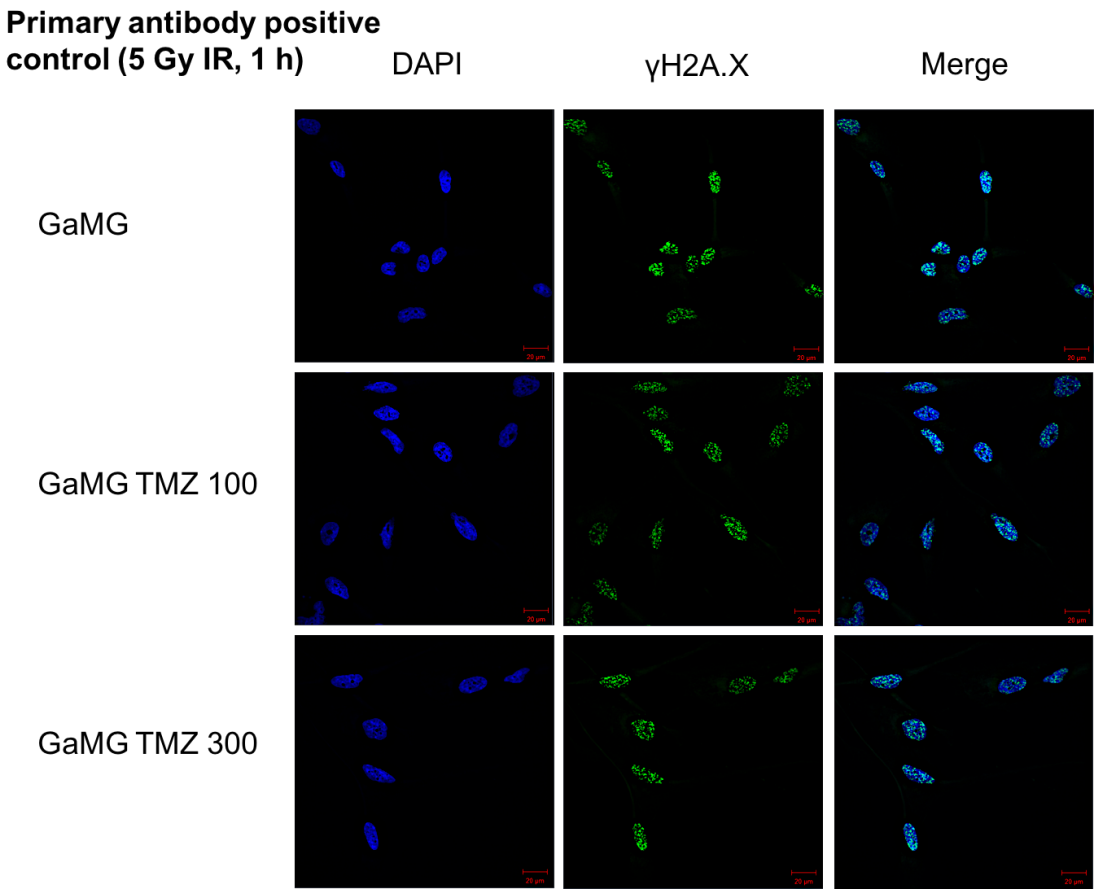
To begin investigation of how TMZ-induced apoptosis was resisted in GaMG TMZ 100 and GaMG TMZ 300 cells, the next experiment assessed DNA damage induced by TMZ in these cells. At several time points after treatment with 100 μM TMZ, GaMG, GaMG TMZ 100, and GaMG TMZ 300 were fixed and stained for phosphorylated histone H2A.X (γH2A.X), a marker of DNA DSBs (Furuta et al., 2003; Paull et al., 2000; Rogakou et al., 1998). As a positive control, cells were subjected to 5 Gy IR, and after 1 hr, clear γH2A.X foci were seen (Figure 4.8A). No foci were seen in the 'no primary antibody' negative control (Figure 4.8B). Without TMZ treatment, all three GaMG lines had very little γH2A.X staining, but GaMG TMZ 300 had the highest basal signal (Figure 4.8C). After one day's treatment with 100 μM TMZ, γH2A.X foci were visible in all three sublines, with an increase on days two and three in GaMG parental cells. In contrast, there was a clear reduction in γH2A.X signal in GaMG TMZ 100 and GaMG TMZ 300 cells on days 2 and 3 (Figure 4.8D-F). At 4-5 days after TMZ treatment, there were fewer parental GaMG cells relative to the TMZ-resistant sublines, as they underwent apoptosis (Figure 4.8G-H). GaMG TMZ-resistant sublines showed very little γH2A.X signal from day 2 onward, which was likely the result of basal DNA damage.

These results suggest that there was reduced DNA damage in response to 100 μM TMZ in TMZ-resistant GaMG sublines. This could be because less DNA damage was induced, and/or the cells were able to more quickly resolve the induced DNA damage, which

likely accounted for the lack of apoptosis observed in response to 100 μM TMZ (Figure 4.7). Conversely, TMZ induced a large amount of DNA DSBs in parental GaMG cells, and these were not resolved, but accumulated with time. This too correlated with the apoptosis seen in Western blotting at similar time points (Figure 4.7A).

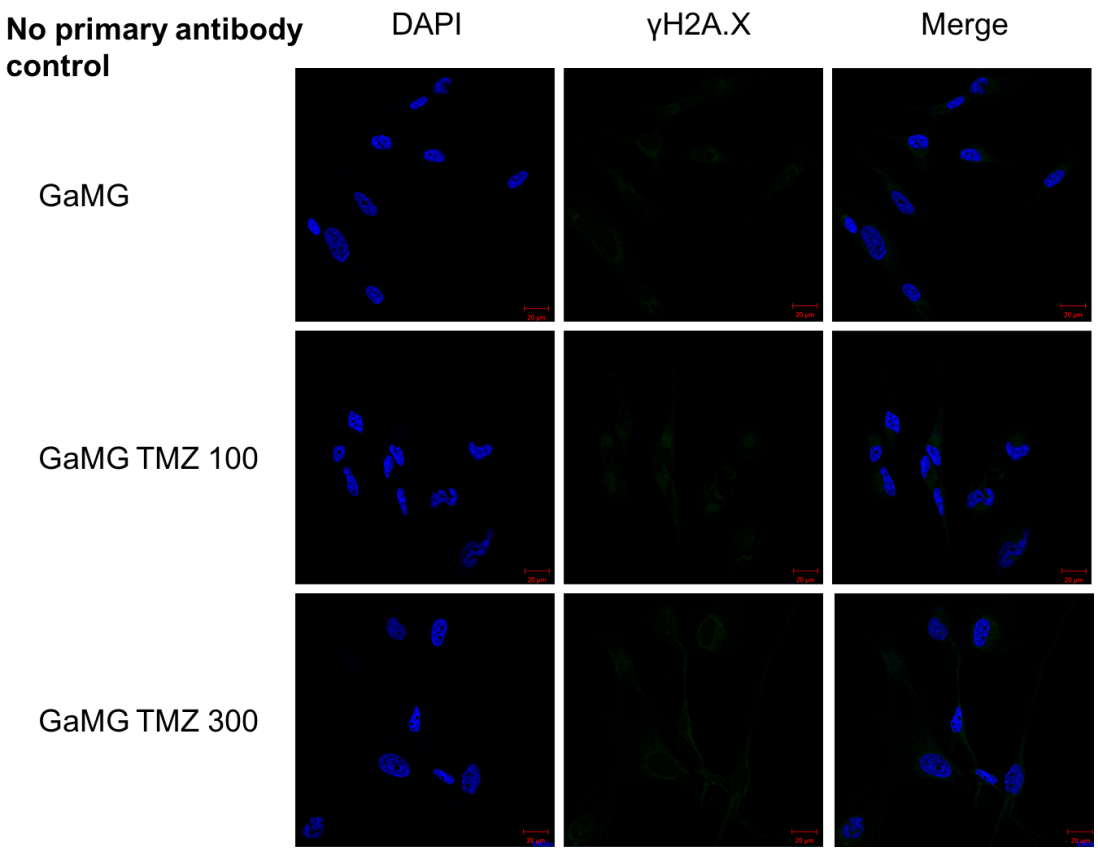
A

Primary antibody positive control (5 Gy IR, 1 h)

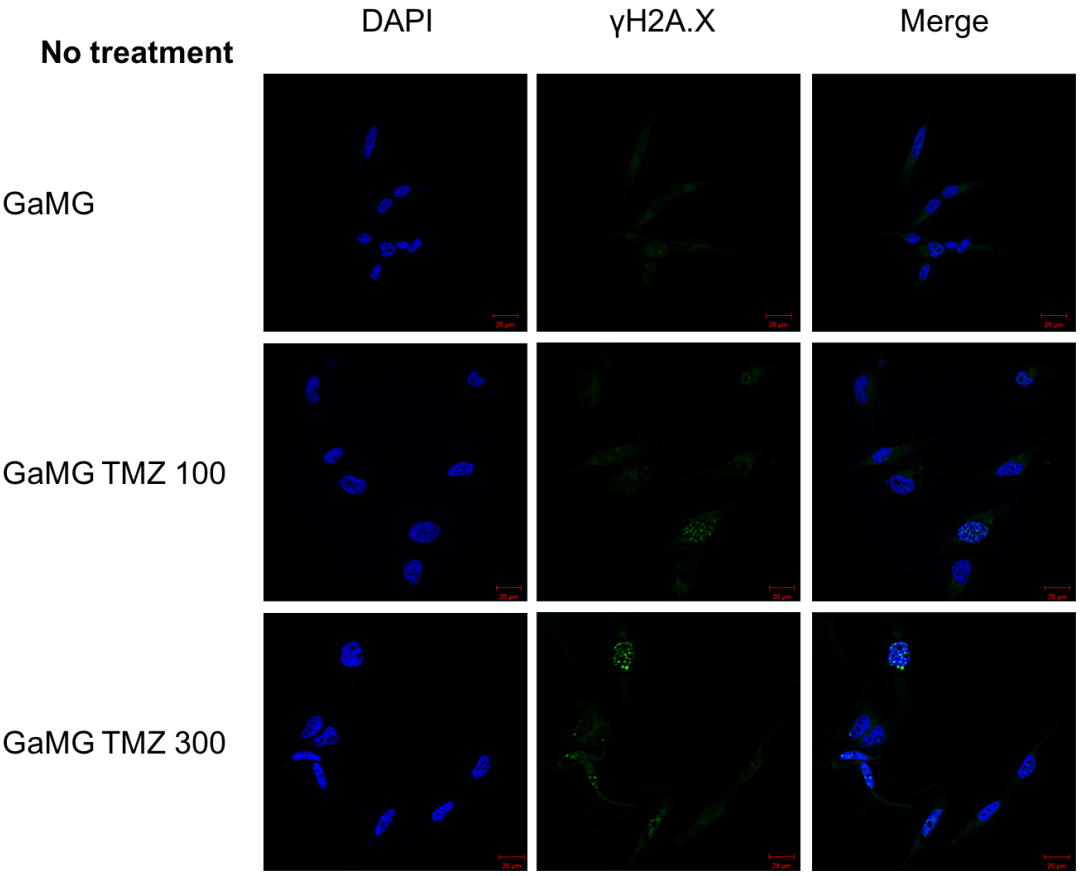


B

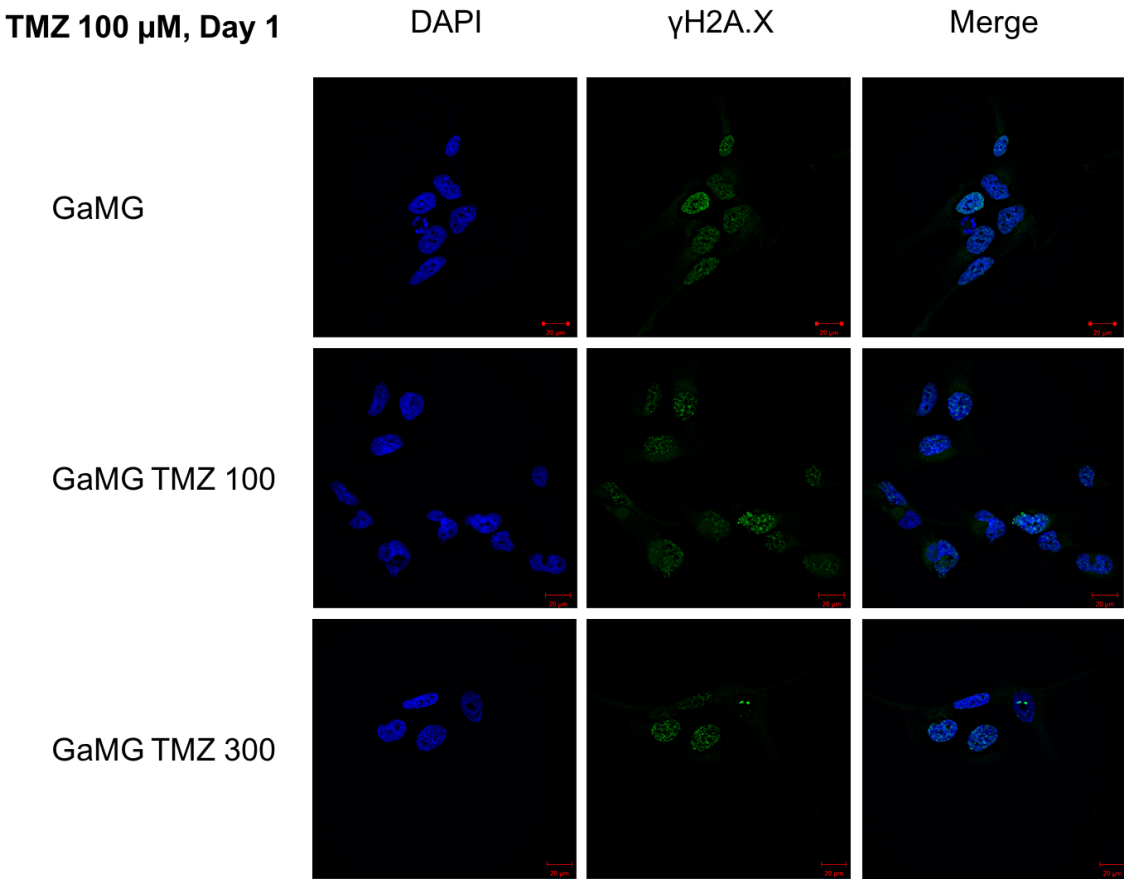
No primary antibody control

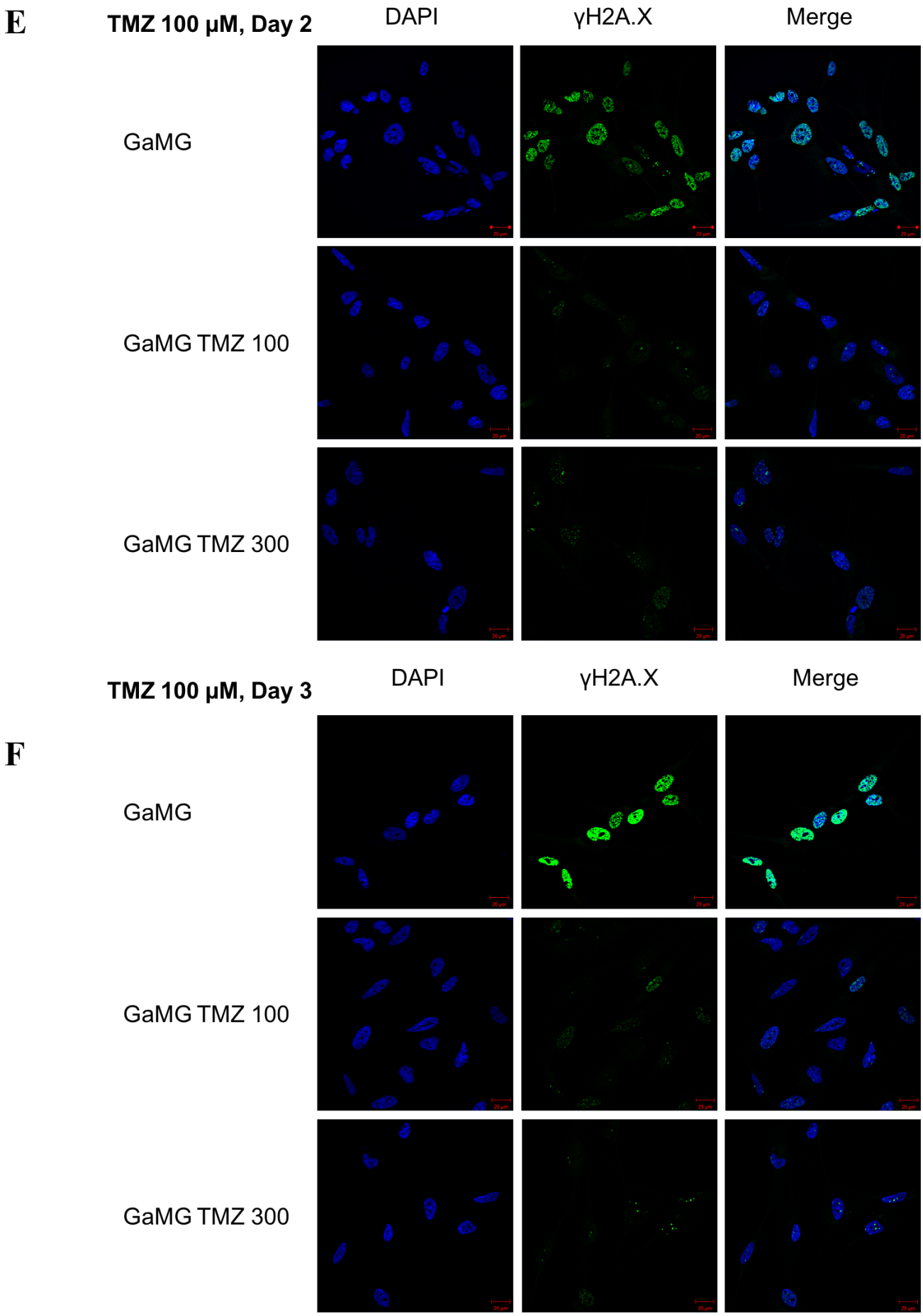


C


No treatment
DAPI
γH2A.X
Merge
GaMG
GaMG TMZ 100
GaMG TMZ 300

D


TMZ 100 µM, Day 1
DAPI
γH2A.X
Merge
GaMG
GaMG TMZ 100
GaMG TMZ 300


E
TMZ 100 µM, Day 2
DAPI
γH2A.X
Merge
GaMG
GaMG TMZ 100
GaMG TMZ 300
TMZ 100 µM, Day 3
DAPI
γH2A.X
Merge
F
GaMG
GaMG TMZ 100
GaMG TMZ 300

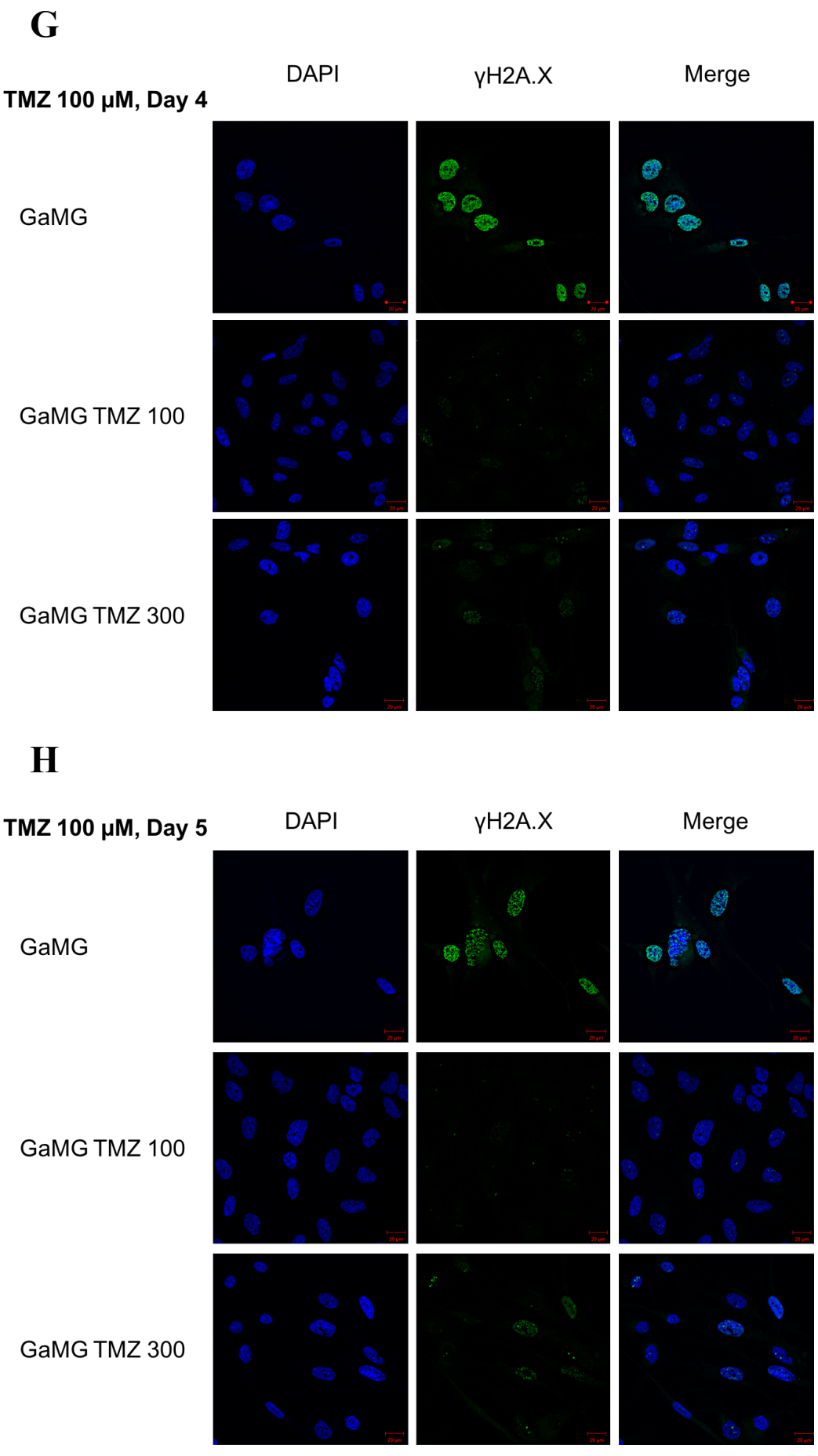


Figure 4.8: γH2A.X induction and resolution in GaMG and GaMG sublines in response to TMZ. GaMG, GaMG TMZ 100, or GaMG TMZ 300 cells were seeded onto coverslips in 6-well plates and incubated overnight. TMZ (100 µM) or DMSO solvent control was added to the culture medium the following day and plates were incubated for 1-5 days after TMZ treatment before fixation and staining with γH2A.X primary antibody and Alexa Fluor® 488 secondary antibody. For a positive control for the primary antibody, wells of cells were irradiated with 5 Gy and fixed 1 hr later. Included for a negative control were cells that were not incubated with primary antibody. A) γH2A.X staining of cells that received 5 Gy IR and fixed after 1 hr. B) Cells that were not incubated with primary antibody. C) γH2A.X staining of cells that received no treatment (DMSO solvent). Fixed at day 2. D-H) γH2A.X staining of cells after treatment with TMZ: 1 day (D), 2 days (E), 3 days (F), 4 days (G), and 5 days (H). DNA was counterstained with DAPI. Cells and immunofluorescence signal were imaged with a Zeiss LSM 710 Observer Z1 confocal microscope. Scale bars represent 20 µm. Original magnification x40.

4.2.4 Effect of O6BG on the sensitivity of GaMG sublines to temozolomide

To investigate whether the reduction in DNA damage and apoptosis in GaMG TMZ 100 cells was the result of direct repair by upregulated MGMT, GaMG TMZ 100, along with GaMG TMZ 300 cells, and LN-18 cells as a positive control, were treated with TMZ after pre-incubation with O6BG as in previous experiments (Section 4.2.1; Figure 4.2). Pre-incubation with O6BG again sensitised LN-18 cells to a range of doses of TMZ in a concentration-dependent manner (Figure 4.9A). In contrast to LN-18 cells, which highly express MGMT, pre-incubation with O6BG at 1 μM or 20 μM did not sensitise GaMG TMZ 100 cells to TMZ, despite their upregulation of MGMT (Figure 4.9B). The response of GaMG TMZ 300 cells to TMZ was also unaffected by the addition of O6BG (Figure 4.9C). These results indicate that despite upregulation of MGMT and its apparent depletion upon addition of TMZ, MGMT alone was not responsible for the resistance of GaMG TMZ 100 cells to TMZ, and that other, additional resistance mechanisms had likely become established.

Together, these experiments confirm that continuous exposure to TMZ can induce acquired TMZ resistance in GBM cells, and validate the establishment of two models that are resistant to different concentrations of TMZ through mechanisms that are independent of MGMT-mediated repair.

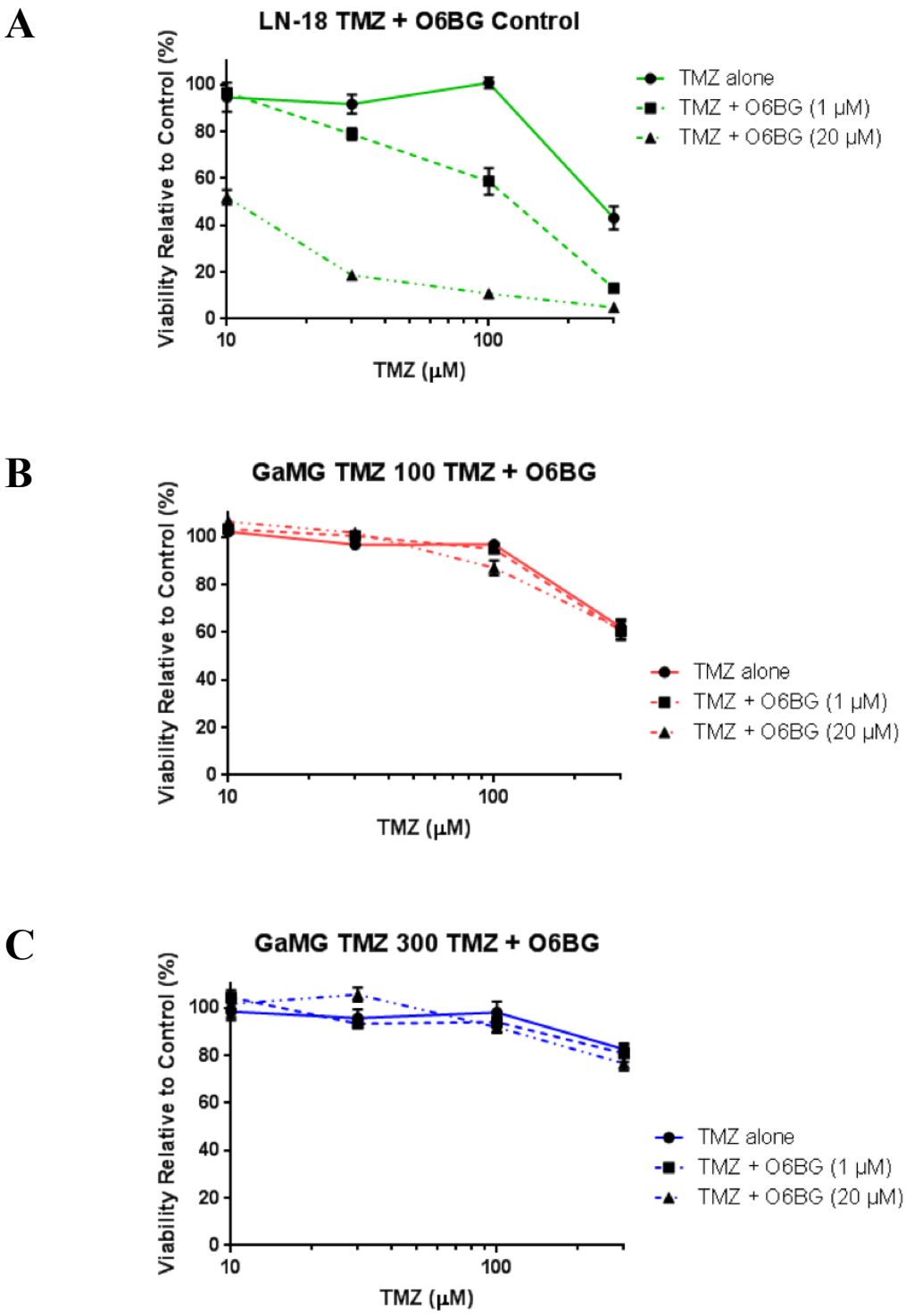


Figure 4.9: Effect of O6BG on the TMZ sensitivity of GaMG sublines. Cells were seeded into 96-well plates (2,000 cells/well) and incubated overnight. O6BG or solvent was added to the culture medium and cells were incubated for a further 2 hr. Different TMZ concentrations were then added to the culture medium in triplicate and cells were incubated for 6 days, then assayed for viability by CellTiter-Blue®. A) TMZ dose response of control cell line LN-18 with or without addition of O6BG. B) TMZ dose response of GaMG TMZ 100 with or without addition of O6BG. C) TMZ dose response of GaMG TMZ 300 with or without O6BG. Points are means ± SEM and represent pooled triplicate data from three independent experiments.

4.3 Discussion

Direct repair of the cytotoxic *O6*-MeG adducts resulting from TMZ is afforded by the activity of MGMT, which removes alkyl adducts to restore guanine and provides the simplest TMZ resistance mechanism (Zhang et al., 2012). It is well known that unmethylated *MGMT* promoters in the tumours of GBM patients and MGMT expression in GBM cells *in vitro* bestow relative resistance to the cytotoxic effects of TMZ (Hegi et al., 2005; Zhang et al., 2012). The intrinsic resistance to TMZ of the GBM cell lines used in this study strongly correlated with MGMT expression status. Pre-inhibition of MGMT with the pseudosubstrate O6BG restored TMZ sensitivity in these cells, which was consistent with previous studies (Wedge et al., 1996a; Wedge et al., 1996b). O6BG has even been found to sensitise xenografts of GBM cells with low MGMT activity to TMZ (Wedge and Newlands, 1996). Despite promising preclinical results, the combination of TMZ and O6BG analogues has been disappointing in the clinical trial setting (Quinn et al., 2009a; Warren et al., 2012). Therefore, it is likely that other targets mediate TMZ resistance, and their inhibition may potentiate the effects of TMZ in GBM. In order to identify new targets, it was decided to establish GBM cell models whose TMZ resistance did not depend on expression of MGMT.

Experiments in this study demonstrated the successful establishment of TMZ-resistant GBM cell sublines from previously sensitive cell lines. Assays for viability and apoptosis confirmed that GaMG TMZ 100 and GaMG TMZ 300 were resistant to TMZ up to 100 μM and 300 μM respectively. This supported the idea that the differences in viability observed between GaMG and the TMZ-resistant sublines was not simply an effect of delayed growth in GaMG, but was due to TMZ-induced death in the parental cells. In addition, GaMG TMZ 100 and GaMG TMZ 300 appeared to sustain less DNA damage from treatment with TMZ than did GaMG, as measured by γH2A.X foci, and the damage was more transient. This suggested that GaMG TMZ 100 and GaMG TMZ 300 had established

or upregulated a mechanism that prevented or reduced the DNA damaging effects of TMZ. Indeed, probing the MGMT expression status of the sublines revealed that GaMG TMZ 100, but not GaMG TMZ 300, had upregulated MGMT at the protein level, which has been observed previously when culturing GBM cells with TMZ (Kohsaka et al., 2012). However, pre-incubation with O6BG to inhibit MGMT did not affect the response of either GaMG subline to TMZ, but did enhance the effect of TMZ on LN-18, which expresses endogenous MGMT. This suggests that although MGMT was upregulated in GaMG TMZ 100 cells, MGMT was not contributing to TMZ resistance.

It has been observed that MGMT expression status does not universally positively correlate with TMZ resistance (Meyer et al., 2015), and the experiments performed here are consistent with this concept. In addition, the expression of MGMT protein does not mean it is inherently active (Zhukovskaya et al., 1992), which, according to the results presented here, is likely the case for GaMG TMZ 100. Assays for MGMT activity would be able to clarify whether MGMT was functional in GaMG TMZ 100 cells.

Before commencing the search for novel drug targets that influence response of GBM cells to TMZ, it may be desirable to further investigate other known mechanisms of TMZ resistance in GaMG TMZ 100 and GaMG TMZ 300, including the status of MMR, alterations in which can confer resistance to TMZ independent of MGMT (McFaline-Figueroa et al., 2015). In the study by McFaline-Figueroa *et al.* (2015), the authors report that expression and activity of components of the MutSα MMR recognition complex, MSH2 and MSH6, were downregulated in cells with induced TMZ resistance. Depletion of these proteins caused substantial resistance to TMZ. Moreover, it would be expected that BER mechanisms remained intact in GaMG TMZ 100 and GaMG TMZ 300, as a failure of these mechanisms would likely have resulted in increased *N7*-MeG and *N3*-MeA adducts from TMZ treatment and consequent cell death, which was not observed in GaMG TMZ 100 or

GaMG TMZ 300. Thus, characterisation of MGMT activity, MMR status, and BER status in the TMZ-resistant GaMG sublines would help to consolidate the interpretation of MGMT-independent resistance, and help to establish whether the induced resistance points towards novel, uncharacterised mechanisms.

Once DNA repair mechanisms have been characterised in these cells, additional experiments towards investigating the induced resistance to TMZ in GaMG TMZ 100 and GaMG TMZ 300 could be pursued. To begin with, global analyses such as gene expression microarrays may be informative in providing clues towards potential resistance mechanisms if genes emerge that are clearly differentially expressed between the parental and TMZ-resistant GaMG sublines. In parallel, assessment of protein activity through performing phospho-protein arrays would provide information not obtainable from analyses of gene expression. Studies have found that the inhibition of a wide range of active proteins has resulted in sensitisation of glioma cells to TMZ, including STAT3, NF-κB, PARP, Mek2, PI3K-AKT and PI3K-mTORC axes, P-glycoprotein, and connexin 43 through EGFR (Daniel et al., 2010; He et al., 2015; Kohsaka et al., 2012; Munoz et al., 2014; Munoz et al., 2015; Wang et al., 2015; Yu et al., 2015; Zhang et al., 2015). Considering this, it may be informative to perform an inhibitor drug screen in combination with TMZ in GaMG TMZ 100 and GaMG TMZ 300 cells to identify new mechanisms of sensitising GBM cells to TMZ, an intervention that is much needed in the treatment of GBM.

This work demonstrates that repeated exposure to TMZ can induce TMZ resistance in GBM cells that are initially sensitive. Further work to identify resistance mechanisms and search for drugs to TMZ-sensitise GaMG TMZ 100 and GaMG TMZ 300 sublines has formed the basis of a new project within our lab.

5 Chapter V: Investigation of the effects of fractionated ionising radiation on GBM cells

5.1 Introduction

Radiotherapy is an important component of the current standard-of-care treatment for GBM. Patient survival is reduced if radiotherapy is not initiated soon after surgical resection, and combining radiotherapy with TMZ chemotherapy has been shown to have an increased survival benefit relative to radiotherapy alone (Stupp et al., 2009; Valduvieco et al., 2013). The current standard-of-care treatment for GBM patients includes radiotherapy administered in 2 Gy fractions, five times per week for six weeks, totalling 60 Gy (Barani and Larson, 2015). However, even after completion and with concomitant and/or adjuvant TMZ therapy, survival remains poor (Barani and Larson, 2015; Stupp et al., 2009; Stupp et al., 2005). Inevitable recurrence, especially at the original tumour site, largely accounts for the near 100% mortality rate in GBM (Hou et al., 2006). It was reasoned that, given the high rate of recurrence in GBM following radiotherapy, the clinical dose of IR may lead to the development of radio-resistant cells, the emergence of pre-existing resistant cells, or may change the cells such that the ones that survive radiotherapy may exhibit a more aggressive phenotype. Therefore, cultured GBM cells were subjected to the clinical dose of IR to investigate what, if any, consequent changes took place as a result of the IR alone.

5.2 Results

5.2.1 Response of GBM cells to repeated irradiation

Adult GBM cell lines GaMG and LN-18 were subjected to the clinically-administered dose of IR of 60 Gy in 2 Gy fractions to generate the sublines GaMGIR60 and LNIR60 respectively (Figure 5.1). One interruption of one week was required between weeks 2 and 3 because cells were not adequately confluent in culture following passaging. After each of the six weeks, cells were passaged before commencing with the next week's irradiation. Following receipt of 60 Gy IR, surviving cells were allowed to recover for one passage before experimentation. Compared with LN-18, subsequent IR dose-response clonogenic assays showed that LNIR60 acquired relative resistance to IR, particularly at 6-10 Gy (Figure 5.2). Statistically significant relative radio-resistance began to appear at single doses of 4 Gy and after a single dose of 10 Gy irradiation, clonogenicity was 10–fold higher in LNIR60 than in LN-18. Increased colony numbers in LNIR60 relative to LN-18 from 4 Gy upwards were also evident from simple observation of the stained dishes (Figure 5.3). In contrast to LNIR60, GaMGIR60 did not show relative resistance to IR when compared with parental GaMG cells at any single IR dose (Figure 5.4A). What was noticeable, however, was a striking change in the morphology of colonies that formed through the duration of clonogenic assays (Figure 5.4B). GaMGIR60 formed colonies that were much more rounded and larger in diameter than GaMG, suggesting that the 60 Gy of IR had altered the growth characteristics of the original cells. GaMGIR60 retained this enlarged colony morphology over time and even after subsequent doses of 2-10 Gy IR (data not shown).

These results show that 60 Gy of IR can change the sensitivity of GBM cells to IR and can alter the cells in such a way as to change the normal patterns of growth, potentially

leading to the emergence of subpopulations of cells with more aggressive phenotypes from heterogeneous populations.

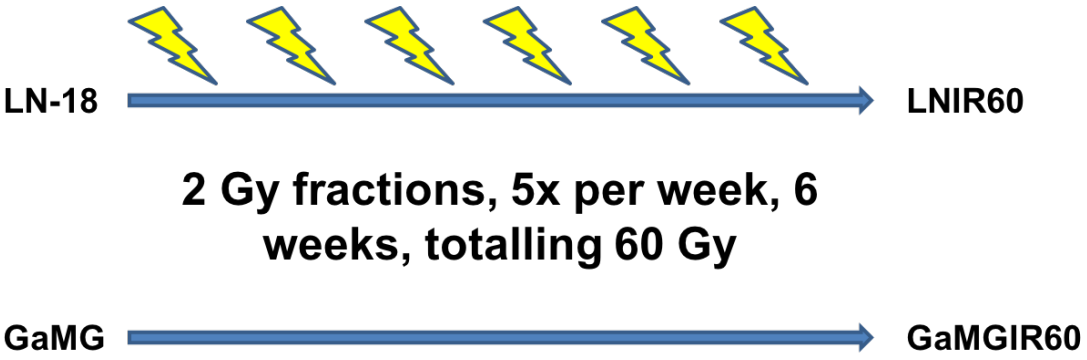


Figure 5.1: Dose schedule applied to GBM cells. Each bolt represents 10 Gy, administered as five 2 Gy fractions. For details, see Section 2.6.2.

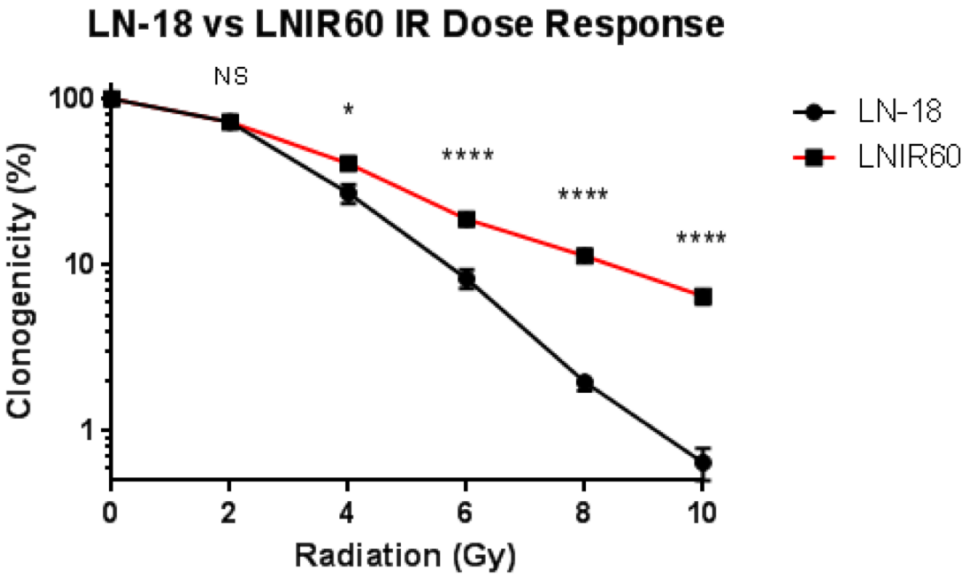


Figure 5.2: Radiation dose response of LN-18 and LNIR60 cells. Radio-sensitivity was tested by clonogenic assays. Single cells were seeded into 10 cm plates at a density of 5000 cells/plate and incubated overnight. Single doses of IR were applied to triplicate dishes 1 day after seeding and cells were incubated 10-12 days to allow formation of colonies of >50 cells. Colonies were counted using a GelCount, and the same settings were used to count LN-18 and LNIR60 colonies. Points represent means ± SEM of pooled triplicate data from three independent experiments. Means were tested for statistically significant differences using unpaired student's *t*-tests (*p < 0.05; ****p < 0.0001).

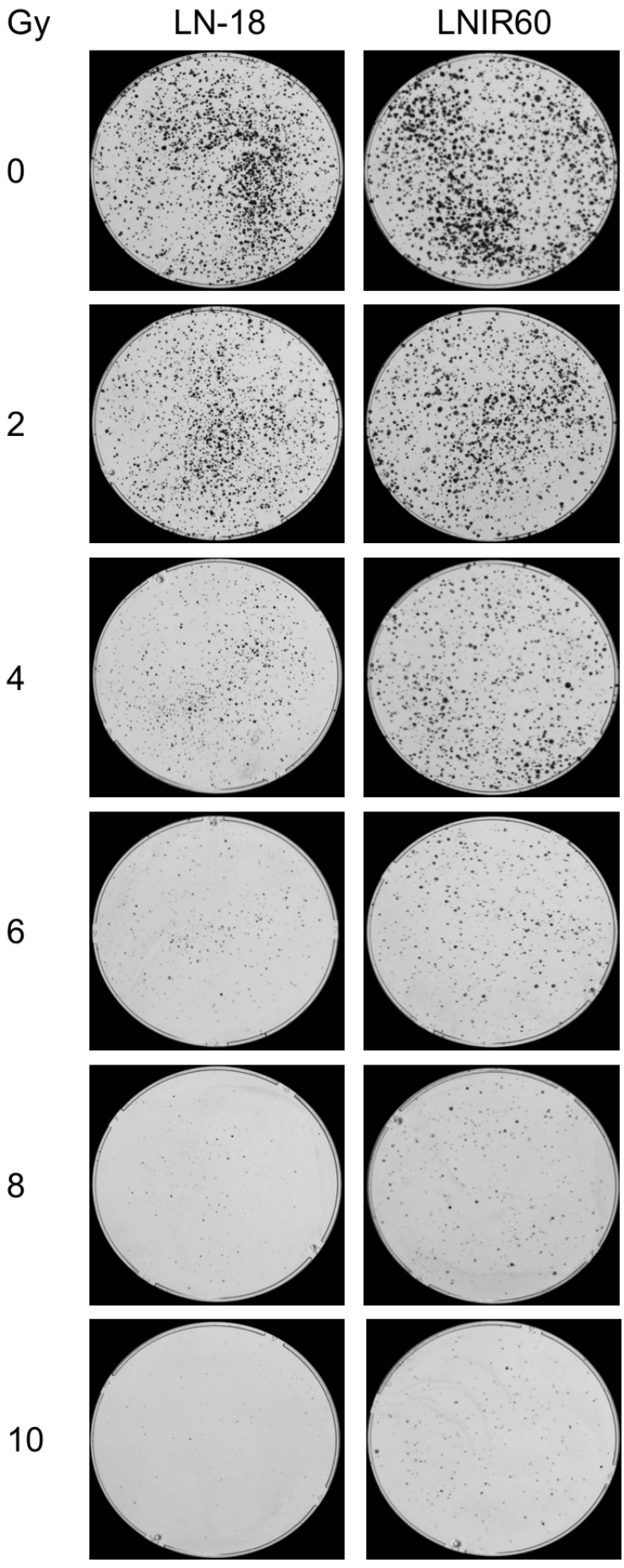
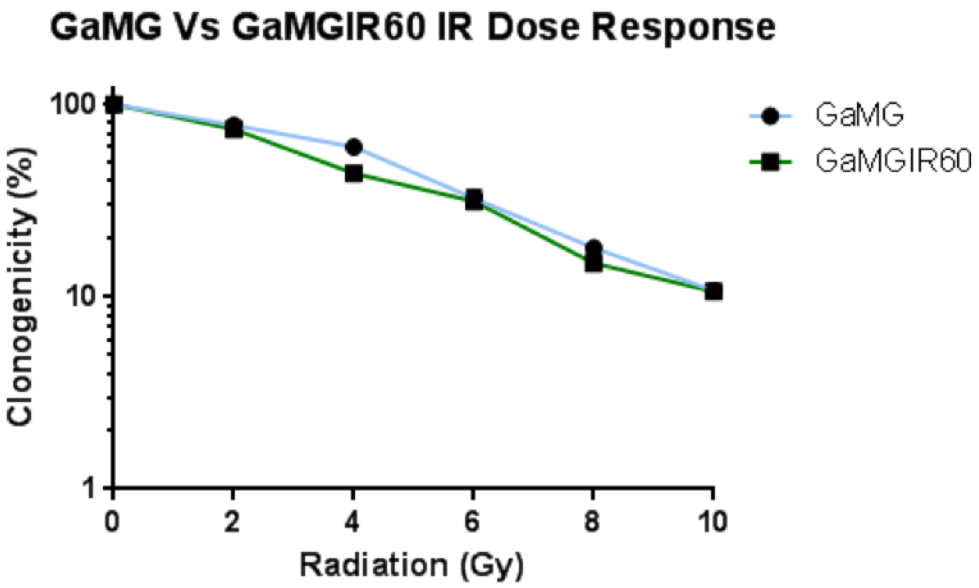


Figure 5.3: Images of LN-18 and LNIR60 colonies at different doses of radiation. Colonies were stained with Coomassie stain and plates were imaged on a GelCount. Images are representative of LN-18 and LNIR60 at each single dose of radiation.

A



B

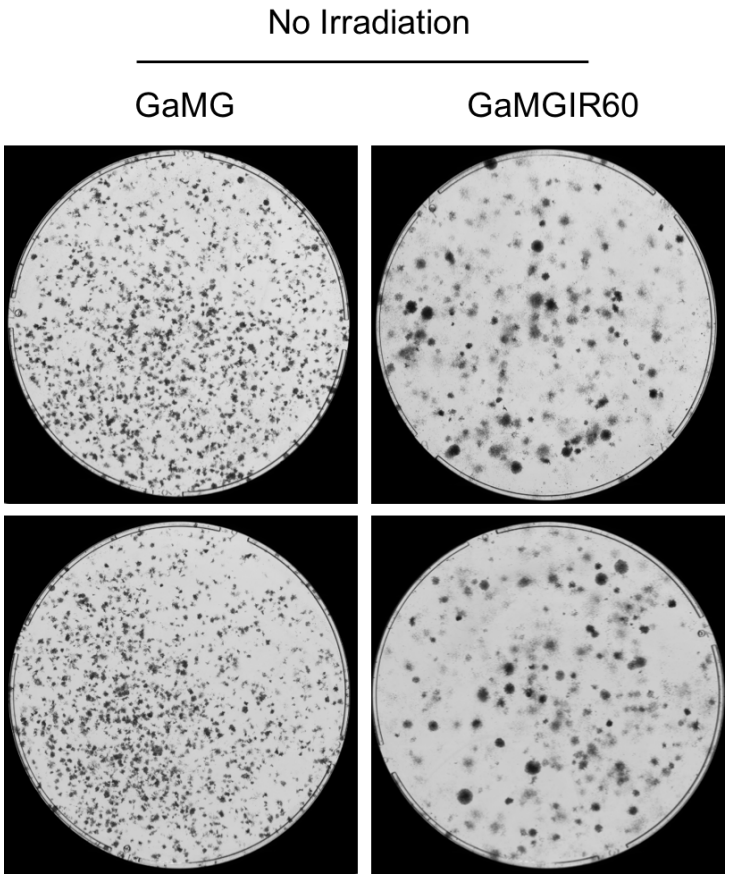


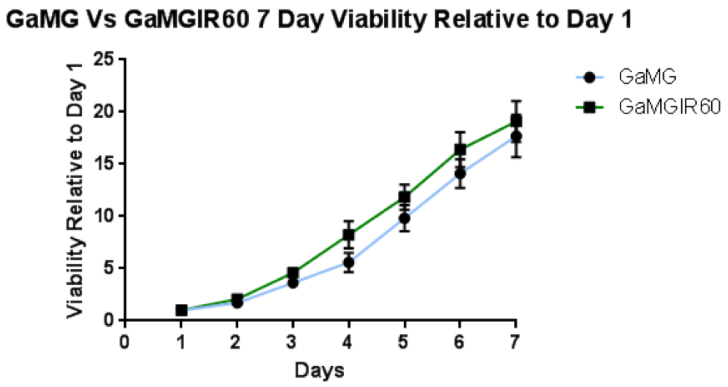
Figure 5.4: Radiation dose response and colony morphologies of GaMG and GaMGIR60 cells. A) Radio-sensitivity was tested by clonogenic assays as in Figure 5.2, following seeding at 5000 or 3000 single cells/plate. B) Images of Coomassie-stained GaMG and GaMGIR60 colonies after no IR treatment. Plates were imaged with a GelCount.

5.2.2 Characterisation and comparison of IR60 sublines and parental cell lines

Following the observations of both increased clonogenicity in response to IR in LNIR60 relative to LN-18, and the emergence of larger colonies with GaMGIR60, it was reasoned that IR60 cells may have been altered by the 60 Gy IR such that the cells were more proliferative. If IR60 cells were more proliferative, it would explain why the colonies that were formed by GaMGIR60 were larger than those of GaMG. Increased proliferation could also possibly explain the difference in clonogenicity seen between LN-18 and LNIR60 in response to IR, as increased proliferation may have allowed more colonies of LNIR60 than LN-18 to exceed the 50-cell cut-off and be included in the colony counts. To test for possible differences in proliferation, GaMG and LN-18 were seeded into viability assays and their viability was followed over periods of 6-7 days and compared against their IR60 sublines. No treatments were applied, so any changes in viability likely represented changes in cell number, changes in metabolism, or both. GaMGIR60 showed only slightly increased viability values relative to GaMG from day 3-7, but these were not statistically significant (Figure 5.5A). No differences in viability were seen between LN-18 and LNIR60 at any point during the time course (Figure 5.5B), suggesting that the relatively increased clonogenicity in LNIR60 at higher doses of IR was an effect of relative resistance to IR.

Given the slight differences in viability seen between GaMG and GaMGIR60, their growth characteristics in a 3D environment were also assessed. When seeded at the same density, the viability values for GaMGIR60 growing in Matrigel were much higher than those of GaMG (Figure 5.6A). In addition, GaMGIR60 colonies established a larger, more diffuse morphology with more evident cellular protrusions than GaMG colonies (Figure 5.6B), suggesting that these conditions favoured the growth of GaMGIR60 over GaMG cells.

A



B

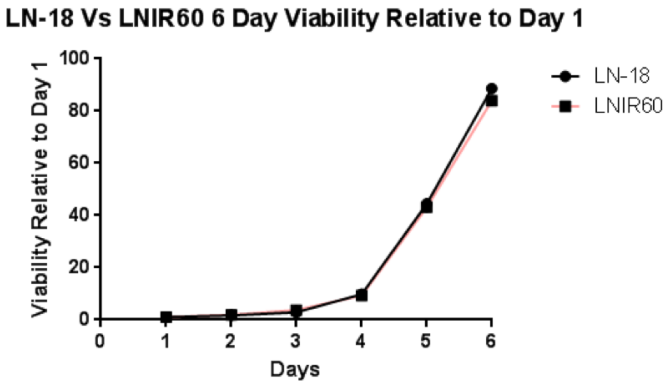
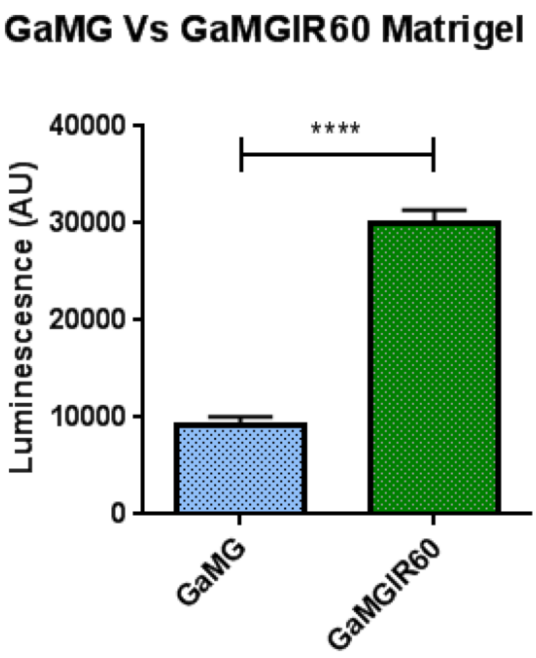


Figure 5.5: Viability of parental GBM cells and IR60 sublines over time. Cells were seeded into 96-well plates at 2000 (GaMG lines) or 1000 (LN-18 lines) cells/well and incubated for 6-7 days. At one day intervals, viability was measured using CellTitre-Blue® and measuring 40 min after addition of reagent to wells. Data are expressed as fluorescence values relative to day 1 ($\frac{Day\ n}{Day\ 1}$). Points represent means ± SEM of pooled triplicate data from three independent experiments for GaMG and GaMGIR60, and means ± SEM of quadruplicate values from a single experiment for LN-18 and LNIR60.

A



B

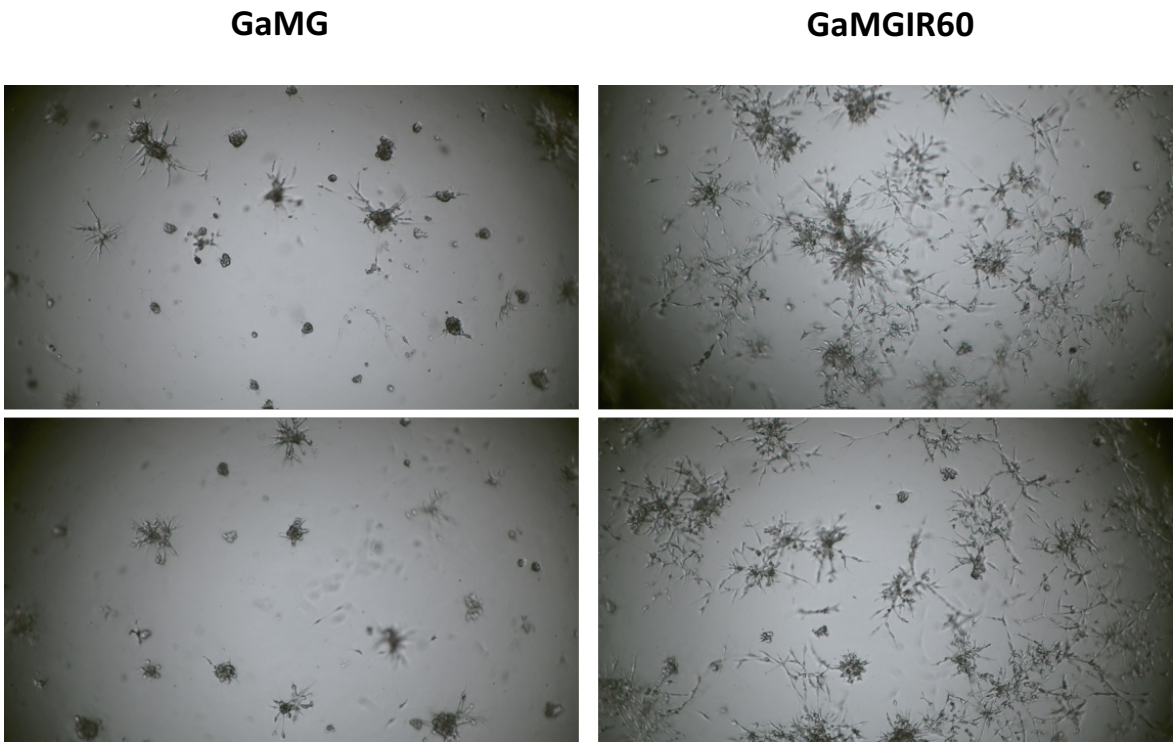
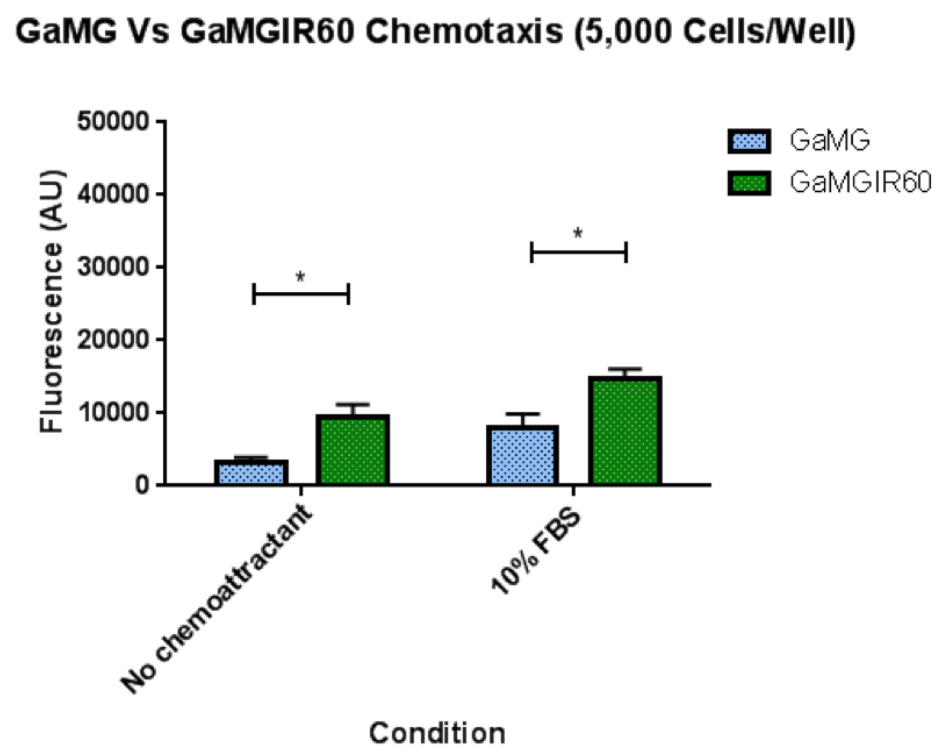


Figure 5.6: Comparison of growth in Matrigel of GaMG and GaMGIR60. Cells were seeded into the '2% on-top' Matrigel 3D environment assay at a density of 735 cells/well. Plates were incubated for 7 days and viability was assayed using CellTitre-Glo® 3D. A) Comparison of viability of GaMG and GaMGIR60 in the Matrigel 3D environment assay. Bars represent means ± SEM of six values from one experiment. A similar pattern of results was observed in a second, independent experiment. Means were tested for statistically significant differences using an unpaired student's *t*-test (****$p < 0.0001$). B) Representative images of the morphologies of GaMG and GaMGIR60 colonies in the Matrigel 3D environment assay. Photographs were taken with a Deltapix microscope camera.

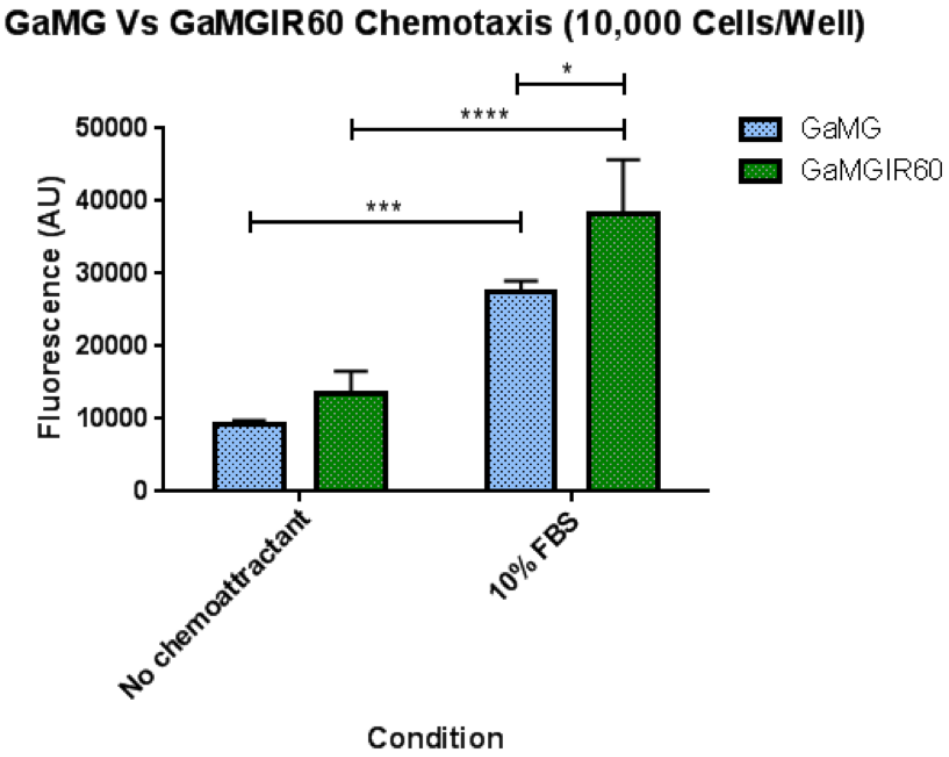
In addition to a possible increase in proliferation in GaMGIR60 cells relative to GaMG, it was also hypothesised that the larger colony sizes seen with GaMGIR60 may have been due to increased motility in GaMGIR60 by way of chemotaxis- that cells were more attracted to one another. To test whether GaMGIR60 cells were more responsive to chemotactic stimuli and thus more mobile than GaMG, Transwell assays were set up to compare migration towards a stimulus. At two different seeding densities, GaMGIR60 were more responsive to chemotactic stimuli (FBS) than were GaMG (Figure 5.7). GaMGIR60 were significantly more migratory in both the absence and presence of FBS at the lower seeding density (Figure 5.7A). At the higher seeding density, the difference was statistically significant in the presence, but not the absence of FBS (Figure 5.7B). Comparing receiver wells from both cell seeding densities, migration was clearly greater in the presence than absence of FBS, and greater in both GaMG and GaMGIR60 at the higher seeding density. In addition, consistent with differences seen in clonogenic assays, GaMG and GaMGIR60 cells showed different morphologies once they had migrated, with GaMG cells forming tight clusters, and GaMGIR60 showing a more diffuse spread of cells (Figure 5.7C-D).

The differences in radio-sensitivity between LNIR60 and LN-18 suggest that the clinically used dose of IR may alter GBM cells to allow the development of an adaptive resistance to IR. In addition, the differences seen between GaMG and GaMGIR60 suggest that the same dose may lead to increased growth, proliferation, and/or motility of GBM cells, especially within a 3D *in vivo* context. All of these differences point towards the development of potentially more aggressive phenotypes, possibly effected by subpopulations of cells that either survive the clinical dose of IR, or establish as a direct result of the IR. These cells may eventually cause recurrence of the tumour following radiotherapy.

A


GaMG Vs GaMGIR60 Chemotaxis (5,000 Cells/Well)
Fluorescence (AU)
50000
40000
30000
20000
10000
0
GaMG
GaMGIR60
*
*
No chemoattractant
10% FBS
Condition

B


GaMG Vs GaMGIR60 Chemotaxis (10,000 Cells/Well)
Fluorescence (AU)
50000
40000
30000
20000
10000
0
GaMG
GaMGIR60
*
****
***
No chemoattractant
10% FBS
Condition

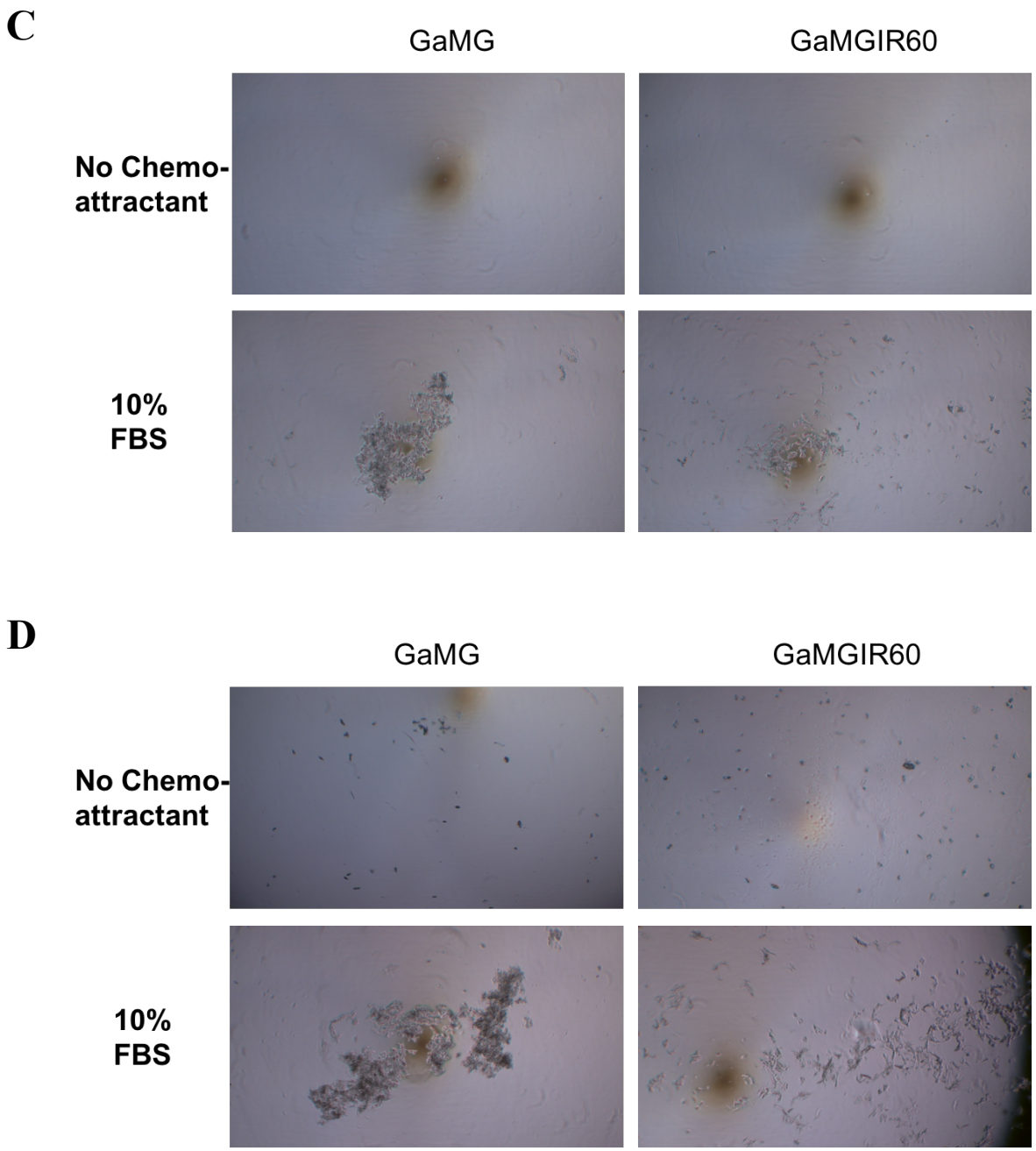


Figure 5.7: Chemotaxis of GaMG and GaMGIR60 cells. The Transwell® assay was used to assess the chemotaxis-induced mobility of GaMG and GaMGIR60. Cells were seeded into insert plates at 5000 or 10,000 cells/ insert in serum-free medium. Receiver wells were filled with serum-free medium (no chemo-attractant) or medium containing 10% FBS. Inserts were placed into receiver wells and plates were incubated for 24 hr before dissociating cells on the underside of the porous membrane, and assaying viability with CellTitre-Blue®. A) Chemotaxis of GaMG and GaMGIR60 cells in response to presence or absence of FBS at 5,000 cells/well. B) Chemotaxis of GaMG and GaMGIR60 cells in response to presence or absence of FBS at 10,000 cells/well. Bars are means ± SEM of four values from one experiment. Similar results were obtained in a second, independent experiment. Results in A and B were analysed by two-way ANOVA (*$p < 0.05$; ***$p < 0.001$; ****$p < 0.0001$). C) Representative images of receiver wells at the end of the 24 hr incubation period in the 5,000 cells/well assay. D) Representative images of receiver wells at the end of the 24 hr incubation period in the 10,000 cells/well assay. Photographs were taken with a Deltapix microscope camera.

It is known that changes in RTK axes can confer resistance of GBM cells to IR and accelerate growth and proliferation (Mukherjee et al., 2009; Osuka et al., 2013). To identify possible molecular changes that may have contributed to the altered phenotypes of GaMG and LN-18 resulting from the clinical dose of IR, expression and activation of selected signalling proteins were characterised (Figure 5.8). The most notable change was the apparent upregulation of PDGFRβ expression in GaMGIR60 compared with GaMG. There was a minor increase in phospho-AKT, but decrease in phospho-Mek in GaMGIR60. In LNIR60, IGF-1R expression and phosphorylation appeared to be greater than in LN-18, although a concomitant increase in phospho-AKT or phospho-Erk was not observed (Figure 5.8). No notable changes in expression or phosphorylation of EGFR were observed. Select proteins involved in the DDR were also analysed. LNIR60 appeared to have upregulation of MGMT relative to the basal levels expressed by LN-18. However, ATM protein was marginally decreased in LNIR60 compared with LN-18 (Figure 5.8).

In order to obtain a more global analysis of changes induced by the clinical dose of IR, gene expression was analysed by microarray to compare the transcriptomes of parental cells with their IR60 sublines. Due to the relative radio-resistance of LNIR60 but not of GaMGIR60, only LN-18 and LNIR60 were analysed following a dose of IR, and GaMG and GaMGIR60 were analysed from basal growth conditions (Figure 5.9). The IR dose (5 Gy) and times at which cells were analysed (6 hr and 24 hr) were informed by previous studies of transcriptional regulation following IR in breast cancer and GBM cells (Lu et al., 2006; Rashi-Elkeles et al., 2014). Of all the comparisons performed, those that were analysed most closely were the basal comparisons, where no additional IR was applied. In total, with the chosen log2-fold change and significance thresholds applied, GaMGIR60 had 29 upregulated and 14 downregulated transcripts relative to GaMG (Figure 5.10A and Tables 5.1, 5.2), while LNIR60 had 34 upregulated transcripts (Table 5.3), and 45

downregulated transcripts (Table 5.4) relative to parental LN-18 cells (Figure 5.10B). Differentially expressed genes were also observed in the other comparisons performed (Figure 5.9, Appendix 7.4).

These results confirm that the clinical dose of IR given to GBM patients can alter the transcriptome of GBM cells, potentially giving rise to subpopulations of cells with altered phenotypes.

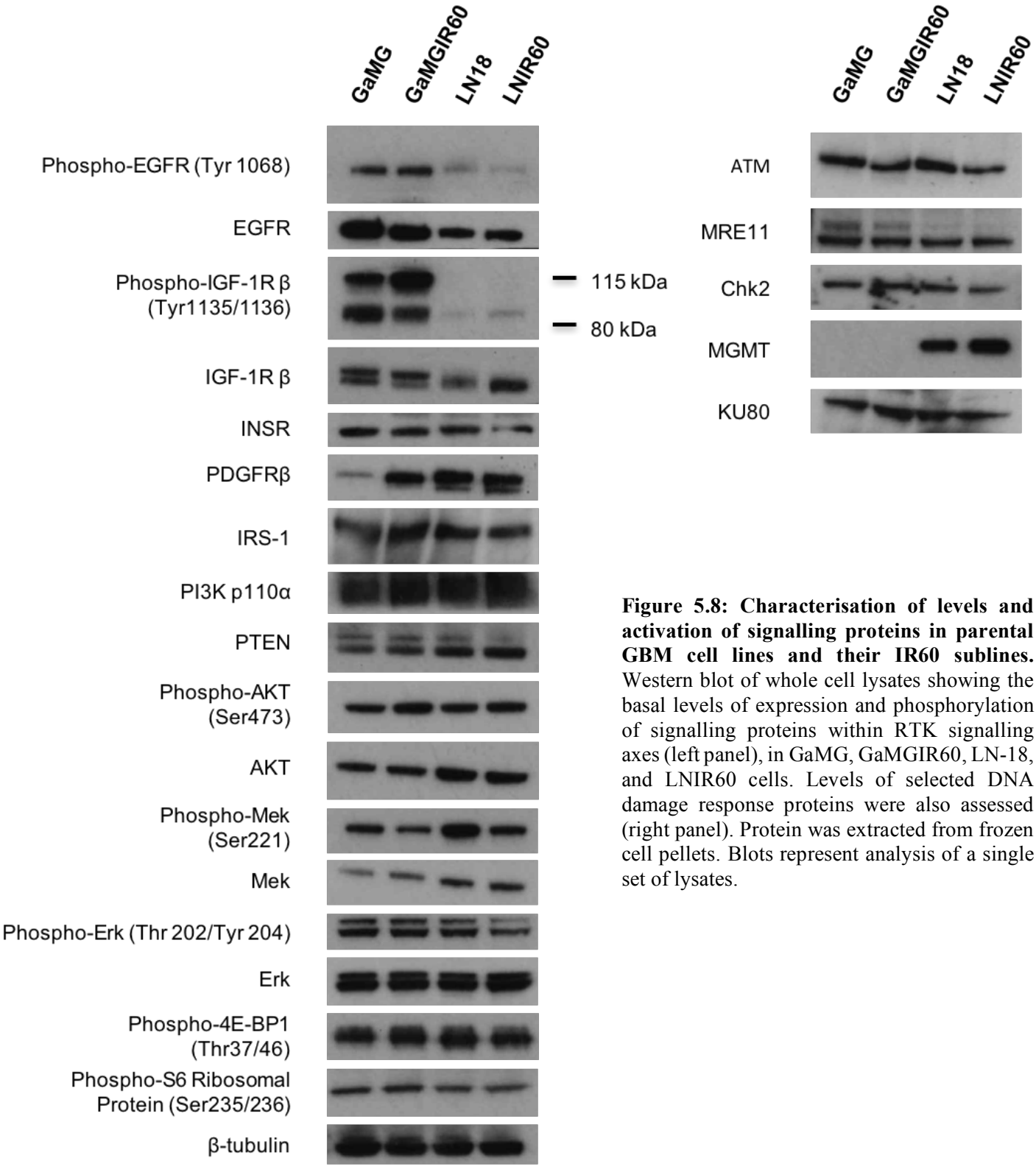


Figure 5.8: Characterisation of levels and activation of signalling proteins in parental GBM cell lines and their IR60 sublines. Western blot of whole cell lysates showing the basal levels of expression and phosphorylation of signalling proteins within RTK signalling axes (left panel), in GaMG, GaMGIR60, LN-18, and LNIR60 cells. Levels of selected DNA damage response proteins were also assessed (right panel). Protein was extracted from frozen cell pellets. Blots represent analysis of a single set of lysates.

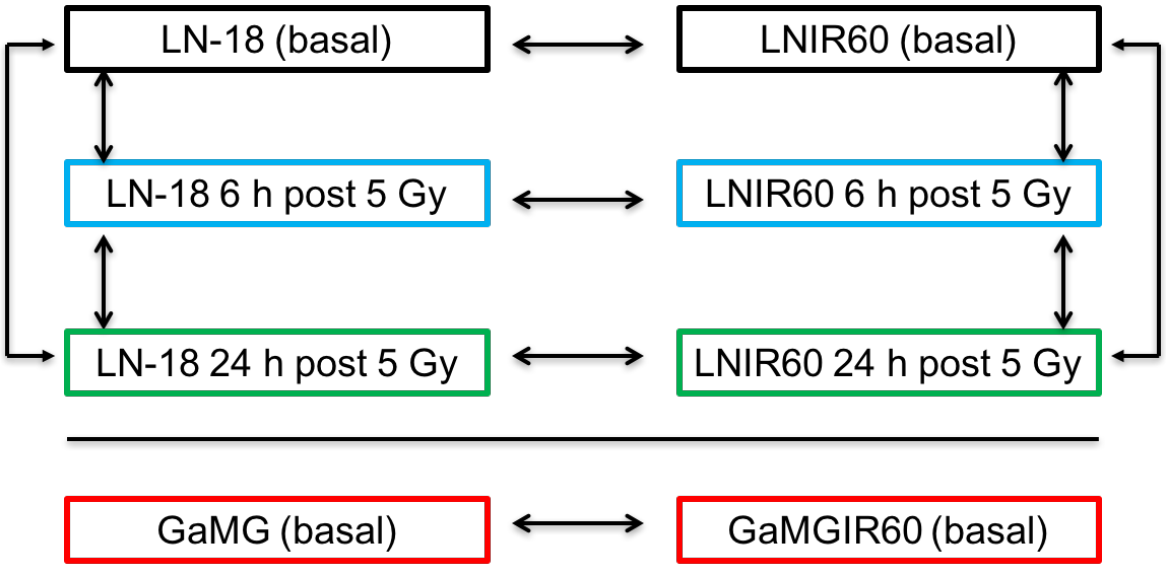
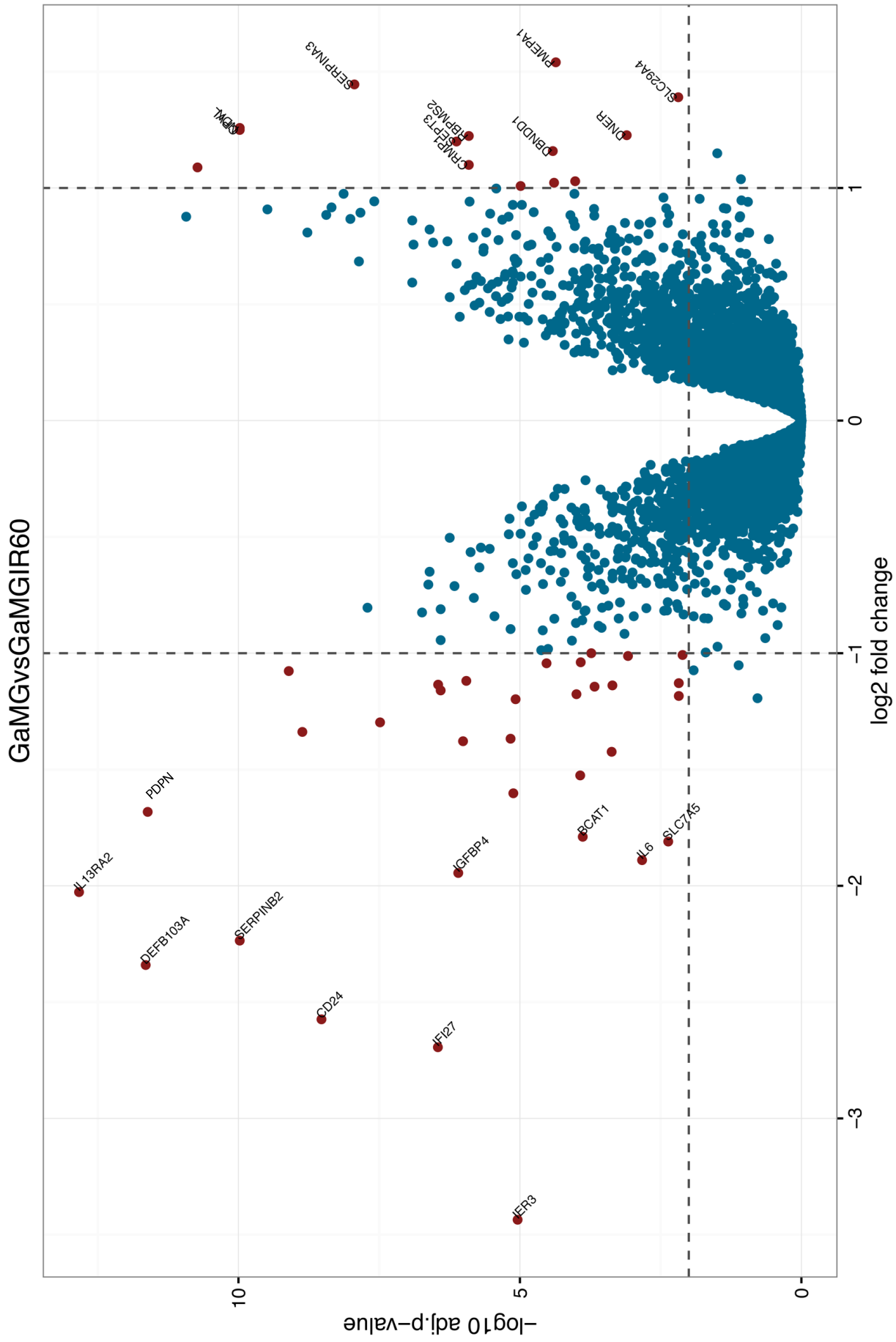


Figure 5.9: Design of Illumina microarray gene expression analysis experiment. Arrows represent comparisons and boxes represent triplicate samples. Total of 24 samples.

A


GaMGvsGaMGIR60
−log10 adj.p−value
log2 fold change
10
5
0
1
0
−1
−2
−3
SERPINA3
PMEPA1
SLC29A4
CRMP1
DUSP1
ONECUT1
PDPN
IL13RA2
DEFB103A
SERPINB2
CD24
IFI27
IGFBP4
BCAT1
IL6
SLC7A5
JUN
JUNB
FOS
FOSB
EGR1
EGR3

B

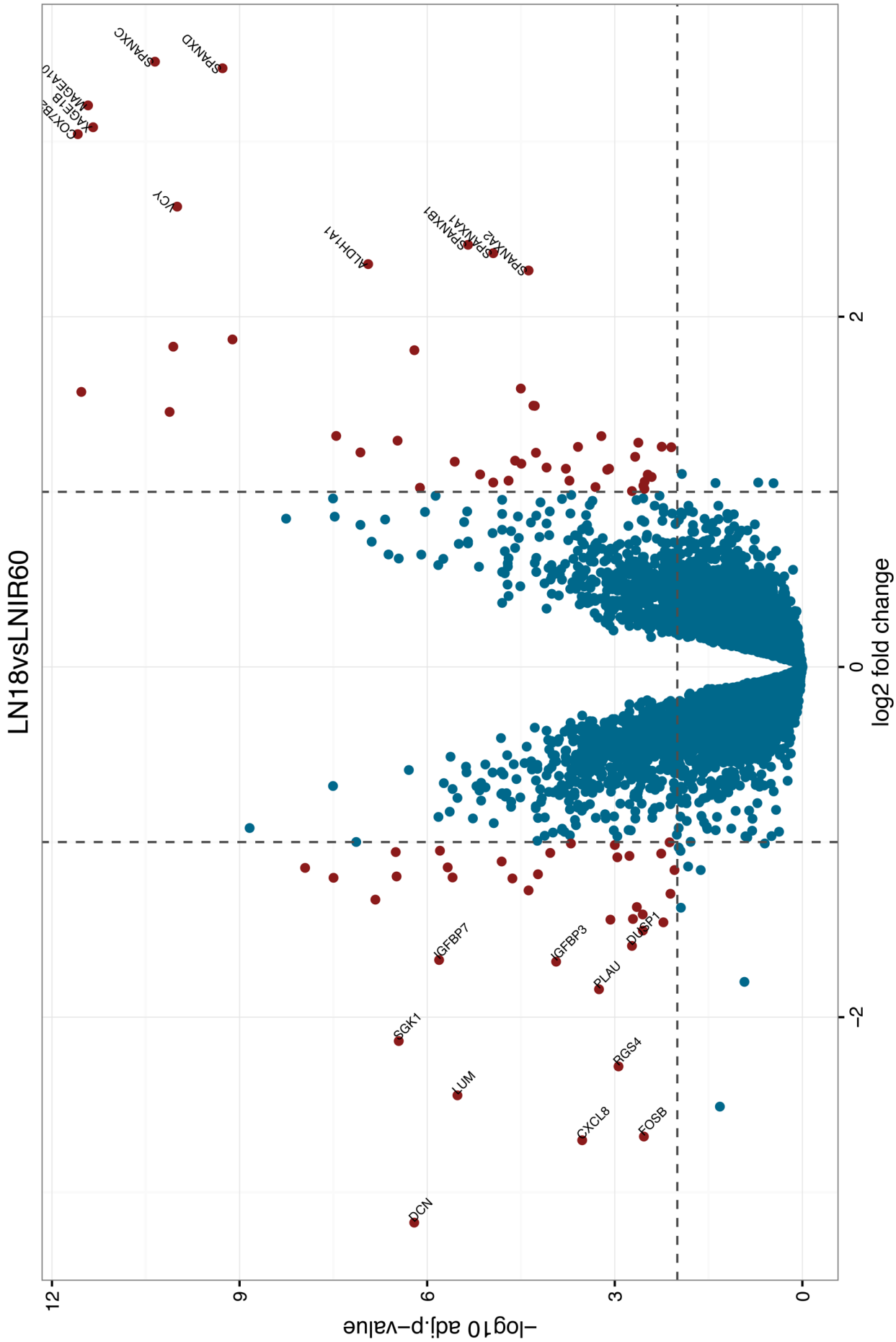

LN18vsLNIR60
−log10 adj.p−value
log2 fold change
12
9
6
3
0
2
0
−2
SPANXC
SPANXD
MAGEA10
MAGEB18
CXorf67
VCY
ALDH1A1
SPANXB1
SPANXA1
SPANXA2
IGFBP7
IGFBP3
DUSP1
PLAU
SGK1
RGS4
LUM
CXCL8
FOSB
DCN

Figure legend accompanying the plots on the previous two pages:

Figure 5.10: Differential gene expressions between parental GBM cell lines and their IR60 sublines. RNA from three independent samples of parental and IR60 sublines was extracted and analysed using the Human HT12v4.0 Illumina array platform. A) Volcano plot showing differential gene expression between GaMG and GaMGIR60. B) Volcano plot showing differential gene expression between LN-18 and LNIR60. Dashed lines represent cut-off values for log2 fold change (vertical), and cut-off for adjusted p-value (horizontal). Red points represent genes that are differentially expressed ('hits'), blue points represent genes that are not differentially expressed. Positive log2 fold change values represent relative upregulation in GaMG or LN-18, negative log2 fold change values represent relative upregulation in GaMGIR60 or LNIR60. The most differentially expressed genes by log2 fold change for each of GaMG, GaMGIR60, LN-18, and LNIR60 are labelled on the plots. The graphs were produced by Anastasia Samsonova.

Table 5.1: List of upregulated genes in GaMGIR60 relative to GaMG. Ranked by log2 fold change.

Gene Symbol	Gene Name	Log2 Fold change	adj.P.Val
IER3	immediate early response 3	3.43526666	1.3361E-04
IFI27	interferon, alpha-inducible protein 27	2.693500674	1.39102E-05
CD24	CD24 molecule	2.573570579	9.59098E-08
DEFB103A	defensin, beta 103A	2.339788769	9.65052E-11
SERPINB2	serpin peptidase inhibitor, clade B (ovalbumin), member 2	2.235657395	6.26205E-09
IL13RA2	interleukin 13 receptor, alpha 2	2.027054183	6.89109E-12
IGFBP4	insulin-like growth factor binding protein 4	1.944446564	5.7539E-06
IL6	interleukin 6	1.889110284	5.263037E-03
BCAT1	branched chain amino-acid transaminase 1, cytosolic	1.788650644	7.20473E-04
PDPN	podoplanin	1.681769845	1.11526E-10
MT1E	metallothionein 1E	1.601623698	2.22007E-04
VASN	vasorin	1.524827976	5.97534E-04
HBEGF	heparin-binding EGF-like growth factor	1.424030106	6.766137E-03
RFTN1	raftlin, lipid raft linker 1	1.378623468	2.31529E-05
FAM133A	family with sequence similarity 133, member A	1.367447288	1.68961E-05
TRIML2	tripartite motif family-like 2	1.33844959	3.44885E-08
IGFBP1	insulin-like growth factor binding protein 1	1.296620852	1.75107E-06
CRISPLD2	cysteine-rich secretory protein LCCL domain containing 2	1.197667442	3.10612E-06
COL6A3	collagen, type VI, alpha 3	1.175733238	1.269179E-03
GALNT9	polypeptide N-acetylgalactosaminyltransferase 9	1.159650483	8.25028E-06
S100A4	S100 calcium binding protein A4	1.143546303	9.91285E-05
FAM107B	family with sequence similarity 107, member B	1.137907968	2.323875E-03
JMJD8	jumonji domain containing 8	1.135028115	1.16377E-05
CXCL5	chemokine (C-X-C motif) ligand 5	1.118484296	3.87558E-05
TGM2	transglutaminase 2	1.076464675	4.31582E-08
IL1B	interleukin 1, beta	1.042840675	7.45525E-04
STMN3	stathmin-like 3	1.038264883	2.9688E-05
TNC	tenascin C	1.011848438	7.143235E-03
PINK1	PTEN induced putative kinase 1	1.000186065	3.79153E-04

Table 5.2: List of upregulated genes in GaMG relative to GaMGIR60. Ranked by log2 fold change.

Gene Symbol	Gene Name	Log 2 Fold Change	adj.P.Val
PMEPA1	prostate transmembrane protein, androgen induced 1	1.540905091	6.29658E-04
SERPINA3	serpin peptidase inhibitor, clade A (alpha-1 antiproteinase, antitrypsin), member 3	1.445113963	6.10433E-07
SLC29A4	solute carrier family 29 (equilibrative nucleoside transporter), member 4	1.390047368	9.97646E-03
NDN	necdin, melanoma antigen (MAGE) family member	1.258938435	6.24095E-09
CPVL	carboxypeptidase, vitellogenic-like	1.249632113	3.95447E-09
DNER	delta/notch-like EGF repeat containing	1.227456828	6.05291E-03
RBPMS2	RNA binding protein with multiple splicing 2	1.224419978	3.6694E-06
Sep-03	septin 3	1.199854745	5.47617E-07
DBNDD1	dysbindin (dystrobrevin binding protein 1) domain containing 1	1.159198078	8.16097E-05
CRMP1	collapsin response mediator protein 1	1.099645697	1.09889E-06
CLEC1A	C-type lectin domain family 1, member A	1.089044184	1.18769E-09
SDC1	syndecan 1	1.0295009	1.09487E-05
H1F0	H1 histone family, member 0	1.023206674	7.67421E-04
SEMA3C	sema domain, immunoglobulin domain (Ig), short basic domain, secreted, (semaphorin) 3C	1.008510954	1.4058E-04

Table 5.3: List of upregulated genes in LNIR60 relative to LN-18. Ranked by log2 fold change.

Gene Symbol	Gene Name	Log2 Fold Change	adj.P.Val
DCN	decorin	3.173672937	6.10433E-07
CXCL8	chemokine (C-X-C motif) ligand 8	2.702975946	3.96851E-04
FOSB	FBJ murine osteosarcoma viral oncogene homolog B	2.681631008	7.45409E-03
LUM	lumican	2.446812448	3.79876E-07
RGS4	regulator of G-protein signaling 4	2.281508784	1.35081E-03
SGK1	serum/glucocorticoid regulated kinase 1	2.13660614	6.6422E-06
PLAU	plasminogen activator, urokinase	1.841035434	4.80072E-03
IGFBP3	insulin-like growth factor binding protein 3	1.683292478	7.33801E-05
IGFBP7	insulin-like growth factor binding protein 7	1.673264033	8.33445E-06
DUSP1	dual specificity phosphatase 1	1.593370304	1.94388E-03
CCPG1	cell cycle progression 1	1.458368949	9.65212E-03
PPAP2A	phosphatidic acid phosphatase type 2A	1.442930766	1.29140E-03
CTGF	connective tissue growth factor	1.439311546	3.07320E-03
JUN	jun proto-oncogene	1.413925908	1.15206E-03
DACH1	dachshund family transcription factor 1	1.371703457	2.90662E-03
PRSS23	protease, serine, 23	1.328603173	6.26205E-09
SOX4	SRY (sex determining region Y)-box 4	1.295255765	9.21495E-03
ATF3	activating transcription factor 3	1.276560137	1.01993E-04
CDH6	cadherin 6, type 2, K-cadherin (fetal kidney)	1.208322358	5.26557E-05
RPS23	ribosomal protein S23	1.204236109	5.36302E-09
KCTD12	potassium channel tetramerization domain containing 12	1.202353523	1.73804E-07
SUSD2	sushi domain containing 2	1.196347123	1.00827E-06
CBX6	chromobox homolog 6	1.184206354	1.39333E-04
SMCO4	single-pass membrane protein with coiled-coil domains 4	1.147963366	3.95447E-09
PRAME	preferentially expressed antigen in melanoma	1.144380858	6.02263E-07
ANTXR2	anthrax toxin receptor 2	1.111339719	2.50956E-05
HSPA5	heat shock 70kDa protein 5 (glucose-regulated protein, 78kDa)	1.087355043	1.62127E-03
CYR61	cysteine-rich, angiogenic inducer, 61	1.078798462	9.0217E-04
PPP1R15A	protein phosphatase 1, regulatory subunit 15A	1.065730456	6.60503E-03
CPED1	cadherin-like and PC-esterase domain containing 1	1.062151477	8.71022E-05
PTPRK	protein tyrosine phosphatase, receptor type, K	1.057169203	4.68454E-08
EVL	Enah/Vasp-like	1.049012492	2.80305E-08
LRCH2	leucine-rich repeats and calponin homology (CH) domain containing 2	1.016965956	8.88137E-05
MMP13	matrix metallopeptidase 13	1.008046303	4.15896E-08

Table 5.4: List of upregulated genes in LN-18 relative to LNIR60. Ranked by log2 fold change.

Gene Symbol	Gene Name	Log2 Fold Change	adj.P.Val
SPANXC	SPANX family, member C	3.455685437	3.74786E-11
SPANXD	SPANX family, member D	3.418257897	6.1968E-10
MAGEA10	melanoma antigen family A10	3.206085876	6.89109E-12
XAGE1B	X antigen family, member 1B	3.081641086	1.17109E-12
COX7B2	cytochrome c oxidase subunit VIIb2	3.042072718	1.65515E-12
VCY	variable charge, Y-linked	2.628473765	5.02188E-12
SPANXB1	SPANX family, member B1	2.411042894	1.55598E-05
SPANXA1	sperm protein associated with the nucleus, X-linked, family member A1	2.363138352	2.9688E-05
ALDH1A1	aldehyde dehydrogenase 1 family, member A1	2.299859284	1.29134E-07
SPANXA2	SPANX family, member A2	2.263871092	1.48099E-04
VCX2	variable charge, X-linked 2	1.870282131	7.04639E-11
MAGEC1	melanoma antigen family C1	1.828341914	7.04639E-11
TFF2	trefoil factor 2	1.808736256	2.70062E-07
CA9	carbonic anhydrase IX	1.590129343	2.98758E-05
MAGEB2	melanoma antigen family B2	1.570240109	1.63063E-12
RAB17	RAB17, member RAS oncogene family	1.492249235	1.12509E-04
HBE1	hemoglobin, epsilon 1	1.490579082	2.3819E-05
DSCR8	Down syndrome critical region 8	1.45641096	6.89109E-12
GCHFR	GTP cyclohydrolase I feedback regulator	1.318725047	2.28791E-08
CDH10	cadherin 10, type 2 (T2-cadherin)	1.318238146	1.371911E-03
AIF1L	allograft inflammatory factor 1-like	1.291824774	1.51661E-07
TK1	thymidine kinase 1, soluble	1.280500074	4.772679E-03
PLEKHS1	pleckstrin homology domain containing, family S member 1	1.256757783	1.414471E-03
PAGE2	P antigen family, member 2 (prostate associated)	1.225285804	4.10775E-10
ADGRL4	adhesion G protein-coupled receptor L4	1.223411841	5.19892E-05
SDC1	syndecan 1	1.178058692	1.09487E-05
MSMO1	methylsterol monooxygenase 1	1.177802819	2.144078E-03
MAGEC2	melanoma antigen family C2	1.171874151	6.98897E-08
CALB2	calbindin 2	1.160190411	3.75564E-04
DAZ4	deleted in azoospermia 4	1.13800378	2.92412E-04
LRRC26	leucine rich repeat containing 26	1.131491115	5.84079E-05
AK4	adenylate kinase 4	1.131476948	5.47318E-04
PLAC8	placenta-specific 8	1.101872883	8.629465E-03
WDR54	WD repeat domain 54	1.098874267	1.64155E-05
HMGB2	high mobility group box 2	1.09799892	4.066851E-03
PTTG3P	pituitary tumor-transforming 3, pseudogene	1.084225981	7.1697E-04
IGFBP6	insulin-like growth factor binding protein 6	1.063872473	1.362707E-03
CARHSP1	calcium regulated heat stable protein 1, 24kDa	1.063697372	2.67686E-05
PTTG1	pituitary tumor-transforming 1	1.057629674	6.27788E-04
IGFLR1	IGF-like family receptor 1	1.05337969	4.43137E-05
NEIL3	nei endonuclease VIII-like 3 (E. coli)	1.035112775	6.173591E-03
APOBEC3B	apolipoprotein B mRNA editing enzyme, catalytic polypeptide-like 3B	1.027046939	7.27646E-04
HMHB1	histocompatibility (minor) HB-1	1.02318201	1.28059E-06
SPC24	SPC24, NDC80 kinetochore complex component	1.017058872	4.746844E-03
DLGAP5	discs, large (Drosophila) homolog-associated protein 5	1.003665526	3.298846E-03

5.2.3 Validation of differentially expressed genes in response the clinical dose of ionising radiation

Of the 122 differentially expressed genes from the GaMG-GaMGIR60 and LN-18-LNIR60 comparisons, four genes were chosen for further analysis and validation of differential expression. From the GaMG-GaMGIR60 comparison, *CD24* and *PDPN* were selected, and from the LN-18-LNIR60 comparison, *SGK1* and *IGFBP3* were selected. *CD24* encodes the cluster of differentiation 24 (CD24) protein, a cancer stem cell (CSC) marker and cell adhesion molecule (Jaggupilli and Elkord, 2012) about which little is known within the context of GBM. *PDPN* encodes podoplanin, a type 1 integral membrane protein that is heavily *O*-glycosylated. It has been shown to have roles in promoting epithelial-mesenchymal-transition and tumour cell motility and invasion through modulating the actin cytoskeleton (Martin-Villar et al., 2006; Wicki et al., 2006). *SGK1* encodes serum and glucocorticoid-regulated kinase 1 (SGK1), a serine/threonine kinase that can be activated by PI3K and mTORC2 in response to IGF-1 and insulin (Kobayashi and Cohen, 1999; Park et al., 1999). Once activated, SGK1 can promote cell survival by translocating to the nucleus and phosphorylating members of the Forkhead family of transcription factors, causing their exclusion from the nucleus and preventing their induction of cell cycle arrest and apoptosis (Brunet et al., 2001). SGK1 also has extensively characterised roles in ion transport (Lang and Shumilina, 2013). *IGFBP3* encodes insulin-like growth factor-binding protein 3 (IGFBP3), which is a member of the IGF-1R signalling axis and serves to bind IGF-1 and IGF-2 in the circulation, regulating interaction with IGF-1R (Firth and Baxter, 2002).

Following observation of their apparent upregulation in GaMGIR60 or LNIR60 cells, qRT-PCR was used to validate the differences in expression of these four genes. Two sets of primers were used to confirm that *CD24* transcription was upregulated in GaMGIR60 compared with GaMG (Figure 5.11A). *PDPN* transcription was also confirmed as

significantly upregulated in GaMGIR60 (Figure 5.11B). In LNIR60, both *SGK1* and *IGFBP3* transcription were confirmed as increased relative to LN-18 (Figure 5.11C and 5.11D respectively). These results confirm that 60 Gy of IR was able to increase the transcription of several genes in these GBM cells.

A recent report showed SGK1 to be upregulated in GBM and that SGK1 inhibition can increase radiation-induced growth inhibition (Talarico et al., 2016). In addition, IGFBP3 has been shown to bind to an EGFR-DNA-PK complex in breast cancer cells, and that IGFBP3 silencing reduced DSB repair by NHEJ (Lin et al., 2014). Given that links between radiation and SGK1 in GBM, and DNA damage and IGFBP3 have already been established, CD24 and podoplanin were chosen for further validation at the protein level. Podoplanin has been linked to increased motility and invasion in GBM cells (Grau et al., 2015) and GaMGIR60 were found to grow better in Matrigel, and to be more motile by chemotaxis (Figures 5.6 and 5.7). Despite clear upregulation of podoplanin at the mRNA level in GaMGIR60, it was difficult to determine whether this was reflected at the protein level (Figure 5.12). Podoplanin is known to be extensively glycosylated, which alters the apparent molecular weights of proteins. Consequently, several molecular weights have been observed for podoplanin, including 24, 35, and 46 kDa. Probing GaMG and GaMGIR60 (and LN-18 and LNIR60 for comparison) lysates for podoplanin revealed a range of bands which may have represented (separately or together) podoplanin protein expression (Figure 5.12A). Upregulation of podoplanin at the protein level was therefore inconclusive by Western blotting. Analysis by immunofluorescence did not show differences in expression levels, but did show that podoplanin localised to a greater density at the projections of GaMG and GaMGIR60 cells (Figure 5.12B).

CD24 is a well-characterised CSC marker (Jaggupilli and Elkord, 2012) and has been

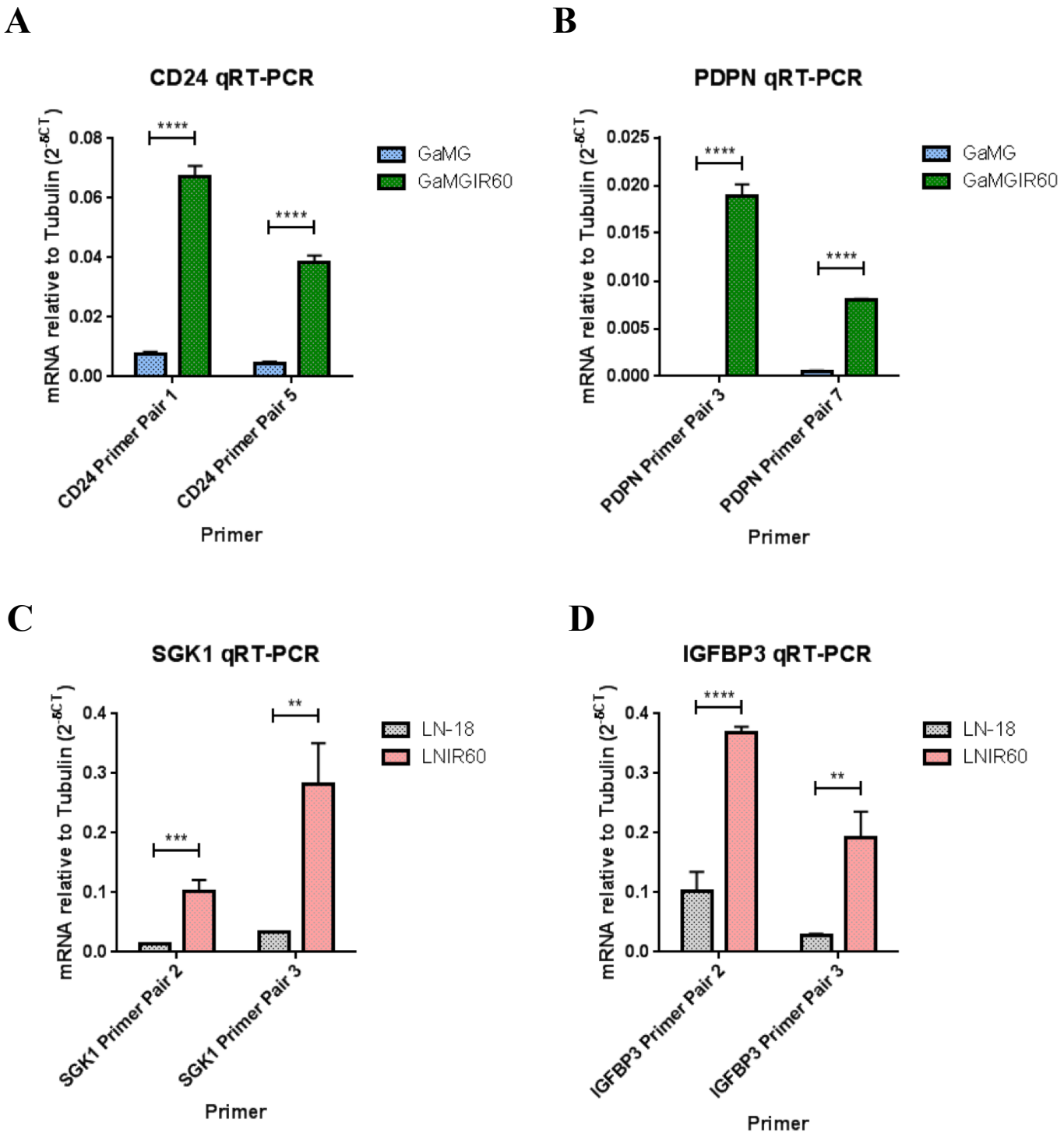


Figure 5.11: Validation of differentially expressed genes at the RNA level. mRNA was converted to cDNA as described in Section 2.18. Relative levels of transcripts for four candidate genes were assessed by qRT-PCR using two sets of primer pairs for each target (section 2.19). Validation of differential expression of A) *CD24* between GaMG and GaMGIR60, B) *PDPN* between GaMG and GaMGIR60, C) *SGK1* between LN-18 and LNIR60, D) *IGFBP3* between LN-18 and LNIR60. Bars are means ± SEM and represent pooled triplicate data from three independent experiments (n = 9) or two independent experiments for *PDPN* (n = 6). The data were analysed by unpaired student's *t*-tests (**p < 0.01; ***p < 0.001; ****p < 0.0001).

A

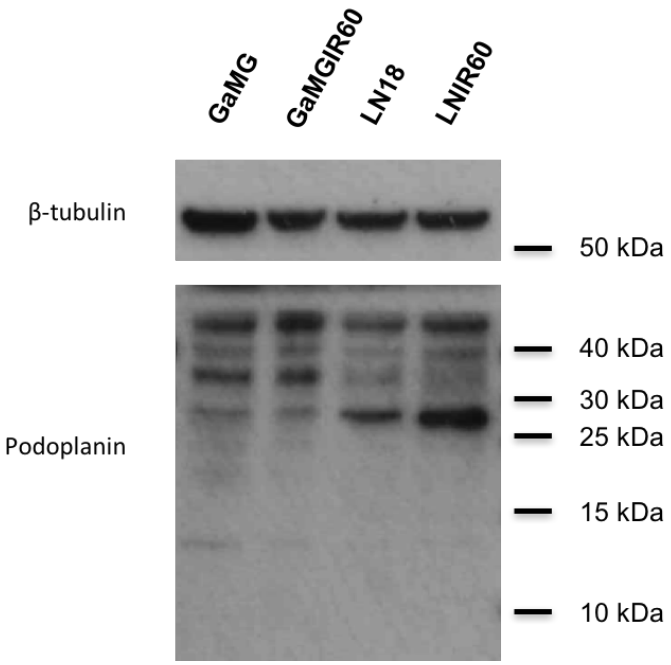


Figure continued on next page.

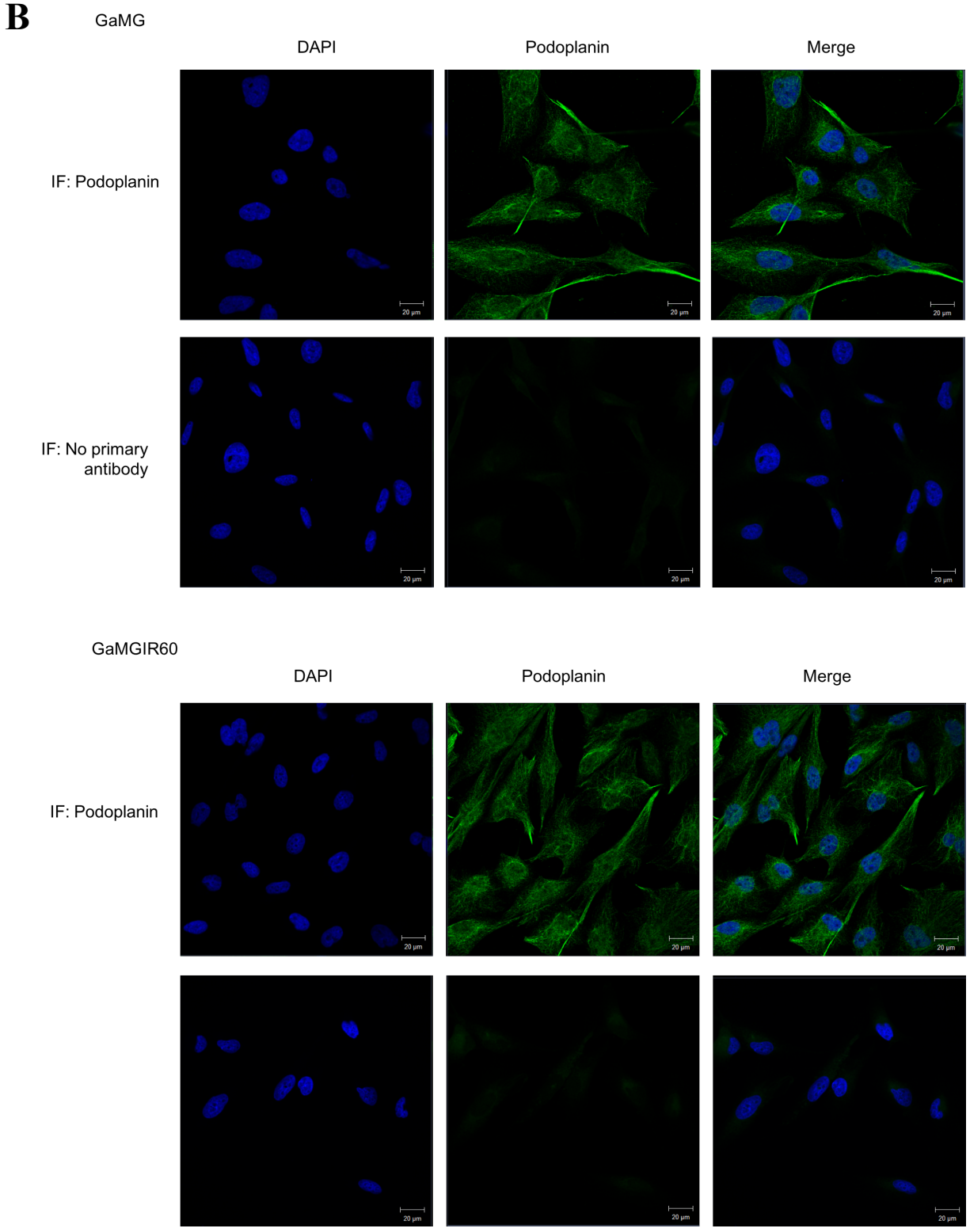


Figure 5.12: Testing for expression of podoplanin in GBM cells at the protein level. A) Protein was extracted from pellets and whole cell lysates were Western blotted with an antibody directed towards PDPN. Blots represent analysis of a single set of lysates. B) GaMG (upper) and GaMGIR60 (lower) were grown on coverslips at 200,000 cells/coverslip overnight and fixed the following day for immunofluorescence staining described in section 2.15.1. Cells were incubated with podoplanin primary antibody or no primary antibody, and bound antibody was detected with secondary antibody conjugated to Alexa Fluor® 488. Nuclei were counterstained with DAPI. Cells were imaged with a Zeiss LSM 710 Observer Z1 confocal microscope. Scale bars represent 20 µm.

shown to mediate adhesion, motility and metastasis in breast and hepatocellular carcinoma cancer cells (Aigner et al., 1998; Zheng et al., 2011). However, CD24 has been studied very little in GBM. Given the observed increased motility by chemotaxis in GaMGIR60 as a result of 60 Gy IR, and confirmed upregulation of CD24 at the mRNA level in GaMGIR60, differences in protein levels of CD24 in GaMG and GaMGIR60 were also validated. Live GaMG and GaMGIR60 cells were probed with an RPE-conjugated CD24 primary antibody and analysed by flow cytometry. CD24 signal was detected above the signal level in IgG-stained controls, and GaMGIR60 showed more positive signal for cell surface expression of CD24 than did GaMG (Figure 5.13A). In addition, GaMGIR60 consistently had a greater proportion of cells with positive signal for CD24 than GaMG, with a statistically significant difference between the mean fluorescence intensity values from four independent experiments (Figure 5.13B).

Taken together, these results confirm that, relative to unirradiated cells, in GaMG cells that had received the clinical dose of IR, CD24 was upregulated at the mRNA level and at the protein level as shown by differences in its expression at the cell surface.

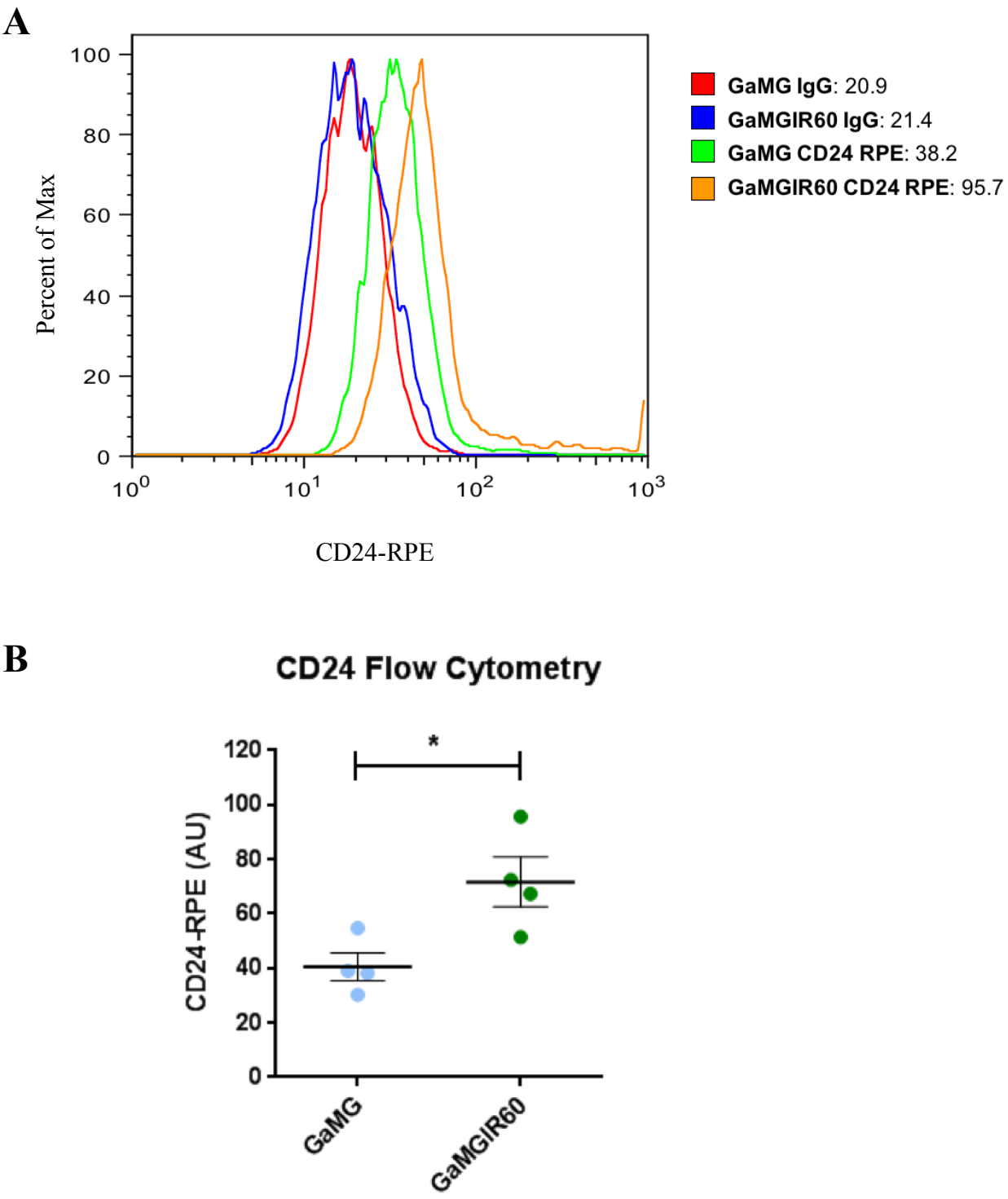


Figure 5.13: Validation of differential expression of CD24 in GaMG and GAMGIR60 cells at the protein level. GaMG and GaMGIR60 cells were disaggregated with 3 mM EDTA, centrifuged, resuspended, and incubated with RPE-conjugated CD24 primary antibody, or human IgG control for 1 hr. Cells were washed and analysed by flow cytometry. A) Expression of CD24 at the cell surfaces of GaMG and GaMGIR60. Fluorescence intensity histogram plot of cells incubated with IgG or CD24-RPE primary antibody. Numbers in the key are the Mean Fluorescence Intensity (MFI) values. The graph displays results from one of four independent experiments. B) Scatter plot showing the means, SEMs, and distributions of MFI values of CD24-RPE signal for GaMG and GaMGIR60 cells from four independent experiments. Data were analysed by an unpaired Student's *t*-test (*p < 0.05).

5.2.4 siRNA Knockdown of CD24

In order to be able to assess the functional relevance of CD24 upregulation in GaMGIR60 cells, an siRNA was selected to knock down *CD24*, using a sequence that has been used with success previously (Ahmed et al., 2009). Upon transfection of GaMG and GaMGIR60 with *CD24* siRNA, two sets of primers were used to test for efficient knockdown by qRT-PCR (Figure 5.14). Both primer pairs confirmed upregulation of *CD24* in GaMGIR60 cells, consistent with Figure 5.11A, and significant knockdown in GaMGIR60 cells transfected with *CD24* siRNA, with 97% reduced expression compared with Allstars-transfected controls. There was also evidence of significant knockdown in GaMG cells transfected with *CD24* siRNA relative to Allstars-transfected controls when testing with primer pair 5 (82% reduced expression), but the differences were not significant when testing with primer pair 1 (Figure 5.14). These results confirm that the *CD24* siRNA was able to degrade its target.

Alongside confirmation of knockdown, the viability of cells following *CD24* siRNA or control transfections was assessed over a period of 7 days (Figure 5.15). Knockdown of *CD24* had a striking effect on the viability readings of GaMG and GaMGIR60. On day 7, fluorescence values for *CD24* siRNA-transfected cells were 13.7-fold and 61-fold lower than untransfected controls in GaMGIR60 and GaMG respectively (Figure 5.15A). However, by day 7, the viability of *CD24* siRNA-transfected GaMGIR60 (and to a lesser extent GaMG) cells had increased relative to day 1. This could be consistent with recovery of *CD24* expression (which would have been tested had time permitted) and suggests that *CD24* knockdown did not completely kill the cells (Figure 5.15B). Despite the rise in viability on day 7 relative to day 1, it is important to note that the raw fluorescence values remained much lower in CD24-depleted cells than in untransfected or Allstars-transfected cells, indicating much lower cell numbers (Figure 5.15A).

The apparent reduction in viability may be explained by examination of the morphologies of *CD24* siRNA-transfected cells. Untransfected and Allstars-transfected cells retained the usual morphology of GaMG and GaMGIR60 cells in 2D growth (Figure 5.16A). However, cells that were transfected with *CD24* siRNA had rounded morphologies and clustered in the centre of the wells (Figure 5.16A). This was distinct from the wide spread of adherent cells within the control wells. The rounded morphologies and lack of cell spreading suggests that knockdown of *CD24* had an effect of reduced adherence on GaMG and GaMGIR60 cells. As the viability of the *CD24* knockdown cells started to recover (Day 6, Figure 5.15), the cells were imaged again. GaMGIR60 cells appeared to have regained the ability to spread to a slightly greater extent than GaMG (Figure 5.16B), potentially suggesting a quicker recovery of *CD24* expression and restoration of growth from the knockdown, as also suggested by the viability assay. This may be due to the higher basal levels of *CD24* mRNA and protein in GaMGIR60.

These results show that *CD24* can be knocked down in GaMG and GaMGIR60 cells, and that CD24 depletion affects the morphologies and viability of these cells. CD24 is therefore likely to be an important protein in the regulation of growth characteristics of GBM cells. Its upregulation in GaMGIR60 cells, as induced by the clinical dose of IR, may contribute to the relative increased chemotactic motility and 3D growth of these cells. Had time permitted, the relationship between upregulated CD24 and increased motility and 3D growth would have been investigated. The implications of upregulated CD24 and potential further experiments are discussed in the next sections.

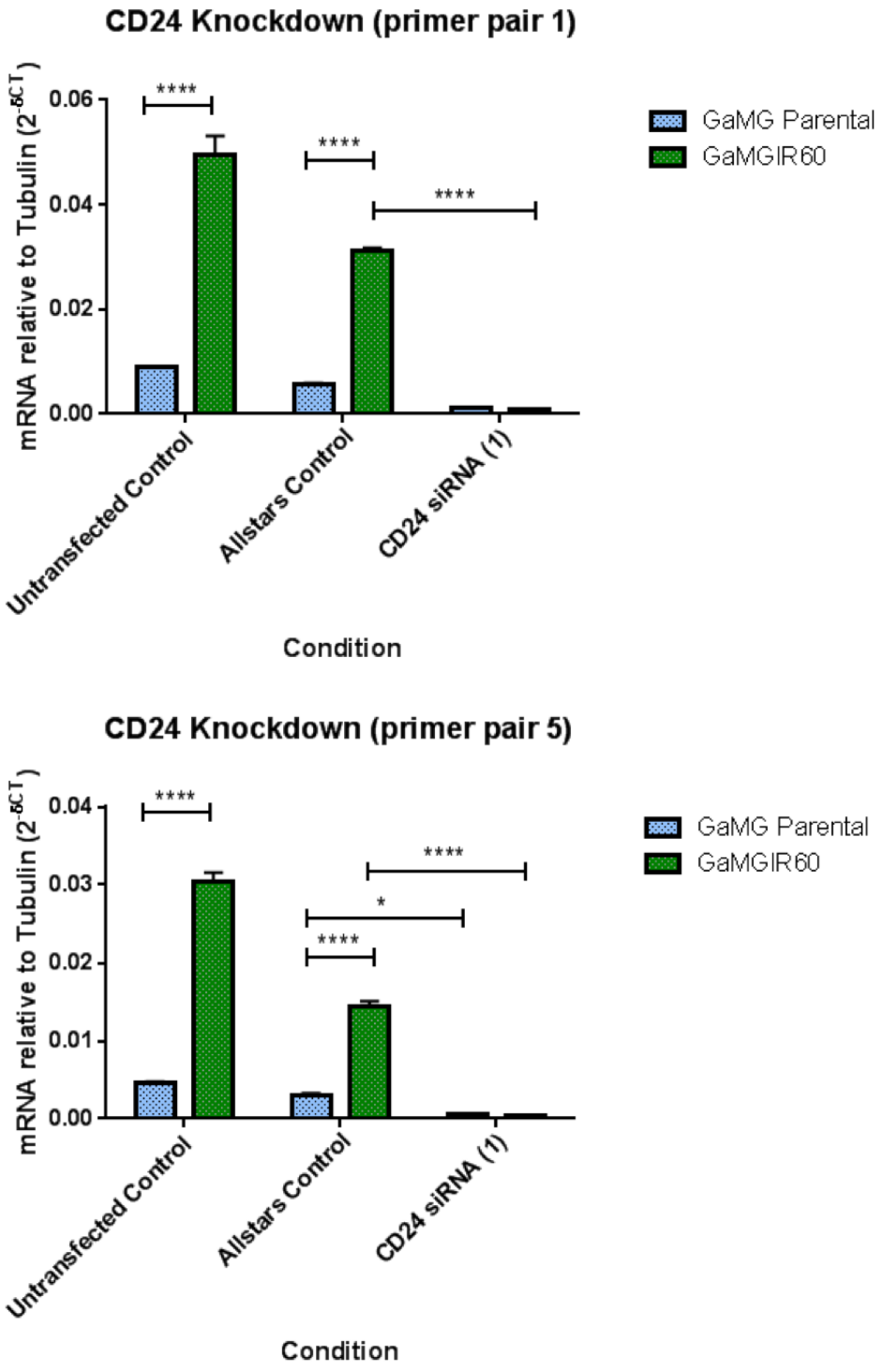
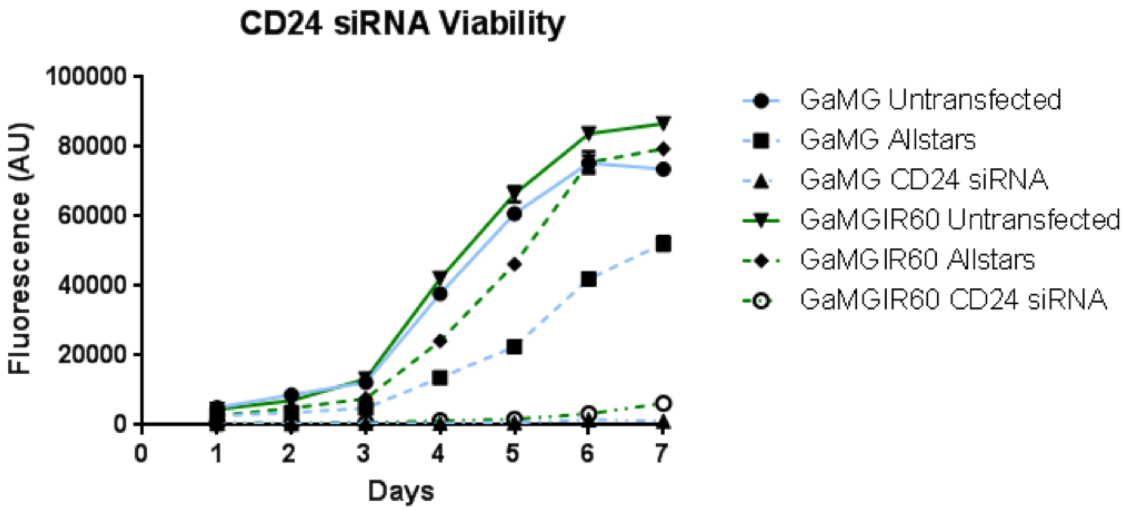


Figure 5.14: Knockdown of *CD24* in GaMG and GaMGIR60. Cells were transfected with *CD24* siRNA, non-silencing siRNA (Allstars), or were not transfected. Cells were harvested as cell pellets on ice at 96 hr post-transfection and frozen until lysis. RNA was extracted and converted to cDNA. *CD24* knockdown was tested by qRT-PCR using CD24 primer pair 1 (upper panel) and primer pair 5 (lower panel). Bars represent means ± SEM of triplicate readings from one experiment. The data were analysed by two-way ANOVAs (*$p < 0.05$; ****$p < 0.0001$).

A



B

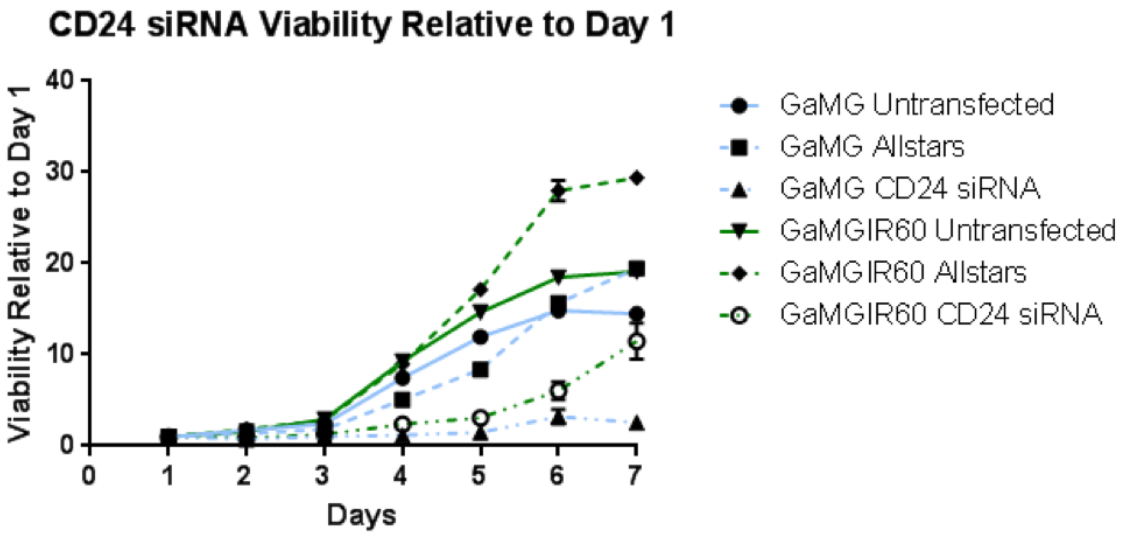


Figure 5.15: Effect of *CD24* knockdown on viability of GaMG and GaMGIR60. Cells were harvested 96 hr post-transfection with *CD24* or Allstars siRNA, or no transfection, and seeded into 96-well plates at a 2000 cells/well and incubated for 7 days. At one day intervals, viability was measured using CellTitre-Blue® and measuring 40 min after addition of reagent to wells. A) Raw viability data readings over 7 days for each experimental condition in GaMG and GaMGIR60 cells. B) Viability data from A expressed as fluorescence values relative to day 1 ($\frac{Day\ n}{Day\ 1}$). Points represent means ± SEM of triplicate data from a single experiment.

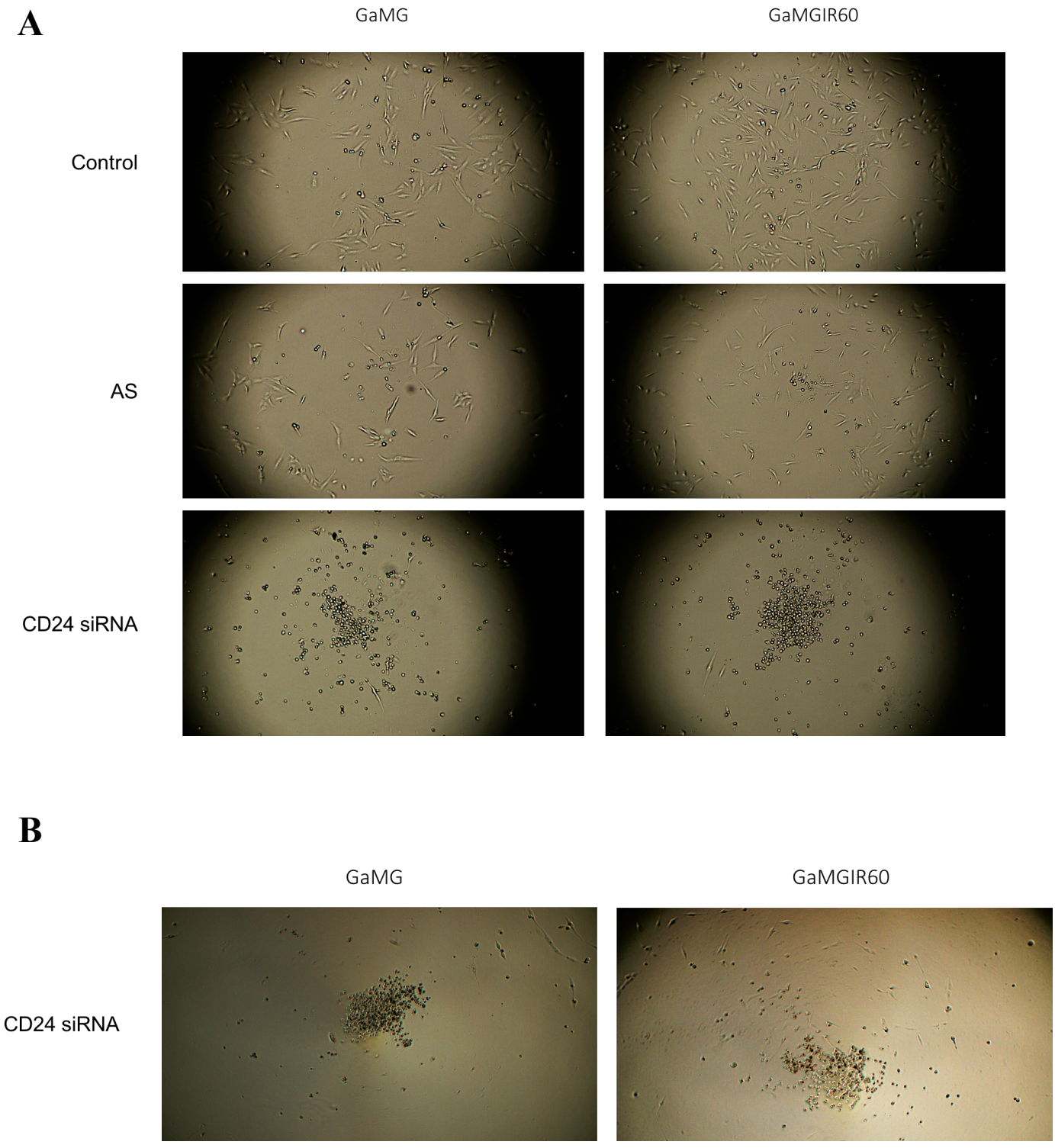


Figure 5.16: Morphologies of GaMG and GaMGIR60 following *CD24* knockdown. A) Representative wells for each condition in the experiment presented in Figure 5.15 were photographed on day 2 of the assay. B) Cells from *CD24* knockdown conditions were photographed again on day 6 of the assay. Photographs were taken with a Deltapix microscope camera.

5.3 Discussion

The intrinsic radio-resistance of the GBM cells studied here was higher than prostate cancer models previously studied in our lab (Chitnis et al., 2014; Turney et al., 2012). It has been suggested that radio-resistance may be due to the failure of p53 to activate the pro-apoptotic $p21^{BAX}$ in response to IR in GBM cells (Shu et al., 1998). Supporting this idea is that *TP53* is the most commonly mutated gene in GBM, and GaMG, LN-18, KNS42, and SF-188 all harbour mutant *TP53*. However, although not directly tested here, SF-188 were found to be sensitive to IR through a TP53-independent mechanism (Yount et al., 2001). Data presented here demonstrate that after treatment with 60 Gy IR, GBM cells can acquire an enhanced resistance to IR that is additional to their intrinsic radio-resistance, but that this does not happen universally. The LNIR60 subline was relatively radio-resistant compared with its LN-18 parental cell line, but GaMGIR60 was not when compared with GaMG. Support for this relative radio-resistance concept is afforded from previous studies that have induced a relative radio-resistance through single-dose, or repeated irradiation, but not with the clinically applicable dose schedule used here (Ding et al., 2014; Kim et al., 2012; Osuka et al., 2013; Xiao et al., 2014). In addition, IR has been shown to alter the viability of GBM cells, with radio-resistant cells displaying a relatively enhanced viability (Ding et al., 2014). This was not true for LNIR60 here, but was seen in GaMGIR60, especially within the 3D context, despite the lack of relative radio-resistance. Of note, what must be remembered when interpreting the data presented here is that the LNIR60 and GaMGIR60 models were not generated in a context where surrounding stroma tissue was present, as would be the case in the *in vivo* situation. It is likely that stromal support allows a survival advantage to tumour cells and may facilitate the induction of a radio-resistant phenotype (Mannino and Chalmers, 2011). The models presented here, particularly the radio-resistant LNIR60, represent only changes that may happen in response to IR as properties of the tumour cells

themselves, and therefore may not be fully indicative of the extent of radio-resistance or phenotypic change induced by IR *in vivo* when stroma tissue is present.

It was reasoned that the relatively radio-resistant phenotype of LNIR60 and increased colony sizes of GaMGIR60 may have been due to altered proliferation of GBM cells following IR, which would agree with what has been observed previously (Kim et al., 2012; Shankar et al., 2014). Increased proliferation was implicated in GaMGIR60, but not LNIR60, supporting the likelihood of a genuine relative radio-resistance in LNIR60 (i.e. it was less likely that more LNIR60 colonies simply exceeded the size cut-off for counting). However, the method used here to ascertain differences in proliferation (monitoring changes in viability over 6-7 days) differed to what were used in previous studies, and was likely not the best method to assess proliferation directly, given its ability to detect both changes in cell number and metabolism. To further consolidate differences (or lack of) in proliferation, total cell counts over a specified time period and analyses of cell cycle distributions could have been performed if time permitted.

Various studies have observed changes in motility and invasion in GBM cells following IR (Ding et al., 2014; Pei et al., 2015; Shankar et al., 2014; Vanan et al., 2012; Wild-Bode et al., 2001). Several methods were used to assess migration, motility and/or invasion in these studies, including wound-healing assays, migration chambers, uncoated, or Matrigel-coated Transwell assays, and analysis of infiltration *in vivo*. The larger colonies of GaMGIR60 were thought to possibly arise from an increase in motility relative to GaMG cells, in that cells had greater propensity to migrate more toward one another. Transwell assays showed that GaMGIR60 were more migratory by chemotaxis than GaMG, suggesting, concurringly, that IR, and in this case repeated IR as opposed to single doses, can promote migration of GBM cells. This has important implications in GBM, because, as implied by Wild-Bode *et al*. (2001), an increased motility, migration, and/or invasiveness

as a response to IR, may facilitate the escape of GBM cells from subsequent doses by movement of cells to areas outside the target volume for radiotherapy. This would result in a geographical miss and possibly render the radiotherapy less effective. In this way, the tumour may establish a more aggressive phenotype and could count towards the recurrence so frequently seen in GBM patients. It would be interesting to assess the invasiveness of both GaMGIR60 and LNIR60 compared with their parental cell lines *in vitro* through use of Matrigel-coated Transwell assays, and *in vivo* through implantation into animal models. Ongoing work in our lab is currently further investigating the migration and adherence of GaMGIR60 using xCELLigence real-time cell analysis.

Along with increased proliferation, viability, and motility, a trait that has been observed in GBM cells following IR is enrichment of stem cell-like characteristics (Kim et al., 2012). IR has been found to enrich GSCs (Bao et al., 2006). The study by Bao *et al.* (2006) showed that the proportion of CD133-expressing GBM cells increased following IR, and that these cells had better survival when challenged with subsequent IR. In the $CD133^+$ cells, activating phosphorylation of the DDR proteins ATM, Rad17, Chk1 and Chk2 was significantly higher than in $CD133^-$ cells, indicating the contribution of preferential activation of the DDR in GSCs. More recent studies have also shown GSCs to have an enhanced DDR compared with bulk, heterogeneous tumour cell populations (Ahmed et al., 2015; Carruthers et al., 2015). Upregulation of expression and activation of ATM, ATR, Chk1 and PARP1 were shown to contribute to the significantly increased radio-resistance in the GSC population. The expression levels of a select few DDR proteins were analysed in LNIR60 and GaMGIR60. In contrast to the studies on GSCs, upregulation of ATM was not observed for the relatively radio-resistant LNIR60. MGMT was upregulated in LNIR60 however, which was consistent with previous reports documenting the effects of IR on *MGMT* expression (Grombacher et al., 1996). What is most evidently missing from the

present study is a thorough investigation of the DDR in the IR60 sublines compared with their parental cell lines. If time allowed, this could have been performed by Western blotting for the phospho- and total levels of DDR proteins such as ATM, ATR, Chk1 and Chk2 at different time-points following single doses of IR. In addition, the DDR could have been further assessed by analysing the formation and resolution of double-strand breaks represented by γH2A.X, Rad50 or p53 binding protein 1 (53BP1) foci over time and in response to different doses of IR. Any differences seen in the DDR may have pointed toward a potential mechanism by which LNIR60 were more resistant to IR. Despite the lack of radio-resistance in GaMGIR60, it would still be important to assess the DDR. Indeed, components of the DDR were found to be involved in a mechanism that coordinated the enhanced motility of GBM cells following IR (Vanan et al., 2012)– an effect observed here with GaMGIR60.

Other than the clear upregulation of PDGFRβ in GaMGIR60, and slight upregulation of phospho- and total IGF-1R in LNIR60, there were no obvious differences in the protein targets representing RTK axes in the IR60 sublines, and *IGF1R*, *EGFR* and *PDGFRB* were not differentially expressed in the microarray analyses. Neither subline showed an increase in expression or phosphorylation of the commonly deregulated EGFR in GBM. However, the IGF axis has been implicated in radio-resistance in murine GSCs (Osuka et al., 2013) and has previously been shown to sensitise to IR in other tumour types (Chitnis et al., 2014; Turney et al., 2012), but IGF-1R inhibition was not found to sensitise adult GBM cells to single IR doses in this study (Chapter 3). Inhibition of PDGFRβ has recently been associated with a reduction of migration in GBM cells (Camorani et al., 2014), and both increased PDGFRβ and migration were seen here in GaMGIR60. It would be interesting to investigate the dependence of GaMGIR60 on PDGFRβ- whether it is active and whether its inhibition affects GaMGIR60 migration. Also, whether LNIR60 had developed a dependency on IGF-

1R following repeated irradiation might be worth investigating. If dependency was observed, it would contrast with the results presented in Chapter 3 and implicate the IGF-1R as a potentially important target following repeated irradiation, which is more applicable clinically.

The transcriptomes of GBM cells are known to be altered following IR, and mRNA sequencing has been used successfully in the context of radio-resistance to identify differentially expressed genes that may confer inhibition of apoptosis following IR (Ma et al., 2013). In addition, the gene expression response to IR has been characterised in breast cancer cells (Rashi-Elkeles et al., 2014). Analyses of the transcriptomes of GaMG, GaMGIR60, LN-18, and LNIR60 in this study showed transcription of many genes had been significantly altered by repeated irradiation, four of which were validated at the mRNA level by qRT-PCR. Importantly, *ATM* mRNA was found to be upregulated in LNIR60 relative to LN-18, but did not exceed the log2-fold change cut-off used in this study to be classified as differentially expressed (*ATM* log2-fold change: 0.60, cut-off: 1.0). Other genes involved in the DDR, including *ATR, CHEK1, CHEK2, RAD50, RAD51* and *TP53BP1* were also not differentially expressed.

SGK1 was found to be upregulated in LNIR60 relative to LN-18. This was consistent with a recent report wherein the authors found that SGK1 inhibition increased the anti-proliferative effects of IR in GBM cells when the two were used in combination, but only at high single doses of IR (Talarico et al., 2016). In contrast, a separate study showed that SGK1, through acting on *N*-myc downstream regulated gene 1 (NDRG1), induced resistance to TMZ, but not radiotherapy, through SGK1-dependent NDRG1 interaction with MGMT, promoting the stability and activity of MGMT (Weiler et al., 2014). In agreement with this second study, a modest increase in MGMT protein was observed in LNIR60 relative to LN-18, suggesting a similar potential link between possible SGK1 and MGMT upregulation in

LNIR60 cells. However, no differential expression was observed for *NDRG1* in the microarray analysis performed here. Further characterisation would be needed at the protein level to determine the contribution of SGK1 to the radio-resistance of LNIR60, or whether SGK1 may enhance TMZ resistance through acting downstream on MGMT.

The IGF axis was again implicated in radio-resistance, with *IGFBP3* upregulation validated in LNIR60 cells. IGFBP3 serves to prevent interaction of IGF-1 with IGF-1R, preventing phosphorylation of IGF-1R, which contrasts with the minor increase in phospho-IGF-1R seen in LNIR60 (Figure 5.8). An alternative mechanism for IGFBP3 in this context though may be the direct involvement in DNA damage repair, as seen in breast cancer cells (Lin et al., 2014). If nuclear translocation of IGFBP3 is true, it may explain the lack of inhibitory effects on IGF-1 activating the IGF-1R in LNIR60, as implicated by the slight increase in basal phospho-IGF-1R seen in LNIR60.

GaMGIR60 were found to have significantly upregulated podoplanin relative to GaMG. Podoplanin is closely associated with cancer cell migration and invasion, and has recently been characterised as having a stabilisation role for invadopodia, facilitating the degradation of extracellular matrix and invasion (Martin-Villar et al., 2015). In the context of GBM, cells that highly express podoplanin have been shown to have increased motility and podoplanin knockdown reduces cell motility (Grau et al., 2015; Peterziel et al., 2012). GaMGIR60 upregulated *PDPN* mRNA and were more migratory. Indeed, podoplanin localised to a greater density at the projections of GaMG and GaMGIR60 cells, suggesting a potential link with motility in these cells. This is the first time that radiation has been implicated in the upregulation of podoplanin in GBM. However, assessment of upregulation of podoplanin at the protein level by Western blotting was inconclusive. Given time, further experiments would seek to characterise the invasive properties of GaMGIR60 and GaMG

and compare the protein levels of podoplanin in GaMG and GaMGIR60 by flow cytometry. The effects of silencing podoplanin could then be assessed.

Perhaps the most noteworthy result obtained from the microarray analysis was the upregulation of *CD24* in GaMGIR60 relative to GaMG, subsequently confirmed at the mRNA and protein levels. CD24 is a CSC marker and adhesion molecule that has not been much studied in GBM. Reports have linked CD24 with increased invasion of GBM cells *in vitro* and *in vivo* (Fukushima et al., 2007; Senner et al., 1999), but again, this is the first study to report a link between repeated radiation and upregulated levels of CD24 in GBM. The effect of *CD24* silencing on GaMG and GaMGIR60 cell growth was tested. Knockdown was achieved, and cells showed clear reductions in viability, possibly due to impedance of adhesion. It would have been beneficial to use a second siRNA to help rule out potential off-target or toxic effects of the siRNA here, which could have accounted for the reduction in growth. In addition, as implied by the long recovery times of *CD24* siRNA-transfected cells, a lower concentration of siRNA may be more suitable for future experiments than the 50 nM used in these experiments. Given the strong links between CD24 and invasion, the characterisation and comparison of the invasive properties of GaMG and GaMGIR60, and subsequent analysis of invasion in the absence and presence of *CD24* silencing will be an important future step. Results of future experiments may therefore link the clinical dose of radiation with increased CD24 expression and increased migration and/or invasion, providing a potential explanation of GBM cells' evasion of IR therapy and establishment of a phenotype that could very well lead to a recurrence. In addition, the upregulation of a CSC marker suggests that it would be worthwhile testing for other GSC markers (such as nanog, CD133, Sox-2, Oct4 and nestin (Safa et al., 2015)) and GSC characteristics (such as the ability to sustain a tumour, produce heterogeneous daughter cells, and an enhanced sphere formation ability (Sampetrean and Saya, 2013)) induced by repeated irradiation in

GaMGIR60. Probing for other CSC markers and assessment of the activity of the DDR in comparison to GaMG would begin to answer this. Ongoing work in our lab is assessing the adherence properties of GaMG and GaMGIR60, the relationship between CD24, motility and invasion, and upregulation of other CSC markers in GaMGIR60.

6 Chapter VI: Future Work

The aim of this project was to investigate radio-resistance and chemo-resistance in GBM. The first angle from which this was tackled was investigation of IGF-1R inhibition as an approach to radio-/chemo-sensitise GBM. Study of the IGF-1R axis in a panel of GBM cell lines showed that paediatric, but not adult, GBM may be responsive to IGF-1R blockade.

To further understand the radio-sensitising effects of IGF-1R inhibition in the paediatric GBM cell line KNS42, it would be necessary to characterise the effects of the combination of IR and IGF-1R inhibition on apoptosis induction and cell cycle distribution. The differentiation between whether there is increased cell death or altered progression through the cell cycle may help to understand the mechanism by which IGF-1R appears to radio-sensitise KNS42 cells. Indeed, radio-sensitivity in mammalian cells varies through the cell cycle, as cells are more radio-sensitive in G1/G2-M and more radio-resistant in S phase, which correlates with the level of activity of HR (S: high; G2-M, G1: low) (Pawlik and Keyomarsi, 2004; Rothkamm et al., 2003). However, IGF-1R inhibition, which can result in G1 accumulation (Flanigan et al., 2010), did not radio-sensitise KNS42 cells when applied 24 hr before IR, but appeared to radio-sensitise KNS42 cells when applied 4 hr before or 24 hr after IR. Therefore, further experiments may also seek to clarify whether IGF-1R inhibition influences the induction and resolution of DSBs in response to IR. Previous work from our group found that IGF-1R inhibition delayed DSB repair by HR and NHEJ (Chitnis et al., 2014). It is possible that similar delayed repair may extend to paediatric GBM, which would highlight the possibility of targeting IGF-1R to increase the efficacy of radiotherapy.

Following modest results from the IGF-1R line of investigation, this project was subsequently successful in establishing and characterising several different models that may be useful for the future study of chemotherapy and radiotherapy resistance in GBM. Two

models of acquired TMZ resistance were established from cells that were initially sensitive to TMZ. GBM cells with intrinsic resistance to TMZ were found here to depend on MGMT for their resistance, but, in contrast, MGMT was not found to confer resistance in the induced-resistance sublines GaMG TMZ 100 and GaMG TMZ 300. The lack of dependence on MGMT shows that TMZ resistance from repeated exposure to TMZ can manifest through other, potentially more complex mechanisms. Initially, assessment of other DNA damage repair pathways, including MMR, BER, and DSB repair, should be assessed in GaMG TMZ 100 and GaMG TMZ 300 cells. Thereafter, in order to gain a global insight into development of TMZ resistance in these cells, gene expression microarray analyses and phospho-proteome array assessments could be performed. In parallel, a drug screen could be performed to commence the search for novel combinations of compounds that sensitise or overcome resistance to TMZ, as is much needed in GBM. A drug screen would make use of MGMT-dependent (LN-18) and MGMT-independent (GaMG TMZ 100 and GaMG TMZ 300) resistant cells. In addition, it would be beneficial to include cells that are resistant to the concentration of TMZ achieved clinically in the cerebrospinal fluid (~20 μM) (Agarwala and Kirkwood, 2000; Middleton et al., 2000), the generation and characterisation of which are underway in our lab. Given that resistance may be multifactorial, initial drug candidates may target components of DNA damage repair, RTK axes, cell cycle progression, multidrug resistance proteins, and other, miscellaneous targets. Initial concentrations usually start in the region of 1 μM, as was used to test O6BG in viability assays performed here. Together, the aforementioned experiments may provide insight into novel mechanisms of TMZ resistance and sensitisation in GBM.

The clinically applicable dose of IR was used here to establish two models of repeatedly irradiated cells. One model showed relative resistance to IR, the other showed changes in morphology and behaviour in culture. To further the characterisation and

functional experiments performed in this study, an important first step may be to assess the extent of stem-like characteristics, especially since LNIR60 were more resistant to IR and GaMGIR60 had upregulated a well-recognised CSC marker, CD24. Generation of stem-like cells by the clinical dose of IR would have important implications for the pathophysiology of GBM, especially in the context of recurrence. Assessment of CSC markers at the cell surface by immunofluorescence and/or flow cytometry and DDR response proteins would represent good starting places to begin stem-like characterisation, as it is very well recognised that GSCs have increased DNA repair capacity (Bao et al., 2006).

The potential link between increased motility and upregulation of CD24 and podoplanin in GaMGIR60 may be worth further investigation, and is one that has not previously been studied in GBM in relation to the clinical dose of IR. Firstly the adherence and invasion of GaMG and GaMGIR60 could be assessed and compared. Secondly, the effects of CD24 and podoplanin (if the latter is validated at the protein level) knockdown on adherence, motility, and invasion could be assessed to question whether upregulated CD24 and/or podoplanin effect a more motile phenotype. Thirdly, depending on results of the prior two sets of experiments, CD24 and/or podoplanin IHC may help to indicate whether the levels of expression of these two proteins correlate with prognosis and survival in GBM patients. Finally, again depending on the results obtained to this point, the use of *in vivo* models could characterise the effects of manipulating expression of CD24 and podoplanin, and may help to understand the role of these two proteins in the behaviour of GBM tumours *in vivo*.

Evidence exists of upregulation of CD24 by activation of the PDGF axis in GBM (Ma et al., 2005). If the upregulation of PDGFRβ is confirmed in a repeat assay in GaMGIR60 cells, it may be interesting to investigate whether the PDGF axis had a role in upregulating CD24 in GaMGIR60 and thus potentially led to increased motility of GBM

cells in response to the clinical dose of IR, an avenue that has not been investigated before. This may be achieved through assessing the response of GaMGIR60 to inhibition of the PDGF axis, and whether PDGF axis inhibition affects the expression of CD24, and the motility and invasion of GBM cells. If so, this would provide a means of manipulating CD24 expression and function, since drugs targeting PDGFR are becoming increasingly more specific (Camorani et al., 2014) and are undergoing clinical testing (ClinicalTrials.gov Identifier: NCT01140568).

The results generated in this study pave the way for several potential avenues of investigation that may help to better understand how GBM cells resist chemotherapy and radiotherapy. This resistance ultimately gives rise to inevitable recurrence in GBM patients, and understanding basic resistance mechanisms may generate results that could inform the design of future clinical trials.

7 Chapter VII: Appendices

7.1 List of Primary Antibodies

Target	Company	Catalogue Number	Application	Dilution Used	2° Antibody Dilution
AKT	CST	#9272	WB	1:1000	1:2000
ATM	CST	#2873	WB	1:1000	1:2000
BrdU	BD Biosciences	#347580	FC	1:100	1:200
CD24-RPE conjugate	Life Technologies	#MHCD2404	FC	1:100	-
Chk2	CST	#2662	WB	1:500	1:2000
Cleaved Caspase-3 (Asp175)	CST	#9661	WB	1:500	1:2000
EGF Receptor	CST	#2232	WB	1:1000	1:2000
IGF-1 Receptor β	CST	#3027	IF	1:200	1:2000
IGF-1 Receptor β	CST	#9750	IHC	1:50	-
IGF-I Receptor β	CST	#3027	WB	1:1000	1:2000
Insulin Receptor β	CST	#3025	WB	1:500	1:2000
IRS-1	CST	#3194	WB	1:500	1:2000
MEK1/2	CST	#4694	WB	1:1000	1:2000
MGMT	Abcam, CST	#ab39253, #2739	WB	1:500, 1:1000	1:2000
MRE-11	CST	#4895	WB	1:1000	1:2000
p44/42 MAPK (Erk1/2)	CST	#4695	WB	1:2000	1:5000
PARP	CST	#9542	WB	1:1000	1:2000
PDGF Receptor β	CST	#3169	WB	1:500	1:2000
Phospho-4E-BP1 (Thr37/46)	CST	#2855	WB	1:1000	1:5000
Phospho-Akt (Ser473)	CST	#4065, #4051	WB	1:500	1:2000
Phospho-EGF Receptor (Tyr1068)	CST	#2236	WB	1:500	1:2000
Phospho-Histone-H2A.X (Ser139)	Millipore	#05-636	IF	1:500	1:2000
Phospho-IGF-I Receptor β (Tyr1135/1136)/Insulin Receptor β (Tyr1150/1151)	CST	#3024	WB	1:300	1:2000
Phospho-MEK1/2 (Ser221)	CST	#2338	WB	1:1000	1:2000
Phospho-p44/42 MAPK (Erk1/2) (Thr202/Tyr204)	CST	#9101	WB	1:1000	1:2000, 1:5000
Phospho-S6 Ribosomal Protein (Ser235/236)	CST	#2211	WB	1:1000	1:2000
PI3 Kinase p110α	CST	#4249	WB	1:500	1:2000

Podoplanin	Abcam	Ab10288	WB	1:200	1:5000
Podoplanin	Abcam	Ab10288	IF	1:500	1:2000
PTEN	CST	#9559	WB	1:500	1:2000
β-tubulin	Sigma	#T4026	WB	1:2000	1:5000

WB: Western Blotting*

IHC: Immunohistochemistry

IF: Immunofluorescence

FC: Flow Cytometry

CST: Cell Signaling Technology

*Primary antibodies for Western blotting were diluted in 5% (w/v) non-fat dairy milk in TBST or 5% (w/v) BSA in TBST according to instructions on their datasheets.

7.2 List of Secondary Antibodies

Secondary antibodies were used for the Western Blotting, Immunofluorescence, and Flow Cytometry procedures. IHC used an antibody detection kit.

Western Blotting:

- Anti-Rabbit IgG, HRP-linked Antibody. CST #7074
- Anti-Mouse IgG, HRP-linked Antibody. CST #7076

Secondary antibodies for Western blotting were diluted in 5% (w/v) non-fat dairy milk in TBST.

Immunofluorescence and Flow Cytometry

- Alexa Fluor® 488 Conjugate Donkey Anti-Rabbit IgG. ThermoFisher Scientific #A21206
- Alexa Fluor® 488 Conjugate Goat Anti-Mouse IgG. ThermoFisher Scientific #A11029

7.3 Recipes

7.3.1 Gels

Protocols used for manually cast polyacrylamide gels were as follows:

Component	8% Resolving Gel	15% Resolving Gel	4% stacking Gel
Deionised Water	9.2 ml	4.4 ml	6 ml
30% Acrylamide-Bis	5.2 ml	10 ml	1.3 ml
1.5 M Tris-HCl pH 8.8	5.2 ml	5.2 ml	-
0.5 M Tris-HCl pH 6.8	-	-	2.5 ml
10% SDS	200 µl	200 µl	100 µl
Tetramethylethylenedia -mine (TEMED)	30 µl	30 µl	10 µl
10% Ammonium persulfate	150 µl	150 µl	50 µl

7.3.2 Buffers

For cell pellet lysis (section 2.7.2), RIPA-100 lysis buffer was used, as follows:

RIPA-100

Component	Concentration	Amount for 1 litre
Tris pH 7.5	20 mM	20 ml 1M stock Then add H_2O to 700 ml
EDTA pH 7.5	1 mM	2 ml 0.5 M stock
NaCl	100 mM	20 ml 5 M stock
Triton X-100	1% (v/v)	10 ml Stir 5 min before adding sodium deoxycholate
Sodium Deoxycholate	0.5% (w/v)	5 g Stir 5 min before adding SDS
SDS	0.1% (w/v)	1 g Stir 5 min, then add H_2O to 1 litre

Buffer was stored at 4°C. Prior to use, 20 µl phosphatase inhibitor cocktails 2 and 3, 20 µl reconstituted cOmplete™ EDTA-free protease inhibitor cocktail (x50), and 10 µl reconstituted Pefabloc® SC (x100) were freshly added per ml of buffer.

For lysis in dish (section 2.7.1), and loading protein samples into gels, 3 x Laemmli Sample Buffer was used, as follows:

3 x Laemmli Sample Buffer

Component	Concentration	Amount for 10 ml
2-Mercaptoethanol	15% (v/v)	1.5 ml
SDS	9% (w/v)	0.9 g
Glycerol	30% (v/v)	3.0 ml
Bromophenol Blue	0.3 mg/ml	3.0 mg
Tris-HCl pH 6.8	150 mM	3.0 ml 0.5 M stock
Deionised Water	-	Up to 10 ml

Buffer was stored at 4°C.

For electrophoresis of manually cast polyacrylamide gels, the running buffer used in SDS-PAGE was:

Running Buffer (20 l)

- 60.4 g Tris Base
- 288 g glycine
- 20 g SDS
- 20 l H_2O

For commercial 4-12% gradient gels, MOPS or MES running buffers (NP0001 and NP0002, Life Technologies) were used depending on the protein separation required. Buffers were stored at room temperature.

For electrotransfers not performed with the Trans-Blot® Turbo™ Transfer System, semi-dry transfer buffer was used, as follows:

Semi-Dry Transfer Buffer (20 l)

- 116 g Tris Base
- 58 g glycine
- 7.8 g SDS
- 16 l H_2O
- 4 l methanol
- Adjust to pH 9.2

Buffer was stored at room temperature.

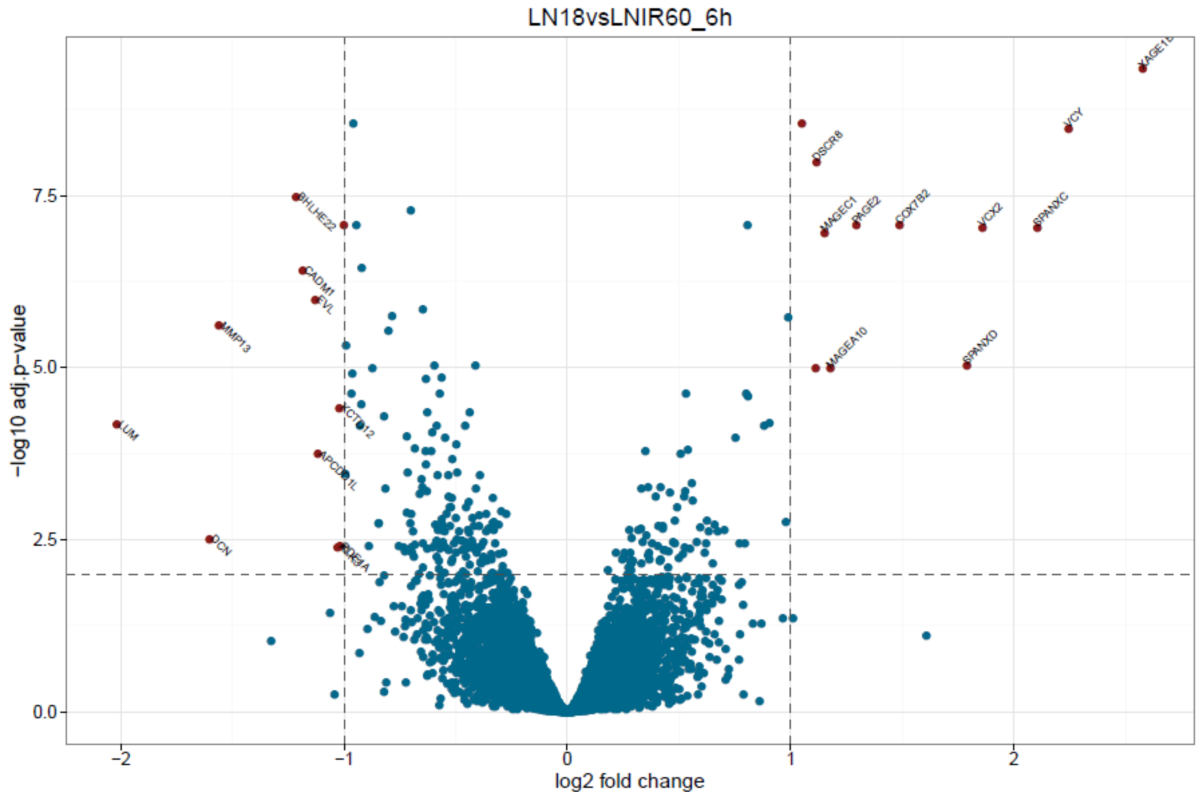
7.4 Additional Microarray Comparisons

To access the microarray data presented in this thesis, please contact Dr. Valentine Macaulay:

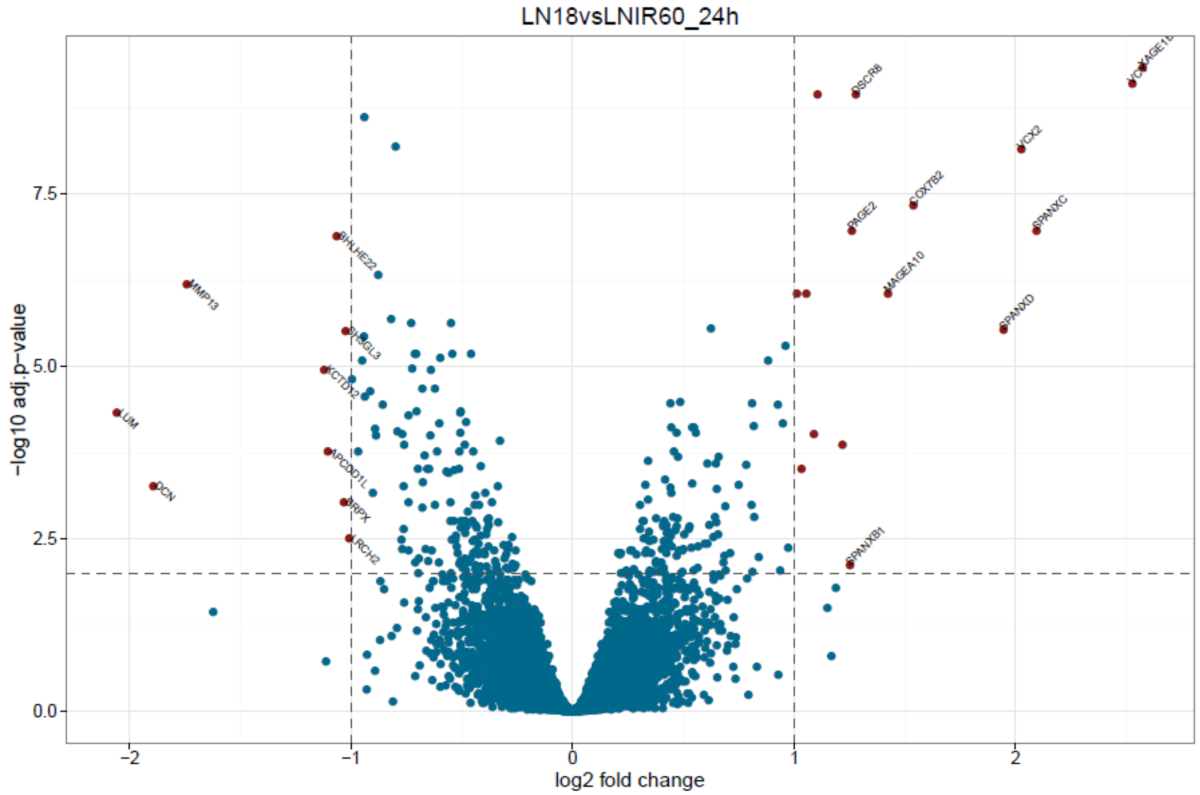
Dr Valentine Macaulay
Old Road Campus Research Building
Roosevelt Drive
Headington
Oxford. OX3 7DQ
Tel: 01865 222458
Email: valentine.macaulay@imm.ox.ac.uk

PA: Penny Berry
Tel: 01865 617435
Email: penny.berry@oncology.ox.ac.uk

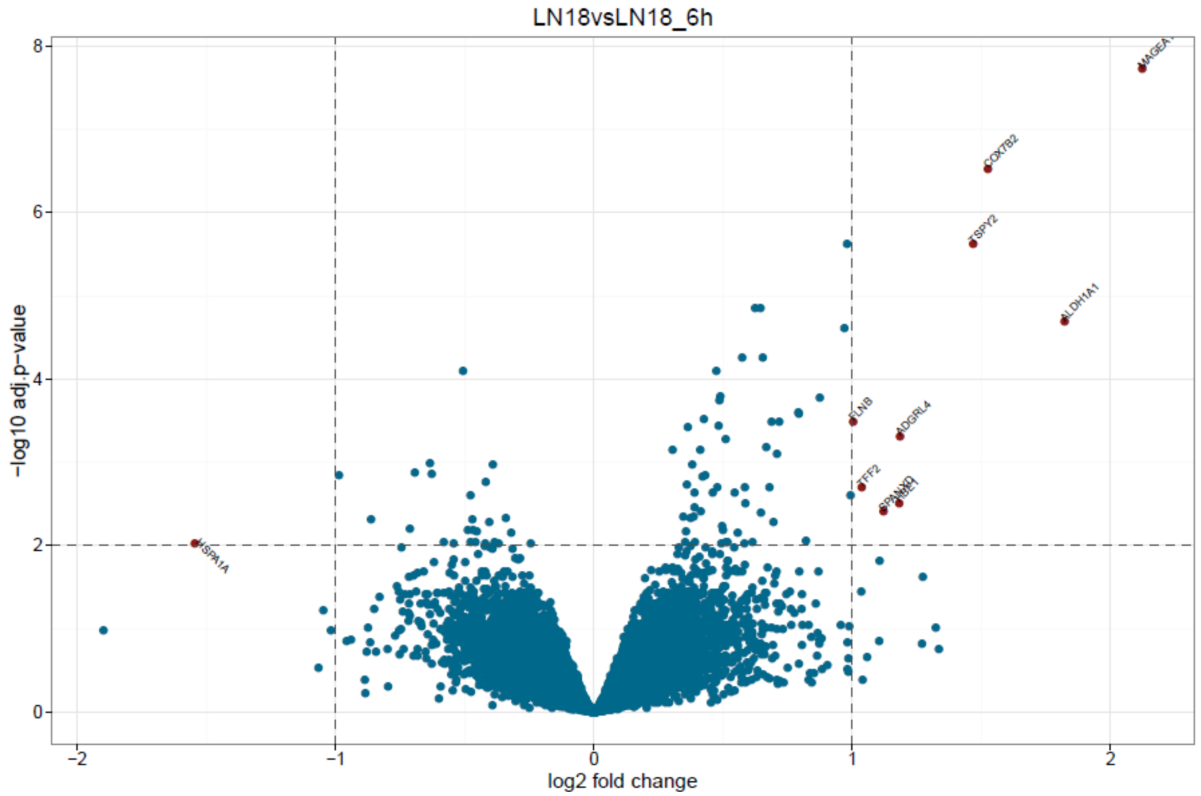
A


LN18vsLNIR60_6h
−log10 adj.p−value
log2 fold change
7.5
5.0
2.5
0.0
−2
−1
0
1
2
PHLHE22
CADM1
MMP13
UM
PCN
PRGE2
COX7B2
VCX2
PANX3
MAGEA10
PANX2

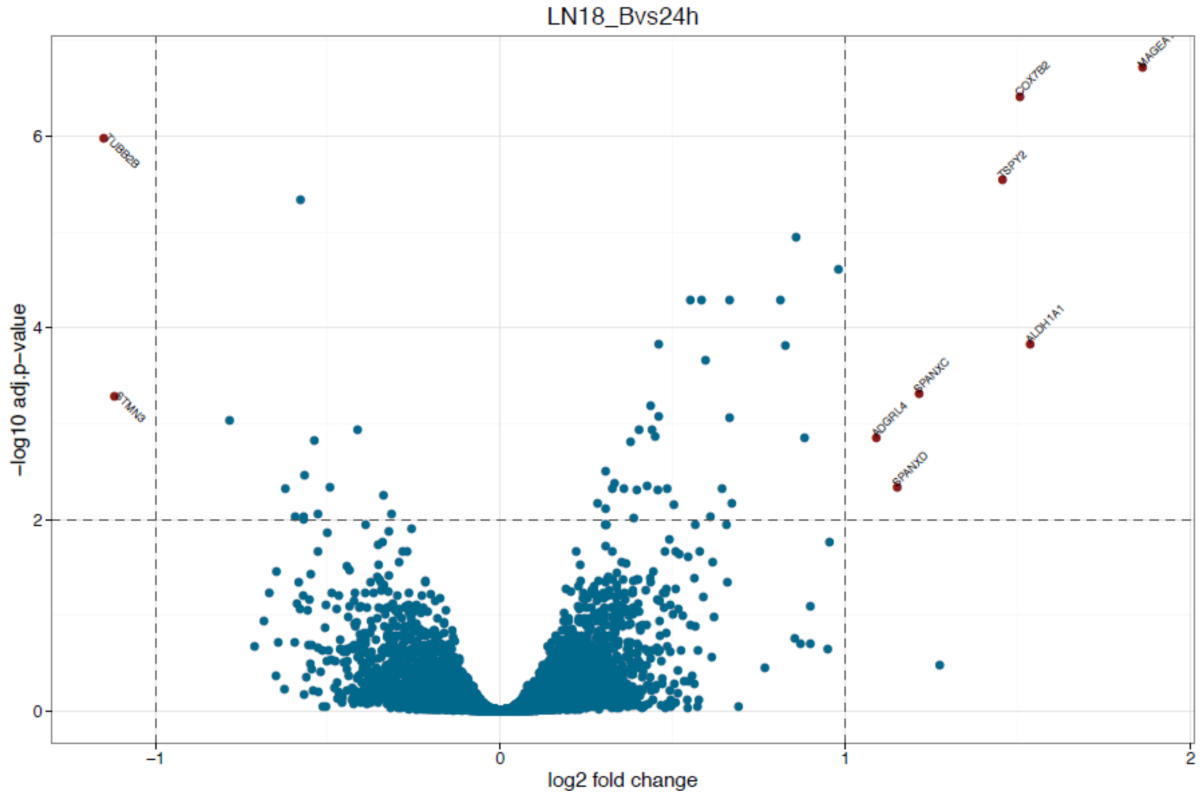
B


LN18vsLNIR60_24h
−log10 adj.p−value
log2 fold change
7.5
5.0
2.5
0.0
−2
−1
0
1
2
PHLHE22
MMP13
UM
PCN
PRGE2
COX7B2
VCX2
PANX3
MAGEA10
PANX2
PANX1

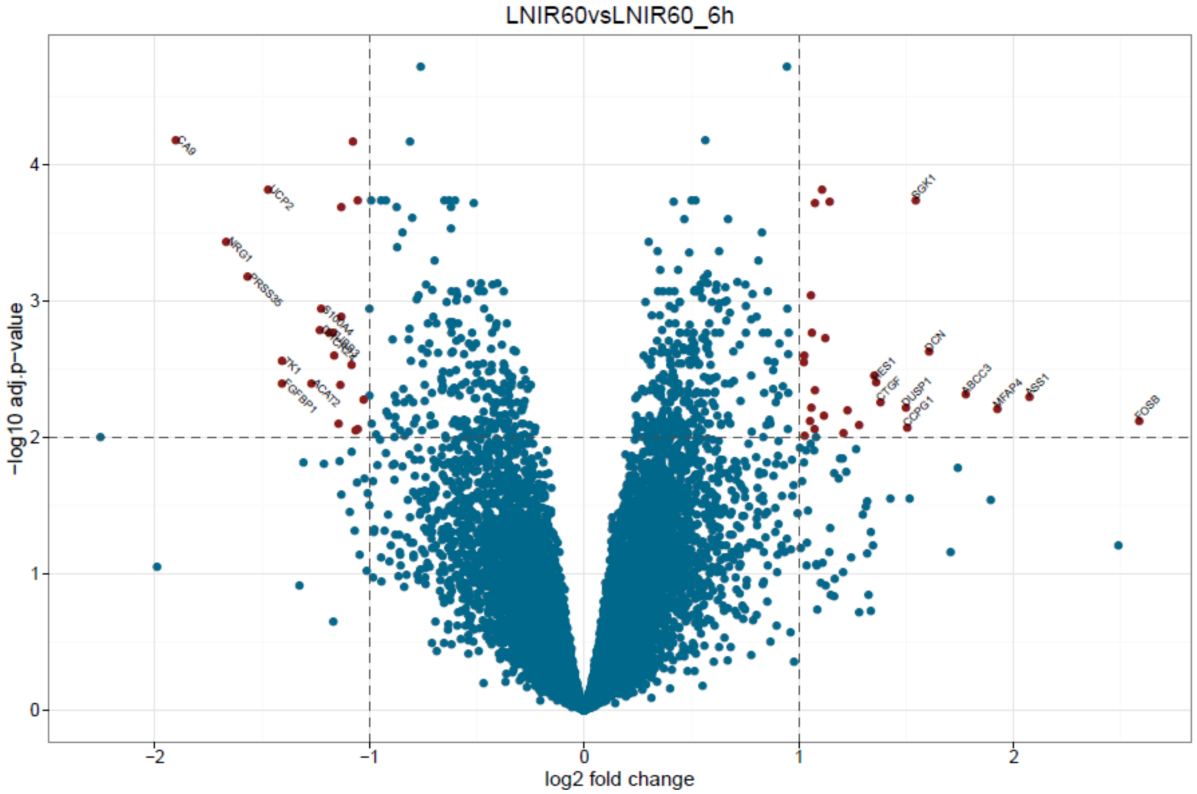
C


LN18vsLN18_6h
−log10 adj.p−value
log2 fold change
HSPA1A
FLNB
ADGRL4
TF2
ALDH1A1
SPY2
COX7B2
8
6
4
2
0
−2
−1
0
1
2

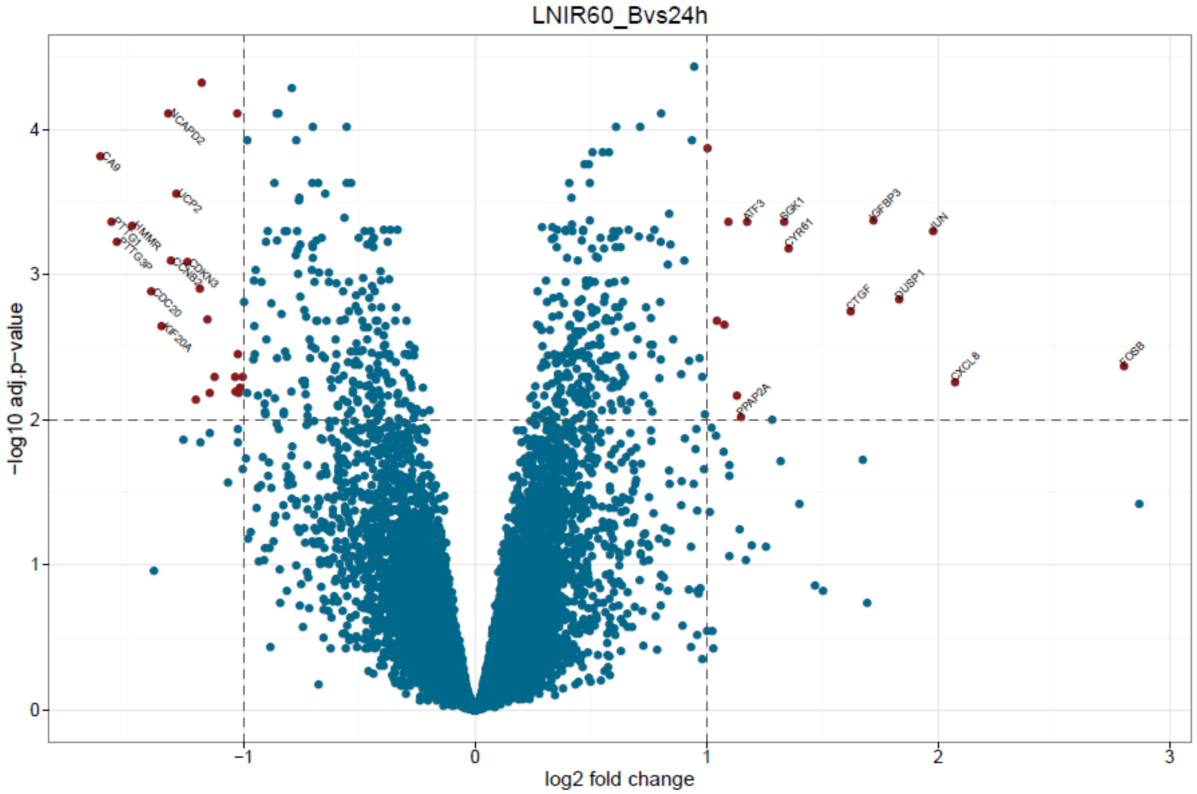
D


LN18_Bvs24h
−log10 adj.p−value
log2 fold change
TUBB2B
STMN3
ADGRL4
PANXC
PANXD
ALDH1A1
SPY2
COX7B2
6
4
2
0
−1
0
1
2

E


LNIR60vsLNIR60_6h
−log10 adj.p−value
log2 fold change
CA9
VCP2
NRG1
PRSS35
SLC2A4
HMOX1
TX1
IGFBP1
CAT2
SGK1
DCN
NES1
CTGF
DUSP1
CPG1
ABCC3
MFAP4
ASS1
FOSB

F


LNIR60_Bvs24h
−log10 adj.p−value
log2 fold change
VCAPD2
CA9
VCP2
HMMR
CDKN3
CDC20
KIF20A
ATF3
SGK1
CYR61
IGFBP3
JUN
CTGF
DUSP1
CXCL6
PAP2A
FOSB

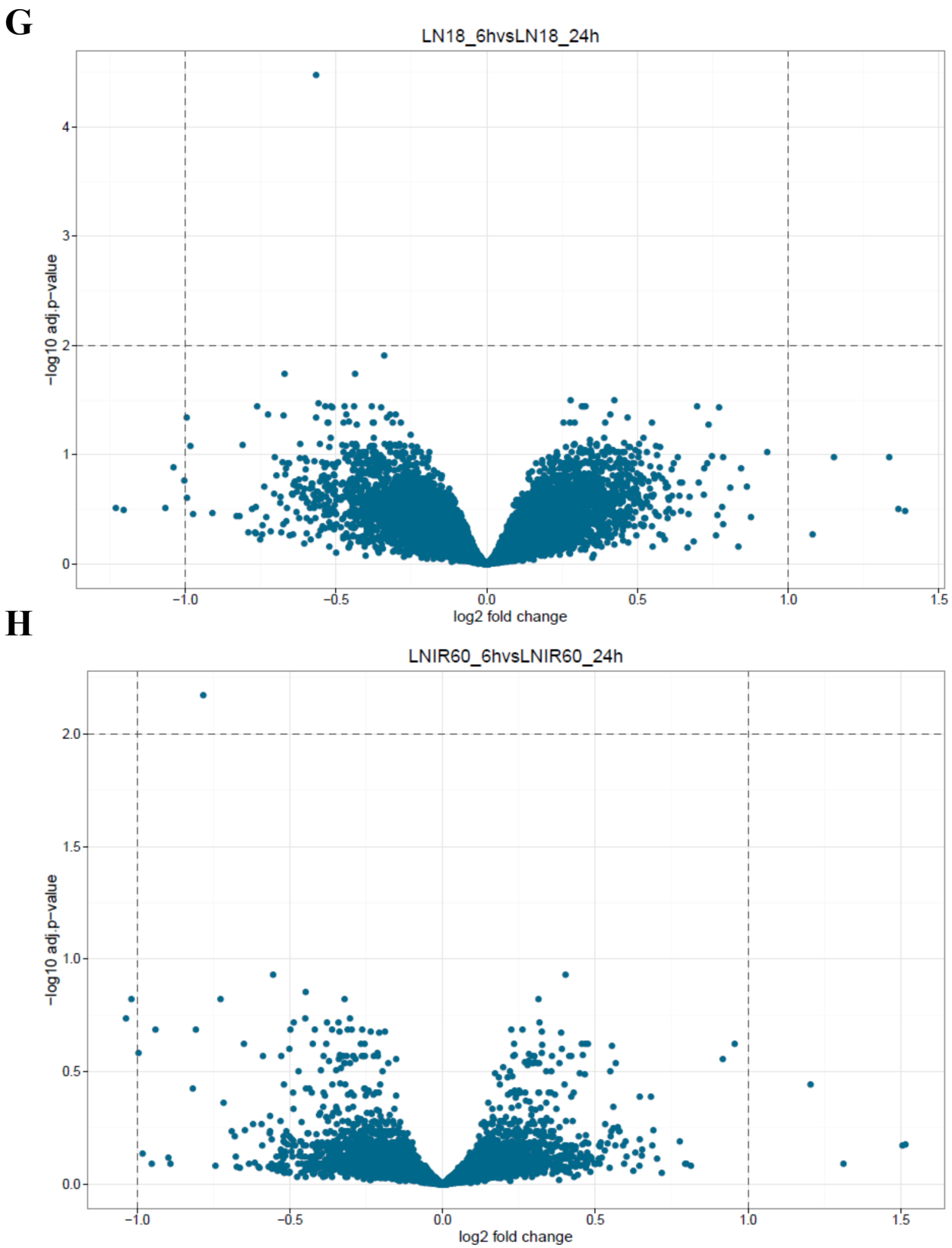


Figure A1: Additional comparisons from the microarray gene expression analysis experiment presented in Chapter 5. Gene expression comparisons for A) LN-18 6 hr post 5 Gy Vs LNIR60 6 hr post 5 Gy; B) LN-18 24 hr post 5 Gy Vs LNIR60 24 hr post 5 Gy; C) LN-18 unirradiated Vs LN-18 6 hr post 5 Gy; D) LN-18 unirradiated Vs LN-18 24 hr post 5 Gy; E) LNIR60 unirradiated Vs LNIR60 6 hr post 5 Gy; F) LNIR60 unirradiated Vs LNIR60 24 hr post 5 Gy; G) LN-18 6 hr post 5 Gy Vs LN-18 24 hr post 5 Gy; H) LNIR60 6 hr post 5 Gy Vs LNIR60 24 hr post 5 Gy. Dashed lines represent cut-off values for log2 fold change (vertical), and cut-off for adjusted p-value (horizontal). Red points represent genes that are differentially expressed ('hits'), blue points represent genes that are not differentially expressed.

8 Chapter VIII: References

Agarwala, S.S., and J.M. Kirkwood. 2000. Temozolomide, a novel alkylating agent with activity in the central nervous system, may improve the treatment of advanced metastatic melanoma. *Oncologist*. 5:144-151.

Agnihotri, S., A.S. Gajadhar, C. Ternamian, T. Gorlia, K.L. Diefes, P.S. Mischel, J. Kelly, G. McGown, M. Thorncroft, B.L. Carlson, J.N. Sarkaria, G.P. Margison, K. Aldape, C. Hawkins, M. Hegi, and A. Guha. 2012. Alkylpurine-DNA-N-glycosylase confers resistance to temozolomide in xenograft models of glioblastoma multiforme and is associated with poor survival in patients. *J Clin Invest*. 122:253-266.

Ahmed, M.A., A. Al-Attar, J. Kim, N.F. Watson, J.H. Scholefield, L.G. Durrant, and M. Ilyas. 2009. CD24 shows early upregulation and nuclear expression but is not a prognostic marker in colorectal cancer. *J Clin Pathol*. 62:1117-1122.

Ahmed, S.U., R. Carruthers, L. Gilmour, S. Yildirim, C. Watts, and A.J. Chalmers. 2015. Selective Inhibition of Parallel DNA Damage Response Pathways Optimizes Radiosensitization of Glioblastoma Stem-like Cells. *Cancer Res*. 75:4416-4428.

Aigner, S., C.L. Ramos, A. Hafezi-Moghadam, M.B. Lawrence, J. Friederichs, P. Altevogt, and K. Ley. 1998. CD24 mediates rolling of breast carcinoma cells on P-selectin. *FASEB J*. 12:1241-1251.

Aleksic, T., M.M. Chitnis, O.V. Perestenko, S. Gao, P.H. Thomas, G.D. Turner, A.S. Protheroe, M. Howarth, and V.M. Macaulay. 2010. Type 1 insulin-like growth factor receptor translocates to the nucleus of human tumor cells. *Cancer Res*. 70:6412-6419.

Aleksic, T., A.R. Worrall, C. Verrill, Turley H., C. L., and V.M. Macaulay. 2016. Improved Immunohistochemical Detection of Type 1 Insulin-Like Growth Factor Receptor in Human Tumors. *Immunochemistry & Immunopathology*. 2:114.

Alessi, D.R., M. Andjelkovic, B. Caudwell, P. Cron, N. Morrice, P. Cohen, and B.A. Hemmings. 1996. Mechanism of activation of protein kinase B by insulin and IGF-1. *EMBO J*. 15:6541-6551.

Alessi, D.R., S.R. James, C.P. Downes, A.B. Holmes, P.R. Gaffney, C.B. Reese, and P. Cohen. 1997. Characterization of a 3-phosphoinositide-dependent protein kinase which phosphorylates and activates protein kinase Balpha. *Curr Biol*. 7:261-269.

Ambrose, D., M. Resnicoff, D. Coppola, C. Sell, M. Miura, S. Jameson, R. Baserga, and R. Rubin. 1994. Growth regulation of human glioblastoma T98G cells by insulin-like growth factor-1 and its receptor. *J Cell Physiol*. 159:92-100.

Aronheim, A., D. Engelberg, N. Li, N. al-Alawi, J. Schlessinger, and M. Karin. 1994. Membrane targeting of the nucleotide exchange factor Sos is sufficient for activating the Ras signaling pathway. *Cell*. 78:949-961.

Backer, J.M., M.G. Myers, Jr., S.E. Shoelson, D.J. Chin, X.J. Sun, M. Miralpeix, P. Hu, B. Margolis, E.Y. Skolnik, J. Schlessinger, and et al. 1992. Phosphatidylinositol 3'-kinase is activated by association with IRS-1 during insulin stimulation. *EMBO J*. 11:3469-3479.

Bao, S., Q. Wu, R.E. McLendon, Y. Hao, Q. Shi, A.B. Hjelmeland, M.W. Dewhirst, D.D. Bigner, and J.N. Rich. 2006. Glioma stem cells promote radioresistance by preferential activation of the DNA damage response. *Nature*. 444:756-760.

Barani, I.J., and D.A. Larson. 2015. Radiation therapy of glioblastoma. *Cancer Treat Res*. 163:49-73.

Baskar, R., K.A. Lee, R. Yeo, and K.W. Yeoh. 2012. Cancer and radiation therapy: current advances and future directions. *Int J Med Sci*. 9:193-199.

Bax, D.A., S.E. Little, N. Gaspar, L. Perryman, L. Marshall, M. Viana-Pereira, T.A. Jones, R.D. Williams, A. Grigoriadis, G. Vassal, P. Workman, D. Sheer, R.M. Reis, A.D. Pearson, D. Hargrave, and C. Jones. 2009. Molecular and phenotypic characterisation of paediatric glioma cell lines as models for preclinical drug development. *PLoS One*. 4:e5209.

Bax, D.A., A. Mackay, S.E. Little, D. Carvalho, M. Viana-Pereira, N. Tamber, A.E. Grigoriadis, A. Ashworth, R.M. Reis, D.W. Ellison, S. Al-Sarraj, D. Hargrave, and C. Jones. 2010. A distinct spectrum of copy number aberrations in pediatric high-grade gliomas. *Clin Cancer Res*. 16:3368-3377.

Belfiore, A., and R. Malaguarnera. 2011. Insulin receptor and cancer. *Endocr Relat Cancer*. 18:R125-147.

Bender, S., Y. Tang, A.M. Lindroth, V. Hovestadt, D.T. Jones, M. Kool, M. Zapatka, P.A. Northcott, D. Sturm, W. Wang, B. Radlwimmer, J.W. Hojfeldt, N. Truffaux, D. Castel, S. Schubert, M. Ryzhova, H. Seker-Cin, J. Gronych, P.D. Johann, S. Stark, J. Meyer, T. Milde, M. Schuhmann, M. Ebinger, C.M. Monoranu, A. Ponnuswami, S. Chen, C. Jones, O. Witt, V.P. Collins, A. von Deimling, N. Jabado, S. Puget, J. Grill, K. Helin, A. Korshunov, P. Lichter, M. Monje, C. Plass, Y.J. Cho, and S.M. Pfister. 2013. Reduced H3K27me3 and DNA hypomethylation are major drivers of gene expression in K27M mutant pediatric high-grade gliomas. *Cancer Cell*. 24:660-672.

Bhaskar, P.T., and N. Hay. 2007. The two TORCs and Akt. *Dev Cell*. 12:487-502.

Bielen, A., L. Perryman, G.M. Box, M. Valenti, A. de Haven Brandon, V. Martins, A. Jury, S. Popov, S. Gowan, S. Jeay, F.I. Raynaud, F. Hofmann, D. Hargrave, S.A. Eccles, and C. Jones. 2011. Enhanced efficacy of IGF1R inhibition in pediatric glioblastoma by combinatorial targeting of PDGFRalpha/beta. *Mol Cancer Ther*. 10:1407-1418.

Bjerke, L., A. Mackay, M. Nandhabalan, A. Burford, A. Jury, S. Popov, D.A. Bax, D. Carvalho, K.R. Taylor, M. Vinci, I. Bajrami, I.M. McGonnell, C.J. Lord, R.M. Reis, D. Hargrave, A. Ashworth, P. Workman, and C. Jones. 2013. Histone H3.3. mutations drive pediatric glioblastoma through upregulation of MYCN. *Cancer Discov*. 3:512-519.

Blanc, J.L., M. Wager, J. Guilhot, S. Kusy, B. Bataille, T. Chantereau, F. Lapierre, C.J. Larsen, and L. Karayan-Tapon. 2004. Correlation of clinical features and methylation status of MGMT gene promoter in glioblastomas. *J Neurooncol*. 68:275-283.

Boriack-Sjodin, P.A., S.M. Margarit, D. Bar-Sagi, and J. Kuriyan. 1998. The structural basis of the activation of Ras by Sos. *Nature*. 394:337-343.

Brennan, C.W., R.G. Verhaak, A. McKenna, B. Campos, H. Noushmehr, S.R. Salama, S. Zheng, D. Chakravarty, J.Z. Sanborn, S.H. Berman, R. Beroukhim, B. Bernard, C.J. Wu, G. Genovese, I. Shmulevich, J. Barnholtz-Sloan, L. Zou, R. Vegesna, S.A. Shukla, G. Ciriello, W.K. Yung, W. Zhang, C. Sougnez, T. Mikkelsen, K. Aldape, D.D. Bigner, E.G. Van Meir, M. Prados, A. Sloan, K.L. Black, J. Eschbacher, G. Finocchiaro, W. Friedman, D.W. Andrews, A. Guha, M. Iacocca, B.P. O'Neill, G. Foltz, J. Myers, D.J. Weisenberger, R. Penny, R. Kucherlapati, C.M. Perou, D.N. Hayes, R. Gibbs, M. Marra, G.B. Mills, E. Lander, P. Spellman, R. Wilson, C. Sander, J. Weinstein, M. Meyerson, S. Gabriel, P.W. Laird, D. Haussler, G. Getz, L. Chin, and T.R. Network. 2013. The somatic genomic landscape of glioblastoma. *Cell*. 155:462-477.

Brodbelt, A., D. Greenberg, T. Winters, M. Williams, S. Vernon, V.P. Collins, and G. National Cancer Information Network Brain Tumour. 2015. Glioblastoma in England: 2007-2011. *Eur J Cancer*. 51:533-542.

Brunet, A., A. Bonni, M.J. Zigmond, M.Z. Lin, P. Juo, L.S. Hu, M.J. Anderson, K.C. Arden, J. Blenis, and M.E. Greenberg. 1999. Akt promotes cell survival by phosphorylating and inhibiting a Forkhead transcription factor. *Cell*. 96:857-868.

Brunet, A., J. Park, H. Tran, L.S. Hu, B.A. Hemmings, and M.E. Greenberg. 2001. Protein kinase SGK mediates survival signals by phosphorylating the forkhead transcription factor FKHRL1 (FOXO3a). *Mol Cell Biol*. 21:952-965.

Camorani, S., C.L. Esposito, A. Rienzo, S. Catuogno, M. Iaboni, G. Condorelli, V. de Franciscis, and L. Cerchia. 2014. Inhibition of receptor signaling and of glioblastoma-derived tumor growth by a novel PDGFRbeta aptamer. *Mol Ther*. 22:828-841.

Cancer Genome Atlas Research, N. 2008. Comprehensive genomic characterization defines human glioblastoma genes and core pathways. *Nature*. 455:1061-1068.

Cantley, L.C. 2002. The phosphoinositide 3-kinase pathway. *Science*. 296:1655-1657.

Carapancea, M., D. Cosaceanu, R. Budiu, A. Kwiecinska, L. Tataranu, V. Ciubotaru, O. Alexandru, M. Banita, C. Pisoschi, M.L. Backlund, R. Lewensohn, and A. Dricu. 2007. Dual targeting of IGF-1R and PDGFR inhibits proliferation in high-grade gliomas cells and induces radiosensitivity in JNK-1 expressing cells. *J Neurooncol*. 85:245-254.

Carboni, J.M., M. Wittman, Z. Yang, F. Lee, A. Greer, W. Hurlburt, S. Hillerman, C. Cao, G.H. Cantor, J. Dell-John, C. Chen, L. Discenza, K. Menard, A. Li, G. Trainor, D. Vyas, R. Kramer, R.M. Attar, and M.M. Gottardis. 2009. BMS-754807, a small molecule inhibitor of insulin-like growth factor-1R/IR. *Mol Cancer Ther*. 8:3341-3349.

Carruthers, R., S.U. Ahmed, K. Strathdee, N. Gomez-Roman, E. Amoah-Buahin, C. Watts, and A.J. Chalmers. 2015. Abrogation of radioresistance in glioblastoma stem-like cells by inhibition of ATM kinase. *Mol Oncol*. 9:192-203.

Cerami, E., J. Gao, U. Dogrusoz, B.E. Gross, S.O. Sumer, B.A. Aksoy, A. Jacobsen, C.J. Byrne, M.L. Heuer, E. Larsson, Y. Antipin, B. Reva, A.P. Goldberg, C. Sander, and N. Schultz. 2012. The cBio cancer genomics portal: an open platform for exploring multidimensional cancer genomics data. *Cancer Discov*. 2:401-404.

Chakravarti, A., J.S. Loeffler, and N.J. Dyson. 2002. Insulin-like growth factor receptor I mediates resistance to anti-epidermal growth factor receptor therapy in primary human glioblastoma cells through continued activation of phosphoinositide 3-kinase signaling. *Cancer Res*. 62:200-207.

Chan, K.M., D. Fang, H. Gan, R. Hashizume, C. Yu, M. Schroeder, N. Gupta, S. Mueller, C.D. James, R. Jenkins, J. Sarkaria, and Z. Zhang. 2013. The histone H3.3K27M mutation in pediatric glioma reprograms H3K27 methylation and gene expression. *Genes Dev*. 27:985-990.

Chandarlapaty, S., A. Sawai, M. Scaltriti, V. Rodrik-Outmezguine, O. Grbovic-Huezo, V. Serra, P.K. Majumder, J. Baselga, and N. Rosen. 2011. AKT inhibition relieves feedback suppression of receptor tyrosine kinase expression and activity. *Cancer Cell*. 19:58-71.

Chellappan, S.P., S. Hiebert, M. Mudryj, J.M. Horowitz, and J.R. Nevins. 1991. The E2F transcription factor is a cellular target for the RB protein. *Cell*. 65:1053-1061.

Chen, M.S., C.E. Ryan, and H. Piwnica-Worms. 2003. Chk1 kinase negatively regulates mitotic function of Cdc25A phosphatase through 14-3-3 binding. *Mol Cell Biol*. 23:7488-7497.

Chitnis, M.M., K.A. Lodhia, T. Aleksic, S. Gao, A.S. Protheroe, and V.M. Macaulay. 2014. IGF-1R inhibition enhances radiosensitivity and delays double-strand break repair by both non-homologous end-joining and homologous recombination. *Oncogene*. 33:5262-5273.

Chitnis, M.M., J.S. Yuen, A.S. Protheroe, M. Pollak, and V.M. Macaulay. 2008. The type 1 insulin-like growth factor receptor pathway. *Clin Cancer Res*. 14:6364-6370.

Clark, M.J., N. Homer, B.D. O'Connor, Z. Chen, A. Eskin, H. Lee, B. Merriman, and S.F. Nelson. 2010. U87MG decoded: the genomic sequence of a cytogenetically aberrant human cancer cell line. *PLoS Genet*. 6:e1000832.

Cosaceanu, D., R.A. Budiu, M. Carapancea, J. Castro, R. Lewensohn, and A. Dricu. 2007. Ionizing radiation activates IGF-1R triggering a cytoprotective signaling by interfering with Ku-DNA binding and by modulating Ku86 expression via a p38 kinase-dependent mechanism. *Oncogene*. 26:2423-2434.

Cross, D.A., D.R. Alessi, P. Cohen, M. Andjelkovich, and B.A. Hemmings. 1995. Inhibition of glycogen synthase kinase-3 by insulin mediated by protein kinase B. *Nature*. 378:785-789.

D'Ambrosio, C., A. Ferber, M. Resnicoff, and R. Baserga. 1996. A soluble insulin-like growth factor I receptor that induces apoptosis of tumor cells in vivo and inhibits tumorigenesis. *Cancer Res*. 56:4013-4020.

D'Atri, S., L. Tentori, P.M. Lacal, G. Graziani, E. Pagani, E. Benincasa, G. Zambruno, E. Bonmassar, and J. Jiricny. 1998. Involvement of the mismatch repair system in temozolomide-induced apoptosis. *Mol Pharmacol*. 54:334-341.

Dale, O.T., T. Aleksic, K.A. Shah, C. Han, H. Mehanna, D.C. Rapozo, J.D. Sheard, P. Goodyear, N.S. Upile, M. Robinson, T.M. Jones, S. Winter, and V.M. Macaulay. 2015. IGF-1R expression is associated with HPV-negative status and adverse survival in head and neck squamous cell cancer. *Carcinogenesis*. 36:648-655.

Daniel, R.A., A.L. Rozanska, E.A. Mulligan, Y. Drew, H.D. Thomas, D.J. Castelbuono, Z. Hostomsky, E.R. Plummer, D.A. Tweddle, A.V. Boddy, S.C. Clifford, and N.J. Curtin. 2010. Central nervous system penetration and enhancement of temozolomide activity in childhood medulloblastoma models by poly(ADP-ribose) polymerase inhibitor AG-014699. *Br J Cancer*. 103:1588-1596.

Datta, S.R., H. Dudek, X. Tao, S. Masters, H. Fu, Y. Gotoh, and M.E. Greenberg. 1997. Akt phosphorylation of BAD couples survival signals to the cell-intrinsic death machinery. *Cell*. 91:231-241.

De Meyts, P., B. Wallach, C.T. Christoffersen, B. Urso, K. Gronskov, L.J. Latus, F. Yakushiji, M.M. Ilondo, and R.M. Shymko. 1994. The insulin-like growth factor-I receptor. Structure, ligand-binding mechanism and signal transduction. *Horm Res*. 42:152-169.

Dhillon, A.S., S. Hagan, O. Rath, and W. Kolch. 2007. MAP kinase signalling pathways in cancer. *Oncogene*. 26:3279-3290.

Ding, H., Y.J. Cheng, H. Yan, R. Zhang, J.B. Zhao, C.F. Qian, W.B. Zhang, H. Xiao, and H.Y. Liu. 2014. Phosphoglycerate kinase 1 promotes radioresistance in U251 human glioma cells. *Oncol Rep*. 31:894-900.

Diserens, A.C., N. de Tribolet, A. Martin-Achard, A.C. Gaide, J.F. Schnegg, and S. Carrel. 1981. Characterization of an established human malignant glioma cell line: LN-18. *Acta Neuropathol*. 53:21-28.

Dittmann, K., C. Mayer, and H.P. Rodemann. 2005. Inhibition of radiation-induced EGFR nuclear import by C225 (Cetuximab) suppresses DNA-PK activity. *Radiother Oncol*. 76:157-161.

Dolan, M.E., R.C. Moschel, and A.E. Pegg. 1990. Depletion of mammalian O6-alkylguanine-DNA alkyltransferase activity by O6-benzylguanine provides a means to evaluate the role of this protein in protection against carcinogenic and therapeutic alkylating agents. *Proc Natl Acad Sci U S A*. 87:5368-5372.

Drablos, F., E. Feyzi, P.A. Aas, C.B. Vaagbo, B. Kavli, M.S. Bratlie, J. Pena-Diaz, M. Otterlei, G. Slupphaug, and H.E. Krokan. 2004. Alkylation damage in DNA and RNA--repair mechanisms and medical significance. *DNA Repair (Amst)*. 3:1389-1407.

Dynlacht, B.D., O. Flores, J.A. Lees, and E. Harlow. 1994. Differential regulation of E2F transactivation by cyclin/cdk2 complexes. *Genes Dev*. 8:1772-1786.

Esteller, M., J. Garcia-Foncillas, E. Andion, S.N. Goodman, O.F. Hidalgo, V. Vanaclocha, S.B. Baylin, and J.G. Herman. 2000. Inactivation of the DNA-repair gene MGMT and the clinical response of gliomas to alkylating agents. *N Engl J Med*. 343:1350-1354.

Evdokimova, V., C.E. Tognon, T. Benatar, W. Yang, K. Krutikov, M. Pollak, P.H. Sorensen, and A. Seth. 2012. IGFBP7 binds to the IGF-1 receptor and blocks its activation by insulin-like growth factors. *Sci Signal*. 5:ra92.

Falck, J., N. Mailand, R.G. Syljuasen, J. Bartek, and J. Lukas. 2001. The ATM-Chk2-Cdc25A checkpoint pathway guards against radioresistant DNA synthesis. *Nature*. 410:842-847.

Favelyukis, S., J.H. Till, S.R. Hubbard, and W.T. Miller. 2001. Structure and autoregulation of the insulin-like growth factor 1 receptor kinase. *Nat Struct Biol*. 8:1058-1063.

Firth, S.M., and R.C. Baxter. 2002. Cellular actions of the insulin-like growth factor binding proteins. *Endocr Rev*. 23:824-854.

Flanigan, S.A., T.M. Pitts, S.G. Eckhardt, J.J. Tentler, A.C. Tan, A. Thorburn, and S. Leong. 2010. The insulin-like growth factor I receptor/insulin receptor tyrosine kinase inhibitor PQIP exhibits enhanced antitumor effects in combination with chemotherapy against colorectal cancer models. *Clin Cancer Res*. 16:5436-5446.

Frech, M., M. Andjelkovic, E. Ingley, K.K. Reddy, J.R. Falck, and B.A. Hemmings. 1997. High affinity binding of inositol phosphates and phosphoinositides to the pleckstrin homology domain of RAC/protein kinase B and their influence on kinase activity. *J Biol Chem*. 272:8474-8481.

Friedbichler, K., M.H. Hofmann, M. Kroez, E. Ostermann, H.R. Lamche, C. Koessl, E. Borges, M.N. Pollak, G. Adolf, and P.J. Adam. 2014. Pharmacodynamic and antineoplastic activity of BI 836845, a fully human IGF ligand-neutralizing antibody, and mechanistic rationale for combination with rapamycin. *Mol Cancer Ther*. 13:399-409.

Friedmann-Morvinski, D., E.A. Bushong, E. Ke, Y. Soda, T. Marumoto, O. Singer, M.H. Ellisman, and I.M. Verma. 2012. Dedifferentiation of neurons and astrocytes by oncogenes can induce gliomas in mice. *Science*. 338:1080-1084.

Fukushima, T., Y. Nakamura, D. Yamanaka, T. Shibano, K. Chida, S. Minami, T. Asano, F. Hakuno, and S. Takahashi. 2012. Phosphatidylinositol 3-kinase (PI3K) activity bound to insulin-like growth factor-I (IGF-I) receptor, which is continuously sustained by IGF-I stimulation, is required for IGF-I-induced cell proliferation. *J Biol Chem*. 287:29713-29721.

Fukushima, T., T. Tezuka, T. Shimomura, S. Nakano, and H. Kataoka. 2007. Silencing of insulin-like growth factor-binding protein-2 in human glioblastoma cells reduces both invasiveness and expression of progression-associated gene CD24. *J Biol Chem*. 282:18634-18644.

Fulci, G., M. Labuhn, D. Maier, Y. Lachat, O. Hausmann, M.E. Hegi, R.C. Janzer, A. Merlo, and E.G. Van Meir. 2000. p53 gene mutation and ink4a-arf deletion appear to be two mutually exclusive events in human glioblastoma. *Oncogene*. 19:3816-3822.

Furnari, F.B., T. Fenton, R.M. Bachoo, A. Mukasa, J.M. Stommel, A. Stegh, W.C. Hahn, K.L. Ligon, D.N. Louis, C. Brennan, L. Chin, R.A. DePinho, and W.K. Cavenee. 2007. Malignant astrocytic glioma: genetics, biology, and paths to treatment. *Genes Dev*. 21:2683-2710.

Furuta, T., H. Takemura, Z.Y. Liao, G.J. Aune, C. Redon, O.A. Sedelnikova, D.R. Pilch, E.P. Rogakou, A. Celeste, H.T. Chen, A. Nussenzweig, M.I. Aladjem, W.M. Bonner, and Y. Pommier. 2003. Phosphorylation of histone H2AX and activation of Mre11, Rad50, and Nbs1 in response to replication-dependent DNA double-strand breaks induced by mammalian DNA topoisomerase I cleavage complexes. *J Biol Chem*. 278:20303-20312.

Gage, F.H., and S. Temple. 2013. Neural stem cells: generating and regenerating the brain. *Neuron*. 80:588-601.

Gao, J., B.A. Aksoy, U. Dogrusoz, G. Dresdner, B. Gross, S.O. Sumer, Y. Sun, A. Jacobsen, R. Sinha, E. Larsson, E. Cerami, C. Sander, and N. Schultz. 2013. Integrative analysis of complex cancer genomics and clinical profiles using the cBioPortal. *Sci Signal*. 6:pl1.

Garcia-Echeverria, C., M.A. Pearson, A. Marti, T. Meyer, J. Mestan, J. Zimmermann, J. Gao, J. Brueggen, H.G. Capraro, R. Cozens, D.B. Evans, D. Fabbro, P. Furet, D.G. Porta, J. Liebetanz, G. Martiny-Baron, S. Ruetz, and F. Hofmann. 2004. In vivo antitumor activity of NVP-AEW541-A novel, potent, and selective inhibitor of the IGF-IR kinase. *Cancer Cell*. 5:231-239.

Gaspar, N., L. Marshall, L. Perryman, D.A. Bax, S.E. Little, M. Viana-Pereira, S.Y. Sharp, G. Vassal, A.D. Pearson, R.M. Reis, D. Hargrave, P. Workman, and C. Jones. 2010. MGMT-independent temozolomide resistance in pediatric glioblastoma cells associated with a PI3-kinase-mediated HOX/stem cell gene signature. *Cancer Res*. 70:9243-9252.

Girnita, L., C. Worrall, S. Takahashi, S. Seregard, and A. Girnita. 2014. Something old, something new and something borrowed: emerging paradigm of insulin-like growth factor type 1 receptor (IGF-1R) signaling regulation. *Cell Mol Life Sci*. 71:2403-2427.

Gottlieb, T.M., and S.P. Jackson. 1993. The DNA-dependent protein kinase: requirement for DNA ends and association with Ku antigen. *Cell*. 72:131-142.

Grau, S.J., F. Trillsch, J.C. Tonn, R.H. Goldbrunner, E. Noessner, P.J. Nelson, and I. von Luettichau. 2015. Podoplanin increases migration and angiogenesis in malignant glioma. *Int J Clin Exp Pathol*. 8:8663-8670.

Grombacher, T., S. Mitra, and B. Kaina. 1996. Induction of the alkyltransferase (MGMT) gene by DNA damaging agents and the glucocorticoid dexamethasone and comparison with the response of base excision repair genes. *Carcinogenesis*. 17:2329-2336.

Haas-Kogan, D.A., G. Yount, M. Haas, D. Levi, S.S. Kogan, L. Hu, C. Vidair, D.F. Deen, W.C. Dewey, and M.A. Israel. 1996. p53-dependent G1 arrest and p53-independent apoptosis influence the radiobiologic response of glioblastoma. *Int J Radiat Oncol Biol Phys*. 36:95-103.

Hanahan, D., and R.A. Weinberg. 2011. Hallmarks of cancer: the next generation. *Cell*. 144:646-674.

Hanks, S.K., and T. Hunter. 1995. Protein kinases 6. The eukaryotic protein kinase superfamily: kinase (catalytic) domain structure and classification. *FASEB J*. 9:576-596.

Harrington, K.J., L.J. Billingham, T.B. Brunner, N.G. Burnet, C.S. Chan, P. Hoskin, R.I. Mackay, T.S. Maughan, J. Macdougall, W.G. McKenna, C.M. Nutting, A. Oliver, R. Plummer, I.J. Stratford, and T. Illidge. 2011. Guidelines for preclinical and early phase clinical assessment of novel radiosensitisers. *Br J Cancer*. 105:628-639.

Hartlerode, A.J., and R. Scully. 2009. Mechanisms of double-strand break repair in somatic mammalian cells. *Biochem J*. 423:157-168.

Hartog, H., W.T. Van Der Graaf, H.M. Boezen, and J. Wesseling. 2012. Treatment of breast cancer cells by IGF1R tyrosine kinase inhibitor combined with conventional systemic drugs. *Anticancer Res*. 32:1309-1318.

He, H., M. Yao, W. Zhang, B. Tao, F. Liu, S. Li, Y. Dong, C. Zhang, Y. Meng, Y. Li, G. Hu, C. Luo, H. Zong, and Y. Lu. 2015. MEK2 is a prognostic marker and potential chemo-sensitizing target for glioma patients undergoing temozolomide treatment. *Cell Mol Immunol*.

Hegi, M.E., A.C. Diserens, P. Bady, Y. Kamoshima, M.C. Kouwenhoven, M. Delorenzi, W.L. Lambiv, M.F. Hamou, M.S. Matter, A. Koch, F.L. Heppner, Y. Yonekawa, A. Merlo, K. Frei, L. Mariani, and S. Hofer. 2011. Pathway analysis of glioblastoma tissue after preoperative treatment with the EGFR tyrosine kinase inhibitor gefitinib--a phase II trial. *Mol Cancer Ther*. 10:1102-1112.

Hegi, M.E., A.C. Diserens, S. Godard, P.Y. Dietrich, L. Regli, S. Ostermann, P. Otten, G. Van Melle, N. de Tribolet, and R. Stupp. 2004. Clinical trial substantiates the predictive value of O-6-methylguanine-DNA methyltransferase promoter methylation in glioblastoma patients treated with temozolomide. *Clin Cancer Res*. 10:1871-1874.

Hegi, M.E., A.C. Diserens, T. Gorlia, M.F. Hamou, N. de Tribolet, M. Weller, J.M. Kros, J.A. Hainfellner, W. Mason, L. Mariani, J.E. Bromberg, P. Hau, R.O. Mirimanoff, J.G. Cairncross, R.C. Janzer, and R. Stupp. 2005. MGMT gene silencing and benefit from temozolomide in glioblastoma. *N Engl J Med*. 352:997-1003.

Hiebert, S.W., S.P. Chellappan, J.M. Horowitz, and J.R. Nevins. 1992. The interaction of RB with E2F coincides with an inhibition of the transcriptional activity of E2F. *Genes Dev*. 6:177-185.

Hinz, J.M., N.A. Yamada, E.P. Salazar, R.S. Tebbs, and L.H. Thompson. 2005. Influence of double-strand-break repair pathways on radiosensitivity throughout the cell cycle in CHO cells. *DNA Repair (Amst)*. 4:782-792.

Holland, E.C. 2000. Glioblastoma multiforme: the terminator. *Proc Natl Acad Sci U S A*. 97:6242-6244.

Hou, L.C., A. Veeravagu, A.R. Hsu, and V.C. Tse. 2006. Recurrent glioblastoma multiforme: a review of natural history and management options. *Neurosurg Focus*. 20:E5.

Iwasa, T., I. Okamoto, M. Suzuki, E. Hatashita, Y. Yamada, M. Fukuoka, K. Ono, and K. Nakagawa. 2009. Inhibition of insulin-like growth factor 1 receptor by CP-751,871 radiosensitizes non-small cell lung cancer cells. *Clin Cancer Res*. 15:5117-5125.

Jackson, S.P., and J. Bartek. 2009. The DNA-damage response in human biology and disease. *Nature*. 461:1071-1078.

Jaggupilli, A., and E. Elkord. 2012. Significance of CD44 and CD24 as cancer stem cell markers: an enduring ambiguity. *Clin Dev Immunol*. 2012:708036.

Jones, C., and S.J. Baker. 2014. Unique genetic and epigenetic mechanisms driving paediatric diffuse high-grade glioma. *Nat Rev Cancer*. 14.

Jones, C., M.A. Karajannis, D.T. Jones, M.W. Kieran, M. Monje, S.J. Baker, O.J. Becher, Y.J. Cho, N. Gupta, C. Hawkins, D. Hargrave, D.A. Haas-Kogan, N. Jabado, X.N. Li, S. Mueller, T. Nicolaides, R.J. Packer, A.I. Persson, J.J. Phillips, E.F. Simonds, J.M. Stafford, Y. Tang, S.M. Pfister, and W.A. Weiss. 2017. Pediatric high-grade glioma: biologically and clinically in need of new thinking. *Neuro Oncol*. 19:153-161.

Jones, J.I., A. Gockerman, W.H. Busby, Jr., C. Camacho-Hubner, and D.R. Clemmons. 1993. Extracellular matrix contains insulin-like growth factor binding protein-5: potentiation of the effects of IGF-I. *J Cell Biol*. 121:679-687.

Kandoth, C., M.D. McLellan, F. Vandin, K. Ye, B. Niu, C. Lu, M. Xie, Q. Zhang, J.F. McMichael, M.A. Wyczalkowski, M.D. Leiserson, C.A. Miller, J.S. Welch, M.J. Walter, M.C. Wendl, T.J. Ley, R.K. Wilson, B.J. Raphael, and L. Ding. 2013. Mutational landscape and significance across 12 major cancer types. *Nature*. 502:333-339.

Kato, J., H. Matsushime, S.W. Hiebert, M.E. Ewen, and C.J. Sherr. 1993. Direct binding of cyclin D to the retinoblastoma gene product (pRb) and pRb phosphorylation by the cyclin D-dependent kinase CDK4. *Genes Dev*. 7:331-342.

Kim, Y., K.H. Kim, J. Lee, Y.A. Lee, M. Kim, S.J. Lee, K. Park, H. Yang, J. Jin, K.M. Joo, J. Lee, and D.H. Nam. 2012. Wnt activation is implicated in glioblastoma radioresistance. *Lab Invest*. 92:466-473.

King, H., T. Aleksic, P. Haluska, and V.M. Macaulay. 2014. Can we unlock the potential of IGF-1R inhibition in cancer therapy? *Cancer Treat Rev*. 40:1096-1105.

Kitange, G.J., B.L. Carlson, M.A. Schroeder, P.T. Grogan, J.D. Lamont, P.A. Decker, W. Wu, C.D. James, and J.N. Sarkaria. 2009. Induction of MGMT expression is associated with temozolomide resistance in glioblastoma xenografts. *Neuro Oncol*. 11:281-291.

Kobayashi, T., and P. Cohen. 1999. Activation of serum- and glucocorticoid-regulated protein kinase by agonists that activate phosphatidylinositide 3-kinase is mediated by 3-phosphoinositide-dependent protein kinase-1 (PDK1) and PDK2. *Biochem J*. 339 (Pt 2):319-328.

Kohsaka, S., L. Wang, K. Yachi, R. Mahabir, T. Narita, T. Itoh, M. Tanino, T. Kimura, H. Nishihara, and S. Tanaka. 2012. STAT3 inhibition overcomes temozolomide resistance in glioblastoma by downregulating MGMT expression. *Mol Cancer Ther*. 11:1289-1299.

Kyriakis, J.M., H. App, X.F. Zhang, P. Banerjee, D.L. Brautigan, U.R. Rapp, and J. Avruch. 1992. Raf-1 activates MAP kinase-kinase. *Nature*. 358:417-421.

Lackey, J., J. Barnett, L. Davidson, I.H. Batty, N.R. Leslie, and C.P. Downes. 2007. Loss of PTEN selectively desensitizes upstream IGF1 and insulin signaling. *Oncogene*. 26:7132-7142.

Lang, F., and E. Shumilina. 2013. Regulation of ion channels by the serum- and glucocorticoid-inducible kinase SGK1. *FASEB J*. 27:3-12.

Lee, G.Y., P.A. Kenny, E.H. Lee, and M.J. Bissell. 2007. Three-dimensional culture models of normal and malignant breast epithelial cells. *Nat Methods*. 4:359-365.

Lee, J.H., and T.T. Paull. 2005. ATM activation by DNA double-strand breaks through the Mre11-Rad50-Nbs1 complex. *Science*. 308:551-554.

Leevers, S.J., H.F. Paterson, and C.J. Marshall. 1994. Requirement for Ras in Raf activation is overcome by targeting Raf to the plasma membrane. *Nature*. 369:411-414.

Lemmon, M.A., and J. Schlessinger. 2010. Cell signaling by receptor tyrosine kinases. *Cell*. 141:1117-1134.

Li, H.F., J.S. Kim, and T. Waldman. 2009. Radiation-induced Akt activation modulates radioresistance in human glioblastoma cells. *Radiat Oncol*. 4:43.

Li, L., and Y. Lu. 2011. Optimizing a 3D Culture System to Study the Interaction between Epithelial Breast Cancer and Its Surrounding Fibroblasts. *J Cancer*. 2:458-466.

Li, P., M.R. Veldwijk, Q. Zhang, Z.B. Li, W.C. Xu, and S. Fu. 2013. Co-inhibition of epidermal growth factor receptor and insulin-like growth factor receptor 1 enhances radiosensitivity in human breast cancer cells. *BMC Cancer*. 13:297.

Lin, M.Z., K.A. Marzec, J.L. Martin, and R.C. Baxter. 2014. The role of insulin-like growth factor binding protein-3 in the breast cancer cell response to DNA-damaging agents. *Oncogene*. 33:85-96.

Liu, C., J.C. Sage, M.R. Miller, R.G. Verhaak, S. Hippenmeyer, H. Vogel, O. Foreman, R.T. Bronson, A. Nishiyama, L. Luo, and H. Zong. 2011. Mosaic analysis with double markers reveals tumor cell of origin in glioma. *Cell*. 146:209-221.

Liu, L., L.M. Backlund, B.R. Nilsson, D. Grander, K. Ichimura, H.M. Goike, and V.P. Collins. 2005. Clinical significance of EGFR amplification and the aberrant EGFRvIII transcript in conventionally treated astrocytic gliomas. *J Mol Med (Berl)*. 83:917-926.

Livak, K.J., and T.D. Schmittgen. 2001. Analysis of relative gene expression data using real-time quantitative PCR and the 2(-Delta Delta C(T)) Method. *Methods*. 25:402-408.

Louis, D.N. 1994. The p53 gene and protein in human brain tumors. *J Neuropathol Exp Neurol*. 53:11-21.

Louis, D.N., H. Ohgaki, O.D. Wiestler, W.K. Cavenee, P.C. Burger, A. Jouvet, B.W. Scheithauer, and P. Kleihues. 2007. The 2007 WHO classification of tumours of the central nervous system. *Acta Neuropathol*. 114:97-109.

Louis, D.N., A. Perry, G. Reifenberger, A. von Deimling, D. Figarella-Branger, W.K. Cavenee, H. Ohgaki, O.D. Wiestler, P. Kleihues, and D.W. Ellison. 2016. The 2016 World Health Organization Classification of Tumors of the Central Nervous System: a summary. *Acta Neuropathol*. 131:803-820.

Lu, X., L. de la Pena, C. Barker, K. Camphausen, and P.J. Tofilon. 2006. Radiation-induced changes in gene expression involve recruitment of existing messenger RNAs to and away from polysomes. *Cancer Res*. 66:1052-1061.

Ma, D., C.L. Nutt, P. Shanehsaz, X. Peng, D.N. Louis, and D.M. Kaetzel. 2005. Autocrine platelet-derived growth factor-dependent gene expression in glioblastoma cells is mediated largely by activation of the transcription factor sterol regulatory element binding protein and is associated with altered genotype and patient survival in human brain tumors. *Cancer Res*. 65:5523-5534.

Ma, H., L. Rao, H.L. Wang, Z.W. Mao, R.H. Lei, Z.Y. Yang, H. Qing, and Y.L. Deng. 2013. Transcriptome analysis of glioma cells for the dynamic response to gamma-irradiation and dual regulation of apoptosis genes: a new insight into radiotherapy for glioblastomas. *Cell Death Dis*. 4:e895.

Ma, Y., N. Tang, R.C. Thompson, B.C. Mobley, S.W. Clark, J.N. Sarkaria, and J. Wang. 2016. InsR/IGF1R Pathway Mediates Resistance to EGFR Inhibitors in Glioblastoma. *Clin Cancer Res*. 22:1767-1776.

Mailand, N., J. Falck, C. Lukas, R.G. Syljuasen, M. Welcker, J. Bartek, and J. Lukas. 2000. Rapid destruction of human Cdc25A in response to DNA damage. *Science*. 288:1425-1429.

Manning, B.D., and L.C. Cantley. 2007. AKT/PKB signaling: navigating downstream. *Cell*. 129:1261-1274.

Manning, G., D.B. Whyte, R. Martinez, T. Hunter, and S. Sudarsanam. 2002. The protein kinase complement of the human genome. *Science*. 298:1912-1934.

Mannino, M., and A.J. Chalmers. 2011. Radioresistance of glioma stem cells: intrinsic characteristic or property of the 'microenvironment-stem cell unit'? *Mol Oncol*. 5:374-386.

Marais, R., Y. Light, H.F. Paterson, and C.J. Marshall. 1995. Ras recruits Raf-1 to the plasma membrane for activation by tyrosine phosphorylation. *EMBO J*. 14:3136-3145.

Margison, G. 2010. O(6)-methylguanine in DNA: bad penny? *Cell Cycle*. 9:441-442.

Maris, C., N. D'Haene, A.L. Trepant, M. Le Mercier, S. Sauvage, J. Allard, S. Rorive, P. Demetter, C. Decaestecker, and I. Salmon. 2015. IGF-IR: a new prognostic biomarker for human glioblastoma. *Br J Cancer*. 113:729-737.

Martin-Villar, E., B. Borda-d'Agua, P. Carrasco-Ramirez, J. Renart, M. Parsons, M. Quintanilla, and G.E. Jones. 2015. Podoplanin mediates ECM degradation by squamous carcinoma cells through control of invadopodia stability. *Oncogene*. 34:4531-4544.

Martin-Villar, E., D. Megias, S. Castel, M.M. Yurrita, S. Vilaro, and M. Quintanilla. 2006. Podoplanin binds ERM proteins to activate RhoA and promote epithelial-mesenchymal transition. *J Cell Sci*. 119:4541-4553.

Mateyak, M.K., A.J. Obaya, and J.M. Sedivy. 1999. c-Myc regulates cyclin D-Cdk4 and -Cdk6 activity but affects cell cycle progression at multiple independent points. *Mol Cell Biol*. 19:4672-4683.

Matsuoka, S., G. Rotman, A. Ogawa, Y. Shiloh, K. Tamai, and S.J. Elledge. 2000. Ataxia telangiectasia-mutated phosphorylates Chk2 in vivo and in vitro. *Proc Natl Acad Sci U S A*. 97:10389-10394.

McCubrey, J.A., L.S. Steelman, W.H. Chappell, S.L. Abrams, E.W. Wong, F. Chang, B. Lehmann, D.M. Terrian, M. Milella, A. Tafuri, F. Stivala, M. Libra, J. Basecke, C. Evangelisti, A.M. Martelli, and R.A. Franklin. 2007. Roles of the Raf/MEK/ERK pathway in cell growth, malignant transformation and drug resistance. *Biochim Biophys Acta*. 1773:1263-1284.

McFaline-Figueroa, J.L., C.J. Braun, M. Stanciu, Z.D. Nagel, P. Mazzucato, D. Sangaraju, E. Cerniauskas, K. Barford, A. Vargas, Y. Chen, N. Tretyakova, J.A. Lees, M.T. Hemann, F.M. White, and L.D. Samson. 2015. Minor Changes in Expression of the Mismatch Repair Protein MSH2 Exert a Major Impact on Glioblastoma Response to Temozolomide. *Cancer Res*. 75:3127-3138.

Meyer, M., J. Reimand, X. Lan, R. Head, X. Zhu, M. Kushida, J. Bayani, J.C. Pressey, A.C. Lionel, I.D. Clarke, M. Cusimano, J.A. Squire, S.W. Scherer, M. Bernstein, M.A. Woodin, G.D. Bader, and P.B. Dirks. 2015. Single cell-derived clonal analysis of human glioblastoma links functional and genomic heterogeneity. *Proc Natl Acad Sci U S A*. 112:851-856.

Middleton, M.R., J.J. Grob, N. Aaronson, G. Fierlbeck, W. Tilgen, S. Seiter, M. Gore, S. Aamdal, J. Cebon, A. Coates, B. Dreno, M. Henz, D. Schadendorf, A. Kapp, J. Weiss, U. Fraass, P. Statkevich, M. Muller, and N. Thatcher. 2000. Randomized phase III study of temozolomide versus dacarbazine in the treatment of patients with advanced metastatic malignant melanoma. *J Clin Oncol*. 18:158-166.

Mukherjee, B., B. McEllin, C.V. Camacho, N. Tomimatsu, S. Sirasanagandala, S. Nannepaga, K.J. Hatanpaa, B. Mickey, C. Madden, E. Maher, D.A. Boothman, F. Furnari, W.K. Cavenee, R.M. Bachoo, and S. Burma. 2009. EGFRvIII and DNA double-strand break repair: a molecular mechanism for radioresistance in glioblastoma. *Cancer Res*. 69:4252-4259.

Mukohara, T., H. Shimada, N. Ogasawara, R. Wanikawa, M. Shimomura, T. Nakatsura, G. Ishii, J.O. Park, P.A. Janne, N. Saijo, and H. Minami. 2009. Sensitivity of breast

cancer cell lines to the novel insulin-like growth factor-1 receptor (IGF-1R) inhibitor NVP-AEW541 is dependent on the level of IRS-1 expression. *Cancer Lett*. 282:14-24.

Munoz, J.L., V. Rodriguez-Cruz, S.J. Greco, S.H. Ramkissoon, K.L. Ligon, and P. Rameshwar. 2014. Temozolomide resistance in glioblastoma cells occurs partly through epidermal growth factor receptor-mediated induction of connexin 43. *Cell Death Dis*. 5:e1145.

Munoz, J.L., N.D. Walker, K.W. Scotto, and P. Rameshwar. 2015. Temozolomide competes for P-glycoprotein and contributes to chemoresistance in glioblastoma cells. *Cancer Lett*. 367:69-75.

Ohgaki, H., P. Dessen, B. Jourde, S. Horstmann, T. Nishikawa, P.L. Di Patre, C. Burkhard, D. Schuler, N.M. Probst-Hensch, P.C. Maiorka, N. Baeza, P. Pisani, Y. Yonekawa, M.G. Yasargil, U.M. Lutolf, and P. Kleihues. 2004. Genetic pathways to glioblastoma: a population-based study. *Cancer Res*. 64:6892-6899.

Ohtani, K., J. DeGregori, and J.R. Nevins. 1995. Regulation of the cyclin E gene by transcription factor E2F1. *Proc Natl Acad Sci U S A*. 92:12146-12150.

Omuro, A., and L.M. DeAngelis. 2013. Glioblastoma and other malignant gliomas: a clinical review. *JAMA*. 310:1842-1850.

Osuka, S., O. Sampetrean, T. Shimizu, I. Saga, N. Onishi, E. Sugihara, J. Okubo, S. Fujita, S. Takano, A. Matsumura, and H. Saya. 2013. IGF1 receptor signaling regulates adaptive radioprotection in glioma stem cells. *Stem Cells*. 31:627-640.

Pandini, G., F. Frasca, R. Mineo, L. Sciacca, R. Vigneri, and A. Belfiore. 2002. Insulin/insulin-like growth factor I hybrid receptors have different biological characteristics depending on the insulin receptor isoform involved. *J Biol Chem*. 277:39684-39695.

Pardo, B., B. Gomez-Gonzalez, and A. Aguilera. 2009. DNA repair in mammalian cells: DNA double-strand break repair: how to fix a broken relationship. *Cell Mol Life Sci*. 66:1039-1056.

Park, J., M.L. Leong, P. Buse, A.C. Maiyar, G.L. Firestone, and B.A. Hemmings. 1999. Serum and glucocorticoid-inducible kinase (SGK) is a target of the PI 3-kinase-stimulated signaling pathway. *EMBO J*. 18:3024-3033.

Parsons, D.W., S. Jones, X. Zhang, J.C. Lin, R.J. Leary, P. Angenendt, P. Mankoo, H. Carter, I.M. Siu, G.L. Gallia, A. Olivi, R. McLendon, B.A. Rasheed, S. Keir, T. Nikolskaya, Y. Nikolsky, D.A. Busam, H. Tekleab, L.A. Diaz, Jr., J. Hartigan, D.R. Smith, R.L. Strausberg, S.K. Marie, S.M. Shinjo, H. Yan, G.J. Riggins, D.D. Bigner, R. Karchin, N. Papadopoulos, G. Parmigiani, B. Vogelstein, V.E. Velculescu, and K.W. Kinzler. 2008. An integrated genomic analysis of human glioblastoma multiforme. *Science*. 321:1807-1812.

Paugh, B.S., C. Qu, C. Jones, Z. Liu, M. Adamowicz-Brice, J. Zhang, D.A. Bax, B. Coyle, J. Barrow, D. Hargrave, J. Lowe, A. Gajjar, W. Zhao, A. Broniscer, D.W. Ellison, R.G. Grundy, and S.J. Baker. 2010. Integrated molecular genetic profiling of pediatric high-grade gliomas reveals key differences with the adult disease. *J Clin Oncol*. 28:3061-3068.

Paull, T.T., E.P. Rogakou, V. Yamazaki, C.U. Kirchgessner, M. Gellert, and W.M. Bonner. 2000. A critical role for histone H2AX in recruitment of repair factors to nuclear foci after DNA damage. *Curr Biol*. 10:886-895.

Pawlik, T.M., and K. Keyomarsi. 2004. Role of cell cycle in mediating sensitivity to radiotherapy. *Int J Radiat Oncol Biol Phys*. 59:928-942.

Pei, J., I.H. Park, H.H. Ryu, S.Y. Li, C.H. Li, S.H. Lim, M. Wen, W.Y. Jang, and S. Jung. 2015. Sublethal dose of irradiation enhances invasion of malignant glioma cells

through p53-MMP 2 pathway in U87MG mouse brain tumor model. *Radiat Oncol*. 10:164.

Perry, J.R., N. Laperriere, C.J. O'Callaghan, A.A. Brandes, J. Menten, C. Phillips, M.F. Fay, R. Nishikawa, J.G. Cairncross, W. Roa, D. Osoba, A. Sahgal, H.W. Hirte, W. Wick, F. Laigle-Donadey, E. Franceschi, O.L. Chinot, C. Winch, K. Ding, and W.P. Mason. 2016. A phase III randomized controlled trial of short-course radiotherapy with or without concomitant and adjuvant temozolomide in elderly patients with glioblastoma (CCTG CE.6, EORTC 26062-22061, TROG 08.02, NCT00482677). *Journal of Clinical Oncology*. 34:suppl; abstr LBA2.

Peterziel, H., J. Muller, A. Danner, S. Barbus, H.K. Liu, B. Radlwimmer, T. Pietsch, P. Lichter, G. Schutz, J. Hess, and P. Angel. 2012. Expression of podoplanin in human astrocytic brain tumors is controlled by the PI3K-AKT-AP-1 signaling pathway and promoter methylation. *Neuro Oncol*. 14:426-439.

Pollak, M. 2012. The insulin and insulin-like growth factor receptor family in neoplasia: an update. *Nat Rev Cancer*. 12:159-169.

Polo, S.E., and S.P. Jackson. 2011. Dynamics of DNA damage response proteins at DNA breaks: a focus on protein modifications. *Genes Dev*. 25:409-433.

Quail, D.F., R.L. Bowman, L. Akkari, M.L. Quick, A.J. Schuhmacher, J.T. Huse, E.C. Holland, J.C. Sutton, and J.A. Joyce. 2016. The tumor microenvironment underlies acquired resistance to CSF-1R inhibition in gliomas. *Science*. 352:aad3018.

Quinn, J.A., S.X. Jiang, D.A. Reardon, A. Desjardins, J.J. Vredenburgh, J.N. Rich, S. Gururangan, A.H. Friedman, D.D. Bigner, J.H. Sampson, R.E. McLendon, J.E. Herndon, 2nd, A. Walker, and H.S. Friedman. 2009a. Phase II trial of temozolomide plus o6-benzylguanine in adults with recurrent, temozolomide-resistant malignant glioma. *J Clin Oncol*. 27:1262-1267.

Quinn, J.A., S.X. Jiang, D.A. Reardon, A. Desjardins, J.J. Vredenburgh, J.N. Rich, S. Gururangan, A.H. Friedman, D.D. Bigner, J.H. Sampson, R.E. McLendon, J.E. Herndon, Jr., A. Walker, and H.S. Friedman. 2009b. Phase I trial of temozolomide plus O6-benzylguanine 5-day regimen with recurrent malignant glioma. *Neuro Oncol*. 11:556-561.

Raizer, J.J., L.E. Abrey, A.B. Lassman, S.M. Chang, K.R. Lamborn, J.G. Kuhn, W.K. Yung, M.R. Gilbert, K.A. Aldape, P.Y. Wen, H.A. Fine, M. Mehta, L.M. Deangelis, F. Lieberman, T.F. Cloughesy, H.I. Robins, J. Dancey, M.D. Prados, and C. North American Brain Tumor. 2010. A phase II trial of erlotinib in patients with recurrent malignant gliomas and nonprogressive glioblastoma multiforme postradiation therapy. *Neuro Oncol*. 12:95-103.

Ramcharan, R., T. Aleksic, W.P. Kamdoum, S. Gao, S.X. Pfister, J. Tanner, E. Bridges, R. Asher, A.J. Watson, G.P. Margison, M. Woodcock, E. Repapi, J.L. Li, M.R. Middleton, and V.M. Macaulay. 2015. IGF-1R inhibition induces schedule-dependent sensitization of human melanoma to temozolomide. *Oncotarget*. 6:39877-39890.

Rashi-Elkeles, S., H.J. Warnatz, R. Elkon, A. Kupershtein, Y. Chobod, A. Paz, V. Amstislavskiy, M. Sultan, H. Safer, W. Nietfeld, H. Lehrach, R. Shamir, M.L. Yaspo, and Y. Shiloh. 2014. Parallel profiling of the transcriptome, cistrome, and epigenome in the cellular response to ionizing radiation. *Sci Signal*. 7:rs3.

Resnicoff, M., D. Abraham, W. Yutanawiboonchai, H.L. Rotman, J. Kajstura, R. Rubin, P. Zoltick, and R. Baserga. 1995a. The insulin-like growth factor I receptor protects tumor cells from apoptosis in vivo. *Cancer Res*. 55:2463-2469.

Resnicoff, M., J.L. Burgaud, H.L. Rotman, D. Abraham, and R. Baserga. 1995b. Correlation between apoptosis, tumorigenesis, and levels of insulin-like growth factor I receptors. *Cancer Res*. 55:3739-3741.

Resnicoff, M., W. Li, S. Basak, D. Herlyn, R. Baserga, and R. Rubin. 1996. Inhibition of rat C6 glioblastoma tumor growth by expression of insulin-like growth factor I receptor antisense mRNA. *Cancer Immunol Immunother*. 42:64-68.

Resnicoff, M., C. Sell, M. Rubini, D. Coppola, D. Ambrose, R. Baserga, and R. Rubin. 1994. Rat glioblastoma cells expressing an antisense RNA to the insulin-like growth factor-1 (IGF-1) receptor are nontumorigenic and induce regression of wild-type tumors. *Cancer Res*. 54:2218-2222.

Riedemann, J., M. Takiguchi, M. Sohail, and V.M. Macaulay. 2007. The EGF receptor interacts with the type 1 IGF receptor and regulates its stability. *Biochem Biophys Res Commun*. 355:707-714.

Robertson, A.B., A. Klungland, T. Rognes, and I. Leiros. 2009. DNA repair in mammalian cells: Base excision repair: the long and short of it. *Cell Mol Life Sci*. 66:981-993.

Rocchi, S., S. Tartare-Deckert, I. Mothe, and E. Van Obberghen. 1995. Identification by mutation of the tyrosine residues in the insulin receptor substrate-1 affecting association with the tyrosine phosphatase 2C and phosphatidylinositol 3-kinase. *Endocrinology*. 136:5291-5297.

Rochester, M.A., N. Patel, B.W. Turney, D.R. Davies, I.S. Roberts, J. Crew, A. Protheroe, and V.M. Macaulay. 2007. The type 1 insulin-like growth factor receptor is over-expressed in bladder cancer. *BJU Int*. 100:1396-1401.

Rochester, M.A., J. Riedemann, G.O. Hellawell, S.F. Brewster, and V.M. Macaulay. 2005. Silencing of the IGF1R gene enhances sensitivity to DNA-damaging agents in both PTEN wild-type and mutant human prostate cancer. *Cancer Gene Ther*. 12:90-100.

Rogakou, E.P., D.R. Pilch, A.H. Orr, V.S. Ivanova, and W.M. Bonner. 1998. DNA double-stranded breaks induce histone H2AX phosphorylation on serine 139. *J Biol Chem*. 273:5858-5868.

Rothkamm, K., I. Kruger, L.H. Thompson, and M. Lobrich. 2003. Pathways of DNA double-strand break repair during the mammalian cell cycle. *Mol Cell Biol*. 23:5706-5715.

Rottenberg, D.A., J.Z. Ginos, K.J. Kearfott, L. Junck, and D.D. Bigner. 1984. In vivo measurement of regional brain tissue pH using positron emission tomography. *Ann Neurol*. 15 Suppl:S98-102.

Rupnik, A., N.F. Lowndes, and M. Grenon. 2010. MRN and the race to the break. *Chromosoma*. 119:115-135.

Rutka, J.T., J.R. Giblin, D.Y. Dougherty, H.C. Liu, J.R. McCulloch, C.W. Bell, R.S. Stern, C.B. Wilson, and M.L. Rosenblum. 1987. Establishment and characterization of five cell lines derived from human malignant gliomas. *Acta Neuropathol*. 75:92-103.

Safa, A.R., M.R. Saadatzadeh, A.A. Cohen-Gadol, K.E. Pollok, and K. Bijangi-Vishehsaraei. 2015. Glioblastoma stem cells (GSCs) epigenetic plasticity and interconversion between differentiated non-GSCs and GSCs. *Genes Dis*. 2:152-163.

Saito, S., A.A. Goodarzi, Y. Higashimoto, Y. Noda, S.P. Lees-Miller, E. Appella, and C.W. Anderson. 2002. ATM mediates phosphorylation at multiple p53 sites, including Ser(46), in response to ionizing radiation. *J Biol Chem*. 277:12491-12494.

Sampetrean, O., and H. Saya. 2013. Characteristics of glioma stem cells. *Brain Tumor Pathol*. 30:209-214.

Sanai, N., A. Alvarez-Buylla, and M.S. Berger. 2005. Neural stem cells and the origin of gliomas. *N Engl J Med*. 353:811-822.

Sandberg-Nordqvist, A.C., P.A. Stahlbom, M. Reinecke, V.P. Collins, H. von Holst, and V. Sara. 1993. Characterization of insulin-like growth factor 1 in human primary brain tumors. *Cancer Res*. 53:2475-2478.

Sarbassov, D.D., D.A. Guertin, S.M. Ali, and D.M. Sabatini. 2005. Phosphorylation and regulation of Akt/PKB by the rictor-mTOR complex. *Science*. 307:1098-1101.

Schwartz, S., J. Wongvipat, C.B. Trigwell, U. Hancox, B.S. Carver, V. Rodrik-Outmezguine, M. Will, P. Yellen, E. de Stanchina, J. Baselga, H.I. Scher, S.T. Barry, C.L. Sawyers, S. Chandarlapaty, and N. Rosen. 2015. Feedback suppression of PI3Kalpha signaling in PTEN-mutated tumors is relieved by selective inhibition of PI3Kbeta. *Cancer Cell*. 27:109-122.

Schwartzentruber, J., A. Korshunov, X.Y. Liu, D.T. Jones, E. Pfaff, K. Jacob, D. Sturm, A.M. Fontebasso, D.A. Quang, M. Tonjes, V. Hovestadt, S. Albrecht, M. Kool, A. Nantel, C. Konermann, A. Lindroth, N. Jager, T. Rausch, M. Ryzhova, J.O. Korbel, T. Hielscher, P. Hauser, M. Garami, A. Klekner, L. Bognar, M. Ebinger, M.U. Schuhmann, W. Scheurlen, A. Pekrun, M.C. Fruhwald, W. Roggendorf, C. Kramm, M. Durken, J. Atkinson, P. Lepage, A. Montpetit, M. Zakrzewska, K. Zakrzewski, P.P. Liberski, Z. Dong, P. Siegel, A.E. Kulozik, M. Zapatka, A. Guha, D. Malkin, J. Felsberg, G. Reifenberger, A. von Deimling, K. Ichimura, V.P. Collins, H. Witt, T. Milde, O. Witt, C. Zhang, P. Castelo-Branco, P. Lichter, D. Faury, U. Tabori, C. Plass, J. Majewski, S.M. Pfister, and N. Jabado. 2012. Driver mutations in histone H3.3 and chromatin remodelling genes in paediatric glioblastoma. *Nature*. 482:226-231.

Sell, C., G. Dumenil, C. Deveaud, M. Miura, D. Coppola, T. DeAngelis, R. Rubin, A. Efstratiadis, and R. Baserga. 1994. Effect of a null mutation of the insulin-like growth factor I receptor gene on growth and transformation of mouse embryo fibroblasts. *Mol Cell Biol*. 14:3604-3612.

Sell, C., M. Rubini, R. Rubin, J.P. Liu, A. Efstratiadis, and R. Baserga. 1993. Simian virus 40 large tumor antigen is unable to transform mouse embryonic fibroblasts lacking type 1 insulin-like growth factor receptor. *Proc Natl Acad Sci U S A*. 90:11217-11221.

Senner, V., A. Sturm, I. Baur, U.H. Schrell, L. Distel, and W. Paulus. 1999. CD24 promotes invasion of glioma cells in vivo. *J Neuropathol Exp Neurol*. 58:795-802.

Shankar, A., S. Kumar, A.S. Iskander, N.R. Varma, B. Janic, A. deCarvalho, T. Mikkelsen, J.A. Frank, M.M. Ali, R.A. Knight, S. Brown, and A.S. Arbab. 2014. Subcurative radiation significantly increases cell proliferation, invasion, and migration of primary glioblastoma multiforme in vivo. *Chin J Cancer*. 33:148-158.

Shiloh, Y., and Y. Ziv. 2013. The ATM protein kinase: regulating the cellular response to genotoxic stress, and more. *Nat Rev Mol Cell Biol*. 14:197-210.

Shin, I., F.M. Yakes, F. Rojo, N.Y. Shin, A.V. Bakin, J. Baselga, and C.L. Arteaga. 2002. PKB/Akt mediates cell-cycle progression by phosphorylation of p27(Kip1) at threonine 157 and modulation of its cellular localization. *Nat Med*. 8:1145-1152.

Shu, H.K., M.M. Kim, P. Chen, F. Furman, C.M. Julin, and M.A. Israel. 1998. The intrinsic radioresistance of glioblastoma-derived cell lines is associated with a failure of p53 to induce p21(BAX) expression. *Proc Natl Acad Sci U S A*. 95:14453-14458.

Spentzos, D., S.A. Cannistra, F. Grall, D.A. Levine, K. Pillay, T.A. Libermann, and C.S. Mantzoros. 2007. IGF axis gene expression patterns are prognostic of survival in epithelial ovarian cancer. *Endocr Relat Cancer*. 14:781-790.

Stojic, L., R. Brun, and J. Jiricny. 2004. Mismatch repair and DNA damage signalling. *DNA Repair (Amst)*. 3:1091-1101.

Stupp, R., M.E. Hegi, W.P. Mason, M.J. van den Bent, M.J. Taphoorn, R.C. Janzer, S.K. Ludwin, A. Allgeier, B. Fisher, K. Belanger, P. Hau, A.A. Brandes, J. Gijtenbeek, C. Marosi, C.J. Vecht, K. Mokhtari, P. Wesseling, S. Villa, E. Eisenhauer, T. Gorlia, M. Weller, D. Lacombe, J.G. Cairncross, R.O. Mirimanoff, R. European Organisation for, T. Treatment of Cancer Brain, G. Radiation Oncology, and G. National Cancer Institute of Canada Clinical Trials. 2009. Effects of radiotherapy with concomitant and adjuvant temozolomide versus radiotherapy alone on survival in glioblastoma in a randomised phase III study: 5-year analysis of the EORTC-NCIC trial. *Lancet Oncol*. 10:459-466.

Stupp, R., W.P. Mason, M.J. van den Bent, M. Weller, B. Fisher, M.J. Taphoorn, K. Belanger, A.A. Brandes, C. Marosi, U. Bogdahn, J. Curschmann, R.C. Janzer, S.K. Ludwin, T. Gorlia, A. Allgeier, D. Lacombe, J.G. Cairncross, E. Eisenhauer, R.O. Mirimanoff, R. European Organisation for, T. Treatment of Cancer Brain, G. Radiotherapy, and G. National Cancer Institute of Canada Clinical Trials. 2005. Radiotherapy plus concomitant and adjuvant temozolomide for glioblastoma. *N Engl J Med*. 352:987-996.

Sugawa, N., A.J. Ekstrand, C.D. James, and V.P. Collins. 1990. Identical splicing of aberrant epidermal growth factor receptor transcripts from amplified rearranged genes in human glioblastomas. *Proc Natl Acad Sci U S A*. 87:8602-8606.

Sugiarto, S., A.I. Persson, E.G. Munoz, M. Waldhuber, C. Lamagna, N. Andor, P. Hanecker, J. Ayers-Ringler, J. Phillips, J. Siu, D.A. Lim, S. Vandenberg, W. Stallcup, M.S. Berger, G. Bergers, W.A. Weiss, and C. Petritsch. 2011. Asymmetry-defective oligodendrocyte progenitors are glioma precursors. *Cancer Cell*. 20:328-340.

Sun, H., R. Lesche, D.M. Li, J. Liliental, H. Zhang, J. Gao, N. Gavrilova, B. Mueller, X. Liu, and H. Wu. 1999. PTEN modulates cell cycle progression and cell survival by regulating phosphatidylinositol 3,4,5,-trisphosphate and Akt/protein kinase B signaling pathway. *Proc Natl Acad Sci U S A*. 96:6199-6204.

Takahari, D., Y. Yamada, N.T. Okita, T. Honda, Y. Hirashima, J. Matsubara, A. Takashima, K. Kato, T. Hamaguchi, K. Shirao, Y. Shimada, and T. Shimoda. 2009. Relationships of insulin-like growth factor-1 receptor and epidermal growth factor receptor expression to clinical outcomes in patients with colorectal cancer. *Oncology*. 76:42-48.

Takeshita, I., T. Takaki, M. Kuramitsu, S. Nagasaka, T. Machi, H. Ogawa, H. Egami, H. Mannoji, M. Fukui, and K. Kitamura. 1987. Characteristics of an Established Human Glioma Cell Line, KNS-42. *Neurologia medico-chirurgica*. 27:581-587.

Talarico, C., V. Dattilo, L. D'Antona, A. Barone, N. Amodio, S. Belviso, F. Musumeci, C. Abbruzzese, C. Bianco, F. Trapasso, S. Schenone, S. Alcaro, F. Ortuso, T. Florio, M.G. Paggi, N. Perrotti, and R. Amato. 2016. SI113, a SGK1 inhibitor, potentiates the effects of radiotherapy, modulates the response to oxidative stress and induces cytotoxic autophagy in human glioblastoma multiforme cells. *Oncotarget*. 7:15868-15884.

Tanno, S., S. Tanno, Y. Mitsuuchi, D.A. Altomare, G.H. Xiao, and J.R. Testa. 2001. AKT activation up-regulates insulin-like growth factor I receptor expression and promotes invasiveness of human pancreatic cancer cells. *Cancer Res*. 61:589-593.

Tiwana, G.S., R. Prevo, F.M. Buffa, S. Yu, D.V. Ebner, A. Howarth, L.K. Folkes, B. Budwal, K.Y. Chu, L. Durrant, R.J. Muschel, W.G. McKenna, and G.S. Higgins. 2015. Identification of vitamin B1 metabolism as a tumor-specific radiosensitizing pathway using a high-throughput colony formation screen. *Oncotarget*. 6:5978-5989.

Toulany, M., K. Dittmann, M. Kruger, M. Baumann, and H.P. Rodemann. 2005. Radioresistance of K-Ras mutated human tumor cells is mediated through EGFR-dependent activation of PI3K-AKT pathway. *Radiother Oncol*. 76:143-150.

Trojan, J., T.R. Johnson, S.D. Rudin, J. Ilan, M.L. Tykocinski, and J. Ilan. 1993. Treatment and prevention of rat glioblastoma by immunogenic C6 cells expressing antisense insulin-like growth factor I RNA. *Science*. 259:94-97.

Turcan, S., D. Rohle, A. Goenka, L.A. Walsh, F. Fang, E. Yilmaz, C. Campos, A.W. Fabius, C. Lu, P.S. Ward, C.B. Thompson, A. Kaufman, O. Guryanova, R. Levine, A. Heguy, A. Viale, L.G. Morris, J.T. Huse, I.K. Mellinghoff, and T.A. Chan. 2012. IDH1 mutation is sufficient to establish the glioma hypermethylator phenotype. *Nature*. 483:479-483.

Turner, B.C., B.G. Haffty, L. Narayanan, J. Yuan, P.A. Havre, A.A. Gumbs, L. Kaplan, J.L. Burgaud, D. Carter, R. Baserga, and P.M. Glazer. 1997. Insulin-like growth factor-I receptor overexpression mediates cellular radioresistance and local breast cancer recurrence after lumpectomy and radiation. *Cancer Res*. 57:3079-3083.

Turney, B.W., M. Kerr, M.M. Chitnis, K. Lodhia, Y. Wang, J. Riedemann, M. Rochester, A.S. Protheroe, S.F. Brewster, and V.M. Macaulay. 2012. Depletion of the type 1 IGF receptor delays repair of radiation-induced DNA double strand breaks. *Radiother Oncol*. 103:402-409.

Ullrich, A., A. Gray, A.W. Tam, T. Yang-Feng, M. Tsubokawa, C. Collins, W. Henzel, T. Le Bon, S. Kathuria, E. Chen, and et al. 1986. Insulin-like growth factor I receptor primary structure: comparison with insulin receptor suggests structural determinants that define functional specificity. *EMBO J*. 5:2503-2512.

Valduvieco, I., E. Verger, J. Bruna, L. Caral, T. Pujol, T. Ribalta, T. Boget, L. Oleaga, E. Pineda, and F. Graus. 2013. Impact of radiotherapy delay on survival in glioblastoma. *Clin Transl Oncol*. 15:278-282.

Valsecchi, M.E., M. McDonald, J.R. Brody, T. Hyslop, B. Freydin, C.J. Yeo, C. Solomides, S.C. Peiper, and A.K. Witkiewicz. 2012. Epidermal growth factor receptor and insulinlike growth factor 1 receptor expression predict poor survival in pancreatic ductal adenocarcinoma. *Cancer*. 118:3484-3493.

Vanan, I., Z. Dong, E. Tosti, G. Warshaw, M. Symons, and R. Ruggieri. 2012. Role of a DNA damage checkpoint pathway in ionizing radiation-induced glioblastoma cell migration and invasion. *Cell Mol Neurobiol*. 32:1199-1208.

Verhaak, R.G., K.A. Hoadley, E. Purdom, V. Wang, Y. Qi, M.D. Wilkerson, C.R. Miller, L. Ding, T. Golub, J.P. Mesirov, G. Alexe, M. Lawrence, M. O'Kelly, P. Tamayo, B.A. Weir, S. Gabriel, W. Winckler, S. Gupta, L. Jakkula, H.S. Feiler, J.G. Hodgson, C.D. James, J.N. Sarkaria, C. Brennan, A. Kahn, P.T. Spellman, R.K. Wilson, T.P. Speed, J.W. Gray, M. Meyerson, G. Getz, C.M. Perou, D.N. Hayes, and N. Cancer Genome Atlas Research. 2010. Integrated genomic analysis identifies clinically relevant subtypes of glioblastoma characterized by abnormalities in PDGFRA, IDH1, EGFR, and NF1. *Cancer Cell*. 17:98-110.

Vidal, S.J., V. Rodriguez-Bravo, S.A. Quinn, R. Rodriguez-Barrueco, A. Lujambio, E. Williams, X. Sun, J. de la Iglesia-Vicente, A. Lee, B. Readhead, X. Chen, M. Galsky, B. Esteve, D.P. Petrylak, J.T. Dudley, R. Rabadan, J.M. Silva, Y. Hoshida, S.W. Lowe, C. Cordon-Cardo, and J. Domingo-Domenech. 2015. A targetable GATA2-IGF2 axis confers aggressiveness in lethal prostate cancer. *Cancer Cell*. 27:223-239.

Wang, S.I., J. Puc, J. Li, J.N. Bruce, P. Cairns, D. Sidransky, and R. Parsons. 1997. Somatic mutations of PTEN in glioblastoma multiforme. *Cancer Res*. 57:4183-4186.

Wang, X., L. Jia, X. Jin, Q. Liu, W. Cao, X. Gao, M. Yang, and B. Sun. 2015. NF-kappaB inhibitor reverses temozolomide resistance in human glioma TR/U251 cells. *Oncol Lett*. 9:2586-2590.

Warren, K.E., A.A. Aikin, M. Libucha, B.C. Widemann, E. Fox, R.J. Packer, and F.M. Balis. 2005. Phase I study of O6-benzylguanine and temozolomide administered daily for 5 days to pediatric patients with solid tumors. *J Clin Oncol*. 23:7646-7653.

Warren, K.E., S. Gururangan, J.R. Geyer, R.E. McLendon, T.Y. Poussaint, D. Wallace, F.M. Balis, S.L. Berg, R.J. Packer, S. Goldman, J.E. Minturn, I.F. Pollack, J.M. Boyett, and L.E. Kun. 2012. A phase II study of O6-benzylguanine and temozolomide in pediatric patients with recurrent or progressive high-grade gliomas and brainstem gliomas: a Pediatric Brain Tumor Consortium study. *J Neurooncol*. 106:643-649.

Watanabe, K., O. Tachibana, K. Sata, Y. Yonekawa, P. Kleihues, and H. Ohgaki. 1996. Overexpression of the EGF receptor and p53 mutations are mutually exclusive in the evolution of primary and secondary glioblastomas. *Brain Pathol*. 6:217-223; discussion 223-214.

Wedge, S.R., and E.S. Newlands. 1996. O6-benzylguanine enhances the sensitivity of a glioma xenograft with low O6-alkylguanine-DNA alkyltransferase activity to temozolomide and BCNU. *Br J Cancer*. 73:1049-1052.

Wedge, S.R., J.K. Porteous, and E.S. Newlands. 1996a. 3-aminobenzamide and/or O6-benzylguanine evaluated as an adjuvant to temozolomide or BCNU treatment in cell lines of variable mismatch repair status and O6-alkylguanine-DNA alkyltransferase activity. *Br J Cancer*. 74:1030-1036.

Wedge, S.R., J.K. Porteus, B.L. May, and E.S. Newlands. 1996b. Potentiation of temozolomide and BCNU cytotoxicity by O(6)-benzylguanine: a comparative study in vitro. *Br J Cancer*. 73:482-490.

Weiler, M., J. Blaes, S. Pusch, F. Sahm, M. Czabanka, S. Luger, L. Bunse, G. Solecki, V. Eichwald, M. Jugold, S. Hodecker, M. Osswald, C. Meisner, T. Hielscher, P. Rubmann, P.N. Pfenning, M. Ronellenfitsch, T. Kempf, M. Schnolzer, A. Abdollahi, F. Lang, M. Bendszus, A. von Deimling, F. Winkler, M. Weller, P. Vajkoczy, M. Platten, and W. Wick. 2014. mTOR target NDRG1 confers MGMT-dependent resistance to alkylating chemotherapy. *Proc Natl Acad Sci U S A*. 111:409-414.

Werner, H., E. Karnieli, F.J. Rauscher, and D. LeRoith. 1996a. Wild-type and mutant p53 differentially regulate transcription of the insulin-like growth factor I receptor gene. *Proc Natl Acad Sci U S A*. 93:8318-8323.

Werner, H., C.T. Roberts, Jr., F.J. Rauscher, 3rd, and D. LeRoith. 1996b. Regulation of insulin-like growth factor I receptor gene expression by the Wilms' tumor suppressor WT1. *J Mol Neurosci*. 7:111-123.

Wicki, A., F. Lehembre, N. Wick, B. Hantusch, D. Kerjaschki, and G. Christofori. 2006. Tumor invasion in the absence of epithelial-mesenchymal transition: podoplanin-mediated remodeling of the actin cytoskeleton. *Cancer Cell*. 9:261-272.

Wild-Bode, C., M. Weller, A. Rimner, J. Dichgans, and W. Wick. 2001. Sublethal irradiation promotes migration and invasiveness of glioma cells: implications for radiotherapy of human glioblastoma. *Cancer Res*. 61:2744-2750.

Willers, H., J. Dahm-Daphi, and S.N. Powell. 2004. Repair of radiation damage to DNA. *Br J Cancer*. 90:1297-1301.

Wittman, M.D., J.M. Carboni, Z. Yang, F.Y. Lee, M. Antman, R. Attar, P. Balimane, C. Chang, C. Chen, L. Discenza, D. Frennesson, M.M. Gottardis, A. Greer, W. Hurlburt, W. Johnson, D.R. Langley, A. Li, J. Li, P. Liu, H. Mastalerz, A. Mathur, K. Menard, K. Patel, J. Sack, X. Sang, M. Saulnier, D. Smith, K. Stefanski, G. Trainor, U. Velaparthi, G. Zhang, K. Zimmermann, and D.M. Vyas. 2009. Discovery

of a 2,4-disubstituted pyrrolo[1,2-f][1,2,4]triazine inhibitor (BMS-754807) of insulin-like growth factor receptor (IGF-1R) kinase in clinical development. *J Med Chem*. 52:7360-7363.

Wu, G., A. Broniscer, T.A. McEachron, C. Lu, B.S. Paugh, J. Becksfort, C. Qu, L. Ding, R. Huether, M. Parker, J. Zhang, A. Gajjar, M.A. Dyer, C.G. Mullighan, R.J. Gilbertson, E.R. Mardis, R.K. Wilson, J.R. Downing, D.W. Ellison, J. Zhang, S.J. Baker, and P. St. Jude Children's Research Hospital-Washington University Pediatric Cancer Genome. 2012. Somatic histone H3 alterations in pediatric diffuse intrinsic pontine gliomas and non-brainstem glioblastomas. *Nat Genet*. 44:251-253.

Xiao, S., Z. Yang, R. Lv, J. Zhao, M. Wu, Y. Liao, and Q. Liu. 2014. miR-135b contributes to the radioresistance by targeting GSK3beta in human glioblastoma multiforme cells. *PLoS One*. 9:e108810.

Yount, G.L., G. Afshar, S. Ries, M. Korn, N. Shalev, D. Basila, F. McCormick, and D.A. Haas-Kogan. 2001. Transcriptional activation of TRADD mediates p53-independent radiation-induced apoptosis of glioma cells. *Oncogene*. 20:2826-2835.

Yu, Z., G. Xie, G. Zhou, Y. Cheng, G. Zhang, G. Yao, Y. Chen, Y. Li, and G. Zhao. 2015. NVP-BEZ235, a novel dual PI3K-mTOR inhibitor displays anti-glioma activity and reduces chemoresistance to temozolomide in human glioma cells. *Cancer Lett*. 367:58-68.

Zhang, J., M.F. Stevens, and T.D. Bradshaw. 2012. Temozolomide: mechanisms of action, repair and resistance. *Curr Mol Pharmacol*. 5:102-114.

Zhang, L.H., A.A. Yin, J.X. Cheng, H.Y. Huang, X.M. Li, Y.Q. Zhang, N. Han, and X. Zhang. 2015. TRIM24 promotes glioma progression and enhances chemoresistance through activation of the PI3K/Akt signaling pathway. *Oncogene*. 34:600-610.

Zhang, Y., X. Chen, H. Lian, J. Liu, B. Zhou, S. Han, B. Peng, J. Yin, W. Liu, and X. He. 2014. MicroRNA-503 acts as a tumor suppressor in glioblastoma for multiple antitumor effects by targeting IGF-1R. *Oncol Rep*. 31:1445-1452.

Zhao, H., J. Dupont, S. Yakar, M. Karas, and D. LeRoith. 2004. PTEN inhibits cell proliferation and induces apoptosis by downregulating cell surface IGF-IR expression in prostate cancer cells. *Oncogene*. 23:786-794.

Zheng, J., Y. Li, J. Yang, Q. Liu, M. Shi, R. Zhang, H. Shi, Q. Ren, J. Ma, H. Guo, Y. Tao, Y. Xue, N. Jiang, L. Yao, and W. Liu. 2011. NDRG2 inhibits hepatocellular carcinoma adhesion, migration and invasion by regulating CD24 expression. *BMC Cancer*. 11:251:251-259.

Zhou, B.P., Y. Liao, W. Xia, B. Spohn, M.H. Lee, and M.C. Hung. 2001. Cytoplasmic localization of p21Cip1/WAF1 by Akt-induced phosphorylation in HER-2/neu-overexpressing cells. *Nat Cell Biol*. 3:245-252.

Zhukovskaya, N., B. Rydberg, and P. Karran. 1992. Inactive O6-methylguanine-DNA methyltransferase in human cells. *Nucleic Acids Res*. 20:6081-6090.

Zong, H., R.G. Verhaak, and P. Canoll. 2012. The cellular origin for malignant glioma and prospects for clinical advancements. *Expert Rev Mol Diagn*. 12:383-394.

Zou, L., and S.J. Elledge. 2003. Sensing DNA damage through ATRIP recognition of RPA-ssDNA complexes. *Science*. 300:1542-1548.